Engineering *Cupriavidus necator* H16 for 3-hydroxypropionic acid production

Jessica Katie Locker (MSc)

Thesis submitted to the University of Nottingham for the degree of Doctor of Philosophy

March 2021

Declaration

Unless otherwise acknowledged, the work presented in this thesis is my own. No part has been submitted for another degree at the University of Nottingham or any other institute of learning.

Jessica Katie Locker, March 2021

Abstract

As chemical production is largely sustained by oil-based products and accounts for 10% of the global final energy consumed, it is an essential target in the fight against climate change and ecosystem destruction. Biological synthesis in microorganisms has been proposed as the choice alternative for production of commodity chemicals using non-petroleum energy sources. Among the many chassis organisms under investigation, *Cupriavidus necator* displays many characteristics that make it ideal for the biosynthesis of such chemicals. Notably, the organism can grow lithoautotrophically (using only CO_2 and H_2 as carbon and energy sources) and on a range of non-traditional substrates.

The main aim of this study was to engineer *C. necator* to produce 3-hydroxypropionic acid (3-HP), a precursor to industrial chemicals such as acrylic acid, 1,3-propandiol and poly-3-HP, with a global market estimated to be worth over $1 billion. There are numerous pathways to produce 3-HP biologically, but the malonyl-CoA pathway has been described as one of the most promising, due to the small number of genes required and its thermodynamic feasibility. The pathway is based on only two enzymes, acetyl-CoA carboxylase (ACC) and malonyl-CoA reductase (MCR): ACC converts acetyl-CoA to malonyl-CoA, which is then reduced by the action of MCR to malonate semialdehyde and finally 3-HP. In the first step, the ACC subunit encoding genes from *Corynebacterium glutamicum* were combined into a synthetic operon controlled by an inducible promoter and expressed in this strain together with the *mcr* gene from *Chloroflexus aurantiacus.* However, no 3-HP production was achieved.

To understand why no 3-HP was seen, strain choice was evaluated, and each step of the malonyl-CoA pathway was assessed. An enzyme-based colorimetric biosensor for malonyl-CoA in *C. necator* H16 was developed, and results showed that neither *C. glutamicum* ACC expression, nor gene deletions (*mcd*, *mmsA1*/2/3, *phaCAB*) had any effect on malonyl-CoA availability. The same assay also demonstrated the detrimental effect of overexpressing the ACC in *C. necator*, with even the lowest induction level reducing cell viability greatly. Although the MCR enzyme was found to be produced, its activity was very low (0.025 μmol min^{-1} mg^{-1}). Modifications known to increase MCR activity were introduced, including splitting of the enzyme into malonyl-CoA reductase and MSA reductase domains, and overexpression of a further hydroxypropionate dehydrogenase gene (*ydfGEc*) to enhance conversion of malonate semialdehyde (MSA) to 3-HP. Again, a 3-HP producing strain could not be generated.

It was found that 3-HP and its degradation intermediate MSA appear to have unforeseen effects on the catabolism of compounds consumed by the Entner-Doudoroff pathway. In wild type cells the acid is consumed preferentially over sugars thereby repressing the genes involved in fructose breakdown. It was uncovered that 3-HP presence had undesirable effects on strains of *C. necator* unable to degrade it, such as such as the inability to grow on fructose and N-acetylglucosamine, and slower growth on gluconate. This could be a contributing factor in the inability of engineered *C. necator* strains to produce 3-HP when grown on these substrates.

Acknowledgments

I would like to show my enormous gratitude to my supervisors, Klaus Winzer and Katalin Kovács. Thank you for supporting me, I whole-heartedly appreciate all your advice, guidance, and expertise. I feel very lucky to have had such understanding and knowledgeable mentors.

I wish to thank my friends and family, who supported me in the lab each day and who encouraged me from afar. Thank you for every inspiring discussion and happy distraction.

The biggest thanks to Mark for all your love and support throughout this whole experience, I couldn't have done it without you. Finally, I would like to thank Arnie, for the company and comfort he provided.

Table of contents

List of figures

List of tables

Abbreviations

Abbreviation	Description
3-HP	3-hydroxypropionic acid
ABC	ATP-binding cassette
ACC	Acetyl CoA carboxylase
BC	Biotin carboxylase
BCCP	Biotin carboxylase carrier protein
CT	Carboxyltransferase
CBB cycle	Calvin-Benson-Bassham cycle
Cm	Chloramphenicol
ED pathway	Entner–Doudoroff pathway
EMP pathway	Embden–Meyerhof–Parnas pathway
eyfp	Enhanced yellow fluorescent protein
Gent	Gentamicin
GlcNac	N-acetyl glucosamine
HPLC	High-performance liquid chromatography
IPTG	Isopropyl ß-D-1-thiogalactopyranoside
KDPG	2-keto-3-deoxy-6-phosphogluconate
KEGG	Kyoto encyclopaedia of genes and genomes
LB	Lysogeny broth
LSLB	Low salt lysogeny broth
MCR	Malonyl CoA reductase
MM	Minimal medium
MMC	Methyl-malonate carboxyltransferase
MSA	Malonate semialdehyde
NCBI	National Centre for Biotechnology Information
OAA	Oxaloacetate
OD	Optical density
PCR	Polymerase chain reaction
PEP	Phosphoenolpyruvate
PHA	Polyhydroxyalkanoate
PHB	Polyhydroxybutyrate
PP pathway	Pentose phosphate pathway
PTS	Phosphotransferase system
RBS	Ribosome binding site
rfp	Red fluorescent protein
rpm	Revolutions per minute
SG	Sodium gluconate
SNP	Single nucleotide polymorphism
TAE	Tris-acetate-EDTA buffer
TCA cycle	Tricarboxylic acid cycle
Tet	Tetracycline
v/v	Volume/volume
w/v	Weight/volume

Chapter 1 – Introduction

Chapter 1 - Introduction

1.1 The requirement for bio-based chemicals

Despite increased funding, awareness and technological advances, the release of greenhouse gases and other waste products into the environment remains one of remains one of humanity's greatest challenges. Described as a "collision course with the natural world", there is enhanced pressure to change behaviours and act in sustainable manner [1]. This includes reducing reliance on fossil fuel derived products, re-evaluating waste release procedures and reducing ecological impact. In order to mitigate the disastrous consequences, new green technologies must be adopted that rely on renewable energy sources [1].

As chemical production is largely sustained by the sale of oil-based products and accounts for 10% of the global final energy consumed, it is an essential target in the fight against climate change and ecosystem destruction [2]. Biological synthesis has been touted as the choice alternative for production of commodity chemicals at a commercial scale using non-petroleum energy sources [3]. For example, biofuels accounted for 7.1% of energy use in transport in the EU in 2019 and over 5 billion litres of bioethanol were produced. Much of this ethanol (over 90%) was produced from primary feedstocks such as sugar beet, corn, or wheat [4]. Although an improvement, plant-derived feedstocks can lead to direct and indirect land use change, reducing biodiversity and decreasing food availability [5]. Carbon dioxide is an alternative, highly-sustainable carbon source, decoupling production from fossil resources, decreasing harmful emissions and producing industrially-desirable platform chemicals simultaneously [6].

1.2 *Cupriavidus necator*

Cupriavidus necator has many characteristics that make it ideal for biosynthesis of chemicals that were previously derived from fossil fuels or feedstocks that compete with food availability. The bacterium is best known for its industrial production of bioplastics, but recent interest is focused on the ability to grow lithoautotrophically, (using only CO_2 and H_2 as carbon and energy sources) [7]. Coupling these two

characteristics, *C. necator* has the potential to be a powerful chassis for synthesis of useful products from waste products such as CO_2.

Isolated in the 1950s, *C. necator* is a Gram-negative, aerobic and non-spore forming bacterium, found ubiquitously in soil and water, such as springs. The first isolates were originally named *Hydrogenomonas eutropha*, and categorised as 'hydrogen bacteria', due to the ability to use hydrogen as a sole energy source. For this reason, the species immediately garnered interest from NASA and industry for use as a bioregenerative system [8]. The name was then changed to *Alcaligenes eutrophus*, as the genus *Hydrogenomonas* contained many distinct species, no longer categorised by the utilisation of hydrogen, but other features [9].

The advancement of phylogenetic analysis using 16S rDNA recategorised *A. eutrophus* and 2 *Burkholderia* species into a new genus, *Ralstonia*, as seen in Figure 1 [10]. A proposal to rename *Ralstonia eutropha* to *Wautersia eutropha* was put forward, distinguishing them from *Ralstonia* strains by their flagella type, acid production, and their susceptibility to colistin. However, the 16S rRNA gene sequence showed that the *Wautersia eutropha* type strain was identical to previously isolated *C. necator* [11] and hence *C. necator* was officially recognised due to rules regarding nomenclature [12]. Both names, *R. eutropha* and *C. necator*, are used regularly in print, but for clarity and to comply with nomenclature guidelines, *C. necator* will be used throughout this thesis.

From the Latin *cuprum* (copper) and *avidus* (desirous of, greedy, loving), the genus is named after its resistance to high copper concentrations. In fact, for some species copper is found to initiate growth phases, *via* copper-related growth initiation factor (GIF), promoting an increase in population size. The species was designated the name 'necator' meaning murderous, due to the predatory nature of some strains of this microorganism in nature [13].

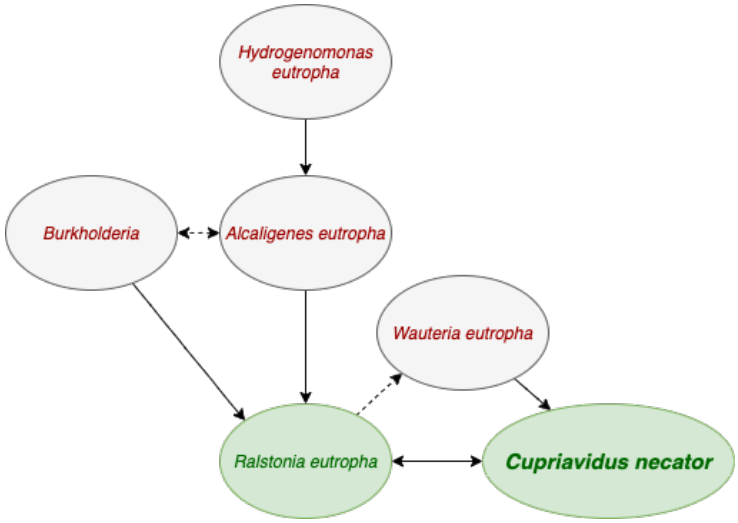

Figure 1 - The current and previous names for the species now recognised as *Cupriavidus necator*. In red are previously held, defunct names. In green are names in current usage. Solid lines indicate show the development of changes to the name. The dashed lines show equivalent names used at the same time.

The NCBI has 5 strains of *C. necator* listed as of 2020, but recent work has reclassified a number of strains using whole genome sequencing [14]. Subtypes such as NH9 and JMP134 are known for the ability to degrade chloroaromatics. This ability, in addition to resistance to metallic compounds, is a defining feature of the species as a whole. *C. necator* has almost all of the main ring-cleavage pathways for the degradation of aromatic compounds [14], [15]. Varieties H16 and N-1 (the type strain) are highly similar (see Figure 2), but N-1 does not possess the H_2-oxidizing hydrogenases required for lithoautotrophic growth [16].

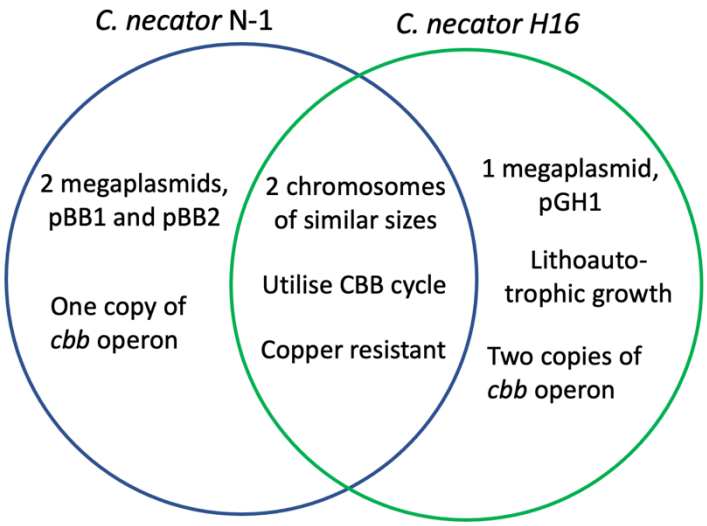

Figure 2 - Simplified comparison of the *C. necator* type strain N-1, and *C. necator* H16. CBB = Calvin–Benson–Bassham cycle, encoded by the *cbb* operon

The presence of these hydrogenases, encoded for on the megaplasmid pHG1, allows *C. necator* H16 to utilise hydrogen as an energy source and carbon dioxide as a carbon source, in the presence or absence of oxygen [17]. The hydrogen and electrons provide energy and reducing power. Even under lithoautotrophic conditions, the bacteria are able to grow to high cell densities (up to 18 g/L) and accumulate intracellular energy stores [18]. The sequence of the 2 chromosomes and the pGH1 megaplasmid (452,156 bp) have both been published for *C. necator* H16 [7], [17], [19]. Much work has been completed on the various and wide-ranging carbon sources that this strain can exploit, and biosynthetic pathways have been introduced to generate commodity chemicals [20]–[29]. The H16 strain is the best studied and will be discussed and used throughout this thesis.

1.2.1 Genetic tools for engineering *C. necator* H16

The abilities discussed make *C. necator* an exciting chassis organism for biotechnology. Many tools are now available for genetic manipulation of the species, including transformation with plasmids and chromosome modifications [30]. Broad host range plasmids that have previously been found to function in a diverse range of Gram-negative bacteria have been favoured for work with *C. necator*. However, issues have been reported with plasmid loss after a relative short growth period. For example, pBBR1-based plasmid loss was reported to be above 38% within 24 hours [31]. For plasmids with an RSF1010 origin of replication, plasmid retention rate was only 48% after 3 subcultures over 72 hours [23]. A major problem with this is the need for antibiotic selection to maintain presence of the plasmid. This can be a costly addition to an industrial scale fermentation set up. Solutions to this have been proposed including addiction systems, where the presence of the plasmid is necessary due to a defect in the strain that would otherwise slow or inhibit growth [31].

This approach has been shown to work in *C. necator*, where a KDPG aldolase gene dependent addiction system was implemented. To achieve this, a KDPG aldolase-deficient mutant was created by knocking out the *eda* gene, which meant the strain was unable to utilise fructose or gluconate as sole carbon source. The *eda* gene was reintroduced on a pBBR1 plasmid and expressed at high levels as it was essential [32]. However, this system only works when the growth medium contains fructose or

gluconate as the sole carbon source, making it ineffectual for autotrophic growth. A *hoxA*-mediated plasmid addiction system has been demonstrated in *C. necator*. In this system, the *hox* genes are necessary for the utilisation of hydrogen. Disrupting the chromosomal hydrogenase operon transcriptional regulator gene (*hoxA*) and placing an intact copy on the plasmid makes it indispensable. This method is functional in autotrophic conditions [33]. However, no addiction system has been found to be satisfactory for industrial use due to insufficient stability or incompatibility with proposed production processes using gas feedstocks [34] . Although plasmid-based systems are excellent for high throughput testing of biosynthesis pathways, the variable copy number, antibiotic resistance and cost are all barriers to implementing plasmid-bearing strains in an industrial setting.

Studies have been conducted to evaluate promoter activities in *C. necator*. Unlike *E. coli*, the *lac* promoter/inducer system does not appear to be functional in this species, due to the absence of the galactose permease gene *lacY* or the inability of *C. necator* to transport IPTG into the cell. When tested, controlling expression of a fluorescent protein, expression levels were similar before and after induction with IPTG [20]. The strong promoter P_{tac} showed better basal expression. This promoter is a hybrid between the *trp* and *lac* promoters. The P_{BAD} promoter is better suited if a fine-tuned expression level is necessary as it is possible to regulate activity using varying levels of the inducer, L-arabinose [35]. This promoter also allows for the uncoupling of growth and product synthesis, resulting in higher titers [36]. Native promoters P_{phaC}, and P_{phaP}, are both mediating moderate strength, constitutive gene expression [35]. More recent work by Johnson *et al.* created a system of 42 constitutive promoters, for tailoring specific expression levels [37]. Similar work by Alagesan *et al.* expanded the dynamic range to over 700 fold using two positively (L-arabinose and L-rhamnose) and two negatively (acrylate and cumate) regulated inducible systems [38]. Hanko *et al.* described a 3-HP inducible promoter system from *Pseudomonas putida*, that provided a 500-fold expression range in *C. necator* [39]. Furthermore, the same authors identified and characterised 15 novel metabolite-inducible systems from *C. necator* H16, induced by compounds such as benzoate, salicylate and formate [40].

In order to genetically engineer the central metabolism of *C. necator* and direct carbon flow to a desired product, it is necessary to have a system for deleting and inserting

coding regions into the chromosome(s). Commonly gene knockouts and integrations are performed using a suicide plasmid system with an antibiotic resistance marker that is introduced by conjugation with the help of a conjugative donor *E. coli* strain (often S17-1). In the case of *C. necator*, the suicide plasmid usually contains the *sacB* gene from *Bacillus subtilis*, with encodes a levansucrase. This enzyme converts sucrose to levans (mostly β-(2,6)-linked fructose polymers), which are toxic to *C. necator* [41]. The accumulation of the harmful product selects for plasmid loss after the homologous regions on the chromosome and plasmid are exchanged (by allowing cells to grow after the plasmid backbone containing the *sacB* gene has been lost). Addition of sucrose hence serves as a counter-selection technique to eliminate cells for which no double crossover (or reversal to the wild type chromosome) has occurred. A benefit of this method is the lack of antibiotic resistance marker left residually in the chromosome(s) of the organism, constructing unmarked mutants [41].

With the recent success of CRISPR-Cas9 gene editing techniques in various bacterial backgrounds, the system was also implemented in *C. necator* H16. This system increased the efficiency and decreased time needed to edit the genomic DNA. Xiong *et al*. were the first to implement the method in *C. necator* H16, demonstrating inactivation of the 4 genes, H16_A1814, H16_A1334, H16_A1437 and H16_B0204. Interestingly, it was reported that it was not possible to delete one of these genes (H16_B0204) using traditional techniques, but the CRISPR-Cas9 method had a 95.7% editing efficiency. However, their approach had shortcomings as they were unable to demonstrate the ability to insert larger fragments of heterologous DNA, as 2 compatible plasmids are required, but were not available at the time of the study. As many biosynthetic pathways consist of multiple genes and are hence encoded by many kilobases of DNA, the full potential of the methodology has not fully been exploited by biotechnology researchers working on *C. necator* [42].

Integration of heterologous DNA into the host chromosome is seen as the best method for selection-free expression of biosynthetic pathways [43]. A popular site of integration is the *phaCAB* locus [28], [36], [44]–[46]. The *phaCAB* operon codes for proteins involved in polyhydroxyalkanoates (PHA) synthesis under conditions of carbon excess but limitation of nutrients, a major carbon sink pathway [28]. Deleting these genes whilst integrating those for heterologous pathways is hypothesized to

divert carbon bound for PHA into acetyl-CoA. This approach has been used to increase the production of fatty acids [28], alkanes [36] and other desired compounds. For this reason, it is considered a useful integration site and the carbon-flux rerouting is perceived as a further advantage. However, the number of genes that may be integrated at a single site and controlled by a single promoter will be limited. Expression of an organophosphohydrolase (OHA) gene, integrated multiple times into the chromosome of *C. necator* H16 greatly increased its production, without the appearance of inclusion bodies seen when this level of protein (4.3 g/L) was expressed in *E. coli* [47]. Bommareddy *et al*., expressed the biosynthetic pathway for 2,3-butanediol in *C. necator* by integration at the *phaCAB* locus. The work compared the titer from the integration strain to a comparable plasmid-based system and there was no difference in final product titer (1.8 vs. 1.9 g/L). However, when the genes for isopropanol were integrated at this site, the integrated strain had an increased final titer of 1.8 g/L compared to the plasmid based strain producing 2.7 g/L [46]. No work has been published on "neutral" integration sites in *C. necator*. Furthermore, there is no information on the consequences of integration at various sites on the transcription of the gene of interest. It has been shown that the insertion site can play a role in the expression levels and protein secretion in other organisms [43], [48].

1.2.2 Central carbon metabolism of *C. necator* H16

C. necator belong to the class *Betaproteobacteria* and the family *Burkholderiaceae*, within the order *Burkholderiales*. The genetic arrangement of *C. necator* is typical of free-living bacteria, for example it has a large number of regulatory genes, vital in a highly changeable habitat with variable carbon sources [7].

Early studies established heterotrophic growth on a large range of carbon sources, this being of interest to researchers in both academic and industrial settings. The bacteria are naturally able to use a range of organic acids, fatty acids and sugars. The utilisation pathways for a selection of common substrates can be seen in Figure 3 [49]. *C. necator* has a complete Entner-Doudoroff (ED) pathway (sometimes also referred to as 2-keto-3-deoxy-6-phosphogluconate (KDPG) pathway) to quickly utilise gluconate, fructose, and *N*-acetylglucosamine. However, these substrates are taken up by different transport mechanisms, suggesting independent control over assimilation [49]. No

complete EMP or oxidative pentose phosphate cycle pathway is found in this species, missing the phosphofructokinase and 6-phosphogluconate dehydrogenase enzymes required [7]. Strain development work has produced genetically modified strains of *C. necator* H16 that are able to metabolise previously unusable carbon sources such as glucose. Interestingly, only a single necessary gene is missing in order to transport and phosphorylate glucose, as glucose-6-phosphate is an intermediate in the established ED pathway. A UV-mutation generated glucose-utilising strain was found to have mutations in the *nag* operon and regulator genes that allowed the change in substrate specificity from GlcNac to glucose [21].

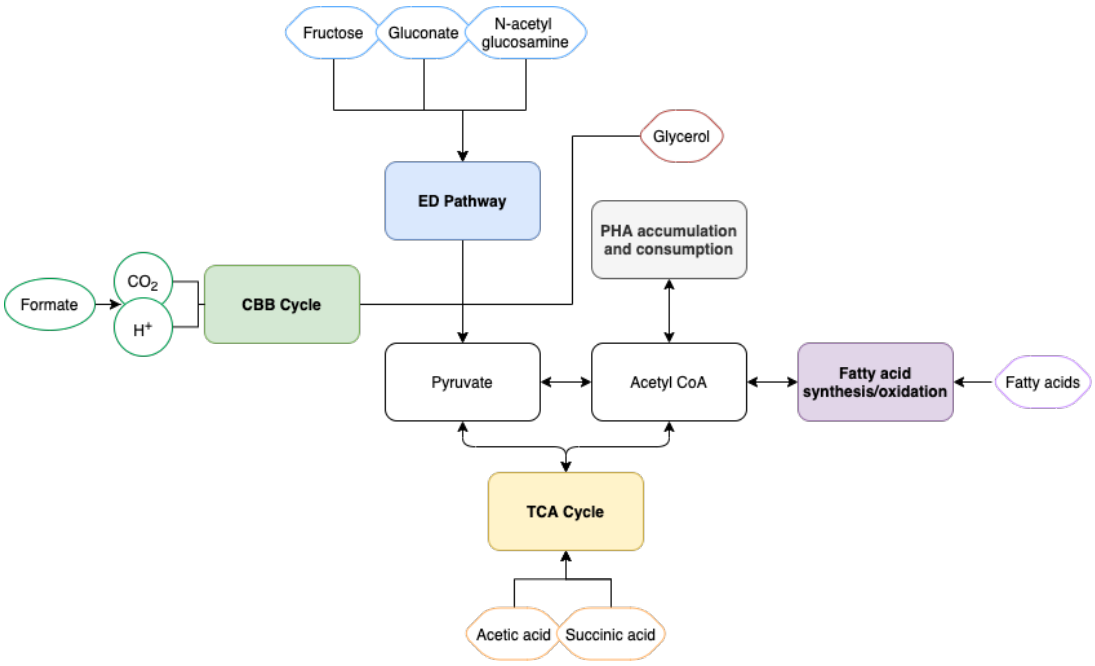

Figure 3 - Outline of the central carbon metabolism of *C. necator* H16. Information shown from Pohlmann *et al.* [7]. CBB = Calvin–Benson–Bassham cycle. ED = Entner-Doudoroff pathway. TCA = Tricarboxylic acid cycle

As previously stated, the ability to utilise hydrogen as an energy source was early identified in *C. necator*. The expression of oxygen tolerant [NiFe]-hydrogenases allows for H_2 oxidation in comparatively high oxygen concentrations, providing the energy required for carbon fixation [50]. The mechanisms by which these bacterial hydrogenases withstand oxygen toxicity are multifaceted, including limited access to the active site [29], [51]. Alongside this, CO_2 is assimilated as a sole carbon source by the Ribulose-1,5-bisphosphate carboxylase-oxygenase (Rubisco) enzyme, part of the Calvin-Benson-Bassham (CBB) cycle, the required reducing equivalents also being derived from hydrogen. The large gene clusters for autotrophic CO_2 fixation form 2

operons, one located on the chromosome and the other on self-transmissible megaplasmid, pHG1 [7]. However, the megaplasmid copy of the *cbb* operon lacks the gene encoding CbbB, formate dehydrogenase like protein [52]. Controlled by a LysR-type transcriptional regulator (CbbR) and modulated by a number of metabolites including phosphoenolpyruvate (PEP), the CBB pathway is tightly co-ordinated and both operons are simultaneously transcribed. Growth of *C. necator* has been demonstrated in fermenters supplied with a gas mixture of H_2, CO_2, and O_2 [53].

Although *C. necator* H16 is naturally unable to utilise carbon monoxide, the strain is insensitive to CO at the levels seen in industrial waste streams. By expressing the heterologous CO dehydrogenase encoded by the *cox* operon (originally from *Oligotropha carboxidovorans*), the bacteria can oxidise CO to CO_2, which can enter the CBB cycle [54]. This engineered strain allows for the possibility of using anthropogenic waste gases, such as those released from steel manufacturing, as cheap, clean carbon sources for *C. necator* [55].

1.2.3 Metabolism of aromatic compounds in *C. necator* H16

Although renowned for the ability to degrade aromatic compounds, *C. necator* can use a vast number of unconventional substrates. Utilisation of benzoate, phenol, and cresol (alongside many others) have all been demonstrated, converted *via* the key common intermediates protocatechuate and catechol, then entering the central metabolism *via* acetyl-CoA and succinyl-CoA [56]. From herbicides, such as 2,4-dichlorophenoxyacetic acid, to pharmaceutical precursors like phenylacetic acid, this bacterium has the potential for bioremediation efforts, as well as to provide vital experimental information on product inhibition in industrial settings [57].

1.2.4 Metabolism of other compounds in *C. necator* H16

Due to the varied metabolism genes in *C. necator*, many studies have been performed, growing the bacteria on non-traditional carbon sources in order to understand bioremediation abilities, or elucidate more information on the metabolism.

For example, Sharma *et al.* demonstrated growth on biodiesel by-product substrates, containing varying amounts of glycerol and fatty acids, although cell dry weight (CDW) and PHA accumulation were decreased [58]. In. *C. necator* H16, the growth rate on glycerol is 11.4 times slower than on the preferred substrate gluconate [59]. Glycerol is transported by an ATP-binding cassette (ABC) transporter (GlpV) or by another glycerol transport protein (GlpF). The internalised glycerol is phosphorylated by glycerol kinase (GlpK) to glycerol-3-phosphate, then to dihydroxyacetone-phosphate (DHAP). The conversion of glycerol-3-phosphate is catalysed by the glycerol-3-phosphate dehydrogenases GlpA and GspA. DHAP is further metabolised to PEP, entering central metabolism, or gluconeogenesis [58]. Utilisation of glycerol by *C. necator* H16 wild type is inefficient, but has been improved by overexpressing the genes of aquaglyceroporin (*glpF*) and glycerol kinase (*glpK*) from *E. coli* [60].

González-Villanueva *et al*., [59] established a strain that can co-utilize gluconate and glycerol. In particular, the growth rate on glycerol was increased over 9-fold, and even co-utilisation of gluconate and glycerol was faster. This strain was achieved by laboratory directed evolution experiments, but genome sequencing showed that in particular, mutations in the glycerol kinase gene (*glpK)* were responsible for the improvement. Interestingly, the adapted strain showed reduced growth rate and increase lag phase on fructose and *N*-acetylglucosamine [59].

Experiments on crude bottom glycerol by Sharma *et al.* also showed that fatty acids in the mixture were also degraded by *C. necator* H16 [58]. Breakdown of fatty acids by the beta-oxidation pathway was explored by Brigham *et al*., [57] using trioleate, a model plant oil composed of three fatty acids joined to a glycerol backbone. Expression studies showed 2 upregulated fatty acid β-oxidation operons, each containing all the necessary genes, except *fadD* which is located separately. The fatty acid is first ligated to CoA, catalysed by FadD, to form acyl-CoA. The enzyme encoded by *fadE* (an acyl-CoA dehydrogenase) converts the acyl-CoA to enoyl-CoA, which is then further changed to 3-hydroxyacyl-CoA by FadB. The same enzyme converts 3-hydroxyacyl-CoA to 3-ketoacyl-CoA. The final stage of β-oxidation involves the FadA catalysed cleavage of 3-ketoacyl-CoA to release an acetyl-CoA and produce a shorter-length fatty acyl-CoA, which can re-enter the cycle [57].

Degradation of the PHA bioplastics in the environment is catalysed by extracellular PHA polymerases, secreted into the environment by microorganisms such as *Acidovorax* sp., *Aspergillus* sp., and *Pseudomonas* sp. [61]. In *C. necator*, PHAs are stored as membrane bound inclusions and are degraded by intracellular PHA-depolymerases [61]. This occurs when carbon sources are scarce Multiple homologues of these enzymes (PhaZs) are found in *C. necator*, but particular, PhaZ1 has been shown to be involved in degradation of PHAs. When *phaZ1* was deleted, lower PHA assimilation was seen [62]. After depolymerisation, the monomeric units enter central carbon metabolism, *via* acetyl-CoA, providing the energy and carbon required to sustain the cell [61].

In *C. necator* H16, experiments found 3-hydroxypropionic acid (3-HP) was also assimilated and used as a carbon source, in a similar way to P*seudomonas denitrificans* [63][64]. Degradation takes place *via* the oxidative pathway, which converts 3-HP to malonate semialdehyde and then to acetyl-CoA. The enzyme responsible for the breakdown of 3-HP to malonate semialdehyde is 3-hydroxypropionate dehydrogenase (HpdH). However, deletion of the HpdH encoding gene in *C. necator* H16 only resulted in delayed consumption of 3-HP [63].

Zhou *et al.* [65] investigating 11 species of bacteria that can use 3-HP as a sole carbon source showed that another gene called (methyl)malonate-semialdehyde dehydrogenase (*mmsA*) was also involved in 3-HP catabolism [66]. This is also the case in *C. necator* H16, where 3 copies of *mmsA* genes have been identified. Their gene products are responsible for the second step of 3-HP breakdown, catalysing the conversion of malonate semialdehyde to acetyl-CoA [65]. Arenas-Lopez *et al.* clarified the degradation pathway of the carboxylic acid 3-hydroxpropionic acid in *C. necator*. As well as creating a strain that no longer degrades 3-HP, the work provided interesting insight into the assimilation pathways for β-alanine, valine and 3-hydroxyisobutyrate. By deleting the 3 homologous, but separately regulated, *mmsA* genes it was possible to stop the degradation of malonate semialdehyde to acetyl-CoA, before entering central carbon metabolism [63].

The substrate range for *C. necator* H16 has been expanded by introducing heterologous genes. For example, in order to utilise mannose, a sugar that is found in the polymerised form in lignocellulosic biomass, non-native enzymes must be employed as no native degradation pathway is present. Sichwart *et al.,* [49] achieved this by introducing a number of genes from *Zymomonas mobilis* and *E. coli*. These genes encoded a glucose-facilitated diffusion transporter (Glf) that transports the mannose, which is then phosphorylated in an ATP-dependent manner by a mannofructokinase (Mak). The final enzyme, a phosphomannose isomerase (Pmi), converts mannose-6-phosphate to fructose-6-phosphate that can enter the ED pathway. As mannose can be a major component of the hemicellulose, a heteropolymer that makes up 11-50% of lignocellulosic biomass [67], this advancement is a step closer to utilising lignocellulose as a sustainable feedstock for commodity chemical production in *C. necator*.

1.2.5 Polymer Production in *C. necator*

In order to combat the effects of changing carbon availability, *C. necator* stores intracellular granules of PHA, like a number of other organisms evolved in a nutritionally unstable environment [68]. These collected granules are easily stained and visible using confocal fluorescence microscopy (Figure 4). Signals produced under nutrient limited conditions cause PHA synthesis when carbon levels are high, but other vital elements like nitrogen or phosphorus are scarce [69].

A

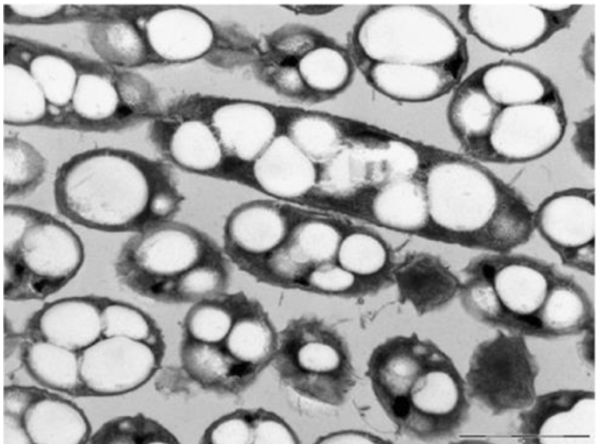

B

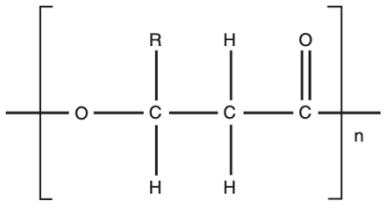

Figure 4 – (A) Transmission electron micrograph showing PHA accumulation in *C. necator* H16 [65]. (B) The general structure of PHB [85]

There are 8 known pathways to generate the hydroxyacyl-CoA precursors for PHA synthesis and the acetyl-CoA dependent pathway present in *C. necator* is the best studied [70]. Two acetyl-CoA molecules are converted to acetoacetyl-CoA by the enzyme β-ketothiolase (PhaA). Acetoacetyl-CoA dehydrogenase PhaB reduces acetoacetyl-CoA into (*R*)-3-hydroxybutyryl-CoA (3HB-CoA) in an NADPH-dependent reaction. Lastly, the PHB synthase (encoded by *phaC*) polymerises the 3HB-CoA monomers into the PHB polymer, structure seen in Figure 4A [71].

The promising applications of the naturally accumulated PHAs have not gone unnoticed. These biopolymers are well known for their biological degradability and their potential to disrupt the fossil-fuel derived plastics industry [72]. The best known of the PHAs is the polymer of 3-hydroxybutyrate (PHB), previously manufactured by Biopol [73]. The molecular weight and compositions of the biogenic PHAs can be varied, resulting in plastics with diverse qualities and applications. Hydroxyvalerate and hydroxypropionate are both monomers that can be incorporated into the bioplastic to tailor the composition and therefore the chemical, thermal, and mechanical properties [72].

The resulting plastics can be biocompatible, making them suitable for uses in implantable devices, cartilage scaffolds and drug encapsulation formulas. These high-value, specialist products are necessary in order for bioderived PHAs to be cost effective [74]. However, there is now a drive towards alternative plastics, due to issues of environmental damage and reliance on fossil fuels. The PHA industry is estimated to grow 11.8% between 2019 and 2024, largely due to the production of food packaging [75].

The greatest benefit of bacterial derived PHAs is the avoidance of the petrochemical industry, with rapidly depleting oil reserves and unpredictable market prices. Furthermore, the energy requirement for bio-based polymers is calculated to be significantly less than those from petroleum supplies. However, these polymers also have the potential to lessen the future addition of plastics to the environment, as they are completely compostable and biodegrade in all aerobic and anaerobic environments [76]. PHAs created in *C. necator* were found to have a high weight-average molecular

mass and exhibited the best thermal stability compared to microbially synthesised PHAs from *Burkholderia cepacia*, using soy bean as a substrate [77].

C. necator is considered a model organism for PHB production, therefore this topic has been explored extensively. Biosynthesis of the bioplastic has been demonstrated from a range of carbon substrate. For example, using syngas (10% CO_2, 75% H_2, 15% O_2), 42.9 g/L PHB was produced in the native *C. necator* H16 strain [78]. PHB has also been synthesised from several different waste streams, including cheese whey and waste frying oil [62], [79]. Several further examples are outlined in Table 1. A comprehensive list of PHB production attempts from waste materials (with titre and productivity rates) is listed by Sohn *et al.* [80].

Metabolic engineering of *C. necator* H16 has allowed for a wider range of substrates to be consumed and producing a wider range of bioplastics to be synthesised. In a glucose-utilising *C. necator* mutant strain, 76% of the dry cell weight was PHB, and the productivity was 2.42 g/L/h, ideal for industrial fermentation of bioplastics [81]. The biosynthesis of co-polymers has been published, using a combination of overexpression of heterologous genes from *C. aurantiacus*, resulting in compounds such as poly(3HB-co-3HP) [82]. Furthermore, recent work by McGregor showed that poly-3HP can be produced, with varying percentages of 3-HP in *C. necator* from β-alanine [83].

Table 1 - Further details of PHB production by native *C. necator* H16 strains on multiple carbon sources

Carbon Source	**Titre (g/L)**	**Productivity (g/L/h)**	**Yield (g/g)**	**Reference**
Fructose	25.7	0.43	-	[84]
CO_2	22	0.314	-	[85]
Molasses	0.78	-	-	[86]
Jatropha oil	15.5	-	0.99	[87]
Waste frying oil	0.62	-	-	[79]
Waste glycerol	0.93	-	-	[58]
Free fatty acids	4.83	-	-	

1.2.6 Commodity chemical production in *C. necator*

With the wide substrate usage, adaptable metabolism and a vast array of genetic tools now available, *C. necator* is considered an attractive industrial chassis [46]. Many articles have been published showing the production of a large range of commodity chemicals and important precursors (other than PHA), with key examples shown in Table 2.

Although the titer and/or productivity from $CO_2/H_2/O_2$ is low in this species, it demonstrates that complex, highly sought-after compounds can be produced from renewable carbon sources. Currently, the metabolism of the organism is not sufficiently understood to be able to divert carbon flux into heterologous pathways and non-native products.

Table 2 - A selection of commodity chemicals previously reported as being synthesised in *C. necator* H16

Product(s)	**Carbon source**	**Strain development**	**Titres and/or productivity achieved**	**Reference**
Acetoin	CO_2	Deletion of *acoABC* and *phaC*	"> 100% carbon efficiency"	[88]
Alkanes	CO_2	Deletion of *phaCAB*	435 mg/L	[36]
Isopropanol	Fructose	-	9.8 g/l	[89]
Fatty acids	Rich media	Deletion of *fadD3*, *H16_A0285* and *H16_A2794*	62 mg/L	[28]
Methyl ketones	Fructose	Deletion of β-oxidation genes (H16_A1526-1531) and *phaCAB*	65 mg/L	[44]
	CO_2		Up to 180 mg/L	
Isobutanol and 3-methyl-1-	CO_2	Deletion of *phaCAB*	1.4 g/l (~846 mg/L isobutanol and ~570 mg/L 3MB)	[90]

butanol (3MB)	Fructose		30 mg/L/h, 14 g/L final titer	[22]
Lipochitooligo-saccharides (LCOs)	CO_2	Deletion of *phaC*	1.4 mg/L	[91]
Isotope-labelled arginine	CO_2	Deletion of *phaC*	500 mg/L	[33]
2,3-Butanediol	Fructose	Deletion of *acoABC* and *phaC*	1.9 g/L	[46]
	CO_2		32 g/L	
Isopropanol	Fructose	Deletion of *phaC*	2.7 g/L	
	CO_2		7.7 g/L	

1.3 3-Hydroxypropionic acid

3-hydroxypropionic acid (also known as 3-hydroxypropionate, 3-hydroxypropanoic acid, 3-HPA and 3-HP) is a 3-carbon, optically inactive precursor to many sought after compounds [92]. The global market for 3-HP-derived compounds is worth over $1 billion [92]. Due to unsatisfactory chemical methods for its production, it has become a noteworthy target for biological manufacture. It is a structural isomer of lactic acid and has bifunctionality due to the presence of an alcohol group and a carboxylic acid group. The presence of two functional groups allows oxidation, reduction and polymerisation of 3-HP into a wide range of industrial chemicals, seen in Figure 5 [93]. For example, 3-HP can be reduced to 1,3-propandiol used in the production of polyesters, or oxidised to malonic acid, an intermediate in the synthesis of vitamins B_1 and B_6 and other pharmaceuticals. The dehydration of 3-HP to acrylic acid has been seen as renewable way to alleviate the environment issues caused by the traditional petrochemical method of making acrylic acid from propylene [94]. A promising 3-HP product results from a polymerisation reaction, creating poly-3HP, a biodegradable, biocompatible plastic [95].

As a valuable platform compound, chemical production methods have been researched for many years, but with little success. Aqueous 3-HP is currently created from β-propiolactone by hydrolysis with alkali and acid catalysts. However, this method is considered extremely dangerous as β-propiolactone is mutagenic and carcinogenic [96]–[98]. Safer routes for 3-HP production, such as hydration of acrylic acid, still have environmental concerns and economic viability is impeded by the increasing cost of acrylic acid [93], [99]. Other methods are not viable for scale up to industrial proportions, such as the synthesis of 3-HP from ethylene chlorohydrine *via* β-hydroxypropionitrile. This process uses harmful reagents such as sodium cyanide limiting the real-life uses [94]. Another method requires a rare, unsustainable metal catalyst such as palladium to oxidise 1.3-propandiol to 3-HP [100] More recently, a method to oxidise allyl alcohol (2-propene-1-ol) to 3-HP using a gold catalyst were proposed. The conditions required were mild (50^{o}C), but other compounds, such as glyceric acid, acrylic acid and glycerol were co-produced [101]. Furthermore, gold catalysts can have issues regarding stability and cost that prevent them from being used industrially [102]. In response to increasing environmental concerns about climate change, fossil fuel reliance and ecological impact, the traditional chemical production of 3-HP has been limited [103]. New methods have been proposed, such as using gold as a catalyst with allyl alcohol. However, the selectivity of the gold catalyst dropped dramatically when the catalyst was recycled [93]. An efficient method of converting levulinic acid to 3-HP with hydrogen peroxide has been suggested, but has yet to reach industrial viability [104].

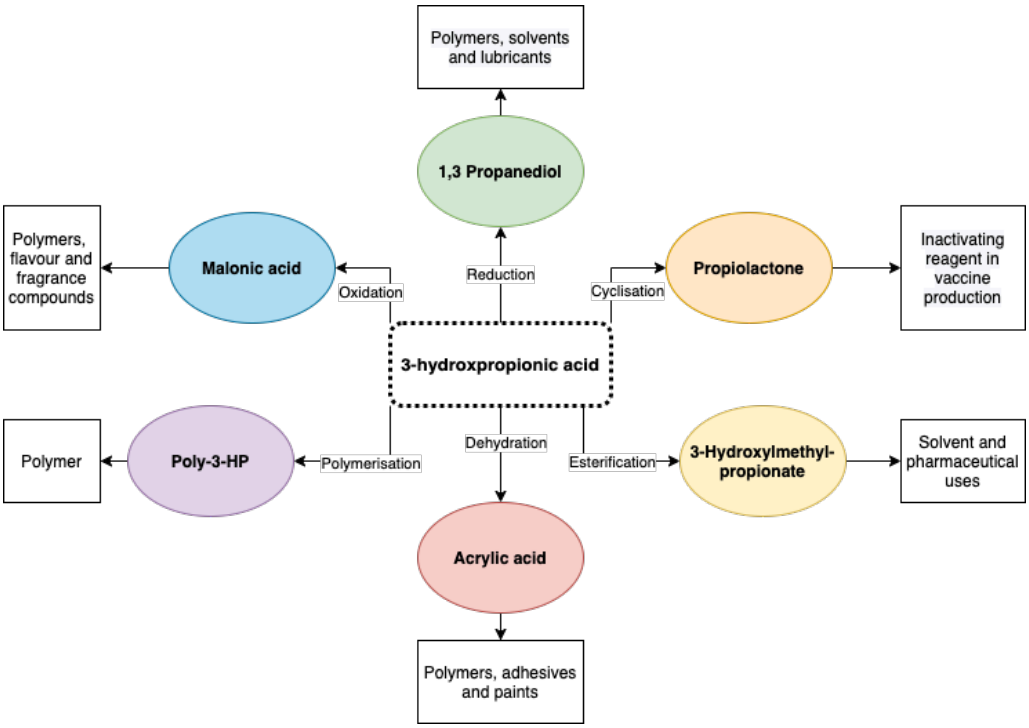

Figure 5 - Possible industrial and pharmaceutical uses for 3-HP. The reaction used to attain the final product is indicated on the arrows. Collated and modified from references [3], [76], [105]

1.3.1 Microbial synthesis of 3-HP

Biological synthesis has been touted as the choice alternative, with 3-HP produced at commercial scale within the next few years without the need of fossil-fuel derived substrates [3]. Promising results have been published in both prokaryotic and eukaryotic host organisms, using a range of carbon feedstocks [105]. Referred to as a "central component in a network of several high volume biorefinery products", 3-HP was in the top ten sugar-derived building blocks reported by the US Office of Energy Efficiency and Renewable Energy. This report outlined the need for the product, the current status and the major elements of improvement. Furthermore, it outlined the problems and challenges associated with biosynthesis in microorganisms (Figure 6) [106]. Despite publication in 2004, the industrial success of biogenic 3-HP has not emerged as predicted, and the need for sustainable commodity chemicals has increased.

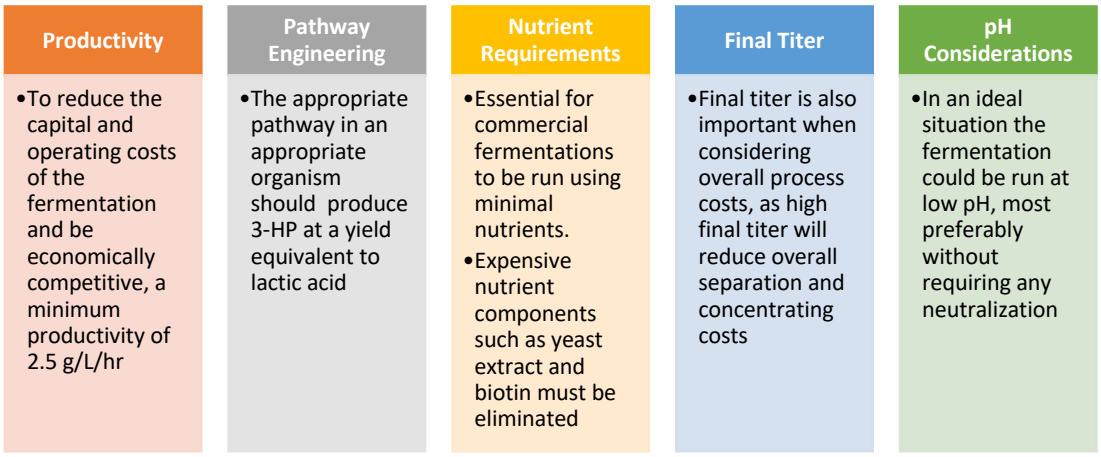

Figure 6 – The challenges to overcome for industrial production of 3-HP using microorganisms. Modified from Werpy and Peterson [106]

Table 3 outlines several examples of 3-HP biosynthesis. Traditionally a titre of 50-100 g/L is considered desirable for commercial processing of 3-HP [107]. Chu *et al.* [108] achieved an impressive titre of 71.9 g/L 3-HP using metabolically engineered *E. coli* grown in media (with concentrated glycerol added to maintain the concentration at 80 g/L). Still, the productivity of 1.8 g/L/h was not considered adequate [108]. In *Klebsiella pneumoniae*, titres of 83.8 g/L, equalling a 54% glycerol conversion rate, have been accomplished. Once again, the productivity in this organism was unsatisfactory [109].

Overall, production of 3-HP from sugars such as glucose has yielded disappointing results. In *Saccharomyces cerevisiae*, only 13.7 g/L 3-HP was achievable, well below the desirable titre. An exception to this was published by Chen *et al.* using *C. glutamicum* fed on glucose: 62.6 g/L 3-HP was produced with a productivity of 1.2 g/L/h [110]. Unfortunately, these plant-derived feedstocks can lead to direct and indirect land use change, reducing biodiversity and decreasing food availability [5].

An alternative, highly-sustainable carbon source would be the use of CO_2, simultaneously decreasing harmful emissions and producing industrially-desirable platform chemicals [6]. Compatibility with current fermentation infrastructure, downstream processing and yield requirements need to be examined when considering 3-HP produced from CO_2, as these constraints have limited commercial implementation thus far [111]. Direct photosynthetic conversion of CO_2 to 3-HP has

been achieved in *Synechococcus elongatus*, a cyanobacterium. In this organism, both malonyl-CoA and the β-alanine pathways (Figure 7) were implemented. However, the titer and productivity of engineered strains (659 mg/L and 102 mg/L/d respectively) were very low. A production titer of over 500 mg/L is uncommon in cyanobacteria, and general low tolerance levels for the acid has limited the economically viable implementation of photobiosynthetic 3-HP [112].

Table 3 – Examples of biosynthesis of 3-HP in microorganisms

Pathway	Species	Carbon source	Titres (g/L)	Productivity (g/L/h)	Yield (g/g)	Reference
Malonyl CoA	*E. coli*	Glucose	40.6	-	0.19	[113]
	Schizosaccharomyces pombe	Cellobiose	11.4	-	0.11	[114]
	Synechococcus elongatus	CO_2	0.665	-	-	[112]
β-alanine	*E. coli*	Glucose	31.1	-	0.423	[115]
	S. cerevisae	Glucose	13.7	0.17	-	[116]
Glycerol	*E. coli*	Glycerol	71.9	1.8	-	[108]
	K. pneumoniae	Glycerol	83.8	1.53	-	[109]
	B. subtilis	Glycerol and glucose	10		-	[117]

1.3.2 Biological routes to produce 3-hydroypropionic acid

Many main routes for biological production of 3-HP have been proposed and shown to be attainable in a range of species of bacteria and yeast. The suggested starting substrates were glycerol and glucose due to their availability and well-studied metabolic pathways [105].

Glycerol is considered a cheap, safe and sustainable substrate for biologically producing 3-HP, as it is a by-product of biodiesel production [92], [118]. There are

two possible pathways from glycerol, the CoA-dependent and CoA-independent routes. In both pathways, a glycerol dehydratase (DhaB) catalyses the conversion of glycerol to 3-hydroxypropanal. However, 3-hydroxypropanal can become toxic upon accumulation, meaning downstream enzymatic activity must be in excess to convert the metabolite before it causes metabolic impairment [119].

The CoA-dependent route is naturally found in *Lactobacillus* species. In this pathway, 3-hydroxypropanal is converted to 3-hydroxypropanoyl-CoA, using a CoA-dependent propionaldehyde dehydrogenase. This compound is then transformed to 3-hydroxypropanoyl-phosphate, catalysed by a phosphotransacylase (PduL). Finally, an ATP-driven 3-hydroxypropionate kinase catalyses the reaction to 3-HP [120]. The CoA-independent route requires only one extra step from 3-hydroxypropanal, using an aldehyde dehydrogenase (ALDH) to convert it to 3-HP. This pathway is more commonly used for 3-HP production in bacteria but it has been observed that a high expression of ALDH can be a burden on the host strain [92], [119].

Generally, the first step in both pathways uses a coenzyme B_{12}-dependent glycerol dehydratase reaction. This is an issue for host strains not naturally capable of producing coenzyme B_{12}. One solution would be to engineer bacteria to generate B_{12}, but this is a highly challenging task given that the pathway requires very large number of genes organised over 6 *cob* operons [121]. Nonetheless, the genes coding for synthesis of coenzyme B_{12} from *Ps. denitrificans* have been expressed in non-native strains, such as *E. coli*. Glycerol dehydratase enzymes have been found that can complete this first step (converting glycerol to 3-hydroxypropanal) independent of coenzyme B_{12}, but they are sensitive to oxygen and the reaction must take place under microaerophilic or anaerobic conditions, limiting the number of appropriate host strains. Furthermore, many glycerol dehydratases can be deactivated by the presence of glycerol [120]. These enzymes must be reactivated by glycerol dehydratase reactivases, which also must be present in heterologous hosts [92]. Despite these difficulties, yields of up to 83.8 g/L have been seen in other better-suited organisms engineered to overcome the discussed issues [109].

1.3.3 3-HP from sugars

More recently, seven routes to produce 3-HP from glucose have been patented by Cargill and reviewed by Kumar, each proceeding *via* pyruvate or PEP [122], [123] and they are outlined in Figure 7. These pathways are of most interest because the starting sugar/substrate can be varied. However, the introduced biosynthetic pathways will be competing for pyruvate (and other intermediates) reserved for native processes. Four of the proposed seven pathways are regarded unfavourable (either thermodynamically or because they are energy inefficient due to considerable ATP input). The 3 pathways that are considered as potential routes to 3-HP proceed *via* malonyl-CoA (1), β-alanine (2) and α-alanine (3) [123].

1.3.4 Routes to 3-HP *via* β-alanine

The path to 3-HP *via* β-alanine (pathway 2 in Figure 7) is often considered to be the most attractive biosynthesis routes, and one has been patented by Novozymes [124]. There are a low number of enzymes involved and the reactions are thermodynamically favourable overall, consuming no ATP. Theoretically, this route gives the highest possible yield of 3-HP from glucose [125]. The biosynthesis starts with the formation of the amino acid β-alanine (3-aminopropionic acid), a product of the decarboxylation of L-aspartate. This molecule is a precursor to vitamin B_5 (pantothenic acid), and hence a precursor of coenzyme A (CoA) [126]. The β-alanine is converted into malonic semialdehyde (3-oxopropanoate), using one of the two enzymes known to catalyse this reaction; β-alanine-pyruvate aminotransferase (BAPAT) or γ-aminobutyrate transaminase (GABT) [116]. The malonic semialdehyde can then be converted to 3-HP, catalysed by a hydroxypropionate dehydrogenase (HPDH), e.g. the gene product of $ydfG_{Ec}$ from *E. coli* [127].

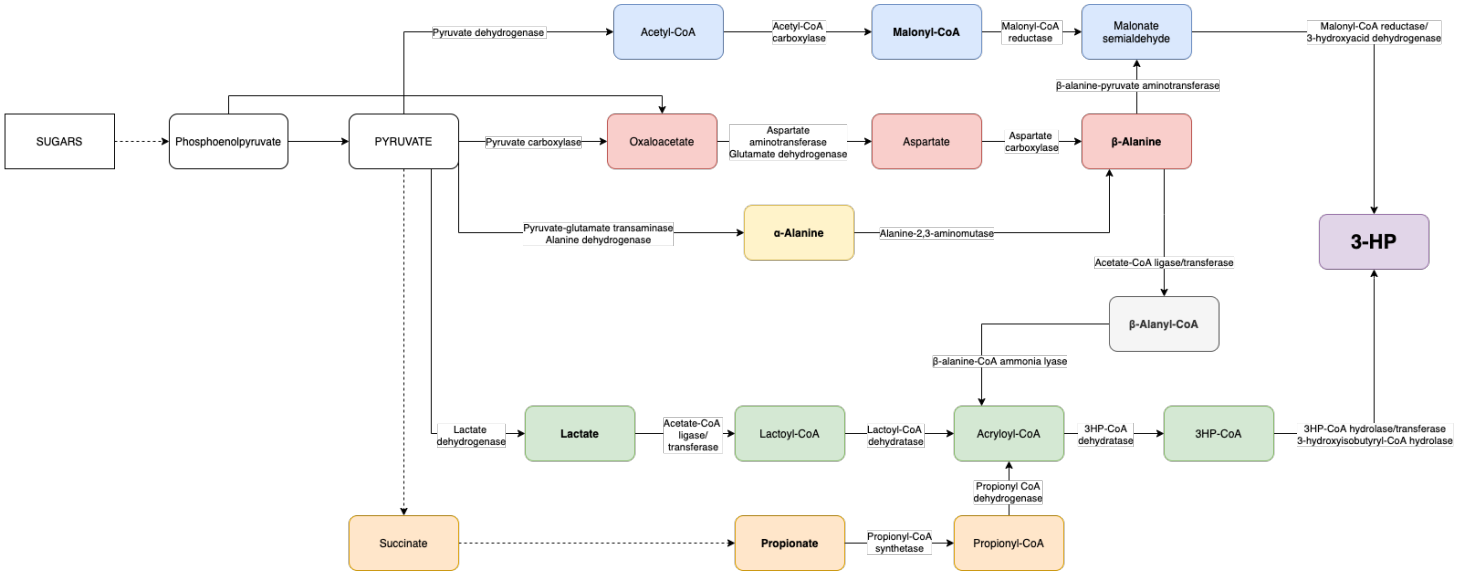

	Pathway		Net ATP Yield* per 3HP	Thermodynamically favourable?	Cofactors required	Benefits	Disadvantages
1	**Malonyl-CoA**		0	Yes	NADH, NADPH, ATP, biotin, CoA	Redox neutral Short pathway Most successful in experimental data	Competition for malonyl-CoA from vital pathways such as fatty acid synthesis Expression of malonyl-CoA reductase subunits must be balanced Cost and delivery of cofactors needs to be considered Tight regulation of acetyl-CoA carboxylases
2	**β-Alanine**		0 or 1 (depending on PEP carboxylase or kinase used)	Yes	NADH, NADPH, ATP	Can give a postive ATP yield Short pathway	No need to add expensive cofactors Difficulty linking to central metabolism
3	**α-Alanine**	via β-Alanyl-CoA	0	No	NADH, NADPH, ATP, B12	Addresses the lack of ATP production in β-alanine pathway as energy consuming steps are bypassed	Conversion of α-alanine to β-alanine is rate limiting step B12 required
		via malonate semialdehyde	1	Yes			
4	**β-Alanyl-CoA**		0 or −1 (depending on acetate-CoA ligase or transferase used)	No	NADH, NADPH, ATP, CoA	Alternative of α-alanine and β-alanine pathways, avoiding toxic malonate semialdehyde	Not thermodynamically favourable and has no postive ATP yield
5	**Lactate**		0 or 1 (depending on acetate-CoA ligase or transferase used)	No	NADH, ATP, CoA	Can give positive ATP yield	Difficult separation of the lactate and 3-HP in the downstream process
6	**Propionate**		-0.33 or -1 (depending on	No	NADH, ATP, CoA	Good for strains that have enhanced propionic acid fermentation	Net consumption of ATP

* based upon 2 ATP molecules produced from glycolysis to pyruvate

Figure 7 - Biosynthesis of 3-HP by various routes outlined in patent by Cargill. Modified from Kumar *et al.* [105] with further data from Matsakas *et al* [92], Jiang *et al.* [123] and Lui *et al.* [139]

This pathway has been explored experimentally and shown to work in model organisms *S. cerevisiae* [116] and *E. coli* [115]. In yeast, the titre and productivity peaked at 13.7 g/L and 0.17 g/L/h, respectively [116]. The efficiency could be improved by using a fed-batch cultivation, increasing the overall yield of C-mol/C-mol glucose from 14% to 29%. However, productivity remained low overall [128]. Using *E. coli* as a host strain was more successful, with a comparable fed-batch cultivation producing 31.1 g/L of 3-HP [115]. Furthermore, aspartate is a precursor in the generation of several amino acids and is itself required for protein synthesis, creating competition for the substrate [129] Further work must be done to improve the carbon and nitrogen flux towards aspartate [116].

The alternative pathway through α-alanine (pathway 3 in Figure 2) has the advantage of avoiding aforementioned issues with the use of aspartate. However, there are no naturally occurring aminomutase enzymes that specifically interconvert α-alanine to β-alanine. Research has shown that lysine 2,3-aminomutase (2,3-LAM) which has a broad substrate range, can complete this reaction but requires further enzyme engineering [130].

Producing 3-HP by the β-alanine pathways in *C. necator* has previously been explored within the research group. A plasmid harbouring the genes encoding a BAPAT from *Chromobacterium violaceum* and $YdfG_{Ec}$ from *E. coli* were inserted into a non-3-HP degrading strain of *C. necator.* This allowed the bacteria to convert β-alanine to 3-HP. From cultures grown in SG-MM supplemented with 50 mM β-alanine, 40 mM 3-HP was detected [131]. However, no successful attempt at producing the precursor β-alanine from central carbon metabolism *via* aspartate (or α-alanine) has been published in *C. necator*.

Other work in our laboratory showed that the 3-HP produced from β-alanine can be incorporated into the PHAs produced by *C. necator*. The genes for 3-HP production enzymes (BAPAT and *YdfGEc*) were overexpressed alongside genes encoding PhaC (PHA synthase) from *Chromobacterium* sp. USM2 and the native Pct (propionate CoA-transferase). This plasmid-based system allowed for accumulation of 80% poly-3HP (as percentage of all PHAs produced), from media containing 50 mM β-alanine [83]. Currently, other researchers in the laboratory are working on linking the 3-HP

production to the central carbon metabolism, allowing for production without the addition of β-alanine, making the process more economically viable.

1.3.5 Malonyl-CoA pathway to 3-HP

Some bacteria and archaea are native producers of 3-HP as part of their CO_2 assimilation pathway which proceeds *via* the Fuchs-Holo bicycle or the 3-hydroxypropionate/4-hydroxybutyrate cycle [132]. The Fuchs-Holo bicycle, also known as the 3-HP bicycle, is a sequence of reactions starting with acetyl-CoA, which is carboxylated to malonyl-CoA in an ATP and biotin-dependent reaction by an acetyl-CoA carboxylase (ACC) enzyme, using bicarbonate as a CO_2 donor. This is followed by the NADPH-dependent conversion of malonyl-CoA to 3-HP by a malonyl-CoA reductase (MCR) [133]. 3-HP is further converted in numerous enzymatic steps to regenerate acetyl-CoA. The 3-HP cycle has the same energy efficiency as the CBB cycle, using ~2.3 mol ATP/mol CO_2 to produce pyruvate [134].

A synthetic version of the 2-step reaction sequence from acetyl-CoA to 3-HP, also known as the malonyl-CoA pathway (Figure 8), has been proven to be feasible and implemented in in *E. coli*, *S. cerevisiae* and cyanobacteria [135].

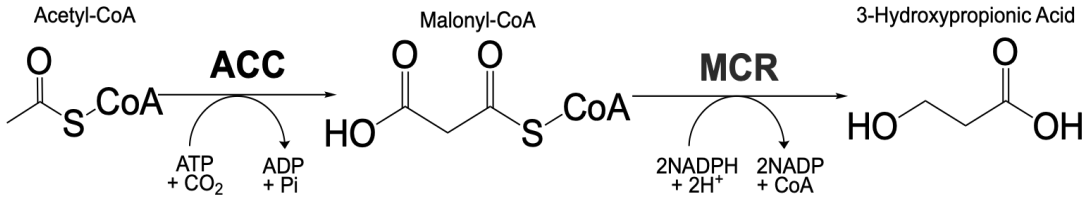

Figure 8 – The simplified malonyl-CoA pathway from acetyl-CoA to 3-HP, as first proposed by Berg *et al,*. [132]. ACC = acetyl-CoA carboxylase, converts acetyl-CoA to malonyl-CoA in an ATP-dependent manner. MCR = malonyl-CoA reductase, catalyses the reaction of malonyl-CoA to 3-HP, requiring NADPH

As outlined above, the first reaction of the malonyl-CoA pathway is the conversion of acetyl-CoA (a central metabolite in intermediary metabolism) into malonyl-CoA, catalysed by an acetyl-CoA carboxylase (ACC). In eukaryotes, the enzyme consists of a single, multi domain protein [136]. Conversely, in prokaryotes it consists of up to 4 separate subunits (commonly *accA*, *accD*, *accB* and *accC*), all encoded by the *acc* operon. The main role of this enzyme in most organisms lies in fatty acid biosynthesis, where malonyl-CoA provides the acetyl-moiety used for chain elongation.

Rathnasingh *et al.,* [137] were the first to show 3-HP production from central carbon metabolism, *via* acetyl-CoA and malonyl-CoA. To achieve this the native *acc* operon was overexpressed in *E. coli,* in addition to *mcr* from *Chloroflexus aurantiacus*. The overexpression of the genes of the ACC operon increased the titer two-fold from 0.71 mmol/L to 1.6 mmol/L of 3-HP. With strain engineering and further pathway design, the final titre was 2.14 mM [137].

The same genes were used by Wang *et al*., for the production of 3-HP, that was then polymerised to poly-3HP using PhaC from *C. necator* and the native PrpE. However, cell yield was low (1.32 g/L) and only very little of this was poly-3HP (0.98% of cell dry weight) [138].

It was further found that utilising the *acc* operon from *Corynebacterium glutamicum* significantly improved the titer of 3-HP in *E. coli* [139]. This was likely due to greater malonyl-CoA availability, as overexpression of the *acc* operon increased malonyl-CoA concentration from 0.01% to 17.7 % of the total CoA metabolite pool [140] . It was hypothesized that the change in the operon structure and/or lack of feedback mechanism was responsible for higher malonyl-CoA pool [141]. However, cell viability was reduced, possibly due to toxic intermediates [142]

The catalytic mechanism of the ACC enzyme has been well studied. Firstly, ATP and bicarbonate are used to carboxylate biotin. The carboxyl group is then transferred from carboxybiotin onto acetyl-CoA to give malonyl-CoA [143]. This reaction is energetically unfavourable and hence coupled to ATP hydrolysis [137]. Furthermore, often it is necessary to add supplementary biotin to the fermentation medium, which can increase the production cost dramatically [139], [144], [145]. However, these issues can be overcome using the right chassis organism that naturally produces biotin.

Malonyl-CoA reductase is a bifunctional enzyme, a natural fusion of an aldehyde dehydrogenase domain (MCR-N) and an alcohol dehydrogenase domain (MCR-C). The 135-145 kDa, NADPH-dependent protein catalyses the reduction of malonyl-CoA to malonate semialdehyde and finally to 3-HP. The most studied MCR is found in *C. aurantiacus* and has been used in most of the assembled synthetic malonyl-CoA

pathways across a range of organisms. For example, the encoding gene has been inserted into recombinant *E. coli* strains, enabling them to produce 2.14 mM of 3-HP [137]. However, MCR homologues are also found in several other organisms that can photosynthesise anoxygenically and are capable of fixing carbon *via* the Fuchs-Holo cycle [146].

The concept of using the MCR from *C. aurantiacus* DSM 635 to catalyse the reaction of malonyl-CoA to 3-HP has been demonstrated in *C. necator* by Fukui *et al.* [35] and resulted in the production of the copolymer poly((R)-3-hydroxybutyrate-co-3-hydroxypropionate) (P(3HB-co-3HP)), with a 3-HP fraction of 0.2-2.1 mol %. This was achieved by expressing the genes for MCR and the N-terminal acyl-CoA synthetase domain of the propionyl-CoA synthase from *C. aurantiacus* (acs_{Ca}) that lead to the generation of 3-HP-CoA and its subsequent incorporation into the copolymer. In the Fukui study, no accumulation of monomeric 3-HP was reported [35]. Previous work has shown the MCR protein to have activity in *C. necator* [24]. The activity of 4 MCR candidates was measured at 30°C using a spectrophotometric assay, monitoring the oxidation of NADPH. The MCR from *C. aurantiacus* was found to have the highest specific activity of 0.01 +/- 0.001 µmol/min/mg [24]. This was somewhat lower than seen in other literature for the same enzyme produced in *E. coli* (11.6 µmol/min/mg), but the latter values were obtained at 55°C, rather than a physiological temperature that is more relevant to *C. necator* [133].

1.4 Proposed pathways to 3-HP in *C. necator*

Previous work published alongside Arenas-López *et al.* [63] resulted in the creation of a *C. necator* strain that does not metabolise 3-HP as a carbon source. This was achieved by the deletion of the 3 (methyl)malonyl-CoA semialdehyde dehydrogenase encoding genes. The work performed to construct this *C. necator* strain (termed H16 Δ3), established the basis for potential 3-HP production in this chassis.

A defining feature of *C. necator* H16, and one that is key to its industrial potential, is the ability to grow on CO_2/H_2 gas mixtures. Carbon fixation *via* the CBB cycle results in the generation of 3-phosphoglycerate, a precursor in the formation of pyruvate and acetyl-CoA. The latter form the starting points for 3-HP formation *via* the β-alanine

and malonyl-CoA pathway, respectively. By contrast, due to inefficient utilisation of glycerol, the glycerol pathway is not an appropriate route for 3-HP biosynthesis in *C. necator*.

Although at least on paper *C. necator* possesses all the enzymes to convert the β-alanine to 3-HP *via* malonate semialdehyde, it has recently been shown to not accumulate any 3-HP, unless all three (methyl)malonyl-CoA semialdehyde dehydrogenases are impaired and the pathway intermediate β-alanine is provided in the media [131]. Most likely this is because the various enzymes do not form part of a single coherent metabolic unit but are part of separate and unrelated metabolic pathways.

As previously discussed, successful attempts have been made to implement sections of an externally sourced β-alanine pathway in *C. necator* Δ3 [83]. Interestingly, for *C. necator,* 3-HP monomers generated in the aforementioned manner have recently been shown to be incorporated into the co-polymer poly(3HB-co-3HP) at a high percentage. Altering the amount of available β-alanine was found to change the composition of the final biopolymer [83].

This project began as an endeavour to produce 3-HP from $CO_2/H_2/O_2$ in *C. necator* H16, but complications along the way lead to a deeper understanding of the central carbon metabolism and adaptability of the organism. *C. necator* is an ideal chassis, growing autotrophically or on a range of substrates, and to a very high cell density [26]. Much work has been performed on developing synthetic biology techniques for *C. necator*, allowing for precise genome editing and plasmid design [37][42]. Despite this, the titer of most desired compounds have remained low (see Table 2). This implies that more focus needs to be applied to understanding the metabolism of *C. necator*, in order to eliminate competing pathways, feedback inhibition and issues relating to the regulation of native and introduced metabolic pathways.

1.5 Aims and objectives

This work explores the unexpected interrelation between 3-HP production and sugar metabolism. Thus, the specific aims of this study were to:

1. Optimise plasmid-based expression of the malonyl-CoA pathway (or a derivative of) for *C. necator* H16
    a. Create an inducible system to modulate expression of a non-native *acc* (or alternative enzyme-encoding genes) to increase available malonyl-CoA
    b. Overexpression and modification of *mcr* gene from *C. aurantiacus* to convert malonyl-CoA to 3-HP
2. Establish an enzyme-based, colorimetric biosensor for malonyl-CoA in *C. necator* H16, which can be used to determine the *C. necator* H16 strain with the highest malonyl-CoA availability, and evaluate the effect of overexpression of ACC enzyme
3. Investigate the consequences of the presence of 3-HP in media alongside other metabolizable carbon sources, particularly in strains unable to degrade 3-HP

Chapter 2 –
Materials and methods

Chapter 2 - Materials and methods

2.1 Bacterial strains and growth conditions

2.1.1 Bacterial strains and strain storage

All bacterial species and strains used in this study are listed in Table 1. All bacterial strains were stored at -80ºC in tubes, as part of the Cryobank microbial cryopreservation system. The cultures were grown in LB overnight, before 1 mL was transferred to vial, where the bacteria bound to the beads. The culture was removed, and the vial was immediately placed in freezer. Bacteria were initially plated onto LB and stored at 4ºC when not in use.

Table 4 - Species and strains used in this study

Species	Strain	Description	Source
E. coli	DH5α	D5-alpha *E. coli* Genotype - (F– *endA1 glnV44 thi*-1 *recA1 relA1 gyrA96 deoR nupG purB20 φ80dlacZΔM15* Δ(*lacZYA-argF*)U169, *hsdR17*(rK– mK+), λ–	NEB
	Lemo21(DE3)	*E. coli* cells (C2528) with tuneable T7 expression Genotype - *fhuA2* [lon] *ompT gal* (λ DE3) [*dcm*] Δ*hsdS*/ pLemo(Cam^R) λ DE3 = λ sBamHIo Δ*EcoRI*-B int::(*lacI*::P$_{lac}$UV5::T7 gene1) i21 Δ*nin5* pLemo = pACYC184-Prha$_{BAD}$-*lysY*	NEB

	MSD42	Reduced genome strain	Umenhoffer *et al.* [147]
	S17-1	Conjugative donor strain, ATCC 47055 Genotype - *recA pro hsdR RP42-Tc*::MuKm::Tn7	Simon *et al*. [148]
Cupriavidus necator	H16 (=DSMZ 428)	*Cupriavidus necator* H16	German Collection of Microorganisms and Cell Cultures GmbH, Braunschweig, Germany
	H16 Δ3	H16 with deletions of *mmsA1*, *mmsA2* and *mmsA3*	Lopez, 2017 [63]
	H16 Δ3 *Δmcd*	H16 with deletions of *mmsA1*, *mmsA2, mmsA3* and *mcd*	This study and Lopez, 2017 [63]
	H16 Δ4	H16 with deletions of *mmsA1*, *mmsA2, mmsA3* and *phaCAB*	Lopez, 2017 [63]
	H16 Δ*mcd*	H16 with deletion of *mcd*	Lopez, 2017 [63]
	H16 Δ*hpdH*	H16 with deletions of *hpdH*	Lopez, 2017 [63]
	H16 Δ3 Δ*hpdH*	H16 with deletions of *mmsA1*, *mmsA2, mmsA3* and *hpdH*	This study and Lopez, 2017 [63]
	H16 Δ3.1 - Δ3.10	H16 with deletions of *mmsA1*, *mmsA2* and *mmsA3,* and SNP adaptations induced by	This study

		growth on fructose and 3HP	
Streptomyces griseus	DSM 40236, ATCC 23345	Type strain	Samantha Bryan, University of Nottingham

2.1.2 General growth conditions in LB medium

E. coli cultures were grown in Lysogeny Broth (LB) (10 g/L sodium chloride, 5 g/L yeast extract and 10 g/L tryptone) liquid or agar (15 g/L bacteriological agar no. 1 added). Both were sterilised by autoclaving. Liquid cultures were incubated shaking at 200 rpm, with plasmid-appropriate antibiotic added. All *E. coli* cells were cultured at 37ºC, unless stated otherwise. *E. coli* S17-1 cells were cultured with 100 µg/mL spectinomycin.

C. necator strains were cultured at 30ºC with gentamicin (10 µg/L) added to prevent contamination, alongside any plasmid-specific antibiotic. *C. necator* strains were grown on/in LB (composed as above) for general storage, and during initial recovery from DNA manipulation, with any required antibiotics. Low salt LB, abbreviated to LSLB, with 2.5 g/L NaCl, rather than 10 g/L was used for overnights of this bacterium before conjugative plasmid transfer procedures. LSLB with 15% (w/v) sucrose added was used to select for plasmid loss in suicide-plasmid aided homologous recombination experiments for chromosomal deletions/insertions.

2.1.3 Growth in minimal media

C. necator H16 strains were grown in minimal medium (composition in

Table 5 and Table 6), with filtered carbon source added (descriptions in Table 7). Medium pH was adjusted to 6.9 using HCl or NaOH. The medium was filter sterilised and stored at room temperature (4ºC for 3-HP containing medium variants).

Component	Concentration
$Na_2HPO_4 \times 12H_2O$	9 g/L
KH_2PO_4	1.5 g/L
NH_4Cl	1 g/L
$MgSO_4 \times 7H_2O$	0.2 g/L
$CaCl_2 \times 2H_2O$	20 mg/L
Fe(III)NH4-citrate	1.2 mg/L
SL7 (trace element solution)	1 mL/L

To make agar plates, microbiological agar 1 (Oxoid) was prepared to give a final concentration of 15 g/L. The agar was autoclaved at 121ºC for 15 minutes separately to sterilise. Pre-warmed, filter sterilised minimal medium was mixed to give the concentrations stated. Plates were poured (with or without antibiotics), stored at 4ºC and dried in a biosafety cabinet before use.

Table 5 - The composition of minimal medium used to grow *C. necator* H16

Table 6 - The composition of SL7 (trace element solution) used in minimal media for growth of *C. necator* H16

Component	Concentration
25% (w/v) HCl	1.3 mL/L
H_3BO_3	62 mg/L
$CoCl_2 \times 6H_2O$	190 mg/L
$CuCl_2 \times 2H_2O$	17 mg/L
$MnCl_2 \times 4H_2O$	100 mg/L
$Na_2MoO_4 \times 2H_2O$	36 mg/L
$NiCl_2 \times 6H_2O$	24 mg/L
$ZnCl_2$	70 mg/L

Table 7 - Carbon sources and concentrations used in minimal media for growth of *C. necator* H16-derived strains

Media	Carbon source

SG-MM	0.2 % sodium gluconate (w/v)
F-MM	0.2 % fructose (w/v)
NAG-MM	0.2 % N-acetylglucosamine (w/v)
SUC-MM	0.2 % succinate (w/v)
SG+3HP-MM	25 mM sodium gluconate + 50 mM 3-hydroxpropionic acid
F+3HP-MM	25 mM fructose + 50 mM 3-hydroxpropionic acid
NAG+3HP-MM	25 mM N-acetylglucosamine + 50 mM 3-hydroxpropionic acid
SUC+3HP-MM	25 mM succinate + 50 mM 3-hydroxpropionic acid

2.1.4 Antibiotic concentrations

All antibiotics were prepared from powdered stocks with an appropriate sterile solvent, outlined below (Table 8).

Table 8 - Antibiotics and their preparation during this work.

Antibiotic	**Plasmid backbone**	**Solvent**	**Conc. (µg/mL)**	
(abbreviation)			***E. coli***	***C. necator***
Tetracycline (Tet)	pMTL71301, pME6032	100% EtOH	10	12.5
Chloramphenicol (Cm)	pMTL71101, pMTL74111, pLEMO, pBBR1-Cm		25	50
Ampicillin (Amp)	pET16b	dH_2O	100	100
Kanamycin (Kan)	pUC57		50	- (>300)
Gentamicin (Gent)	-		-	10

2.1.5 Testing toxicity of cerulenin on *E. coli* strains

To test the toxicity effect of cerulenin (Stratech Scientific) on *E. coli* strains, the culture was grown in M9 media at 37° C, 200 rpm for 16 hours. A sterile, flat bottomed, clear 96 well plate (Corning) was set up with M9 medium [149] and varying concentrations of cerulenin from 50 µM down to 0 µM (50 µM, 25 µM, 12.5 µM, 6.25 µM, 3.125 µM, 1.5625 µM, 0 µM). All the experiments were performed in triplicate. Seed culture was added to a starting OD of 0.1. The OD600 of the wells were read every 15 minutes using TECAN Infinite M NanoPlus microplate reader for 20 hours.

2.1.6 Testing toxicity of cerulenin on *C. necator* strains

C. necator H16 strains were grown in SG-MM at 30°C, 200 rpm for 20 hours. A sterile, flat bottomed, clear 96 well plate (Corning) was set up with SG-MM and varying concentrations of cerulenin (as above). Seed culture was added to give a starting OD of 0.1. The OD600 of the wells were read every 15 minutes using TECAN Infinite M NanoPlus for 22 hours.

2.2 Extraction of genomic DNA

Genomic DNA (gDNA) was extracted using GenElute Bacterial Genomic DNA Kit (Sigma-Aldrich), using 1 mL sample of a 5 mL LB overnight, grown from a single colony. This was performed according to the included instructions. Purity and concentration of gDNA was checked by SimpliNano microvolume spectrophotometer (GE Healthcare Life Sciences). A small volume (equivalent to ~10 ng) was loaded on to a 0.75 % agarose gel with a molecular weight ladder to verify the integrity of the DNA.

2.3 Amplification and visualisation of DNA fragments

Amplification of genetic material was performed using Q5 High-Fidelity DNA Polymerase (NEB). Annealing temperatures were calculated according to the NEB online calculator (https://tmcalculator.neb.com/). Primers were designed according to guidelines by Dieffenbach *et al*. [150]. A full list of primers can be found in Table 10. Gene products were visualised by gel electrophoresis on 1% TAE agarose for 30 minutes at 100 volts using Gel Doc™ XR+ (Bio-Rad). 2-Log DNA Ladder (NEB - discontinued) or Quick-Load® 1 kb Extend DNA Ladder (NEB) were used as markers.

DNA fragments (PCR or digest products) were extracted from the agarose gel using Monarch DNA Gel Extraction Kit (NEB). The concentration of DNA was measured using a SimpliNano microvolume spectrophotometer (GE Healthcare Life Sciences).

2.4 Plasmid manipulation and construction

Plasmids were purified using QIAprep Spin Miniprep Kit (Qiagen) and associated protocol. Digests were performed with Thermo-Fisher Scientific FastDigest enzymes and buffers at 37ºC for 1 hour. NEBuilder® HiFi DNA Assembly Master Mix was used to construct indicated plasmids. Primer design guidelines and the HiFi assembly protocol from the NEB website were used. Benchling.com was used as a visualisation and editing tool, for designing plasmids and primers, performing sequence alignments and virtual digests.

2.4.1 Plasmids and oligonucleotide primers

All plasmids and oligonucleotides used in this thesis are listed in Table 9 and Table 10, respectively.

Table 9 - Plasmids used in this study

Plasmid Name	Description	Source
pMTL71301	pMTL71301, high copy number plasmid with tetracycline resistance and pBBR1 *oriV*	Muhammad Eshaan, University of Nottingham (unpublished)
pMTL71301_*eyfp*	pMTL71301_with *eyfp* controlled by P*phaC* promoter	Muhammad Eshaan, University of Nottingham (unpublished)
pMTL74111	pMTL74111, low copy number plasmid with IncP/ColEI origins of replication and chloramphenicol resistance	Muhammad Eshaan, University of Nottingham (unpublished)
pMTL74111_*rfp*	pMTL74111 with P_{tac} promoter controlling *rfp*	Muhammad Eshaan, University of Nottingham (unpublished)
pBBR1 P*phaC accCB/dtsR1-glut*	pBBR1 with P_{phaC} promoter controlling *acc* pseudo-operon from *C. glutamicum*	Christian Arenas, University of Nottingham
pBBR1 P*phaC eyfp*	pBBR1 with P_{phaC} promoter controlling *eyfp*	Christian Arenas, University of Nottingham
pBBR1 P*phaC mcr*$_{635}$	pBBR1 with P_{phaC} promoter controlling *mcr* from *C. aurantiacus*	Christian Arenas, University of Nottingham

pBBR1 P*phaC mcr*$_{nit}$	pBBR1 with P_{phaC} promoter controlling *mcr* from *Nitrosopumilus maritimus*	Christian Arenas, University of Nottingham
pBBR1 P*phaC mcr*$_{osc}$	pBBR1 with P_{phaC} promoter controlling *mcr* from *Oscillochloris trichoides*	Christian Arenas, University of Nottingham
pBBR1 P*phaC eyfp*	pBBR1, medium-low-copy-number with P_{phaC} promoter from *C. necator* controlling *eyfp*	Christian Arenas, University of Nottingham
pBBR1_PphaC-CvBAPAT-Ec*ydfGEc*	pBBR1 with P_{phaC} promoter controlling a gene encoding BAPAT from *Chr. violaceum and ydfG*$_{Ec}$ from *E. coli*	Katalin Kovacs, University of Nottingham
pME6032Δ*lacIQ* P*tac mcr635*	Modified pME6032 with *lacIQ* deletion, carrying the *mcr*$_{635}$ from *C. aurantiacus*	Christian Arenas, University of Nottingham
pME6032Δ*lacIQ* P*tac eyfp*	Modified pME6032 with *lacIQ* deletion, carrying the *eyfp*	Christian Arenas, University of Nottingham
pMTL71301_TdcB/R_ *araC*_P*bad_rfp*	pMTL71301_with *rfp* controlled by P_{BAD} promoter	Giorgia Tibaldero, University of Nottingham
pMTL71301_*acc*	pMTL71301_with P_{BAD} promoter controlling *acc* pseudo-operon from *C. glutamicum*	This study
pMTL71301_*acc_ydfGEc*	pMTL71301_with P_{BAD} promoter controlling acc pseudo-operon from *C. glutamicum* and *ydfG*$_{Ec}$ from *E. coli*	This study
pMTL71301_*mmc*	pMTL71301_with P_{BAD} promoter controlling *mmc* operon from *P. freudenreichii*	This study
pMTL71301_*rfp*	pMTL71301_with *eyfp* controlled by P_{phaC} promoter and P_{tac} promoter controlling *rfp*	This study
pMTL74111_*mcr*635	pMTL74111 with P_{tac} promoter controlling *mcr*$_{635}$ from *C. aurantiacus*	This study
pMCR635-His	pET16B expression plasmid with T7 promoter controlling *mrc*$_{635}$ from *C. aurantiacus* with HisTag encoded at N-terminus	Christian Arenas, University of Nottingham
pMTL71301_*acc_mcr*	pMTL71301_with P_{BAD} promoter controlling *acc* pseudo-operon from *C. glutamicum,* and P_{tac} promoter controlling *mcr*$_{635}$ from *C. aurantiacus*	This study
pMTL71301_*acc*_ *ydfGEc_mcr*	pMTL71301_with P_{BAD} promoter controlling *acc* pseudo-operon from *C. glutamicum, and ydfG*$_{Ec}$ *from E. coli,* and P_{tac} promoter controlling *mcr*$_{635}$ from *C. aurantiacus*	This study

pMTL71301_*eyfp_mcr*	pMTL71301_with *eyfp* controlled by P_{phaC} promoter and P_{tac} promoter controlling mcr_{635} from *C. aurantiacus*	This study
pMTL71301_*mmc_mcr*	pMTL71301_with P_{BAD} promoter controlling *mmc* operon from *P. freudenreichii* and P_{tac} promoter controlling *mcr* from *C. aurantiacus*	This study
pMTL71301_*acc_rppA*	pMTL71301_with P_{BAD} promoter controlling acc pseudo-operon from *C. glutamicum* and P_{tac} promoter controlling *rppA* from *S. griseus*	This study
pMTL71301_*acc_ydfGEc_rppA*	pMTL71301_with P_{BAD} promoter controlling *acc* pseudo-operon from *C. glutamicum, and* $ydfG_{Ec}$ *from E. coli,* and P_{tac} promoter controlling *rppA* from *S. griseus*	This study
pUC57-mini-*mcr*	pUC57-mini plasmid containing dissected and mutated *mcr* cassette. The two subunits of *mcr* are controlled by different promoters (P_{tac} promoter controls mcr_N and P_{15} promoter controlling mcr_C). Mutations introduced at N940V, K1106W and S1114R	Synthesised by Genscript Biotech
pMTL_*acc_*mcr_m	pMTL71301_with P_{BAD} promoter controlling *acc* pseudo-operon from *C. glutamicum,* P_{tac} promoter controlling mcr_N and P*15* promoter controlling mcr_C	This study
pMTL_*acc_ydfGEc_*mcr_m	pMTL71301_with P_{BAD} promoter controlling *acc* pseudo-operon from *C. glutamicum* and $ydfG_{Ec}$ from *E. coli,* P_{tac} promoter controlling mcr_N and P*15* promoter controlling mcr_C	This study
pMTL_*eyfp_*mcr_m	pMTL71301_with *eyfp* controlled by P_{phaC} promoter, P_{tac} promoter controlling mcr_N and P_{15} promoter controlling mcr_C	This study
pMTL74111_*rppA*	pMTL74111 with P_{tac} promoter controlling *rppA* from *S. griseus*	This study
pMTL71301_*rppA*	pMTL71301_with *eyfp* controlled by P*phaC* promoter and P_{tac} promoter controlling *rppA* from *S. griseus*	This study

Table 10 - Oligonucleotide primers used in this study

Name	Sequence	Function
71301_accglut_FW	GCTTTTTATCGCAACTCTCTACTGTCATATGTCAGTCGAGACTAGGAAGATC	Amplification of pseudo-operon *acc* from pBBR1 P_{phaC} *accCB*/*dtsR1*, for

71301_accglut_R	GTAAAACGACGGCCAGTGCCAAG CTTACAGTGGCATGTTGCCGTGCT TGC	construction of pMTL71301_*acc*
71301_ACCYDFGEC_R	CGTTGTAAAACGACGGCCAGTGCC AAGCTTGCATGTCTGCAGGCCTCG AGTTACTGACGGTGGACATTCAGT CCGGCATA	Amplification of *ydfG*$_{Ec}$ (originating in *E. coli*) from pBBR1_PphaC-CvBAPAT-Ec*ydfGEc*, for construction of pMTL71301_*acc_ydfGEc*
71301_MCR_FW	CCTGCATTTGCAGGCTTCTTATTTT TATGGCGCGTTGACAATTAATCAT CGGCTCGTATAATGTGTGGAA	Amplification of cassettes encoding either *mcr*$_{635}$ or *rppA* in pMTL71301
71301_MCR_R	CTCTCTGGCGGCCTTCTGGCGCTC CTGCGGCCGGCCATAAAAATAAG AAGCCTGCAAA	
71301_MMC_MCR_FW	GGAAACAGCTATGACCGCGCGGC CGGCCGCTTATGACAACTTGACGG CTACATCATTCAC	Amplification of P$_{tac}$ and *mcr* from pMTL74111_*mcr*635, for construction of pMTL_*mmc_mcr*
71301_MMC_MCR_R	CCACACATTATACGAGCCGATGAT TAATTGTCAAATAAAAATAAGAA	
71301_MMC_MCRlink_FW	GCCTGCATTTGCAGGCTTCTTATTT TTATTTGACAATTAATCATCGGCT CGTATAATGTGTGG	Amplification of MMC encoding genes from pMTL71301_*mmc*, for construction of pMTL_*mmc_mcr*
71301_PBAD_FW	GGAAACAGCTATGACCGCGGCCG CTTATGACAACTTGACGGCTACAT C	Amplification of *AraC*/P$_{BAD}$ from pMTL71301_*TdcB*/R_araC_P$_{BAD}$_*rfp* for construction of pMTL71301_*acc*
71301_PBAD_R	GATCTTCCTAGTCTCGACTGACAT ATGACAGTAGAGAGTTGCGATAA AAAGC	
71301_rfp_FW	CATTTGCAGGCTTCTTATTTTTATG GCGCGATACGCCGCCCCCTGACCA GGAACGCCGGG	Amplification of P$_{tac}$ and *rfp* from pMTL74111_*rfp*, for construction of pMTL71301_*eyfp_rfp*
71301_YDFGEC_FW	CTGCTCGCAAGCACGGCAACATGC CACTGTAACTGATCAACTAGTGAT CCAGGAGATATACCCATGGCCGTT TTAGTAACTGGAGCAACGGCAGGT TTTG	Amplification of *ydfG*$_{Ec}$ (originating in *E. coli*) from pBBR1_PphaC-CvBAPAT-Ec*ydfGEc*, for construction of pMTL71301_*acc_ydfGEc*
74111_ptac_MCR_FW	CACATTATACGAGCCGATGATTAA TTGTCAACCTGCAGGCAGAAGTGG TCAGCTTGGCTGCC	Amplification of P$_{tac}$ and *mcr* genes from pME6032Δ*lacIQ* P$_{tac}$ *mcr635*
74111_tac_FW	GATCCTCTAGAGTCGACGTCACGC GTCCATGGAGATCTCG	Amplification of P$_{tac}$ promoter from pMTL74111
74111_tac_R	AATTGTTATCCGCTCACAATTCCA CACATTATACGAGCCG	
acc_B1_FW	GCACCTTACGTTGACGCTTCCG	Sequencing of *acc* pseudo-operon (originating in *C. glutamicum*)
acc_B1_R	GCTTCCTCATCGGTCGCAGCGGTG TAG	

acc_C1_FW	GGGTTCCAAGGGCTTGGGCTCTG	
acc_C1_R	GCGGTCAACTTCGCCCGATTCCG	
accCB_seq_FW	CAATCGCCATCAAGGCAGCTTTCG	
accCB_seq_R	CCTCCTACCTTCACTATTCG	
dtsR1_seq_FW	CGAATAGTGAAGGTAGGAGG	
M13F	TGTAAAACGACGGCCAGT	Sequencing of all pMTL71301_plasmids
M13R	CAGGAAACAGCTATGAC	
MCR_pUC57_FW	GATGCCAGTGGCCGCACGACGCTCATCTGCGCCGGCGACCAGATTGAAGAGGTGATGGCGCTCAC	Amplification of dissected and mutated *mcr* cassette from pUC57-mini
MCR635_new_seq_FW1	CGCGTTAATACGATCTTTCCCG	Sequencing of *mcr*635 (originating in *C. aurantiacus*)
MCR635_new_seq_FW2	GGACAGCTCAATTGCTCCATAG	
MCR635_new_seq_FW3	GCTGCTGAACCGTTCAATTGCC	
MCR635_seq1_R	CGGGAAAGATCGTATTAACGCG	
MCR635_seq2_R	CTATGGAGCAATTGAGCTGTCC	
MCR635_seq3_R	GGCAATTGAACGGTTCAGCAGC	
MCR635_seq4_R	CTCTTGCGGGATATCCGGATATAG	
MMC_MCR_pUC57_R	GTGAGCGCCATCACCTCTTCAATCTGGTCGCCGGCGCAGATGAGCGTCGTGCGGCCACTGGCATC	Amplification of MMC encoding genes from pMTL71301_*mmc_mcr*, for construction of pMTL71301_*mmc_mcr*$_m$
MMC_SDM_FW	CCTTGGGAGCGTCTGCGCACGTTCCGCAAGCTGATGCCCAACAGCCGTCTCCAGATGC	Used for site directed mutagenesis to correct the SNP in pMTL71301_*mmc*
MMC_SDM_R	GCATCTGGAGACGGCTGTTGGGCATCAGCTTGCGGAACGTGCGCAGACGCTCCCAAGG	
MMC_Seq_F1	GTGACGGCAGAGAGACAATCAAC	Sequencing of genes encoding MMC from *P. freudenreichii*
MMC_Seq_F2	GAAGACGCAGATCAACCTGC	
MMC_Seq_F3	GAGTGGGAGAAGCAGTCCAAG	
MMC_Seq_F4	CAAGATGTTCTTCGCCAACG	
MMC_Seq_F5	CATGTGCAACCGTGACCTTG	
MMC1_FW	ATCGCAACTCTCTACTGTATGAGTCCGCGAGAAATTGAGG	Amplification of synthesised gene fragment *mmc1*
MMC1_R	GCTTCAAATTGTTGTTTTCAGCC	
MMC2_FW	CGAAGTCACCGTTCAGCAGGCG	Amplification of synthesised gene fragment *mmc2*
MMC2_R	AGGTCCTTCTCTTCCTCATCAGCC	
MMC3_FW	GAAGCATGGAAACTTCCCCTG	Amplification of synthesised gene fragment *mmc3*
MMC3_R	TCACGACGTTGTAAAACGACGG	
mcd_int_FW	CCTTCGACACGGGTGACCAGAAG	

mcd_int_R	GTTGCCGGCGCCCAAGCGTGC	Amplification of internal *mcd* region for sequencing and diagnostic
rppA_FW	CGGCTCGTATAATGTGTGGAATTG TGAGCGGATAACAATTAGTATCAG TAAAAGGAGGTATATACATGGCG ACCCTGTGCCGACCGGCCATCGCT GTGCC	Amplification of *rppA* gene with RBS from S. griseus for malonyl-CoA biosensor plasmids
rppA_R	CGAGATCTCCATGGACGCGTGACG TCGACTCTAGAGGATCCTCAGCCG GACAGCGCAACGCCGGCGGTCAG CTCCAGCTC	
rfp_int_FW	GGCGAGTAGCGAAGACGTTATCA AAG	Sequencing of *rfp*
rfp_int_R	GCACCGGTGGAGTGACGACC	
hpdh_seq_FW	CACATGAGCAGGCTGCGCCAC	Sequencing of *hpdH* from *C. necator* H16

2.4.2 Construction of plasmids for 3-HP production

To create the vectors for 3-HP production, the plasmid pMTL71301_was digested with NotI and HindIII restriction enzymes. The promoter of the arabinose ara_{BAD} operon (called P_{BAD}), and the gene encoding the regulator of this promoter (*araC*) were amplified from pMTL71301_TdcB/R_araC_Pbad_*rfp*, using primers 71301_P_{BAD}_FW and 71301_P_{BAD}_R. The *acc* pseudo-operon (originating from *C. glutamicum*) was amplified from plasmid pBBR1-P_{phaC}- *acc* using primers 71301_*acc*glut_FW and 71301_*acc*glut_R. HiFi assembly was used to construct the plasmid named pMTL71301_*acc*. The plasmid was sent Sanger sequencing with the primers described.

To create the plasmid pMTL71301_*acc_ydfGEc*, the gene $ydfG_{Ec}$ from *E. coli* was amplified from pBBR1_PphaC-CvBAPAT-Ec*ydfGEc*, using primers 71301_*YDFGEC*_FW and 71301_ACC*YDFGEC*_R. The plasmid pMTL71301_*acc* was digested using HindIII and SpeI restriction enzymes, and HiFi assembly was used to recombine the fragments to form plasmid pMTL71301_*acc_ydfGEc*, aided by complementary overhangs on PCR products and plasmid.

The genes encoding the 4 subunits of the methylmalonyl-CoA carboxyltransferase (MMC) from *Propionibacterium freudenreichii* were synthesised by ThermoFisher.

Three codon-optimised "gene strings" (sequences in Appendix 7.1) were amplified using primers MMC1_FW, MMC1_R, MMC2_FW, MMC2_R, MMC3_FW and MMC3_R. The plasmid named pMTL71301_*acc* was h linearised with HindIII and SacI restriction enzymes and HiFi assembly was used construct the plasmid named 71301_*mmc* in the second generation. The plasmid was sent Sanger sequencing with primers denoted as "sequencing for *mmc*" in primers list.

The entire biosynthetic pathway to 3-HP *via* malonyl-CoA and malonate semialdehyde was united on a single plasmid. To achieve this, the vectors pMTL71301_*acc* and pMTL71301_*acc_ydfG*$_{Ec}$ were digested with AscI and FseI restriction enzymes. Primers 71301_MCR_FW and 71301_MCR_R were used to amplify the *mcr* gene and associated P$_{tac}$ promoter from pMTL74111_*mcr*635. Once assembled, the coding regions of the plasmids pMTL71301_*acc_mcr* and pMTL71301_*acc_ydfGEc_mcr* were confirmed by sequencing using primers described in table.

To construct the pMTL_*mmc_mcr* plasmid, pMTL71301_*mmc* was digested with NotI and FseI restriction enzymes. Two separate PCR products were generated: one for MMC encoding genes (using primers 71301_MMC_MCR_FW and 71301_MMC_MCR_R) and one for the *mcr* cassette (using primers 71301_MMC_MCRlink_FW and 71301_MCR_R). The PCR fragments were assembled with the linearised vector using HiFi assembly and the correct sequence was confirmed by sequencing,

There was a need to correct SNPs in plasmid 71301_*mmc_mcr* that arose during cloning. This was performed by the same procedure outlined previously in Section 2.4.3, using primers MMC_SDM2_FW and MMC_SDM2_R.

The control plasmid (pMTL71301_*rfp*) was generated by digestion of pMTL71301_*eyfp* with AscI and FseI restriction enzymes and the subsequent insertion of the P$_{tac}$-*rfp* cassette (amplified from pMTL74111_*rfp* using primers 71301_*rfp*_FW and 71301_MCR_R with appropriate overhangs) by HiFi assembly. Correct assembly was confirmed by Sanger sequencing.

Variations of the pMTL71301_*acc_mcr* plasmid were generated by separating the C and N-terminal domain encoding regions of the *mcr* gene and putting them under control of two different promoters, P_{tac} and P*15* promoter-like sequence, according to details in Lui [144].

To generate the plasmids pMTL_*acc_mcr*$_m$, pMTL_*acc_ydfGEc_mcr*$_m$ and pMTL_*eyfp_mcr*$_m$, the backbones were provided by plasmids pMTL71301_*acc_mcr*, pMTL71301_*acc_ydfGEc_mcr* and pMTL71301_*eyfp*, linearised with MreI and FseI restriction enzymes. Primers MCR_pUC57_FW and 71301_MCR_R were used to amplify the dissected and mutated *mcr* cassette from pUC57-mini-*mcr*. HiFi assembly was used to assemble.

Due to the presence of unwanted restriction sites, the pMTL71301_*mmc_mcr*_sdm plasmid was generated by a different cloning strategy. The plasmid pMTL71301_*mmc_mcr* was digested with MreI and FseI restriction enzymes. Two separated PCR products (with complementary overhangs) were amplified. The promoter and MMC encoding region were amplified with primers 71301_MMC_MCR_FW and MMC_ MCR_pUC57_R. The second product (including the dissected/mutated *mcr* and associated promoters) was created as above. The digested vector and the two PCR products where then combined by HiFi assembly.

2.4.3 Site directed mutagenesis to remedy single nucleotide changes

In the process of cloning, plasmid 71301_*mmc* acquired a single nucleotide deletion (T) at position 248 in the gene denoted as *M1870*. In order to correct this, QuikChange site-directed mutagenesis kit was used to insert a T base at the correct position. The entire plasmid was amplified using Q5 polymerase and primers MMC_SDM_FW and MMC_SDM_R. The thermocycler temperature and timing settings are outlined in the manufacturers protocol. To eliminate the parent template, 1 µl DpnI was added to the reaction mix and incubated at 37° C for 1 hour. Competent cells were transformed immediately using this digested, error-free plasmid. The entire region was re-sequenced to ensure no other mutations occurred. The corrected plasmid is referred to as pMTL71301_*mmc*.

2.4.4 Construction and assembly of vectors for the expression of *rppA* alongside *eyfp, acc* or *acc/ydfGEc*

The *rppA* gene and its RBS was amplified by PCR from a single colony of *S. griseus* using primers *rppA*_FW and *rppA*_R. The gene was originally cloned into plasmid pMTL74111 under the control of a *tac* promoter to create pMTL74111_*rppA*. For this, the plasmid backbone including the P_{tac} promoter was amplified from pMTL74111_*mcr*635 using primers 74111_ptac_FW and 74111_ptac_R. The fragments were combined by HiFi assembly and correct assembly confirmed by Sanger sequencing.

pMTL74111_*rppA* did not function correctly, so the gene (with promoter and RBS) was transferred to pMTL71301 (a higher copy number plasmid with a different origin of replication and a superior resistance gene for *C. necator*) to create pMTL71301_*rppA*. The P_{tac}-*rppA* cassette was amplified by PCR from pMTL74111_*rppA* using primers 71301_MCR_FW and 71301_MCR_R. To construct pMTL71301_*rppA*, pMTL71301_*eyfp* was cut with FseI and AscI restriction enzymes. The same enzymes were used to cut pMTL71301_*acc* and pMTL71301_*acc_ydfGEc* to create pMTL71301_*acc_rppA* and pMTL71301_*acc_ydfGEc_rppA* respectively. The fragments were joined using HiFi assembly. The plasmids were transformed into *E. coli* DH5α by heat shock protocol. Once confirmed by PCR and diagnostic digest, the plasmid was sent for Sanger sequencing.

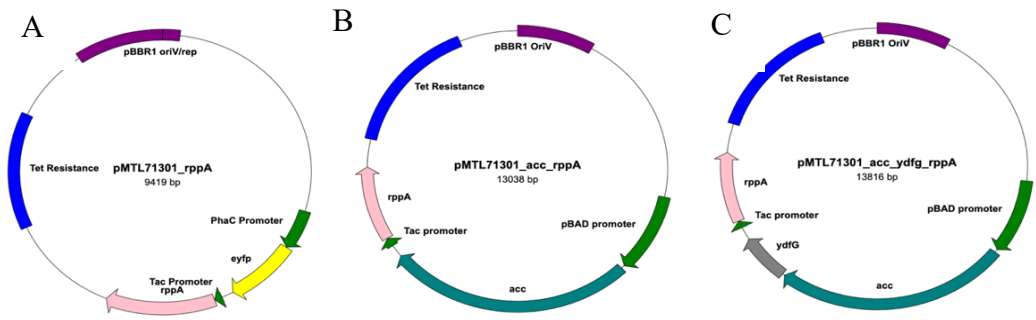

Figure 9 - Schematic plasmid maps of A) pMTL71301_*rppA*, B) pMTL71301_*acc_rppA* and C) pMTL71301_*acc_ydfGEc*_rppA.

2.5 Transformation of *E. coli* cells

E. coli competent cells were bought from NEB or created using the following protocol: 10 mL of culture was grown at 37ºC for 16 hours. This was used as a seed culture for 50 ml LB. This culture was grown until an OD of 0.6 was reached. The culture was cooled and kept at 4ºC throughout the rest of the procedure. The cells were collected by centrifugation at 3000 x g for 15 minutes. The pellet was gently resuspended in 5 mL of sterile 10% (v/v) glycerol and then centrifuged to wash. This procedure was repeated 3 times total. The final pellet was resuspended in 10% (v/v) glycerol, used immediately or stored at -80ºC in 100 µl aliquots.

The previously described competent cells (50 µl) were transformed with 2 µl constructed vectors in a pre-chilled 2 mm electroporation cuvette (BioRad). A MicroPulser Electroporator (Bio-Rad) was used to electroporate (EC2 program 2.5 kV) before recovery in 800 µl SOC medium for 1 hour at 37ºC. Following incubation, 200 µl of culture was plated on LB agar with appropriate antibiotic selection.

Competent *E. coli* cells purchased from NEB (DH5α and LEMO) were transformed by heat shock protocol (30 minutes on ice, 2 minutes at 42ºC, 2 minutes on ice). The competent cells (50 µl) were transformed with 2 µl constructed vectors (approximately 200 ng) and recovered in 800 µl SOC medium for 1 hour, before being plated on LB agar with appropriate antibiotic selection. SOC medium was provided with the purchased cells.

2.6 Transformation of *C. necator* cells

To generate *C. necator* H16 electrocompetent cells, overnight culture from a single colony were set up in 5 mL LB broth. The cells were harvested by centrifugation in a centrifuge at 8000 rpm for 5 minutes, then washed 3 times in filter sterilised 15% sucrose (w/v) at room temperature. The final washed pellet was resuspended in 15% sucrose (w/v) for immediate use or storage at -80ºC in 100 µl aliquots.

C. necator cells were transformed by electroporation using a modified version of the protocol published by Sato *et al*. [23]. 100 µl electrocompetent cells were mixed with

2 µl plasmid in a 2 mm electroporation cuvette at room temperature. The MicroPulser Electroporator program EC2 was used to electroporate *C. necator* (same as *E. coli*), followed by a longer, 3-hour recovery period in 800 µl SOC medium at 30ºC, 200 rpm. After incubation on an antibiotic plate, colony PCR with Taq-polymerase was performed to confirm transformations.

2.7 Conjugative plasmid transfer from *E. coli* S17-1 into *C. necator* H16

Conjugation of pLO3-based suicide plasmids into *C. necator* was achieved using a modified method, based upon Park *et al*. [151]. The conjugative donor strain (*E. coli* S17-1) containing the pLO3-based plasmid was grown overnight at 37ºC in LB with tetracycline. The receiving *C. necator* strains were grown at 30ºC in LSLB. The culture was centrifuged at 8000 rpm for 5 minutes to generate a cell pellet, which was then washed 3 times with LB. The pellets of the donors and receivers were combined in a 1:1 ratio and centrifuged. The resulting pellets were resuspended in 30 µl LB, spotted onto LB agar plates and incubated at 30ºC for 6 hours. The cultures were scraped from the plate with a 10 µl loop and resuspended in 200 µl PBS. The resuspended culture was spread plated on antibiotic SG-MM with plates and incubated for 48-72 hours at 30ºC. Colonies from each plate were streaked to single colonies on antibiotic SG-MM. This was repeated after 48 hours of incubation at 30ºC. A single colony from each streak was resuspended in 200 µl PBS and spread onto LSLB + 15% sucrose plate, allowing for selection of plasmid-free colonies. After incubation, colonies from these plates were plated on both on LB and LB with tetracycline. Any colonies that grew on the LB plates only (and did not show antibiotic resistance) were tested for chromosomal integration/deletion using colony PCR.

2.8 Colony PCR to confirm transformants

The protocol for confirming transformants was a PCR based approach using OneTaq 2X Master Mix (NEB). The protocol and thermocycler program were as advised by the manufacturer. Single colonies were picked with a sterile pipette tip. The colony was transferred to a fresh, dry agar plate, before residual biomatter was used as the template in the PCR reaction. Primers used for each construct are described in Table 10.

2.9 Crude lysate generation by sonication

Cell pellets were resuspended in 100 mM Tris-HCl pH 7.8 with EDTA-free protease inhibitor (concentration according to manufacturer's recommendation) to avoid protein degradation during manipulations, diluted to an OD_{600nm} of 50. The cells were then disrupted by sonication at a maximum amplitude of 10 microns using the Soniprep 150 Plus Digital Ultrasonic Disintegrator (MSE). The samples were kept on ice during the sonication, which took place for 60 seconds, divided into 6 x 10 second intervals. The disrupted cells were centrifuged at 14,000 rpm for 20 minutes at 4°C. The supernatant was kept on ice. Using the Soniprep 150 Plus Digital Ultrasonic Disintegrator (240V) (MSE, UK) the samples were sonicated in 10 second intervals at a maximum amplitude of 10 microns, resting on ice between lysing cycles. The lysed cells were centrifuged at 8000 rpm for 10 minutes at 4°C.

2.10 SDS-PAGE analysis of expressed proteins

Samples were prepared by incubating at 95°C for 5 minutes with LDS Sample Buffer (4X) and NuPAGE™ Sample Reducing Agent (10X). NuPAGE 4-12% Bis-Tris Protein Gels, 1.0 mm, 10/12/15 wells were used for the SDS-PAGE analysis, ran in an XCell SureLock™ Mini-Cell Electrophoresis System (ThermoFisher Scientific) at 120 V for 90 minutes. ThermoFisher PageRuler Prestained Protein Ladder used as a marker. Gels were stained using Pierce Silver Stain Kit (by manufacturer's instructions) or 0.1% Coomassie (0.1% w/v Coomassie Blue R-250, 50% v/v methanol, 10% v/v acetic acid). Gels were stained for 1 hour, lightly shaking, and de-stained overnight in water.

2.11 Western blotting identification of His-tagged proteins

Western blotting was used to confirm presence of the His tagged MCR protein. Trans-Blot Turbo Transfer Packs (BioRad) with Trans-Blot Turbo Transfer System (BioRad) were used to transfer the protein from polyacrylamide gel to nitrocellulose membrane (mixed MW (Turbo) program; 1.3A, up to 25 V per gel, 7 minutes). The membrane was washed with TBS before blocking in 5% milk powder in PBS for 1 hour. The blocking solution was disposed of. The membrane was incubated for 18 hours at 4° C

with a 1:5000 diluted primary Anti-His antibody (in TBS with 1% BSA). After incubation, the membrane was washed three times with TBS buffer and the band corresponding to the His-tagged protein was visualised using the 1-Step Ultra TMB-Blotting Solution (ThermoScientific).

2.12 Purification and concentration of His-tagged proteins

Once confirmed, the His-tagged MCR protein was purified from the supernatant using Thermo Scientific's HisPur Ni-NTA Purification Kit. The equilibration of the spin column was performed using 10 mM imidazole pH 7.4. The wash steps were performed using concentrations of imidazole, (60 mM, 75 mM and then 100 mM) and the protein was eluted using a buffer containing 250 mM imidazole. All collected fractions (washing and elutions) were analysed by SDS-PAGE. The protein was concentrated, and the buffer exchanged (for PBS with 20% glycerol) using the Vivaspin 6 Centrifugal Concentrator with a 75,000 MW cut off. The enzyme was quantified and stored at -20^{o} C in in a cryopreservation vial contains 20% glycerol.

2.13 Quantification of proteins

Quick Start™ Bradford Protein Assay kit (BioRad) was used to quantify purified proteins and crude extracts. Known concentration of BSA between 0 and 1 mg/mL were used as standards. Experiments were performed following the manufacturers protocol in 1 ml cuvettes. The absorbance was read at 595 nm after 10-minute incubation.

2.14 Heterologous production of MCR enzyme in *E. coli* for enzyme activity measurements

Plasmid pMCR635-His encoding His-tagged MCR enzyme from *C. aurantiacus* was transferred into competent *E. coli* Lemo21(DE3) cells (NEB) by the previously outlined heat-shock procedure (outlined in Methods 2.5). New strains were freshly prepared as level of expression decreases in older cells.

After the recovery step in SOC medium, 200 µl of culture was also added to 10 mL SOC medium in a 100 mL flask, containing the plasmid specific antibiotics (tetracycline for pMCR635-His and chloramphenicol for pLEMO). After 16 hours incubation at 30° C, 200 rpm, the entire seed culture was added to 600 mL LB media, containing the appropriate antibiotics. Cultures were incubated for a further 6 hours, before the cells were induced with 400 µM IPTG (for the overexpression of pMCR635-His) and 500 µM L-rhamnose (for the induction of the pLEMO). The culture was incubated for a further 24 hours at 30°C. The cells were harvested and pelleted by centrifugation at 8000 rpm for 5 min, keeping the cultures at 4°C throughout the purification process.

2.15 Determination of malonyl-CoA reductase (MCR) activity

The activity of the purified enzyme was validated by adding malonyl-CoA to a reaction mix and monitoring the NADPH oxidation at 340 nm. The assay mixture of 300 µl contained 100 mM MOPS–KOH buffer (pH 7.8), 2 mM $MgCl_2$, 4 mM ATP, 0.4 mM NADPH and recombinant MCR, as per Kroeger *et al.* [152]. The amount of the recombinant MCR was varied to establish a linear reaction. The reaction was started by the addition of 0.3 mM malonyl–CoA. The assay was carried out at 30° C. on a TECAN Infinite M NanoPlus plate reader in Corning® UV-transparent 96-well microplate. The oxidation of NADPH was followed at 340 nm ($\varepsilon 340nm = 6.22 \times 10^3$ M^{-1} cm^{-1}). Enzyme activity was calculated using equation below, where A is absorbance at 340 nm, V_t indicates the total volume of the solution and Vs represents the volume of the substrate (malonyl-CoA) added. The pathlength, I, for the 96 well plate used, was attained from the manufacturer.

$$Specific\ activity = \left(\frac{\Delta A/\min}{\varepsilon\ x\ I} \times \frac{V_t}{V_s}\right) \div conc.of\ protein\ \div 2$$

2.16 Determination of acetyl-CoA carboxylase activity in crude cell extracts

The plasmid pMTL71301_*acc* was introduced by electroporation into competent *C. necator* H16 cells. Colonies were taken from the resulting transformation agar plate and grown overnight in 10 mL LB (with appropriate antibiotic). A fresh

transformation was performed each time to ensure maximum gene expression. After incubation, the cell pellet was disrupted by sonication, detailed in section 2.9.

Following the protocol outlined by Kroeger *et al.*, [152] the assay reaction mix contained 100 mM MOPS–KOH buffer (pH 7.8), 5 mM $MgCl_2$, 4 mM DTT, 10 mM $NaHCO_3$, 4 mM ATP, 0.4 mM NADPH and 3.5 µg tagged MCR protein (expression protocol in section 2.14). Varying concentrations of *C. necator* supernatant were added to the reaction mix. The reaction was started by the addition of 0.4 mM acetyl–CoA. The progress of the reaction was monitored at 340 nm by the equation in section 2.15.

2.17 Production of 3-HP in *C. necator*

C. necator H16 strains carrying the production plasmid(s), were grown in 25 mL 2 % SG-MM in 250 mL baffled flasks, with appropriate antibiotic(s). The cultures were incubated at 30° C and 200 rpm for 72 hours. 0.04 g/L biotin and 20 mM $NaHCO_3$ were added to ensure no cofactors were lacking. Arabinose (2mM) was used to induce when necessary. Sampling occurred every approximately every 12 hours, by sterile removal of 800 µl from the culture flasks. This was used to measure the OD, 3-HP concentration and substrate utilisation.

2.18 HPLC analysis of carbon sources

A HPLC-based method was used to quantify the amount of 3-HP, fructose, SG, N-acetylglucosamine and succinate concentrations in the culture supernatants. After centrifugation and filtration, samples were added to an HPLC vial along with the mobile phase (5 mM H_2SO_4 and 50 mM valerate as internal standard) in a 1:1 ratio. Appropriate standards curves were generated for each compound. Samples were run at 55° C for 50 using an Aminex HPX-87H 300 mm x 7.8 mm x 9µm column (Bio-Rad), at a 0.5 mL/min flow rate using 5 mM H_2SO_4 mobile phase.

2.19 Validation of the *rppA* biosensor and comparison between strains of *C. necator*

This assay detects and quantifies the production of malonyl-CoA derived flaviolin. For *E. coli*, the reporter plasmid carrying cells were incubated at 37ºC, 200 rpm, as indicated by Yang *et al.* [153]. Precultures were grown in triplicate in 3 mL LB with 12.5 µg/mL tetracycline in 50 mL falcons. 60 µl of preculture was added to 3 mL M9 with glycerol, with 12.5 µg/mL tetracycline and varying concentrations of cerulenin (0, 1.5625, 3.125, 6.25, 12.5, 25 and 50 µM) in a 15 mL falcon tube. The cultures were incubated for a further 16 hours at 37ºC, 200 rpm. The OD of the cultures was read at 600 nm. The cells were pelleted by centrifugation (3000 rpm, 10 minutes). Initially the absorption of the supernatant was read by wavelength scan between 200-1000 nm to find peaks specific for flaviolin. This was performed in a Corning® UV-transparent 96-well microplate and read in a TECAN Infinite M NanoPlus microplate reader. For continuing, the supernatant OD was read at 340 nm and 520 nm. Both the OD of the culture and absorption of the supernatant was adjusted by deducting the media only value. The signal output was found by dividing the adjusted supernatant absorption (340 nm or 520 nm) by OD 600 nm (adjusted to remove media background signal).

For *C. necator,* the cells were incubated at 30ºC, 200 rpm for 20 hours (due to slower growth). SG-MM was prepared, and 60 µl seed culture was added to 3 mL with 12.5 µg/mL tetracycline and varying concentrations of cerulenin (0, 1.5625, 3.125, 6.25, 12.5, 25 and 50 µM) in 15 mL falcon tubes. After cultivation for 20 hours at 30ºC, 200 rpm, the culture OD was read at 600 nm. The supernatant was retrieved by centrifugation of the cultures at 3000 rpm for 10 minutes. The OD340 and OD520 of the supernatant was read by TECAN Infinite M NanoPlus plate reader in Corning® UV-transparent 96-well microplate. The signal of the biosensor (normalised absorption) was defined as the media-normalised absorption of the supernatant at 340 and 520 nm divided by the media-normalised OD of the culture.

2.20 Isolation of mutant capable of growth in the presence of fructose and 3-HP

Cultures were added to 25 mL 3-HP/F-MM (50 mM 3-HP and 25 mM fructose minimal media) to a starting OD of 0.1 in 250 mL baffled flasks. This was repeated

in triplicate for the wild type strain, and 10 times for *C. necator* H16 Δ3 strain. The cultures were incubated conditions outlined in Figure 10. Samples were taken every 12 hours. Final samples were plated on F-MM media plates to provide single colonies. New flasks containing fresh media were inoculated to an OD of 0.1. Samples were taken as previously.

2.21 Whole genome sequencing

Genomic DNA extraction from the *C. necator* cells was performed as outlined in section 2.2. The quality of the gDNA was confirmed by gel electrophoresis on an 0.75% agarose gel, and the concentration measured by SimpliNano microvolume spectrophotometer (GE Healthcare Life Sciences). The gDNA was standardised to a

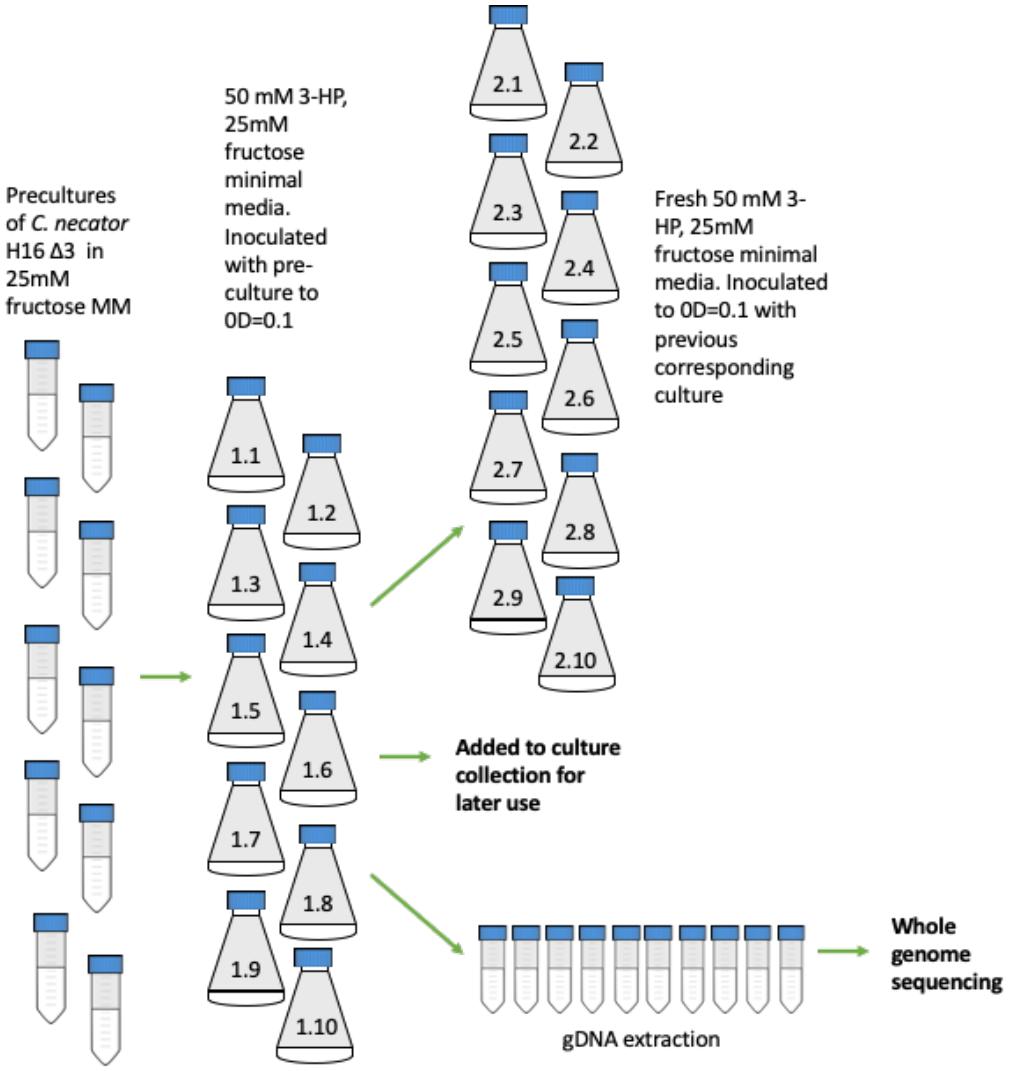

Figure 10 - Graphical description of method used to investigate the consumption of fructose and 3-HP. The initial cultures were set up from single colonies on a F-MM agar plate. All incubations took place at 30°C and 200 rpm shaking.

concentration of 30 ng/L. Whole genome sequencing performed on the Illumina sequencing platform was undertaken by MicrobesNG (protocol can be found at https://microbesng.com/microbesng-faq/).

2.21.1 Mapping reads to the reference genome

CLC Genomics Workbench 12 (Qiagen) was used to map the sequencing reads, align to the reference genomes and detect variants. The published genomes of *C. necator* H16 [19] were downloaded from NCBI, and the genome was used as a template to map paired ends. The mapping options parameters are in Table 11.

2.21.2 Identification of single nucleotide variants

Mapped reads were used to identify single nucleotide variants (SNVs) using CLC Genomics Workbench 12 (Qiagen). The parameters (Table 12) were set and tested by Dr Alex Grosse (University of Nottingham) and used for the Mapping and Variants workflow.

Table 11 - Parameters used in CLC Genomics to map reads to reference. Description of mapping options and default values from the CLC Genomics Workbench user manual [154]

Mapping Options	Selected	Further information
Masking mode	No masking	All regions of the genome considered when mapping reads to reference
Match score	1	Positive score for a match between the read and the reference sequence. Default = 1, maximum = 10
Mismatch cost	2	The cost of a mismatch between the read and the reference sequence. Default = 2, maximum = 3
Insertion cost	3	The cost of an insertion in the read resulting in a gap in the reference sequence. Default = 3, maximum = 3
Deletion cost	3	The cost of a deletion in the read, resulting in a gap in the read sequence. Default = 3, maximum = 3

Insertion open cost	6	The cost of opening an insertion in the read. Lowered as looking for small variations between reference and reads. Default = 10.
Insertion extend cost	1	The cost of extending an insertion in the read. Default = 1
Deletion open cost	6	The cost of opening a deletion in the read. Lowered as looking for small variations between reference and reads. Default = 10.
Deletion extend cost	1	The cost of extending a deletion in the read by 1 base. Default = 1
Length fraction	0.5	Minimum length fraction of read that must match the reference sequence. Default = 0.5 (50%)
Similarity fraction	0.8	Minimum fraction of identity between reads and reference sample. Related to length fraction so 0.8 = >50% of reads have >80% identity. Default = 0.8
Non-specific match handling	Map randomly	When read aligns at >1 place with the same score, the read is mapped randomly

Table 12 - Parameters used to map SNPs in CLC Genomics. Description of parameter options and default values from the CLC Genomics Workbench user manual [154]

Parameter	**Selected**	**Further information**
Ploidy	1	
Ignore positions with coverage above	100,000	Ignores areas of extremely high coverage
Ignore broken pairs	Yes	Ignore reads that may have been mapped in error or other reason resulting in broken pairs
Ignore non-specific matches	Reads	Reads means ignore non-specific matches. Non-specific matches are likely to come from regions of repeats where exact mapping location is uncertain

Minimum coverage	10	Minimum number of valid reads at the current position Default = 10
Minimum count	2	Only variants present in this many reads are included. Default = 2
Minimum variant frequency (%)	35	At least 35% of the reads at a given position should have a different base than the reference to be considered heterozygous
Require presence in both forward and reverse reads	Yes	Variant must be present in both forwards and reverse reads
Base quality filter	Yes	Removes all variants having alleles with an average base quality of less than the given threshold
Neighbourhood radius	5	Default = 5. How far away from the current variant the quality assessment should extend
Minimum central quality	20	Default = 20. Minimum quality score for the central base
Minimum neighbourhood quality	15	Default = 15. Minimum quality score for the neighbourhood
Read direction filter	Yes	Removes variants that are exclusively present in only the forward or reverse reads
Direction frequency (%)	5	Default = 5. Variants that are not present in this frequency of reads from each direction are removed
Relative read direction filter	Yes	Removes variants that are statistically only in forward or reverse reads, not both
Relative read direction filter significance (%)	1	In order to not filter out variants, the significance was set low
Read position filter	No	Similar to the read direction filter but used for sequencing types not studied here

Remove pyro-error variants	No	Remove insertion and deletion variants that occur neighbouring identical consecutive base pairs

Chapter 3 – Production and activity of heterologous malonyl-CoA pathway enzymes in *C. necator* H16

Chapter 3 - Production and activity of heterologous malonyl-CoA pathway enzymes in *C. necator* H16

3.1 Introduction

3.1.1 3-hydroxypropionic acid

3-hydroxypropionic acid (3-HP) is a useful chemical building block that the US Department of Energy considers one of the most important value-added chemicals that has the potential to be made from biomass [106]. This 3-carbon, non-chiral compound can be used to synthesise industrially important products such as biodegradable polymers (polyhydroxyalkanoates) [135], acrylic acid [3] and 1,3-propandiol [155]. The versatility of 3-HP is due to the presence of hydroxyl and carboxyl groups, allowing it to be oxidised, reduced and esterified into desirable commodities for numerous industries. However, to date chemical methods of production have proved uneconomical and environmentally infeasible, using fossil fuels as starting material and the utilisation of expensive and toxic acids [156].

3.1.2 Using genes from the 3-HP bicycle for biosynthesis

Cargill patented the use of the MCR enzyme in a biological method to make 3-HP [122]. Named the malonyl-CoA pathway, the company proposed using the first part of two carbon fixation cycles to create 3-HP from glucose (*via* pyruvate) in heterologous hosts. The idea to overexpress an acetyl-CoA carboxylase (encoded by *acc*) in combination with heterologous expression of the *mcr* gene from *C. aurantiacus* (Figure 8) has been successfully implemented in many different organisms [105]. It has several advantages over other biosynthesis pathways as it is thermodynamically feasible, redox neutral and has the potential to produce 3-HP from a range of substrates [113].

3.1.3 Acetyl-CoA carboxylase

As the first step of fatty acid biosynthesis, ACCs (EC 6.4.1.2) are crucial metabolic enzymes found across all branches of life [157]. The substrate for this enzyme, acetyl-CoA, is the most common acyl-CoA species [158]. This compound is carboxylated to malonyl-CoA, in a biotin-dependent reaction [159]. As a first step, biotin carboxyl carrier protein (BCCP) is covalently attached by an amide bond to the vitamin biotin. The reaction is split into half-reactions, catalysed by 2 subunits: biotin carboxylase (BC) and carboxyltransferase (CT). In the first reaction, the BCCP-bound biotin is carboxylated by BC in an ATP-dependent manner, with CO_2 provided by bicarbonate. In the second half, a carboxyltransferase then transfers the CO_2 from the carboxy-biotin to acetyl-CoA, forming malonyl-CoA. This reaction sequence is described diagrammatically in Figure 11 [160].

Although ACCs are distributed throughout all organisms, generally the same 3 catalytic domains are present; BCCP, BC and CT [161]. Broadly, eukaryotic ACCs are multifunctional polypeptide chains that can assemble to form larger multimers. Eukaryotic ACCs come in 2 isoforms (ACC1 and ACC2), whereas the prokaryotic enzymes are made of separate subunits, encoded distinctly [162]. It is interesting to note that most plants have both types [163]. The rate of transcription of *acc* genes is directly correlated to the rate of cell growth in both *E. coli* and *Bacillus subtilis* [159]. The expression of fatty acid biosynthesis genes must be strictly regulated, as many of the enzymes in the pathway require significant energy investment [164]. Although much is known about the eukaryotic form of ACC, until recently little was known about the regulation in prokaryotes or archaea [162]. In bacteria, the genes for the domains (*accABCD*) tend to be split into 2 operons, located separately on the chromosome. In *E. coli*, the genes for BCCP (*accB*) and BC (*accC*) are organised and translated in a two-gene operon. *accA* coding for the α subunit of CT and *accD* encoding the β subunit are also simultaneously transcribed, but are located almost directly opposite each other in the chromosome [159]. This arrangement is not uncommon and is found in both Gram-positive and -negative bacteria, including *C. necator* but other configurations exist within prokaryotes [165]. For example, in *C.*

glutamicum only genes *accBC* (found in an operon) and *accD1* (also known as *dtsR1*) are required for efficient catalysis [166], [167].

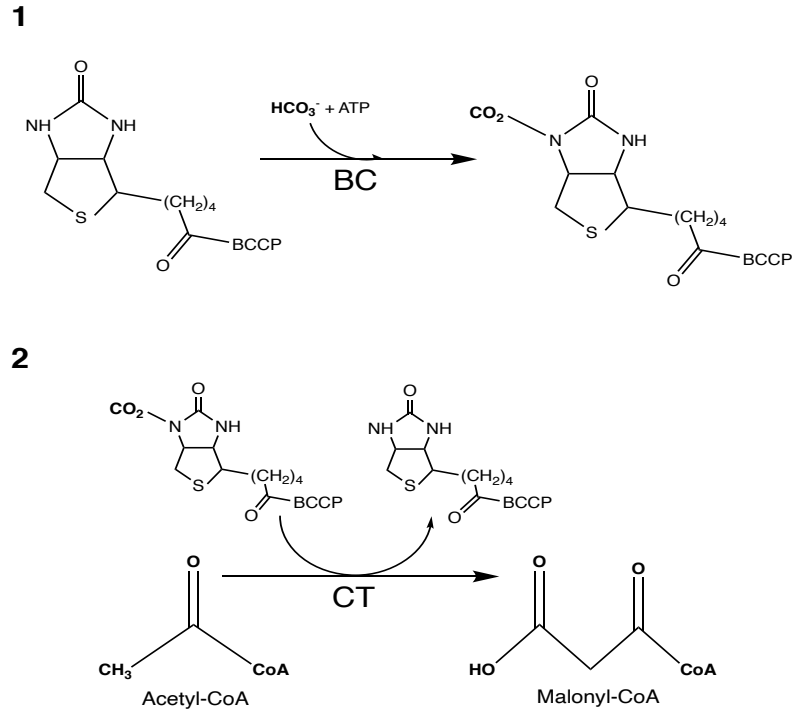

Figure 11 - The ACC catalysed half reactions for the conversion of acetyl-CoA to malonyl-CoA.
Reaction 1 - biotin carboxylase carrier protein (BCCP) is carboxylated by biotin carboxylase (BC). Reaction 2 – acetyl-CoA is carboxylated to malonyl-CoA by the carboxyltransferase (CT) subunit, reverting carboxy-biotin back to biotin. Diagram taken from Smith and Cronan [160]

Due to the importance in controlling fatty acid synthesis, regulation of the catalysis of acetyl-CoA to malonyl-CoA is multifaceted. In many bacteria (with the standard AccABCD configuration) studies suggest that the CT and BCCP/BC subunits are regulated independently [168]. The CT subunit, encoded by *accA* (α) and *accD* (β), is controlled at the translation level [169]. The CT subunit binds to the mRNAs for *accA* and *accD* when acetyl-CoA levels are low, preventing translation. This approach ensures that the stoichiometric ratio of α:β subunits remains, despite the distally located genes. The binding of the mRNA also inhibits the catalytic function of CT, reducing activity of the ACC enzyme. This inhibition is released when acetyl-CoA levels increase, allowing the cell to respond to changing levels [168]. The regulation of BCCP/BC has been studied but the mechanism remains unknown [168]. It has been shown that *accB* autoregulates, as elevated levels of AccB decreased transcription of *accBC.* Downregulation occurs when more BCCP protein is present compared to BC [170].

In the non-standard AccBCD arrangement (such as seen in *C. glutamicum*), the predicted regulatory mechanism is different. It is hypothesised that the acyl-CoA molecules form a complex with the transcriptional regulator FasR, which directly inhibits transcription of the *accBC* and *accD* genes. Binding sites have been shown upstream of the *accBC* and *accD* genes, as well as of *fasA* and *fasB*; genes involved in fatty acid formation [171], [172].

Furthermore, work in *E. coli* shows that accumulated acyl-ACPs are inhibitors of ACC activity by feedback inhibition, preventing fatty acid synthesis [173]. Using palmitoyl-ACP (PACP) as a model acyl-ACP, Evans *et al.* [174] showed that the pantothenic acid arm of the PACP binds allosterically to the complete ACC and acts antagonistically, when the majority of ACPs are bound to an acyl residue. The PACPs exhibit partial competitive inhibition, which can be reversed by acetyl-CoA [174].

The conversion of acetyl-CoA to malonyl-CoA is considered the rate-limiting step in the pathway to fatty acids. Numerous methods for measuring the activity of the ACC enzyme have been described, often finding that the ACC enzyme has the slowest maximum velocity of the fatty acid synthesis (FAS) enzymes [175]. It has been suggested that this will need to be overcome in order to produce acceptable yields of 3-HP in any organism [176]. A common method to increase intracellular malonyl-CoA availability is to overexpress a non-native ACC. This method has been employed successfully in several organisms, in pathways to produce a range of products centred around fatty acid biosynthesis or other secondary metabolites requiring malonyl-CoA as a building block [140], [142], [145]. For example, flavonoid production in *E. coli* was increased by overexpression of the 4 subunits of ACC (each with their own T7 promoter and RBS) from *Photorhabdus luminescens* [177].

Overexpression of homologous or heterologous ACC is a common method of increasing 3-HP production by the malonyl-CoA pathway [135], [137]–[139]. This has previously been attempted in *C. necator* by Arenas-Lopez using an archaeal ACC [24]. In the few archaeal ACCs studied, the reaction from acetyl-CoA to malonyl-CoA is catalysed by one single large enzyme, similar to eukaryotic enzymes. Archaeal ACCs are likely free from the same regulation and acyl-ACP inhibition seen in other enzymes, as they do not use fatty acids in membrane lipid metabolism [178]. For this

reason, an ACC from the archaea *Nitrosopumilus maritimus* was chosen to be tested in *C. necator* by Arenas-Lopez [24]. It was hypothesised that differences in regulation might result in higher expression levels of the expression. Furthermore, it was theorised that introducing heterologous ACCs from distantly related organisms (with distinct fatty acid metabolisms) could reduce the allosteric inhibition by acyl-ACPs. However, the expression of the *N. maritimus* ACC was not successful in the study [24].

Previous studies showed that the overexpression of the *accBCD* operon from *C. glutamicum* resulted in an 8-fold increase in malonyl-CoA formation from acetyl-CoA in the native strain [179]. The protein product of this operon was also successful at increasing malonyl CoA levels 3-fold in *E. coli* [142]. As it has a different genetic arrangement to *C. necator* (3 genes vs. 4 genes), and more is known about the control mechanisms, it was hypothesised that it would be an attractive candidate for overexpression to increase the free malonyl CoA that can be converted to 3-HP [172], [180]. In this study, the genes were combined to form a single operon under the control of the P_{BAD} promoter and overexpressed in *C. necator* as part of the malonyl-CoA pathway to 3-HP.

Previously, quantifying the activity of the ACC enzyme was performed by following the incorporation of [^{14}C]-labelled compounds. The addition of labelled bicarbonate would be added to an assay mixture containing the enzyme and substrate, acetyl-CoA. The bicarbonate is required by the enzyme so the turnover can be followed by quantifying the radioactivity [152]. Due to the dangers and precautions related to the use of radioactive substances, this method is demanding.

The activity of the ACC enzyme can now be assayed using a spectrophotometric approach, requiring the purification of the malonyl-CoA reductase (MCR) enzyme from *C. aurantiacus*. In this method, published by the Fuchs laboratory [152], the reaction couples the ACC catalyzed carboxylation of acetyl-CoA with the reduction of the generated malonyl-CoA by the purified *C. aurantiacus* malonyl-CoA reductase (MCR). This reduction is NADPH dependent, so the ACC activity can be quantified by measuring NADPH consumption using a spectrophotometer at 365 (or 340) nm to follow the oxidation. Theoretically, the carboxylation of 1 acetyl-CoA results in the

reduction of 1 malonyl-CoA, and the production of 2 mol NADP. The study reported close to this value, with 1.8 mol NADP observed per mol of acetyl-CoA [152].

3.1.4 An ACC alternative?

As discussed, several synthetic malonyl-CoA pathways to 3-HP attempted to utilise an overexpressed ACC operon. However, this may often have limited effect due to allosteric competitive inhibition of the enzyme by acyl-ACPs. A novel and promising alternative for the production of malonyl-CoA has been described. This ACC bypass, a methylmalonyl-CoA carboxyltransferase (MMC) from *Propionibacterium freudenreichii* (DSMZ 20271, ATCC 6207, type strain) is able to convert acetyl-CoA and oxaloacetate to malonyl-CoA and pyruvate (Figure 12) [181]. Conventionally, this enzyme would catalyse the reaction methylmalonyl-CoA + pyruvate → oxaloacetate + propionyl-CoA, but in the 1980s it was noted that acetyl-CoA can be accepted as an alternative substrate in this *Propionibacterium* species [182]. The enzyme is comprised of 4 subunits, encoded by 4 genes found in an operon (Table 13). In order to evaluate the effectiveness of the MMC to convert acetyl-CoA to malonyl-CoA, this operon could be implemented in place of the ACC in the 3-HP biosynthesis pathway.

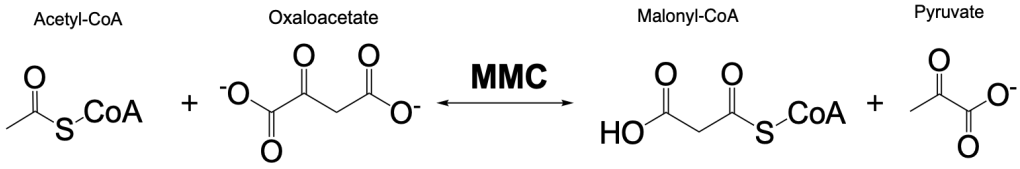

Figure 12 - Reaction schematic showing action of the *P. freudenreichii* MMC enzyme on acetyl-CoA and oxaloacetate to produce malonyl-CoA and pyruvate.

Table 13 - Genes of the *P. freudenreichii* MMC operon, proposed representing subunits of the MMC enzyme (names based on Shin and Lee [181]

Gene	Locus ID (old/new)	Gene Description	Subunit
M18870	RM25_1795/ RM25_RS08850	Oxaloacetate decarboxylase alpha	5S
mmdA	RM25_1794 /RM25_RS08845	Carboxyltransferase	12S
HY	RM25_1793 /RM25_RS08840	Hypothetical protein	Unknown
bccP	RM25_1792 /RM25_RS08835	Acetyl-CoA carboxylase biotin carboxyl carrier protein subunit	1.3S

3.1.5 Malonyl-CoA reductase

In 1989, a novel CO_2 assimilation pathway was discovered in *C. aurantiacus*, and later in other bacteria and archaea [183]. This series of reactions, later named the Fuchs-Holo bicycle, is one of the 6 natural pathways to assimilate CO_2 into cell biomass [184]. Many of the enzymes involved in the bicycle are present in other pathways related to central metabolism and it is thought that this is a relatively recently carbon fixation pathway, that evolved incrementally in species of the order *Chloroflexales*.[185]. It is believed that many of these genes were acquired by horizontal gene transfer, and were retained as they increase the growth rate in the presence of organic acids [186].

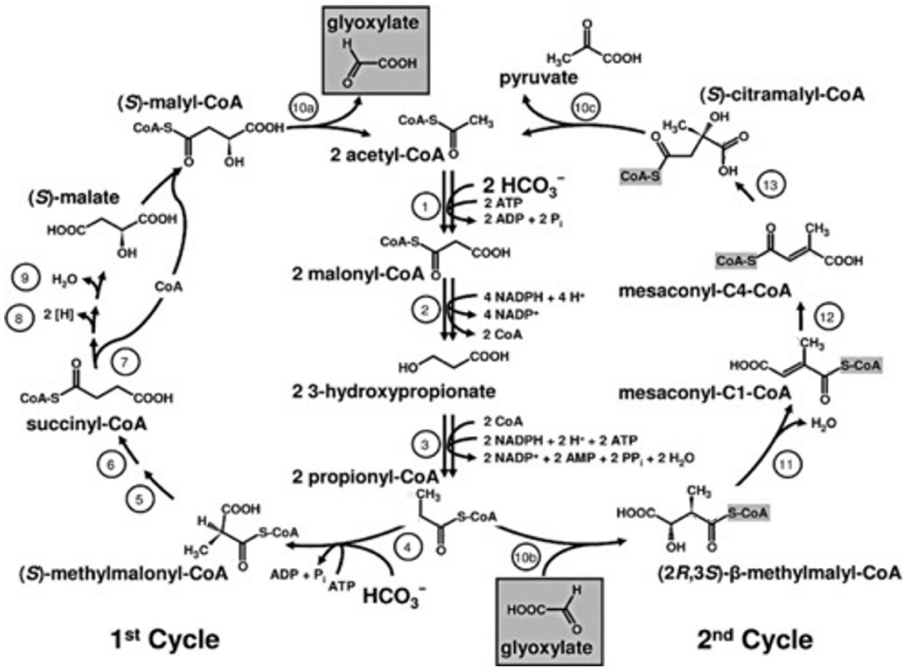

Figure 13 – The 3-HP bicycle in *C. aurantiacus.* Enzymes catalysing the numbered reactions (1) ACC (2) MCR (3) 3-hydroxypropionyl-CoA synthetase, 3-hydroxypropionyl-CoA dehydratase and acryloyl-CoA reductase (4) propionyl-CoA carboxylase, (5) methylmalonyl-CoA epimerase, (6) methylmalonyl-CoA mutase, (7) succinyl-CoA:(S)-malate-CoA transferase, (8) succinate dehydrogenase, (9) fumarate hydratase, (10a,b,c) (S)-malyl-CoA/β-methylmalyl-CoA/(S)-citramalyl-CoA lyase, (11) mesaconyl-C1-CoA hydratase (β-methylmalyl-CoA dehydratase), (12) mesaconyl-CoA C1-C4 CoA transferase, (13) mesaconyl-C4-CoA hydratase.

Also known as the 3-hydroxypropionic (3-HP) bicycle, this sequence starts with acetyl-CoA, which is carboxylated to malonyl-CoA in an ATP and biotin-dependent reaction (Figure 13). This is catalysed by a biotin-dependent acetyl-CoA carboxylase (ACC) enzyme, using bicarbonate as a CO_2 donor. The initial step is followed by the

NADPH-dependent conversion of malonyl-CoA to 3-HP by a malonyl-CoA reductase (MCR) [133]. A propionyl-CoA synthase converts 3-HP to propionyl-CoA. This compound is either converted to (S)-malyl-CoA (via methylmalonyl-CoA, succinyl-CoA and malate) or is combined with glyoxylate to regenerate pyruvate [184]. The 3-HP cycle has the same energy efficiency as the CBB cycle, using ~2.3 mol ATP/mol CO_2 to produce pyruvate [134].

A second natural cycle incorporating 3-HP is found in autotrophic members of the archaeal order *Sulfolobales*, such as *Sulfolobus*, *Archaeoglobus*, *Cenarchaeum* and *Metallosphaera* species [132]. This cycle has been called the hydroxypropionate/hydroxybutyrate (HP/HB) cycle. The first 2 steps from acetyl-CoA to malonyl-CoA and 3-HP are identical to the Fuchs-Holo cycle. The 3-HP is assimilated into succinyl-CoA in a similar fashion, but is then converted to succinate semialdehyde, then 4-hydroxybutyrate (4HB). Using a 4-hydroxybutyryl-CoA dehydratase, the 4HB is converted further via various steps to acetoacetyl-CoA and split into two molecules of acetyl-CoA [187].

The second enzyme in the malonyl-CoA pathway to 3-HP is the malonyl-CoA reductase seen in the 3-HP bicycle and HP/HB cycle. It is encoded by a single gene, *mcr* (GenBank: AY530019.1), but is a bifunctional enzyme, a natural fusion of an aldehyde dehydrogenase domain (MCR-N) and an alcohol dehydrogenase domain (MCR-C). The 135-145 kDa NADPH-dependent protein catalyses the reduction of malonyl-CoA to malonate semialdehyde and finally to 3-HP. As previously explained, this enzyme is part of the CO_2 fixation cycle in some thermophilic organisms [133]. The most studied MCR is found in *C. aurantiacus* and has been used in most synthetic malonyl-CoA pathways across a range of organisms. This gene has also been tagged and purified, to be used in the ACC activity assay described previously [152].

The concept of using the MCR from *C. aurantiacus* DSM 635 to catalyse the reaction of malonyl-CoA to 3-HP has already been demonstrated in *C. necator.* Fukui *et al.* [35] produced the copolymer poly((R)-3-hydroxybutyrate-co-3-hydroxypropionate) (P(3HB-co-3-HP)), with 0.2-2.1 mol % of 3-HP fraction. This was achieved by expressing the genes for MCR and the N-terminal 3-HP-CoA synthetase domain of

the propionyl-CoA synthase (acs_{Ca}), which incorporated free 3-HP-CoA into the copolymer. However, no accumulation of monomeric 3-HP was reported [35].

3.1.6 Improving MCR

Although the traditional 2-enzyme pathway (ACC and MCR) to 3-HP has successfully been implemented in several organisms, modifications have been suggested that could increase the 3-HP yield. Dalwadi and King suggest that a 3-hydroxypropionate dehydrogenase (encoded by $ydfG_{Ec}$ in *E. coli*) must be present alongside the ACC and MCR to maximise 3-HP production [188]. The inclusion of this enzyme should allow sufficient conversion of malonate semialdehyde to 3-HP, reducing the accumulation of the toxic intermediate.

Furthermore, it was hypothesized and proven that dissection of the two subunits, into MCR-N and MCR-C, improves microbial 3-HP production. It was suggested by Liu *et al.* that initial low yield was due to serious imbalance between the enzymes catalysing the 2 half-reactions [113]. The MCR-C fragment reduces malonyl-CoA with NADPH to malonate semialdehyde. The free intermediate is reduced to 3HP by the MCR-N fragment, using a second NADPH (Figure 14). By using a method to alter the level of gene expression, the respective activities can be matched [144]. Liu *et al.* also identified multiple mutation sites that increase the MCR enzyme activity, from 1.51 to 8.37 mmol/min/µmol protein. These changes also lowered the optimal pH from 7.2 to 6.2 [113]. Using site directed mutagenesis, the dissected *mcr* subunit genes were modified to increase 3-HP production.

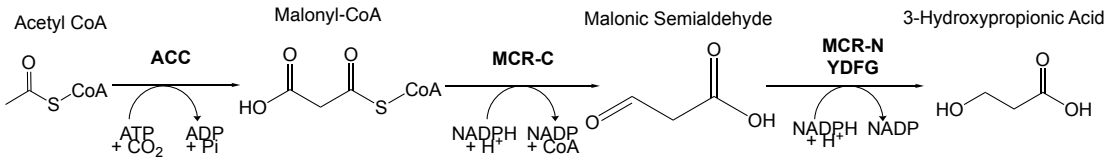

Figure 14 - Schematic of the biosynthesis of 3-HP from acetyl-CoA, via a modified malonyl-CoA pathway. ACC = acetyl-CoA carboxylase from *C. glutamicum*, MCR-C = C terminus of malonyl-CoA reductase from *C. auranticus*, MCR-N = N terminus of malonyl-CoA reductase from *C. auranticus*, $YDFG_{EC}$ = 3-hydroxypropionate dehydrogenase from *E. coli*

3.2 Aims and Objectives

The aim of this chapter was to produce 3-HP in *C. necator* by the malonyl-CoA pathway or one of its derivatives. To achieve this, the objectives were to -

- Implement the traditional malonyl-CoA pathway using an ACC and MCR in *C. necator* for production of 3-HP
- Modify the plasmid-based system to express alternative or additional enzymes.
    - Including an MMC (instead of ACC) to convert acetyl-CoA to malonyl-CoA, in order to overcome inhibition
    - Addition of a 3-hydroxypropionate dehydrogenase enzyme from *E. coli*, coded for by $ydfG_{Ec}$ to reduce toxic intermediates
    - Modification of the *mcr* gene, dissecting the distinct functional subunit and introducing point mutations that increase activity
- Test the expression and activity of the enzymes produced to understand the mechanisms behind the inability to produce 3-HP

3.3 Results

3.3.1 Testing of MCR candidates

To achieve the overall goal of 3-HP production, it was first necessary to test whether introduction of *mcr* genes from various origins resulted in their expression and hence measurable enzymatic activity. *C. aurantiacus* belongs to the green non-sulphur bacteria and is thermophilic, growing at temperatures up to 70°C [133]. Hence its MCR may not be best suited for metabolic pathways operating at 30°C e.g., in *C. necator*. Alternatives exist such as the MCR produced by the related mesophilic *Oscillochloris trichoides* and the ammonia-oxidizing archaeon *Nitrosopumilus maritimus* [189], [190].

Working with plasmids pBBR1-P_{phaC}-mcr_{635}, pBBR1-P_{phaC}-mcr_{osc} and pBBR1-P_{phaC}-mcr_{nit} from Arenas-Lopez [24], carrying the the *mcr* genes from *C. aurantiacus*, *O. trichoides* and *N. maritimus*, respectively, the activity of the encoded 3 MCR candidates was established in cell extracts of *C. necator* H16 Δ3. As outlined above, this was done using a spectrophotometric enzyme assay, measuring the oxidation of NADPH (see methods 2.15). Although Arena-Lopez [24] had previously established that the introduction of these plasmids did not result in 3-HP production in *C. necator*, protein gels and enzyme assays had suggested that the genes were being expressed. The enzyme assay performed in this study confirmed these results and showed that the MCR enzyme from *C. aurantiacus* (from here on referred to as MCR_{635} to indicate that it originated from the DSM 635 strain, also known as ATCC 29366, NCBI:txid324602) had the highest activity at 0.025 µmol min^{-1} mg^{-1} (Figure 6). This was significantly ($p < 0.0001$) different from the MCR enzymes from *N. maritimus* and *O. trichoides* (both 0.006 µmol min^{-1} mg^{-1}) and the empty-plasmid control (0.004 µmol min^{-1} mg^{-1}). The measured specific activities of the *C. aurantiacus* enzyme in *C. necator* crude extracts at 30°C were similar to those reported for cell extracts of the native organism at 55°C, which showed a specific activity of 0.08 and 0.03 µmol min^{-1} mg^{-1} for autotrophically and heterotrophically grown cells, respectively [144]. This suggested that further improvements might be made the heterologous expression of the gene e.g., by modifying copy number, promoter, RBS or operon arrangement.

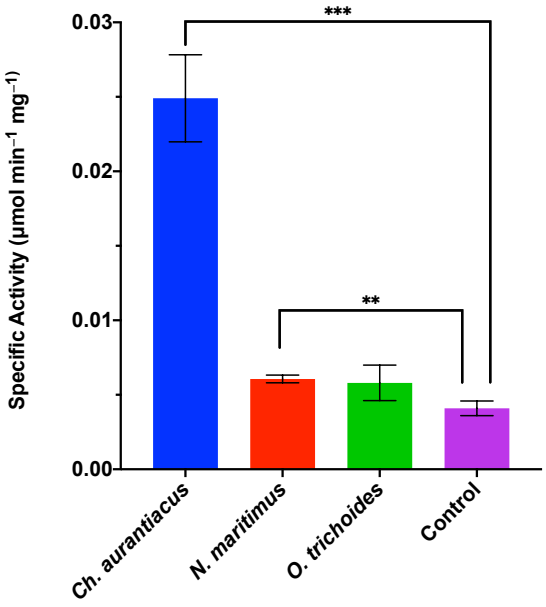

Figure 15 - Specific MCR activity in crude extracts of *C. necator* H16 strains episomally expressing *mcr* genes from *C. aurantiacus*, *N. maritimus* and *O. trichoides*. **(p value < 0.001), *** (p value < 0.0001). Error bars mean ± SD, n = 3.

3.3.2 Heterologous production of MCR in *E. coli* and generation of cell lysates

Once activity of MCR_{635} was confirmed, the gene was overexpressed, and the protein purified to compare specific activities to those reported in the literature for the pure enzyme. Furthermore, pure MCR was needed to measure the activity of the ACC enzyme in a coupled enzymatic assay, based on the conversion of the generated malonyl-CoA by the *C. aurantiacus* MCR enzyme. This required the production of a tagged MCR to allow rapid purification as described by Kroeger *et al* [152].

In order to express and quantify the activity of the enzyme, the mcr_{635} gene was fused to a histidine tag encoding sequence. This construct, $pMCR_{635}$-His, was transferred into *E. coli* Lemo21 cells, to allow fine tuneable expression of the generated tagged gene through addition of the inducer rhamnose. The produced protein was purified using nickel affinity chromatography columns. The MCR protein was observable in the elution fractions between 155 kDa and 140 kDa (Figure 16A and B). This was confirmed by Western blot, using an Anti-His antibody (Figure 16C). The elution fractions were concentrated. Elution 3 was particularly pure so was quantified by Bradford assay and found to contain 362 µg/ml protein. This enzyme was aliquoted,

and glycerol was added to the concentrated fractions to a final concentration of 20% (v/v) to prevent freeze/thaw damage and stored at -20ºC.

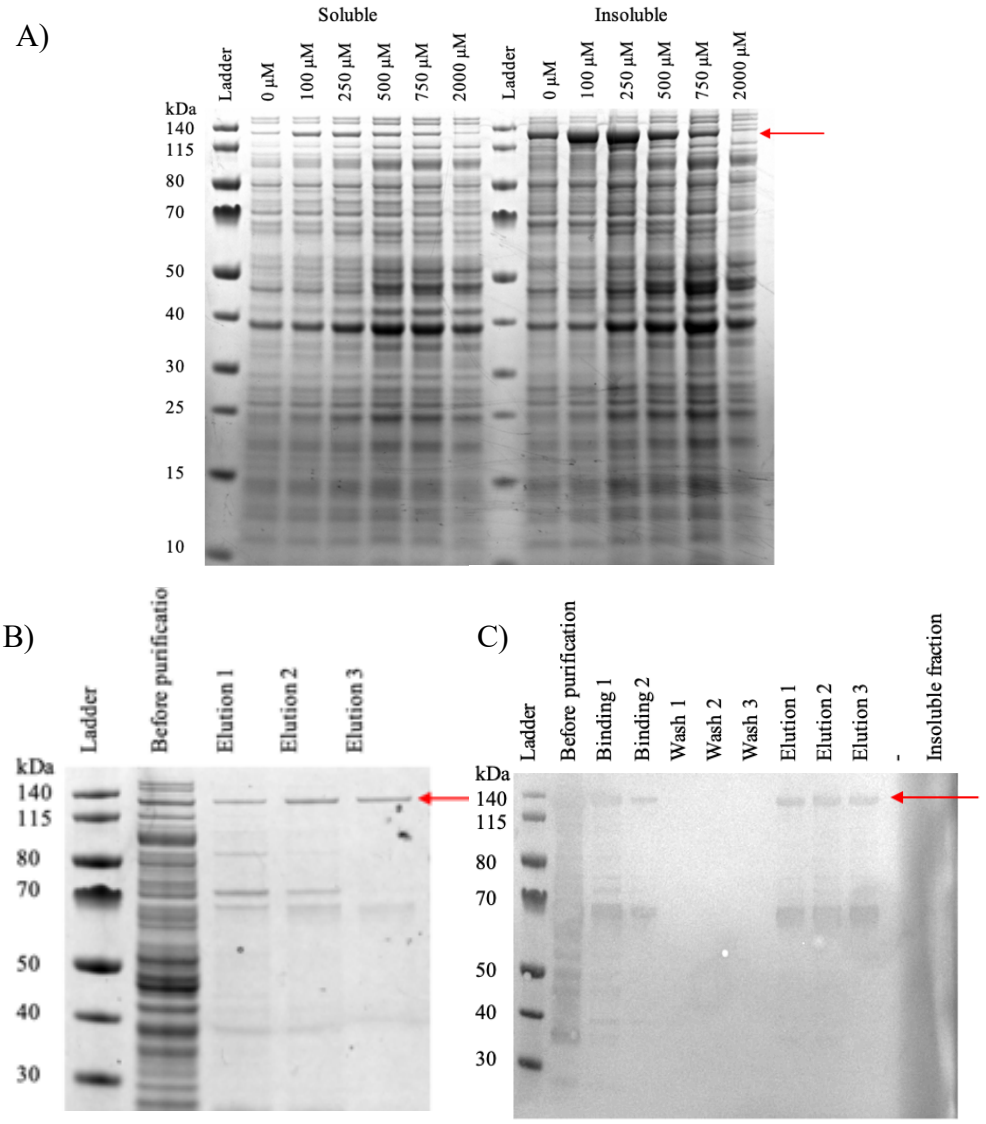

Figure 16 – Purification of MCR6$_{35}$ A) SDS-PAGE analysis of MCR$_{635}$ expression levels in *E. coli* Lemo21(DE3) pMCR$_{635}$, induced at different concentrations of L-rhamnose, ranging from 0-2000 µM and 400 µM IPTG. The soluble fractions are shown on the left, insoluble on the right. 10 µl samples were taken from the lysates and boiled in a 1:1 ratio with loading buffer. 6 µl of this boiled lysate was loaded. B) SDS-PAGE analysis of final elution fractions of His-tagged MCR$_{635}$ after nickel column purification from *E. coli* Lemo21(DE3) cell extracts. Extracts were obtained from *E. coli* Lemo21(DE3) pMCR$_{635}$ induced with 500 µM L-rhamnose and 0.04% IPTG. C) Western blot on fractions collected during purification with nickel column, using anti-His tag antibody to detect the His tagged MCR protein, visible in the elution fractions.

3.3.3 Validation of MCR activity

The activity of the purified MCR enzyme was tested by addition of malonyl-CoA, monitoring the oxidation of NADPH to NADP at 340 nm, as the substrate is converted to 3-HP (Figure 17A). The protein was active, but the change in absorbance was low. The assay with 5 µg MCR added showed a linear reduction that continued for more than 8 minutes until the end of the experiment (data for 5 µg shown in Figure 17B). The specific activity was calculated to be 0.05 µmol min^{-1} mg^{-1}.

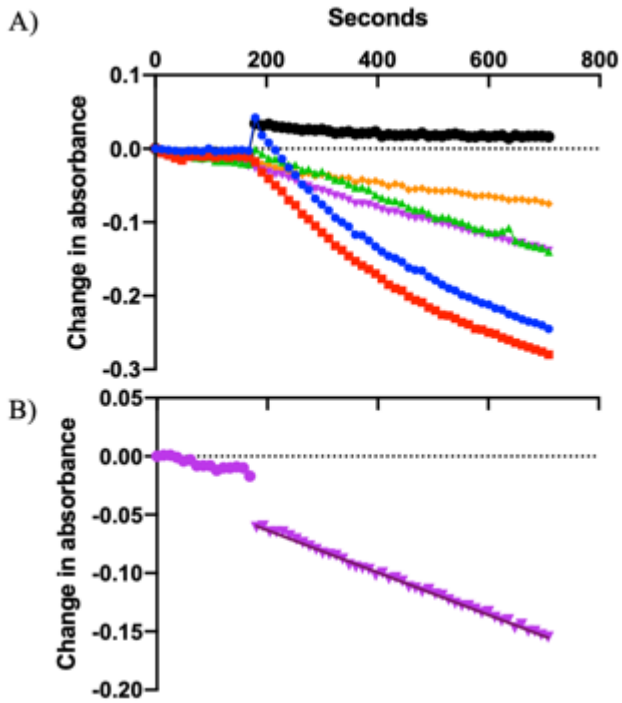

Figure 17 – Spectrophotometric assay used to determine the specific enzyme activity of purified MCR. The change in absorbance was followed photometrically at 340 nm, to monitor the oxidation of NADPH. The amount of purified MCR protein used in the reaction were differed between 0 µg and 40 µg. The reaction was started by the addition of 0.3 mM malonyl–CoA at 180 seconds. A) Each line indicates a different amount of MCR; blue circles = 40 µg, red squares = 20 µg, green triangles = 10 µg, pink triangles = 5 µg, orange rhombus = 2.5 µg, black circles = 0 µg (extra buffer added as control). B) Showing data for reaction mix containing 5 µg purified MCR.

3.3.4 Design and construction of plasmids for heterologous expression of the malonyl-CoA pathway

The project began with 1st generation plasmids (Figure 18), built by a previous PhD student, Christian Arenas (University of Nottingham). These plasmids, pBBR1-P_{phaC}-*accCB-dtsR1* and pME6032Δ*lacIQ*-P_{tac}-mcr_{635}, contained the required genes for the 3-HP biosynthetic pathway, i.e., the *C. glutamicum acc* genes (acc_{Cg}) and the *C.*

aurantiacus DSM 635 *mcr* (*mcr*$_{635}$) gene under control of the *phaC* and P$_{tac}$ promoter, respectively. These were tested in *C. necator*, but failed to produce 3-HP. They were hence modified as follows to generate a set of 2nd generation constructs: (i) plasmid backbones were upgraded to a modular vector format as designed for *C. necator* (created by Muhammed Elsaan, University of Nottingham) to facilitate further future changes and (ii) an inducible promoter was introduced for controlling *acc* expression.

In the second generation of improved vectors for 3-HP production (Figure 18), the plasmid pMTL71301 encoded the promoter of the arabinose *araBAD* operon (called P$_{BAD}$), and the gene encoding the regulator of this promoter (*araC*). The *acc* pseudo-operon (combining *accCB* and *dtsR1* from *C. glutamicum*) was amplified from plasmid pBBR1 P$_{phaC}$ *accCB-dtsR1* and introduced into pMTL71301, to give pMTL71301_*acc*. The gene *ydfG*$_{Ec}$ from *E. coli* was added to the pathway, to create the plasmid pMTL71301_*acc_ydfG*$_{Ec}$ in the second generation, providing another enzyme that can convert malonate semialdehyde to 3-HP.

As outlined in section 1.4, an alternative pathway from acetyl-CoA to malonyl-CoA can be achieved by implementing the genes encoding a methylmalonyl-CoA carboxyltransferase (MMC) from *P. freudenreichii*. The genes encoding the 4 subunits of this enzyme were synthesised by ThermoFisher. Three codon optimised "gene strings" (sequences in appendix 7.1) were amplified used to construct the plasmid named pMTL71301_*mmc* in the second generation. Each of the aforementioned pMTL71301 derivatives were matched with pMTL74111_*mcr*, harbouring the MCR protein with a constitutive P$_{tac}$ promoter, to complete the 3-HP pathway. This was possible because these vectors contained compatible origins of replication and could be selected for by different antibiotics (pBBR1 origin of replication (ori) and tetracycline resistance for the pMTL71301 derivatives, and ori *IncP* and ori *ColEI* and chloramphenicol for pMTL74111).

During construction of pMTL71301_*mmc*, issues arose with mutations appearing in the coding region of the *mmc* operon. This problem was initially corrected by site directed mutagenesis. However, upon sequencing, a second SNP was discovered within the operon. To resolve, an *E. coli* strain with low evolvability and a low mutation rate was selected. Use of the strain MSD42 allowed the cloning to be

completed. 3-HP production experiments were performed in this strain as shown in sections 3.3.7. This plasmid was tested alongside the other 2nd generation plasmids in this MSD42 strain, but no 3-HP was seen.

Issues emerged with introducing and maintaining two separate plasmids in *C. necator,* as detailed in section 3.3.5. Therefore, all pathway components were combined into single constructs as outlined in section 3.3.4 and Figure 7, generating 3rd generation plasmids pMTL71301_*acc_mcr*, pMTL71301_*acc_ydfGEc_mcr* and pMTL71301_*eyfp_mcr*. To achieve this, the second-generation vectors were digested and the *mcr* gene and associated P_{tac} promoter were added downstream of the bidirectional terminator.

Further variations of the above 3rd generation plasmids were generated to improve activity of MCR_{635}. and putting them under control of two different promoters, P_{tac} and P_{15}, according to details in Liu [144]. Following up on the reported improvements in terms of MCR activity and 3-HP production in *E. coli* [113], achieved after separate expression of N- and C-terminal MCR domain encoding *mcr* gene sections (here referred to as mcr_N and mcr_C), an analogous strategy was adopted for *C. necator*. mcr_N and mcr_C coding regions were designed as described by Liu *et al.,* [113] encoding domains comprising amino acids 1-549 and 550-1219 respectively, with expression driven by P_{tac} and P_{15} promoters. The constructs called "final plasmids (4th generation)" in Figure 18, are represented by pMTL71301_*acc_*mcr_m, pMTL71301_*acc_ydfGEc_*mcr_m and pMTL71301_*mmc_*mcr_m

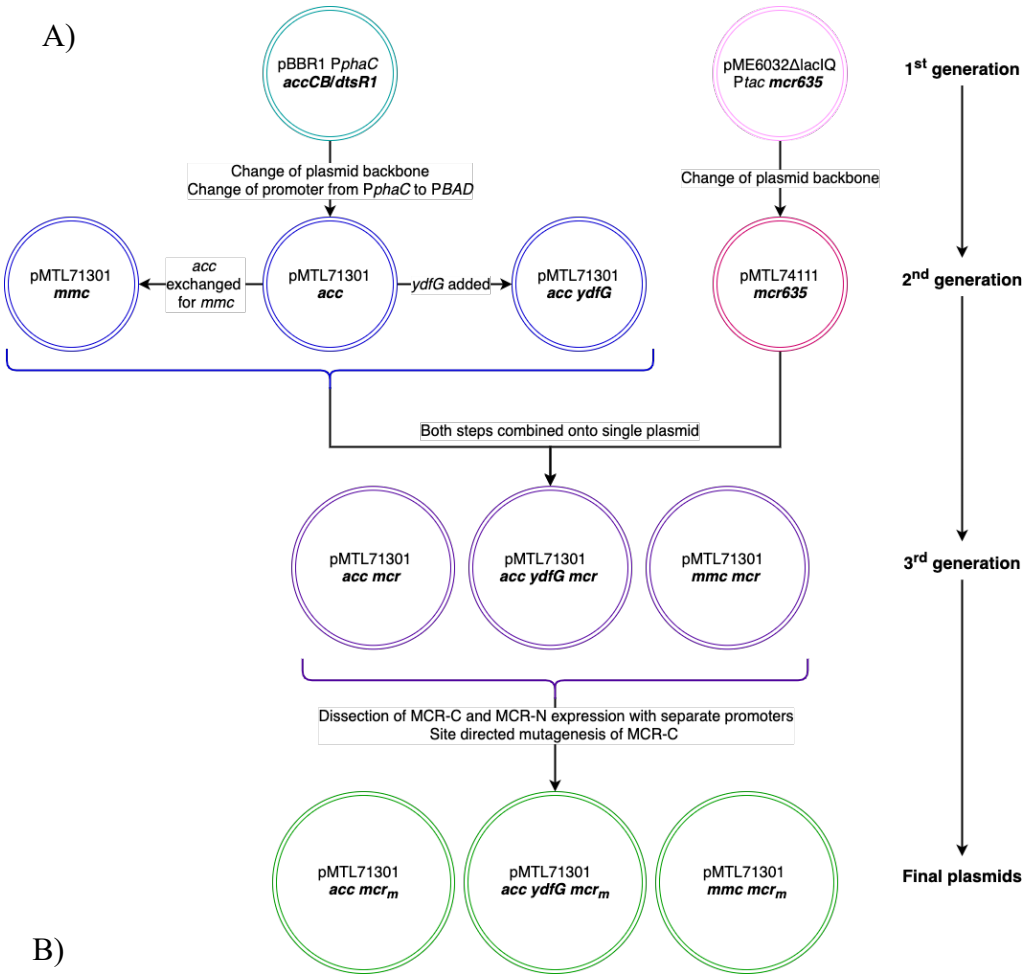

B)

1st generation	pBBR1 P*phaC accCB/dtsR1* + pME6032 ΔlacZ P*tac mcr635*	P*PhaC* → *accC* → *accB* → *dtsR1* + P*tac* → *mcr635*
2nd generation	pMTL71301_*acc* pMTL71301_*acc_ydfG* pMTL71301_*mmc* + pMTL74111 P*tac mcr635*	P*BAD* → *accC* → *accB* → *dtsR1* P*BAD* → *accC* → *accB* → *dtsR1* → *ydfG* P*BAD* → *M1870* → *mmdA* → *HY* → *BCCP* + P*tac* → *mcr635*
3rd generation	pMTL71301_*acc_mcr* pMTL71301_*acc_ydfG_mcr* pMTL71301_*mmc_mcr*	P*BAD* → *accC* → *accB* → *dtsR1* ↔ P*tac* → *mcr635* P*BAD* → *accC* → *accB* → *dtsR1* → *ydfG* ↔ P*tac* → *mcr635* P*BAD* → *M1870* → *mmdA* → *HY* → *BCCP* ↔ P*tac* → *mcr635*
Final plasmids	pMTL71301_*acc_mcrm* *pMTL71301_acc_ydfG_mcrm* pMTL71301_*mmc_mcrm*	P*BAD* → *accC* → *accB* → *dtsR1* ↔ P*tac* → *mcrN* → P*15* → *mcrC* P*BAD* → *accC* → *accB* → *dtsR1* → *ydfG* ↔ P*tac* → *mcrN* → P*15* → *mcrC* P*BAD* → *M1870* → *mmdA* → *HY* → *bccP* ↔ P*tac* → *mcrN* → P*15* → *mcrC*

Figure 18 – A) Schematic diagram of plasmids constructed to achieve 3-HP production in *C. necator* H16. Plasmid names are given. Genes are indicated in bold and italics. Subscript M indicates that the genes contain mutations to improve protein activity. Operon *accCB-dtsR1* encodes the subunits of acetyl-CoA carboxylase from *C. glutamicum*. *ydfGEc* encodes 3-hydroxy acid dehydrogenase from *E. coli.* The operon *mmc* encodes a methylmalonyl-CoA carboxyltransferase from *P. freudenreichii,* consisting of 4 genes *M1870*, *mmdA*, *HY* and *bccP* (names from Shin *et al* [181]. Gene *mcr* encodes malonyl-CoA reductase from *C. aurantiacus*. mcr_{365} indicate the complete *mcr* gene from strain DSMZ 635. The modified version of the *mcr* gene is indicated by mcr_m. In mcr_m, $mcr\text{-}_N$ and $mcr\text{-}_C$ encoding the separate domains of the naturally fused MCR are under the control of different promoters. Changes in the base sequence of $mcr\text{-}_C$ were made to increase the activity. B) Gene organisation on the plasmids, showing promoters controlling genes necessary for 3-HP production from acetyl-CoA. Both pBBR1 and pMTL71301 plasmids have the pBBR1 origin of replication, pME6032 has both pVS1 ori, and p15A ori. and pMTL74111 has IncP/ColE1 ori. Arrows indicate direction of transcription. Bidirectional terminator indicated on the arrow as a red loop.

3.3.5 Expression of heterologous enzymes for 3-HP production in *C. necator*

Initially, *C. necator* H16 Δ3 cells were transformed with the first generation plasmids (pBBR1-P$_{phaC}$-*accCB-dtsR1* and pME6032Δ*lacIQ*-P$_{tac}$-*mcr*$_{635}$) provided by Arenas-Lopez, or appropriate control plasmids [24]. As reported previously, no 3-HP was seen in the supernatant. The growth of the strain bearing the two biosynthesis plasmids was slightly slower than that of the control strain, as seen in Figure 19.

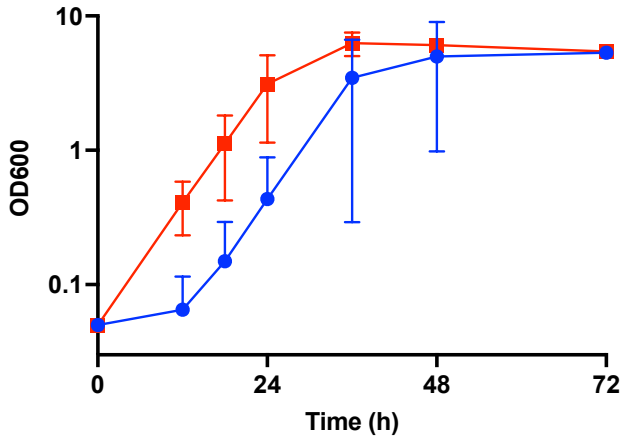

Figure 19 - Growth profile for *C. necator H16* Δ3 strains with 3-HP biosynthesis genes encoded on two separate plasmids (1st generation). Cultures were initially inoculated to an OD_{600} of 0.05 and grown in SG-MM in the presence of tetracycline and chloramphenicol to select against plasmid loss. Blue circles = strain carrying plasmids pBBR1-P$_{phaC}$-*accCB-dtsR1* and pME6032Δ*lacIQ*-P$_{tac}$-*mcr*$_{635}$. Red squares = strain carrying plasmids pBBR1-P$_{phaC}$-*eyfp* and pME6032Δ*lacI*Q-P*tac-eyfp*. Error bars mean ± SD, n = 3.

Several modified malonyl-CoA pathways were established as outlined in Figure 18, and the genes split over 2 vectors for expression. The same genes were used as for the first generation, but promoters and plasmid backbones were changed to modular vectors, pMTL71301 and pMTL74111. However, problems occurred when introducing the plasmids into *C. necator* H16 Δ3. Sequential transformations yielded few colonies on double antibiotic plates. Slow growth and lack of growth was seen during overnight cultures, suspected to be due the loss of one or more of the plasmids. In order to test for the presence of the plasmids, the resulting overnight cultures were plated on LB media plates with either tetracycline, chloramphenicol or both. Few bacterial colonies appeared on the plates containing chloramphenicol, but a large number of colonies propagated on tetracycline containing media. These results indicated that the pMTL74111 plasmid, carrying chloramphenicol resistance gene

catP, was not present in the H16 Δ3 cells. This was further confirmed by absence of product after PCR amplification of segments of the *acc* and *mcr* genes.

Given the issues encountered with parallel maintenance of second-generation plasmids, the constructed single 3rd generation plasmids were introduced into *C. necator.* Although growth on solid minimum media was normal, the H16 Δ3 strains bearing these plasmids only grew to higher ODs in LB (data not shown). The strains grew very slowly in SG-MM (taking over 72 hours for OD to increase) and did not grow at all in fructose minimal media. Growing the initial seed culture in LB before inoculation of SG-MM was also attempted, but again very slow/no growth was seen.

3rd and 4th generation plasmid had been constructed in parallel and sequenced to ensure they were correctly assembled and carried no mutations. However, for *C. necator* H16 Δ3 strains carrying 4th generation plasmids it was not possible to attempt a cultivation due to time restraints caused by COVID-19-related limitation of laboratory access. It was hoped that whatever issues caused the lack of growth of cells harboring the 3rd generation of plasmids could be overcome first. Further work would include transforming H16 Δ3 with these plasmids and performing the cultivation in minimal media with different carbon sources.

The remaining experiments in this chapter aimed to understand why 3-HP production was not possible using the current strategy in *C. necator*. Work was undertaken in *C. necator* where feasible, and *E. coli* when this was not possible. As previous work had shown Mcr_{635} to be active, these investigations focused on confirming expression and activity of the other introduced genes.

3.3.6 Assaying the activity of the ACC enzyme, using a coupled spectrophotometric assay dependent on the previously produced MCR enzyme

C. necator H16 Δ3 carrying pMTL71301_*acc* was used to determine whether the enzyme ACC from *C. glutamicum* was expressed in this background. Using crude extract from cells grown overnight in SG-MM, the activity of the enzyme was monitored using the coupled enzyme assay described by Kroeger et al. (2011) (see methods 2.15.) with 5 µg purified MCR added. For the assay to provide accurate ACC activity data, MCR activity had to be provided in excess. Hence this amount had been

chosen as a starting concentration which could be further increased or decreased if necessary. The overall reaction was started using acetyl-CoA, to be converted by the ACC to malonyl-CoA. This then serves as the substrate for the MCR enzyme, reducing malonyl-CoA to 3-HP. This reaction can be detected by monitoring the change in absorbance at 340 nm, as it is coupled to the oxidation of NADPH. The amount of crude extract added was varied to find the optimum. However, no change in absorbance was seen for any of the differing amounts, nor was a background signal seen from the native ACC. This implies that the assay was not operating as desired, and it was not possibly to measure ACC activity in this manner. For this reason, other methods were considered to evaluate the conversion of acetyl-CoA to malonyl-CoA

3.3.7 Expression of heterologous enzymes for 3-HP production in E. coli

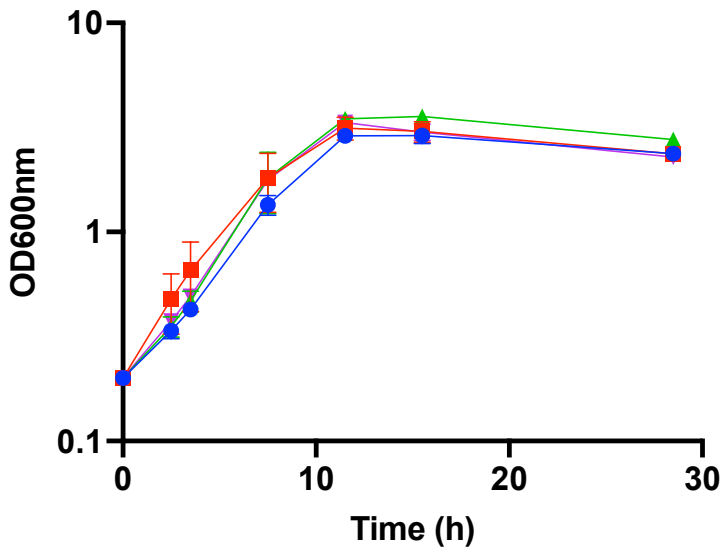

Figure 20 - Growth profile for *E. coli* MDS42 strains with 3-HP biosynthesis genes encoded on two separate plasmids 2nd generation). Cultures were initially inoculated to an OD_{600} of 0.2 and grown in LB in the presence of tetracycline and chloramphenicol to select against plasmid loss. Gene expression was induced at 7.5 hours with 5 mM arabinose. Blue circles = strain carrying plasmids pMTL71301-*acc* and pMTL74111-mcr_{365}, red squares = strain carrying plasmids pMTL71301-*acc-ydfGEc* and pMTL74111-mcr_{365}, green triangles = strain carrying plasmids pMTL71301-*mmc* and pMTL74111-mcr_{365}. Pink triangles = control strain carrying pMTL71301-*eyfp* and pMTL74111-*rfp*. Error bars mean ± SD, n = 3To see if the genes were being expressed, and proteins produced, SDS-PAGE was performed on the samples taken at 12 hours, to allow time for protein synthesis after induction with arabinose at 7.5 hours.

After it proved difficult to sustain two plasmids simultaneously in *C. necator*, the combination of plasmids detailed in Figure 18A second generation were inserted into *E. coli* MDS42 to test for 3-HP production: pMTL71301_*acc*, pMTL71301_*acc*_$ydfG_{Ec}$ and pMTL71301_*mmc* were individually combined with pMTL74111_mcr_{635}. MDS42 was chosen as it is a low evolvability strain, reducing

mutations [147]. The growth profiles for all the generated strains were similar (Figure 20), with no inhibition by *acc* expression, but the amount of 3-HP produced was below the limit of detection.

Given the absence of 3-HP production in the generated *E. coli* strains, the protein profiles for each strain were analysed by SDS-PAGE to establish whether or not the introduced genes were expressed and resulted in detectable protein production (Figure 11). The three *E. coli* MDS42 strains carrying pMTL74111_*mcr* and either pMTL71301_*acc*, pMTL71301_*acc_ydfG*$_{Ec}$ or pMTL71301_*mmc* were grown in M9 minimal media for 3 hours before induction with 0.1% arabinose and incubated for a further 12 hours. This experiment was performed in triplicate and samples were taken at the point of induction ("0-hour sample") and twelve hours later ("12-hour sample) and compared to those of an empty-plasmid MDS42 control strain. Although the subunits of ACC coded for by *accBC* and *dtsR1* were visible in the soluble fraction (Figure 21A), the levels were low and most product was insoluble. Furthermore, due to their similar size of 63 and 58 kDa, they could not be distinguished and hence it is possible that only one of them was expressed. The *E. coli YdfG*$_{Ec}$ protein was also visible and soluble (Figure 21B). The higher molecular weight (56.7 and 54.7 kDa) subunits of the MMC enzyme were apparent on the SDS-PAGE gels (Figure 21C). Overall, this suggested that the genes on the pMTL71301 plasmids are being expressed. However, the Mcr enzyme from *C. aurantiacus* was not seen in the soluble fraction at all but is clear in the insoluble fraction at 130 kDa. Given the measured MCR activities described for *E. coli* in section 3.3.2, it remained unclear whether this was one of the reasons why 3-HP was not produced in detectable amounts.

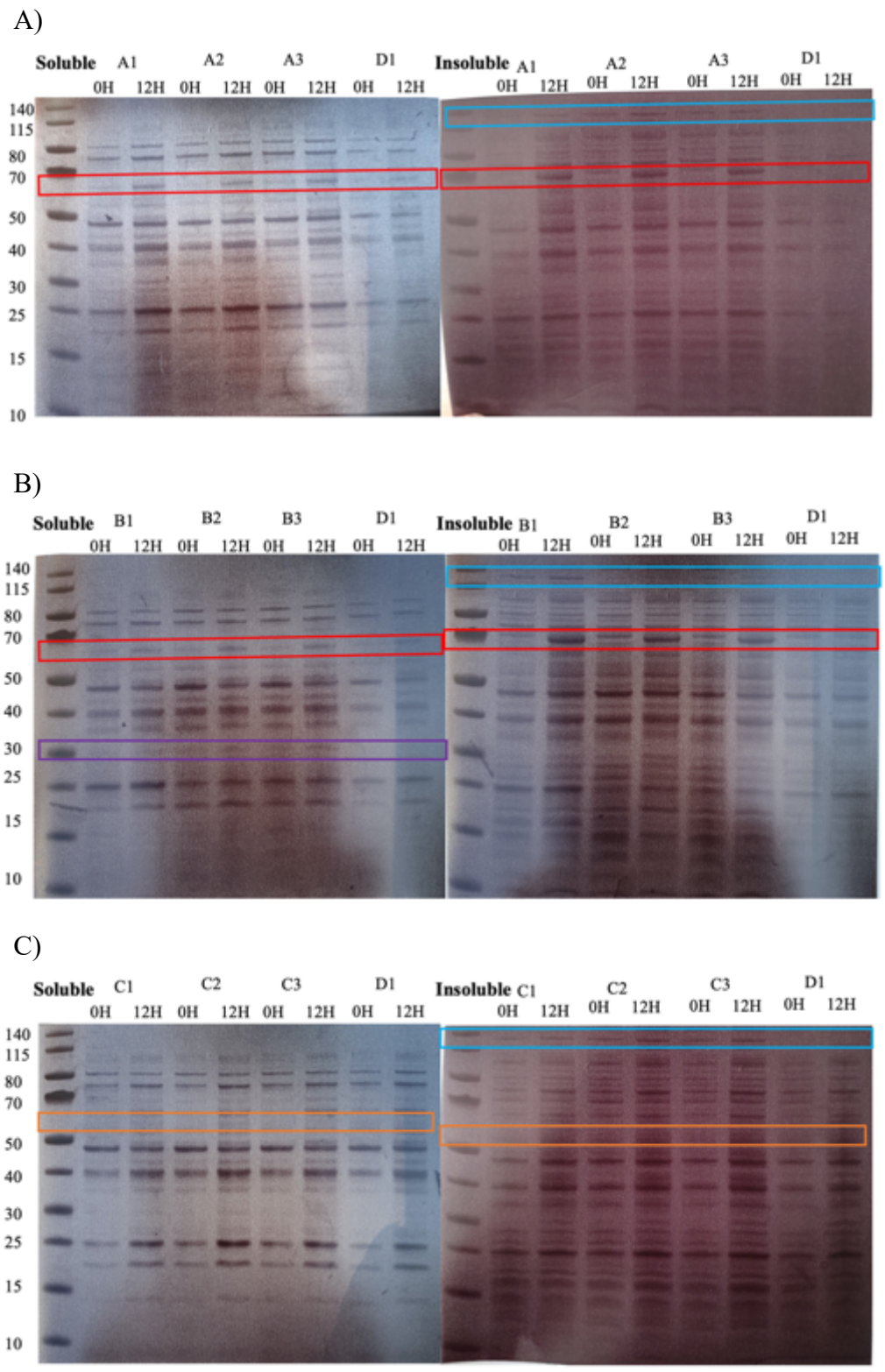

Figure 21 – SDS-PAGE images showing the protein products from *E. coli* MDS42 carrying 3-HP biosynthesis genes on two separate plasmids. Soluble fraction on the left-hand side, insoluble on the right. D1 is the empty-plasmid MSD42 control strain. 0H, 0-hour sample; 12H, 12-hour sample. Red box = AccBC and DtsR1 (AccD) at 63 and 58 kDa. Blue box = Mcr from *C. aurantiacus* at 130 kDa, in the insoluble fraction only. Purple box = *YdfGEc* from *E. coli* at 30 kDa. Orange box = MMC subunits at 55 and 57 kDa. A) pMTL71301_*acc* + pMTL74111_mcr_{635}. A1, A2 and A3 denote replicates. B) pMTL71301_*acc_ydfGEc* + pMTL74111_mcr_{635}. B1, B2 and B3 denote replicates. C) pMTL71301_*mmc* + pMTL74111_mcr_{635}. C1, C2 and C3 denote replicates.

3.4 Discussion

3.4.1 Testing of MCR candidates

Following work completed by Arenas-Lopez [24], MCR enzymes were tested in *C. necator* to confirm that they were active. Of the 3 tested, the enzyme from *C. aurantiacus* had the highest activity, comparable to results seen previously [24]. This experiment was performed at 30°C, the optimum temperature for *C. necator,* but much lower than the optimum for the enzyme from *C. aurantiacus*, which is reported to be 57°C [152]. However, it still had the highest activity of the 3 and the gene from this construct was used in further experiments.

The 3 candidates were chosen to cover multiple structural types and, presumably, temperature optima. The enzymes from *C. aurantiacus* and *O. trichoides* are encoded by single gene called *mcr*, whereas 2 separate genes from *N. maritimus* are necessary to encode the enzymes that catalyse the reaction from malonyl-CoA to 3-HP [24], with malonic semialdehyde (MSA) forming the intermediate of this reaction sequence. The first reaction from malonyl-CoA to MSA is catalysed by MCR. The second enzyme, malonic semialdehyde reductase (*msr*) from this organism has been characterised in *E. coli* [190]. In this current study, only very low activity was seen when the *mcr*/*msr* gene combination from *N. maritimus* was expressed in *C. necator*. The activity of the enzyme was only 1.5-fold higher than those observed for the empty plasmid control strain. It is unfortunate that this enzyme does not function well in *C. necator* as it can utilize both NADH and NADPH, which could relieve the need for NADPH exclusively (as seen in other MCR enzymes) [190]. Given more time, this enzyme could have been improved, however the experiments continued with the better performing enzyme available.

The use of the MCR from *O. trichoides*, alongside $YdfG_{Ec}$ (hydroxypropionic acid dehydrogenase) and MmsB (hydroxyisobutyrate dehydrogenase), has been mentioned in a patent by OPX Biotechnologies Inc., but no other data on the enzyme could be found at time of writing [191]. However, it can be presumed that the optimum temperature of the enzyme would be closer to 30°C as *O. trichoides* grows optimally at 28°C [192]. This was also the reason why it had been selected for the current study.

Unfortunately, its production in *C. necator* resulted in very low activity (Figure 15), so no further work was attempted with this construct.

In the future, it may be worth investigating the reasons for the poor performance of the *N. maritimus* and O. *trichoides* enzymes. It is possible that protein production was poor due to suboptimal codon usage or that there were other addressable causes for low level transcription and/or translation.

3.4.2 Validation of MCR activity for the His-tagged purified enzyme

Since the activity of MCR_{635} had been demonstrated, a histidine tagged fusion protein was produced and purified. The purified MCR enzyme was shown to be active by suppling the substrate, malonyl-CoA, and monitoring the oxidation of 2 molecules of NADPH that occurs as the final product (3-HP) is formed. Varied amounts of the enzyme were included in the reaction mix to ensure that the activity of the enzyme can be measured in an appreciable amount of time.

The most appropriate amount of MCR enzyme in this study was found to be 5 µg and the reaction was linear throughout. The activity was calculated to be 0.05 µmol min^{-1} mg^{-1}. This may be partially explained by the lower than ideal temperature used in this study. The MCR protein originates in a thermophilic organism and activity was shown to be highest at 55 – 60°C [152], whereas the assay was performed at 30°C, the optimum growth temperature for *C. necator*. As production of 3-HP in this organism will take place at this lower temperature, accurate rates were required for the enzyme in these conditions. However, in the specific activity reported by Kroeger *et al.* [152] was around 3 µmol min^{-1} mg^{-1} at 30°C, much higher than this enzyme's specific activity of 0.05 µmol min^{-1} mg^{-1}. It is suspected that the majority of the purified enzyme was inactive. Whilst still soluble or in suspension during the purification process, it may not have been properly folded, as suggested by the presence of large amount of insoluble product, or it may have become increasingly insoluble during storage.

3.4.3 Construction of improved plasmids for the production of ACC_{Cg} and MCR635

Literature search suggested that the ACC_{Cg} and MCR_{635} candidate chosen by Arenas-Lopez [24] were the most suitable (and most popular) choice for 3-HP production [113], [137], [139], [145], [193]. It was hypothesized that the lack of 3-HP production in *C. necator* (in the previous work by Arenas-Lopez) was not due to the genes chosen, but an unknown issue, potentially related to their expression. Initial work included changing the plasmid backbones to a modular system, allowing for easier subsequent alterations. The *acc* genes from *C. glutamicum* were put under the control of a AraC/P_{BAD} promoter system, as this step is considered rate limiting and native genes tend to be under strict regulation [157], [176]. Overexpression of the ACC enzyme has previously caused issues with cell viability [142], [194]. However, many other studies show that malonyl-CoA derived fatty acids concentration increases when ACC is overexpressed [142], [173].

A further gene from *E. coli* was added to one of the plasmid constructs. This gene, *ydgG*, encodes a 3-hydropropionic acid dehydrogenase that additionally converts malonate semialdehyde to 3-HP. The addition of this enzyme was supposed to facilitate the second step of the reaction catalysed by the MCR enzyme. Mathematical modelling by Dalwadi *et al.* [188] suggested that this enzyme was necessary and vital to produce 3-HP, and in order to prevent the accumulation of toxic MSA.

As the regulation of the native acetyl-CoA carboxylase in *C. necator* in unknown, the effect of overexpression of a heterologous ACC is unknown. To circumvent any potential negative effects such an overexpression may have, an alternative route that converts oxaloacetate and acetyl-CoA to malonyl-CoA and pyruvate was designed and the encoding genes used for plasmid construction. Originating in *P. freudenreichii*, the MMC enzyme was shown to increase free fatty acid titer by 44% [181]. Issues arose when constructing this plasmid, as multiple SNPs appeared when sequencing the initial plasmid. After correcting the first mutation through site-directed mutagenesis, sequencing revealed that a second mutation had appeared nearby. This suggested a potential toxicity issue in the *E. coli* DH5α used in cloning, so a "reduced evolvability" strain was used to continue cloning MMC encoding plasmids in MDS42 [147].

The 3rd generation of plasmids involved the amalgamation of the previous constructs, encoding the entire genetic pathway to 3-HP on a single plasmid. However, this resulted in large, complex plasmids, as seen in Figure 16. Initially this strategy was dismissed due to the size of the resulting plasmids, which can reduce transformation efficiency [195]. Furthermore, plasmid size and copy number are inversely proportional, reducing the number of copies of the pathway genes present [196].

To create the 4th generation plasmids, the *mcr* was split into the 2 subunits, N and C, each of which was placed under control of a different constitutive promoter. This was done due to work done by Liu *et al.* [113] who investigated the overall MCR activities resulting from expression of mcr_{635} gene fragments which encoded various portions of the N and C-terminal domains of the enzyme. In addition, Liu *et al.* identified several beneficial mutations (in regard to enzyme activity) and hence these were also incorporated into this new design. Mutations in the C-terminal subunit of the *mcr* gene were reported to have the largest effect on 3-HP titer *via* the malonyl-CoA pathway. A combination of three mutations, clustered in the C-terminal region of mcr_c (N940V, K1106W, S114R) increased the activity of the purified enzyme from 1.51 to 8.37 mmol/min/μmol. Interestingly, the mechanism behind the improvements is unknown as the alterations took place outside of the NADPH binding region or the reactive site.

3.4.4 Expression of heterologous enzymes for 3-HP production in *C. necator*

As described in section 3.3.5, *C. necator* strains carrying two supposedly compatible 2nd generation plasmids appeared to be unstable and strains showed either no (or very low) growth. It was established that this was due to the loss of pMTL74111-*mcr*. Previous work by Muhammed Elsaan (University of Nottingham. unpublished) determined the stability and copy number of both vectors in *C. necator*. This work also showed that the origins of replication of the two plasmids were compatible, however these two exact plasmids had not been tested together in *C. necator* or *E. coli* previously. The exact reasons for this remained unclear but consistent loss of pMTL74111 may point towards selection against the plasmid due to negative effects associated with expression of the encoded gene. One possibility might be that

production of MCR results in metabolic issues, especially given the potential toxicity [197] of the generated malonic semialdehyde intermediate.

Interestingly, *C. necator* strains carrying the 1st generation plasmids also have two plasmids each, similar to the second-generation strains, but they appear to be stable. The difference is likely due to the change in promoters and/or backbones. In particular, the change in promoter of the *acc* genes from P_{phaC} to P_{BAD} was likely to have increased the expression, resulting in the previously detailed growth defects. The P_{phaC} promoter is known to be weak [38], and although expression was previously shown by Arenas-Lopez [63], activity was not shown in that study. Furthermore, the initial pME6032 vector carried the p15A/pVS1 origins of replications, compared to IncP/ColE1 in pMTL74111, which may contribute to the encountered problems.

To overcome these issues observed in the presence of two separate plasmids, the genes for the biosynthetic pathway to 3-HP were combined on a single plasmid, retaining their own promoters and RBS. However, growing *C. necator* H16 Δ3 strains carrying these plasmids was still problematic. Although growth was seen in liquid LB, this was not the case for SG-MM or F-MM.

There are several possible explanations for this behavior. it was suspected that this was due to leaky expression of the P_{BAD} promoter (alongside gene encoding *araC* repressor) controlling the *acc* operon. Work in Chapter 4 investigates how the induction of the *acc* operon with arabinose causes this severely weakened growth for *C. necator*. In order to tighten promoter control [42], precultures were grown with fructose as a carbon source, but this did not resolve the issue.

Another possible explanation may lie in the finding shown in Chapter 5 which suggest that growth of *C. necator* H16 Δ3 on fructose, and to a certain extent gluconate, is inhibited in the presence of an unknown intermediate or other factor, of the 3-HP pathway. Hence, in future work, pathway functionality may instead be tested for 3rd generation plasmid carrying strains grown on succinate.

Disappointingly, the available 4th generation constructs could not be tested as part of this study. This was due to lab closures, necessary due to COVID-19, and because of

the above issues with growing *C. necator* strains carrying the constructed 3rd generation plasmids. Although a small number of papers reported 3-HP biosynthesis in a number of species using the traditional mcr_{635} gene, the results were largely disappointing. However, functional domain analysis suggested that the MCR enzyme was a natural fusion protein. Independent expression of the two MCR domain gave a modest increase in 3-HP production [144]. The greatest improvement was seen by Liu *et al.* who increased the 3-HP titer from 0.15 g/L to 40.6 g/L [113]. This was achieved by balancing the enzyme subunits, MCR-C and MCR-N, followed by random, saturation and site directed mutagenesis. The mutations with the greatest effect on enzyme activity were combined to give the final modified *mcr* gene [113]. Hence as part of this study, 4th generation plasmids were constructed containing *mcr-N* under the control of the P_{tac} promoter, and the *mcr-C* controlled by P_{j5}. Future investigation should establish whether presence of these plasmids is also growth-inhibiting and how this inhibition might be overcome. Production and activity of the encoded 3-HP pathway components may then be analysed and compared to those of obtained for 3rd generation constructs, the ultimate performance criterion being 3-HP titre and productivity.

The remaining work aimed to elucidate which hypothesised mechanism was resulting in the disappointing results. Work was performed in *C. necator* where possible, and *E. coli* where it was not.

3.4.5 Expression of heterologous enzymes for 3-HP production in *E. coli*

As described in section 3.3.5, no 3-HP production was possible for *C. necator* strains carrying 2nd generation plasmids due to unstable vectors. The plasmids were introduced into *E. coli* MDS42, as seen in Figure 20. Despite satisfactory growth, no 3-HP was detected in the supernatant. This suggested that at least in *E. coli* one of the 2 main enzymes (ACC or MCR) were not working as expected. Analysis of protein expression by SDS-PAGE revealed faint bands for ACC, *YDFG* and MMC, thus supporting the hypothesis that at least some of the genes were sub-optimally expressed.

The overexpressed MCR from pMTL74111-mcr was only visible in the insoluble fraction at around 135 kDa. Insolubility was observed during extraction, but this may not necessarily reflect the enzyme's state in the intact cell. This insolubility could be down to poor choice of extraction buffer, which may have influenced the target protein solubility, hence leading to incorrect conclusions [198].

Previous results for *E. coli* strain that showed that the MCR from *C. aurantiacus* was active and had a specific activity of 0.015 μmol min^{-1} mg^{-1} (Figure 15). However, the backbone plasmid had been changed from pBBR1 to pMTL74111, allowing compatibility with pMTL71301. The reason for the observed insolubility remained unknown.

3.4.6 Assaying the activity of the ACC enzyme, using a coupled spectrophotometric assay dependent on the previously produced MCR enzyme

With respect to ACC production and activity, the conducted *E. coli* experiments confirmed that proteins of the expected size were produced in an *acc* expressing strain, but not the control (Figure 21). As the pMTL71301 backbone appeared more stable, it was desirable to keep the *acc* genes on this vector. For the coupled enzyme assay for ACC activity described by Kroeger *et al.*, the previously purified MCR enzyme was required. However, no activity could be measured in crude extracts of *C. necator* H16 Δ3 cells expressing acc_{Cg}, when using a coupled enzymatic assay described by Kroeger et al. [152]. Whilst this would suggest that the produced ACC complex was not active in the generated crude extracts, this requires further confirmation, especially in the light of the malonyl-CoA reporter data presented in chapter 4.

It is possible that this particular assay failed, hence alternative assay systems should be employed. The coupled system used here relied on His-tagged, purified MCR, which was shown to be active based on its ability to convert malonyl-CoA to 3-HP with a specific activity of 0.05 μmol min^{-1} mg^{-1} for the purified enzyme. An alternative reporter-based approach was implemented as part of this study, and is described in Chapter 4, and provided evidence that introduction of acc_{Cg} genes increased malonyl-CoA availability.

3.5 Key outcomes

Although no 3-HP production was reported in this chapter, much was learnt about the

- The MCR enzyme to convert malonyl-CoA to 3-HP is active in *C. necator*, despite the lower than optimum temperature, indicating potential success in future
- However, poor buffer choice may have hindered protein folding or activity in the purified MCR. Due to this, the activity assay requiring the purified MCR was not successful in measuring the activity of ACC from *C. glutamicum*
- The pathway to 3-HP was introduced into *E. coli*, and whilst no 3-HP was found in the supernatant, the expressed proteins were visible on SDS-PAGE

Chapter 4 –
Construction of a *C. necator* malonyl-CoA biosensor

Chapter 4 - Construction of a *C. necator* malonyl-CoA biosensor

4.1 Introduction

4.1.1 Malonyl-CoA

Malonyl-CoA, a 3-carbon compound composed of malonic acid bound to coenzyme A, is the precursor to fatty acid biosynthesis and plays an important role in carbon metabolism. For this reason, malonyl-CoA is a major building block in the synthesis of industrially relevant compounds, such as 3-hydroxypropionic acid, polyketides and fatty acid derived biodiesels [199]. It is synthesised from acetyl-CoA, using the enzyme acetyl-CoA carboxylase [200]. However, only a small amount of the generated acetyl-CoA is converted to malonyl-CoA, with the rest going into the TCA cycle. This topic is discussed in more detail in Chapter 3.

As malonyl-CoA is an essential precursor in both eukaryotes and prokaryotes, its generation and accumulation are of interest with respect to biotechnological applications. However, the intracellular concentration of malonyl-CoA has been found to be low in model organisms [201]. Metabolic engineering can artificially increase the metabolic flux towards malonyl-CoA by overexpressing heterologous genes/operons that generate it, and its intracellular concentration may be increased by inactivating or down-regulating genes for competing malonyl-CoA-utilising pathways. The excess malonyl-CoA can then be used to produce a commodity chemical, without being detrimental to the health of the cells [202]. The addition of heterologous genes can unbalance the natural carbon and co-enzyme flux of the cell, resulting in sub-optimum expression of a synthetic pathway due to feedback inhibition and stringent response. Now that reliable synthetic biology tools have been developed, screening is the bottleneck in strain engineering [203].

4.1.2 Quantifying intracellular malonyl-CoA

Due to its importance in fatty acid biosynthesis and many other metabolic pathways, malonyl-CoA is ubiquitous but can be laborious and difficult to quantify. It is desirable to have information on its intracellular concentration under different conditions and in

different cellular backgrounds. McGarry *et al.* [200] developed a radioisotopic method for measuring malonyl-CoA levels in hepatic tissue of rats. This assay was based on the malonyl-CoA-dependent conversion of acetyl-CoA to palmitic acid and was sensitive down to picomole quantities. The malonyl-CoA containing sample was added to radioactively labelled acetyl-CoA in the presence of a fatty acid synthase and excess cofactors. The acetyl-CoA and malonyl-CoA are combined to form palmitic acid, which can be dissolved in petroleum ether and the radioactivity measured. Despite the sensitivity of this assay, the use of expensive, hazardous, radiolabelled acetyl-CoA makes it unsuitable for many laboratories [200].

Takamura *et al.* [204] developed another indirect enzymatic assay. In this assay a malonate decarboxylase is used to catalyse the reaction of acetyl-CoA to malonyl-CoA. As a result of this reaction, malonate is converted to acetate, which can then be phosphorylated by acetate kinase (Ack) (Figure 22). The final stage of the assay is to add a ferric reagent, resulting in an amount of malonyl-CoA-derived acetohydroxamate that is proportional to acyl-CoA concentration, and can be read at 540 nm. However, this method reads all acyl-CoAs that are converted by the promiscuous enzyme. In order to specifically measure malonyl-CoA, other acyl-CoAs (particularly acetyl-CoA) are eliminated by the addition of an acetyl-CoA-specific citrate synthetase and oxaloacetate to the sample before the procedure. This converts the acetyl-CoA into citrate and eliminates any interference in the assay. Despite the benefits of a one-tube, relatively high throughput method, this protocol uses an unstable enzyme (malonate carboxylase) so a new calibration curve must be established for each use [204].

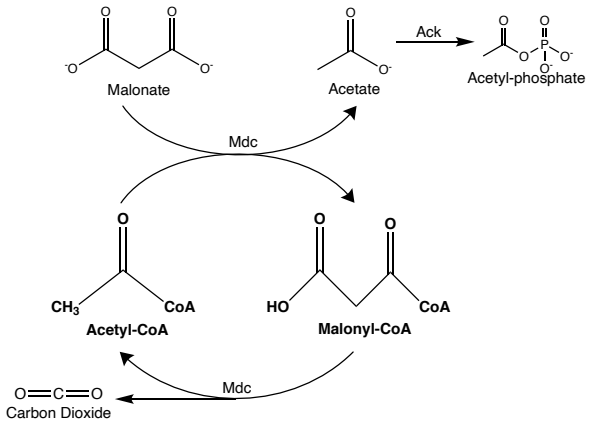

Figure 22 - Principle of malonate decarboxylase reaction used to measure acyl-CoA. Modified from Takamura et al. Ack = acetate kinase, Mdc = malonate decarboxylase

Quantification can also be achieved using HPLC- and MS-based methods. Mass spectrometry techniques have superior sensitivity and specificity, but require expensive equipment and specialised expertise [205]. HPLC detection is often problematic, requiring long run times and struggling to separate and correctly identify acyl-CoAs [206]. New LC/MS methods are better suited, shortening the run time per sample from 20 to only a few minutes, and distinguishing between the 8 most common acyl-CoAs, despite the analogues having similar masses. Issues with pH and temperature stability during sample preparation have been reported, however studies have shown that malonyl-CoA is stable at -80ºC for 55 days and stable at 4ºC for 24 hours [201].

Still, there is a need for a method capable of handling a large number of samples, without intensive methodology and complex machinery. A sandwich enzyme immunoassay kit for malonyl-CoA (MyBioSource) is commercially available, and has a reported detection range of 0.625 ng/ml-40 ng/ml. The malonyl-CoA in the testing sample is bound to an immobilised enzyme on the assay plate. A biotin-conjugated antibody specific to malonyl-CoA is added and Horseradish Peroxidase is added to the wells, which can then be developed using a substrate solution, allowing for colourimetric, quantitative analysis of malonyl-CoA concentration. Unfortunately, this kit is only recommended for serum, plasma and tissue homogenates from humans, mice and rats, making it unsuitable for prokaryotic researC. The cost can also be prohibitive depending on the number of samples [207].

4.1.3 Biosensors for quantifying malonyl-CoA

It is apparent that there is a need for a better procedure for measuring intracellular malonyl-CoA in prokaryotes. The low abundance of the compound (4–90 μM or 0.01–0.23 nmol/mg dry weight in *E. coli* [202]) means that most methods are not sensitive enough to be suitable [205]. To overcome this, biosensors have been designed that allow metabolites such as malonyl-CoA to be quantified *in situ* (Table 14). These biosensors have the advantage of being specific, sensitive and adaptable to different organisms. This can allow for high-throughput, non-destructive, economical screening of metabolically engineered cells and allow to for the selection of high malonyl-CoA-producing strains [202].

Generally, in order to validate a biosensor, the substrate is included in the media and the output is measured to create a calibration curve. In this case, exogenous feeding of malonyl-CoA is not possible, so the antibiotics cerulenin [202] or triclosan [201] can be used to artificial perturb the intracellular concentrations. Cerulenin works by reducing fatty acid chain extension by inhibiting β-ketoacyl-acyl carrier protein synthase enzymes (FabB and FabF) [202]. Triclosan inhibits the activity of FabI, an NADH-dependent enoyl-acyl carrier protein reductase [208]. As a result, both of these biocides impede fatty acid biosynthesis, which significantly increases the malonyl-CoA levels within the cell [209]. By titrating the antibiotic, the levels of malonyl-CoA can be gradually increased to create a calibration curve that indirectly measures the substrate [201]. Predictably, these antibacterials can have a marked effect on the growth of the cells, with optical density greatly reduced by their presence [210]. Additionally, the use of these fatty acid inhibitors in industrially applications is uneconomical [202].

Table 14 - Biosensors for measuring malonyl-CoA levels in multiple organisms

Biosensor	**Details**	**Organism**	**Reference**
FapR/FapO	Malonyl-CoA binds to and separates the FapR-*fapO* complex that blocks RNA polymerase. FapR released from its DNA binding site on *fapO*, and a fluorescent reporter module is transcribed.	*E. coli*	Xu *et al.* [211] Feher *et al.* [203] Liu *et al.* [176]
		Saccharomyces cerevisiae	Liu *et al.* [176] David *et al.* [212]
		Cupriavidus necator H16	Johnson [202]
		Mammalian cells	Ellis and Wolfgang [194] (COS-1) Du *et al.* [213] (HeLa)

AraC-TAL	Malonyl-CoA converted to TAL. TAL interacts with mutated AraC regulator. AraC-TAL interaction can be combined with a P_{BAD} promoter to control the expression of the *lacZ* gene which produces a blue colour.	*E. coli*	Tang *et al.* [201]
RppA	Type III polyketide synthase RppA produces red-coloured flaviolin	*E. coli* *C. glutamicum* *Pseudomonas putida*	Yang *et al.* [150]

Most of the malonyl-CoA biosensors are based upon transcriptional factors and have a repressor module and a reporter module. Many are developed using the interaction between a naturally occurring FapR transcriptional repressor module and *fapO* operator sequence. In bacteria such as *Bacillus subtilis*, the FapR protein binds to the *fapO* DNA sequence, forming a FapR-*fapO* complex that blocks RNA polymerase and represses fatty acid synthesis genes. Malonyl-CoA binds to the ligand-binding domain on FapR, causing a conformational change and releasing it from *fapO*. This allows the downstream genes to be transcribed [214]. In the biosensor design, the FapR repressor module is driven by a suitable promoter and a separate reporter module comprising of a fluorescence protein is driven by a hybrid promoter with the *fapO* sequence combined. As the malonyl-CoA levels increase, the FapR-malonyl-CoA interaction causes the release of the FapR from its DNA binding site on *fapO*, and the reporter module is transcribed. Within certain limits, the level of malonyl-CoA is proportional to the fluorescence output [202].

A benefit of this FapR-based method is the ability to modify the components for successful integration into many organisms. By altering the plasmid backbone, copy number, promoter region and other regulatory elements (such as ribosome binding sites, mRNA stem loops etc.), the expression of the FapR repressor can be modulated

to suit the organism of interest to give an acceptable sensitivity and detection range. However, there is no algorithm for selecting the most suitable genetic components, so work must be performed by trial and error [202]. Despite this, the FapR-*fapO* system has been adapted for use in bacteria, yeast and mammalian cells.

This FapR/*fapO* system has also been used as an actuator to control the expression of a repressor gene, so the cell can self-regulate the expression of other genes to regulate the levels of malonyl-CoA. In *E. coli*, a negative feedback circuit has been used to control the expression of an acetyl-CoA carboxylase (ACC), that catalyses the reaction of acetyl-CoA to malonyl-CoA. When malonyl-CoA levels are low the expression of the ACC is increased. Conversely, when malonyl-CoA accumulates, the ACC is downregulated. This dynamic regulation minimises any adverse effects and toxicity of the increased intracellular substrate levels [176].

Other biosensors, not based on FapR, have also been reported in bacteria. A triacetic acid lactone (TAL) based system has been shown to work in *E. coli*. In this construct, the malonyl-CoA was converted to TAL by heterologous 2-pyrone synthase. TAL is stable and is not utilised as a respiratory substrate. TAL is detected by a mutated AraC regulator, responsive to TAL. This AraC-TAL interaction can be combined with a P_{BAD} promoter to control the expression of the *lacZ* gene. LacZ activity can then be quantified. A significant benefit of this method is the ability to select for colonies by eye, as growth on a media supplemented with X-GAL will turn the colonies with high malonyl-CoA levels blue. However, this must be done in early growth stage before the LacZ output is saturated and all colonies turn the same shade of blue regardless of malonyl-CoA level [201]. LacZ-based assays have also been shown to inhibit cell growth when expression is high [215].

4.1.4 Polyketide synthases

A biosensor by Yang *et al.* [150] is most promising for use in *Cupriavidus necator* and other industrial strains, as it is a one-enzyme reaction that produces a visible, colourimetric output that can be measured easily. The method involves the expression of a polyketide synthase gene, *rppA*. The encoded enzyme (1,3,6,8-tetrahydroxynaphthalene synthase, THNS) catalyses the reaction of 5 x malonyl-CoA molecules to 1,3,6,8-tetrahydroxynaphthalene (THN). THN is then spontaneously oxidised to flaviolin non-enzymatically. Flaviolin has an observable red colour and can be detected and quantified at 340 nm [150], but it has also been reported that 520 nm can reduce background interference [216].

There are 3 types of polyketide synthases (PKS), that result in a large range of diverse products, including medicinal-important compounds for the treatment of cancer, fungal infections and antibiotics [217]. The difference in the types of polyketide synthases comes from the structure of the enzyme and assembly mechanisms. Type I pass the growing polyketide chain from one active site to the next, whereas type II repeatedly uses the same active site during extension. Type III use completely different system where the polyketide chain is never attached to the enzyme [218].

The PKS used in this biosensor (RppA) is of type III and uses malonyl-CoA preferentially as a starter substrate, although it has been shown to use 4-8 carbon acyl-CoAs when substrate concentrations are high [219]. Like most PKS, RppA is found in the order *Actinomycetales*, in particular *Streptomyces* species. Yang *et al.* [150] found that the enzyme from *Steptomyces griseus* was the most proficient at producing flaviolin [150]. In nature, the enzyme performs four successive extensions of malonyl-CoA. The structure is then cyclised to THN, which is oxidised to yield flaviolin, as part of melanin biosynthesis [219].

It is suggested that other polyketides may have similar functions and outputs [150]. The simplicity and reliability of this single-gene *rppA*-based biosensor make it ideal for use as a malonyl-CoA detection method.

4.2 Aims of the study

The work in this chapter aimed to elucidate the reasons for low 3-HP production in *C. necator* strains, which were hypothesised to be caused by low intracellular malonyl-CoA concentrations. The specific aims were –

- To design and implement a plasmid-based malonyl-CoA biosensor in *C. necator*
- To validate the system using an antibiotic to artificially inflate malonyl-CoA levels
- To use the biosensor to evaluate the strains designed to increase malonyl-CoA availability
- To use the biosensor to evaluate the use of a heterologous acetyl-CoA carboxylase (ACC) to amplify the amount of available intracellular malonyl-CoA

4.3 Results

4.3.1 Characterisation of the RppA biosensor in *E. coli*

An RppA-based malonyl-CoA biosensor was constructed as outlined in 2.4.4, consisting of the modular vector backbone pMTL71301 and the *S. griseus rppA* gene under control of the P_{tac} promoter The DH5α strain carrying the generated pMTL71301_*rppA* reporter plasmid (hereafter referred to as DH5α rppA reporter) was tested against a control strain carrying plasmid pMTL71301_*rfp* (named DH5α *rfp* control). A photometric scan was performed to find the best absorption wavelength to determine the flaviolin content of the supernatant. The culture was grown in the presence of cerulenin (0-50 µM) to ensure that the chosen wavelength was best for all concentrations of flaviolin.

As reported in the literature, absorption spectra using DH5α *rppA* reporter supernatant revealed the highest peak for flaviolin at 360 nm, but also showed high background levels, due to other substances present in the media. Both 340 nm [150] and 520 nm [216] have been reported to show acceptable signal to background ratio. However, for this study the signal output was much higher at 340 nm and this was the wavelength chosen for future experiments, although data for 520 nm was retained (Figure 23A). The coefficient of variation (SD as a percentage of the mean) was similar for both 340 nm and 520 nm. The control strain did not show any change in absorbance, regardless of cerulenin level (Figure 23B).

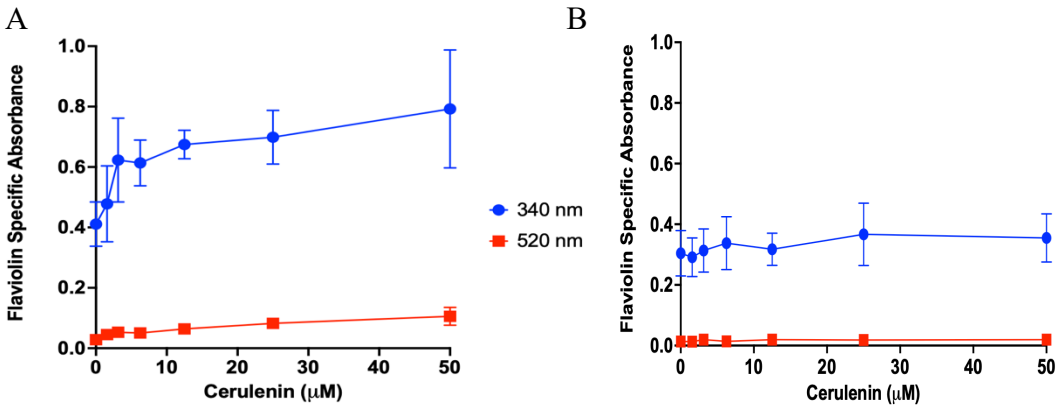

Figure 23 – *E. coli* strains DH5α *rppA reporter* (A) and DH5α *rfp control* (B) were grown in M9 medium for 16 hours in the presence of the indicated concentrations of cerulenin added at 0 h. Relative flaviolin concentrations in cell-free supernatants were determined as described in section 4.3.4.1, by deducting the media only signal then dividing absorption at 340 and 520 nm, respectively, by the achieved optical density of the cultures. Data points and error bars are the mean ± SD, n = 3.

In this study, the pink colour of the supernatant was visible by eye for the DH5α *rppA* reporter strain, both on plate and in liquid culture. However, it did oxidise to a brown colour gradually. The background level of absorbance signal was high for the control strain DH5α *rfp* control. Nonetheless, it did not increase with cerulenin concentration, staying invariable between 0.21-0.46 at 340 nm (Figure 23B). The final optical density of DH5α cells was not affected by the cerulenin (Figure 24).

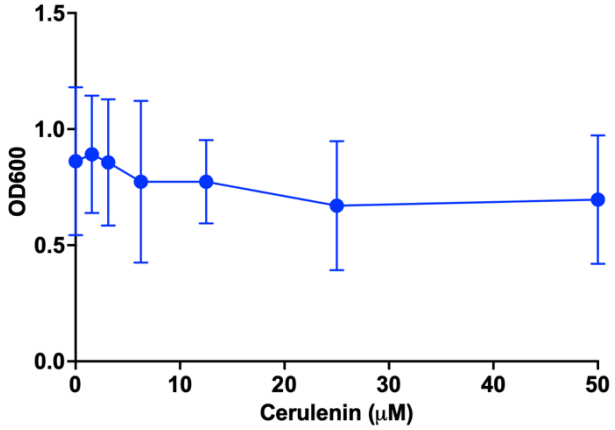

Figure 24 - *E. coli* strain DH5α was grown in M9 medium for 16 hours in the presence of the indicated concentrations of cerulenin added at 0 hours. The optical density of the cells was read at 600 nm. Error bars mean ± SD, n = 3.

As the cerulenin concentration in the media was increased, there was a dose-dependent response in the production of flaviolin (Figure 25A). The output signal plateaued when the cerulenin level was higher than approximately 3 µM. When cerulenin was added, the difference in absorption between DH5α *rppA* reporter and DH5α *rfp* control was obvious (including by eye). However, at low concentrations of

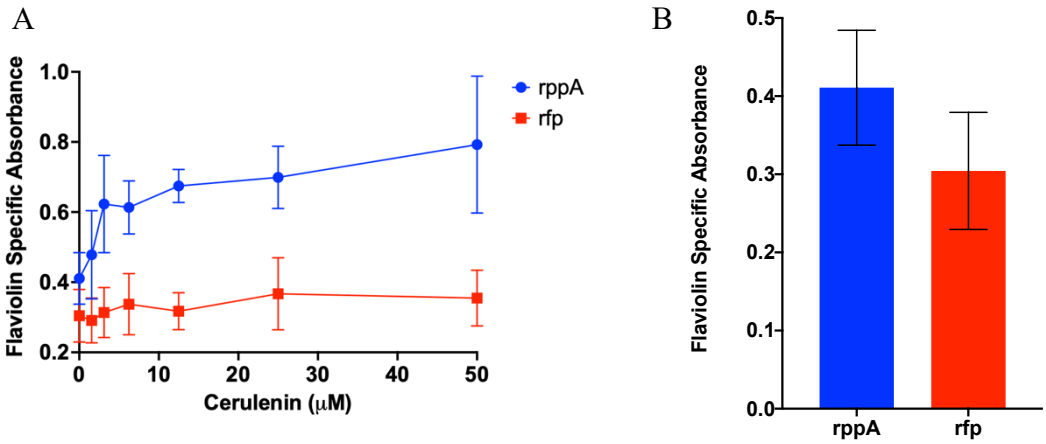

Figure 25 – A) The normalised absorption for strains DH5α *rppA* reporter and DH5α *rfp* control as different cerulenin concentrations were added to M9 medium (at 0 Hs) to perturb malonyl-CoA levels. The absorbance was read at 340 nm, the media only absorbance was deducted, then normalised by dividing by OD600 to give flaviolin specific absorbance B) The normalised absorption for DH5α *rppA* reporter and DH5α *rfp* control with no cerulenin present. Both measured at 16 hours. No significant difference was observed. Evaluated by Students T Test, P value = 0.154. Error bars mean ± SD, n = 3.

cerulenin there was no discernible distinction between the two. This sensor could be problematic in strains with low malonyl-CoA levels, as the difference between the *rppA* reporter and *rfp* control strains was not significant when no cerulenin was added (P value = 0.154) (Figure 25B).

4.3.2 Testing the effect of cerulenin on *C. necator* H16 Δ3 Δ*mcd*

Having established that the constructed pMTL71301_*rppA* reporter was functional in *E. coli* and that flaviolin-specific absorption increased in the presence of cerulenin, the plasmid was transferred into *C. necator* for further testing. Flaviolin production and the effects of cerulenin were evaluated in strain H16 Δ3 Δ*mcd*, as preceding research indicated that this was to be the 3-HP production strain (see chapter 3). Cerulenin levels of up to 50 µM were used, as previous research had shown that above this concentration the compound had a substantial negative impact on growth of *C. necator* H16 wild type strain (Kamran Jawed, University of Nottingham, personal communication). This was backed up by preceding studies that had shown that 40 µM cerulenin completely inhibited Fab proteins in *Ralstonia solanacearum*, a species closely related to *C. necator* [220].

However, cerulenin at 50 µM and below did have a significant effect on cell growth in H16 Δ3 Δ*mcd*. Even with the minimum concentration (1.6 µM), growth was reduced (Figure 26A). However, the lag phase of the samples did not appear to be affected by the cerulenin as seen in the log plot of the data (Figure 26B). By 50 µM, the final optical density at 20 hours of growth was reduced by 82.5% (Figure 26C) and there was a strong negative correlation between cerulenin concentration and the achieved final densities (Spearman rank coefficient, R^2 value = 0.9736). The most marked difference in growth was between 25 µM and 50 µM. The final OD600 for this strain was taken at 20 hours for Figure 26 as this would be the final time point during the testing of strains harbouring pMTL71301_*rppA* reporter. The experiment was allowed to continue to 22 hours for Figure 26A and Figure 26B to allow for any variation in lag phase that occurred due to the growing of the cells in a 96-well plate rather than a 15 ml falcon. It could not be continued longer than this due to the evaporation of liquid from the culture making optical density results unreliable. The normalised absorption is defined as the media-corrected absorption at 340 nm divided

by OD_{600}, so this reduction in growth was accounted for when calculating output of the biosensor.

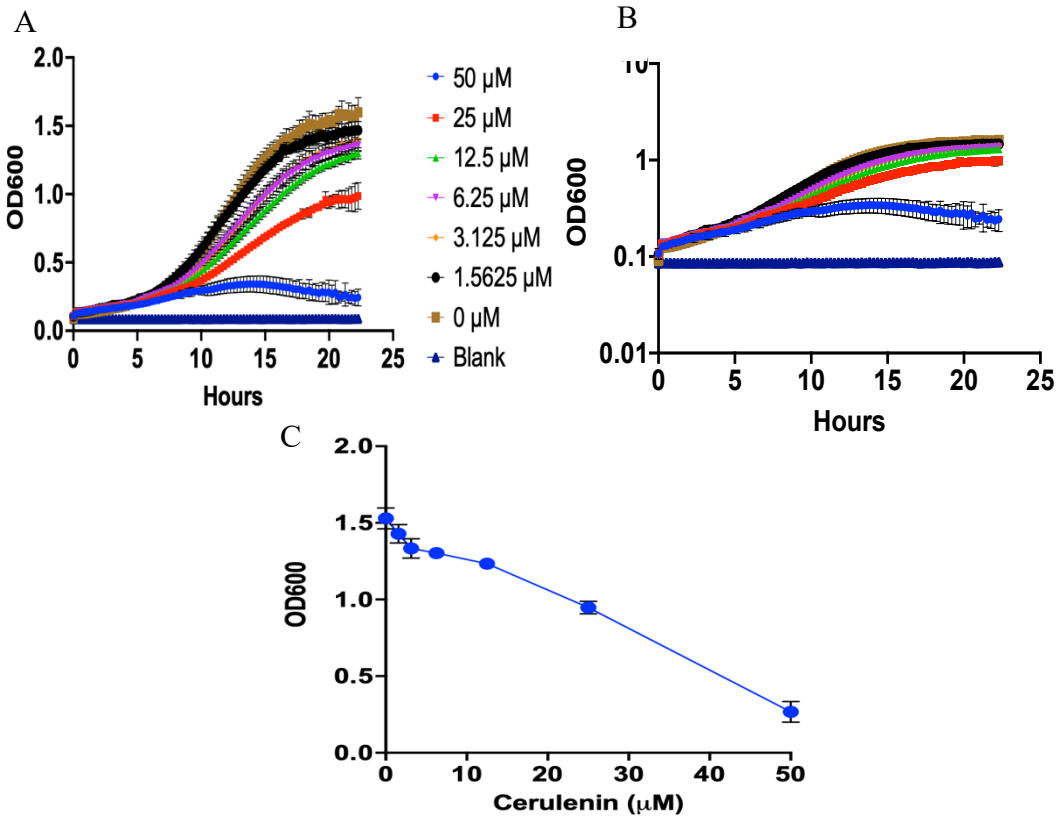

Figure 26 – Growth of *C. necator* H16 *Δ3 Δmcd* in the presence of different concentrations of cerulenin. A) Growth of H16 Δ3 Δ*mcd* in SG-MM in the presence of increasing cerulenin concentrations (added at 0 hours) as determined by OD_{600}. B) Log plot of figure 6A to show growth profile of H16 Δ3 Δ*mcd*. C) The effect of cerulenin concentration on OD600 of H16 Δ3 Δ*mcd* after 20 h of growth in SG-MM. Final OD_{600} values are inversely proportional to the concentration of cerulenin (R^2=0.9736).

4.3.3 Characterization of the RppA biosensor in *C. necator*

The sensor was assessed in H16 Δ3 Δ*mcd*, the anticipated chassis for 3-HP production. Variants of this strain carried either the reporter plasmid pMTL71301_*rppA* or the control vector pMTL71301_*rfp*, hereafter referred to as H16 Δ3 Δ*mcd rppA* reporter and H16 Δ3 Δ*mcd rfp* control, respectively. In the H16 Δ3 Δ*mcd* the reporter showed a clear dose-dependent response when exposed to increasing concentrations of cerulenin (Figure 27). This suggested that the biosensor is functional in *C. necator*. For this strain background, the difference between the signals for the reporter and its control at 0 µM cerulenin were significantly different (Student T test, P value = 0.0013), meaning even small differences in malonyl-CoA availability should be detectable in H16 strains.

Furthermore, the detrimental effect of cerulenin on growth appeared to have been alleviated by the presence of the RppA enzyme. Most likely this is because malonyl-CoA is no longer accumulating, instead being converted into the non-toxic THNS then flaviolin. Although flaviolin-specific absorption at 340 nm was low in the absence of cerulenin, accumulation in solid media allowed the colour change to be seen on agar plates, allowing for selection of plasmid-carrying strains by eye. In liquid media, the production of flaviolin was very obvious and produced maroon coloured culture.

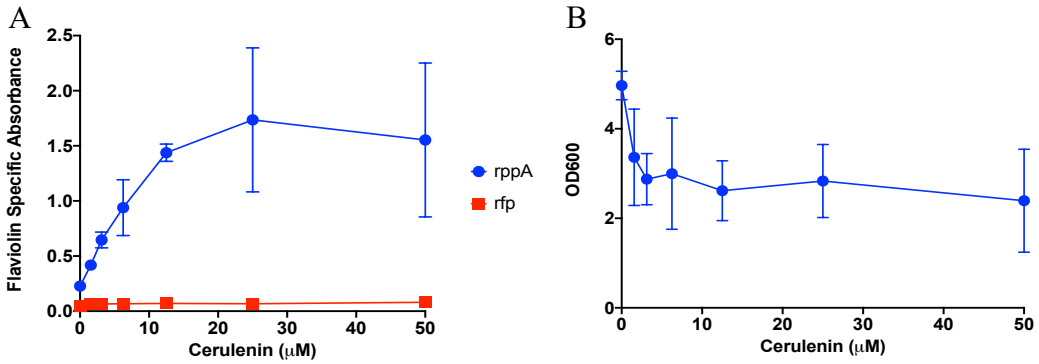

Figure 27 – A) Absorption at 340 nm for cell-free supernatants of H16 Δ3 *Δmcd rppA* and the control strain H16 Δ3 *Δmcd rfp*. in the presence of cerulenin. B) Optical density read at 600nm. Cultures were grown in SG-MM in the presence of the indicated cerulenin concentrations. Absorption at 340 nm was determined after 20 h as a measure of flaviolin production. Error bars mean ± SD, n = 3.

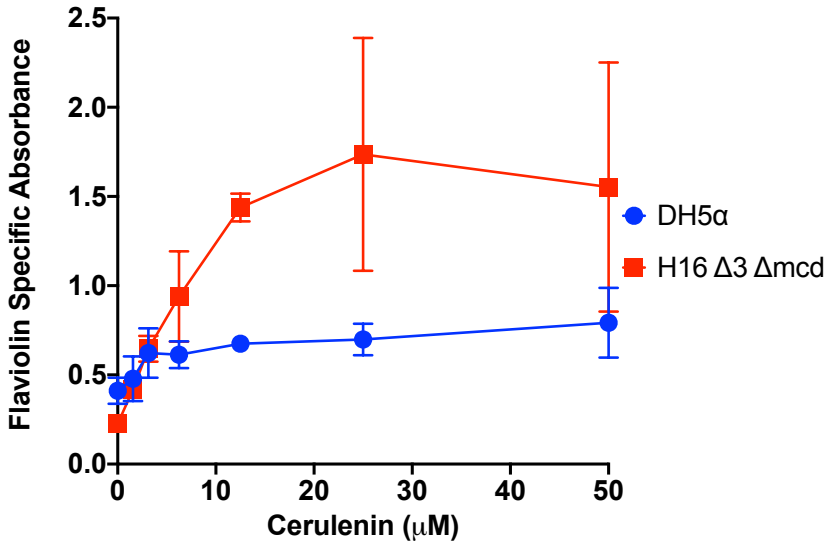

Figure 28 - Comparison of biosensor output between *E. coli* DH5α *rppA* and *C. necator* H16 Δ3 *Δmcd rppA* at different cerulenin concentrations. Absorption at 340 nm for cell-free supernatants was measured for cultures were grown in SG-MM medium in the presence of the indicated cerulenin concentrations. Absorption was determined after 20 h as a measure of flaviolin production.

The signal produced by H16 Δ3 Δ*mcd rppA* in broth was twice as high than the signal seen for DH5α *rppA* reporter (maximum mean signal of 1.55 vs. 0.79 with 50 µM cerulenin, a 1.96-fold increase).

4.3.4 Comparison of biosensor signal between genetically engineered strains of *C. necator*

In order to evaluate the best strain in terms of malonyl-CoA availability, strains of *C. necator* that had numerous gene knockouts were tested with the created *rppA* biosensor, seen in Figure 29. The strains were tested with different levels of cerulenin from 0-25 µM. The H16 wild type (WT), H16 Δ3 and H16 Δ*mcd* strains had a very similar pattern and maximum absorption at 340 nm of approximately 1 with 25 µM cerulenin. The H16 Δ3 Δ*mcd* strain, however, had a higher maximum signal. However, the signal output in the absence of cerulenin was very similar for all 4 tested strains. This suggests that the pool of malonyl-CoA is unaffected by any of the knockouts necessary to stop 3-HP consumption.

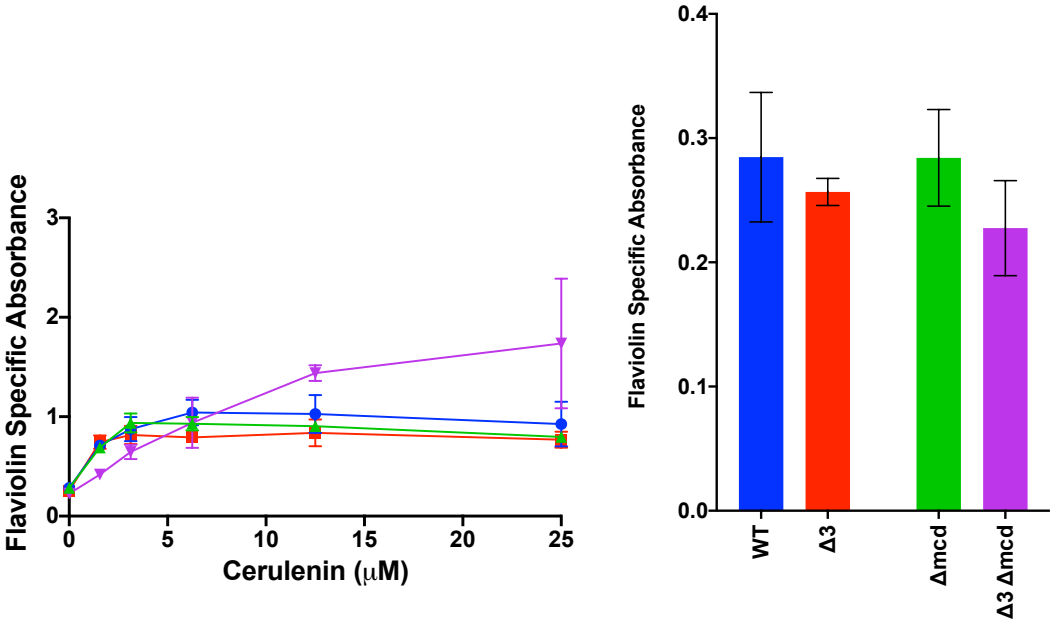

Figure 29 – Comparison of biosensor outputs for four different *C. necator* mutant strains at different cerulenin concentrations. A) Absorption at 340 nm for cell-free supernatants of H16 WT = blue, H16 Δ3 = red, H16 *Δmcd* = green, and H16 Δ3 *Δmcd* = pink). Absorption was determined as a measure of flaviolin production after 20 h of growth in SG-MM medium in the presence of the indicated concentrations of cerulenin. There is no significant difference between the signals between the strains. B) Flaviolin-dependent absorption in the absence of cerulenin in the 4 strains after 20 h shows no significant difference. Error bars mean ± SD, n = 3

Previous work (completed in conjunction with Christian Arenas-Lopez [24]) had generated another *C. necator* H16 derivative, named H16 Δ4, with the aim of increasing acetyl-CoA availability for the generation of 3-HP *via* malonyl-CoA. This strain cannot convert acetyl-CoA to PHB, due to a deletion of the *phaCAB* operon. It

was therefore of interest to see how our RppA-based reporter behaved in this genetic background. However, the H16 Δ4 strain cannot be easily compared to the other strains as its lack of PHB affects cell shape and size, resulting in reduced OD values (Arenas-Lopez, University of Nottingham, personal communication). Furthermore, its growth in batch culture it is characterised by an increased lag-phase. This means the OD of Δ3 and Δ4 are not directly comparable. The density of the culture is influenced by the PHB present; therefore, cell numbers could be vastly different between the strains with the same OD. H16 Δ4 has been shown to have a reduced final OD and an increased lag-phase [151]. Both of these factors could affect the accuracy of the biosensor.

As described above for the other *C. necator* strains, the reporter plasmid pMTL71301_*rppA* was also introduced into H16 Δ4. This strain showed a dose-dependent response to the cerulenin and the signal reached a maximum at 25 µM (Fig. 8). A control strain harbouring pMTL71301_*rfp* did not show any increase in flaviolin-specific signal, with background absorptions at 340 nm remaining stable throughout the experiment. In the absence of cerulenin, the signals between the biosensor strain and the control strain were not significantly different. Compared to the other *C. necator* reporter strains, culture supernatants of the Δ4 *rppA* strain were less red by eye and showed a reduced 340 nm signal output. However, when this was corrected for OD, the signal was higher than seen other strains (Figure 30).

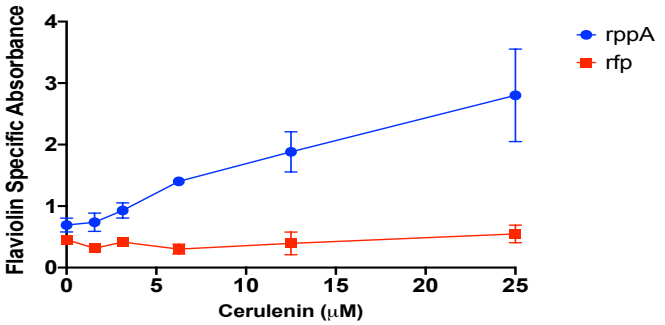

Figure 30 - The biosensor output for *C. necator* H16 Δ4. Derivatives of this strain carried either pMTL71301_*rppA* (blue line and circles) or pMTL71301_*rfp* (red lines and circles). Cells were grown in SG-MM medium for 20 hours before absorption of the culture supernatants was analysed at 340 nm. Error bars mean: ± SD, n = 3.

4.3.5 Investigating the Effect of ACC on Biosensor Signal

The overarching aim of this chapter was to use a biosensor to evaluate whether overexpressing a heterologous acetyl-CoA carboxylase gene would increase intracellular levels. To test this, the *acc* genes from *C. glutamicum* under control the arabinose-inducible *araC*-P_{BAD} promoter were integrated into the reporter construct as described in 4.3.6, resulting in plasmid pMTL71301_ACC_*rppA*. This was designed so a single plasmid could be used to express the full pathway, in a similar way to that seen in Chapter 3 for 3-HP production.

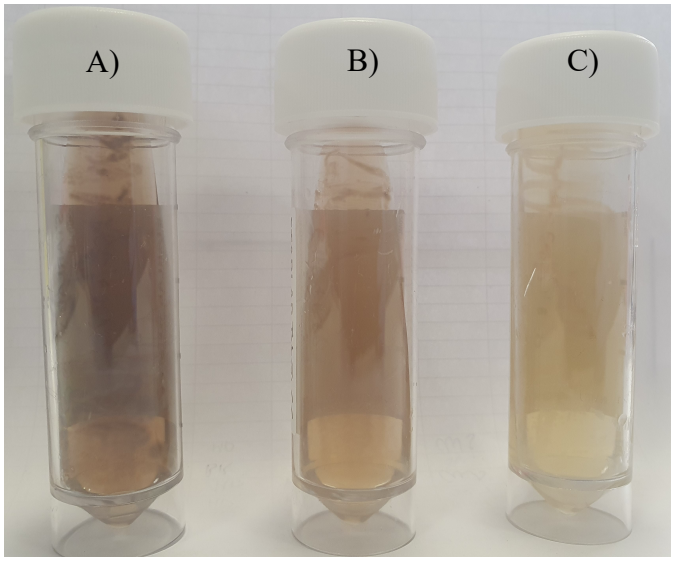

Figure 31 - Flaviolin produced diffuses into the media. Bacteria grown on sloped agar at 30°C for 48 hours. Each slope is a strain of *C. necator* Δ3 carrying different plasmids. A) strain carrying pMTL71301_*acc_rppA* shows darkest colour. B) carrying pMTL71301_*rppA* shows intermediate colour, and C) strain carrying pMTL71301_*rfp* for control and comparison.

Plasmid pMTL71301_ACC_*rppA* was tested in strain H16 Δ3 Δ*mcd*. Once the transformation was confirmed, the production profile for flaviolin was followed. No cerulenin was added on this occasion, but differing concentrations of arabinose were present in the medium to allow fine-tuning of ACC production. Too much expression of the encoding genes has been shown to be detrimental to cell health [176], [181], [221]. Initially the concentration of arabinose was varied from 0% to 0.5%, a range covering the most commonly used concentrations in *C. necator* and reported to give a linear range for expressing fluorescent proteins [38].

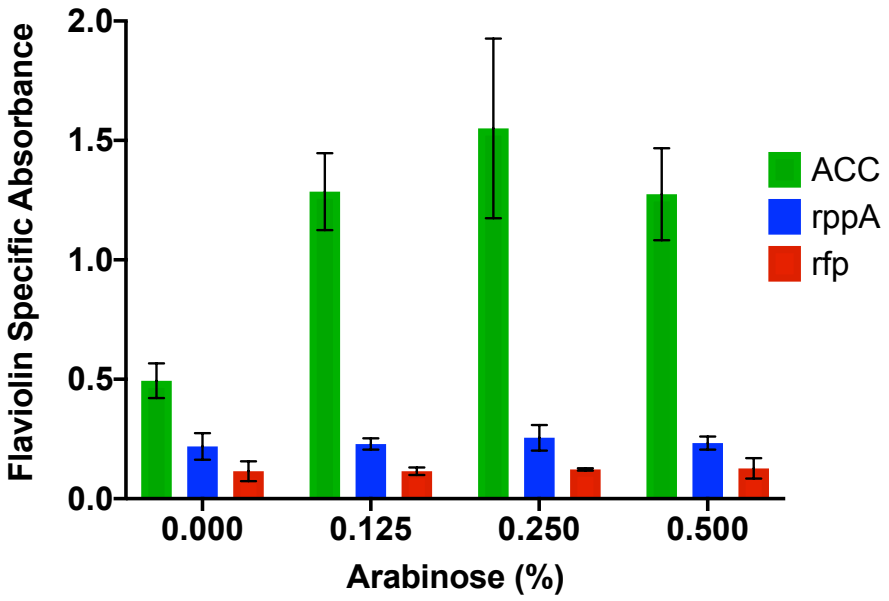

Figure 32 - Flaviolin-specific absorption for H16 Δ3 Δmcd carrying reporter derivatives pMTL71301_ACC_*rppA* (green), pMTL71301_*rppA* (blue) and pMTL71301_*rfp* (red). Cells were grown in SG-MM medium for 20 hours at the indicated arabinose concentrations before absorption of the culture supernatants was analysed at 340 nm. Error bars mean: ± SD, n = 3.

In this experiment, the strains bearing the ACC showed significantly increased signal output (Figure 32). The OD-corrected absorption signal was 5-6-fold higher in the strains with the ACC. This implies that more malonyl-CoA was available when the ACC was expressed.

However, the health of the strains was seriously affected by the expression of the ACC at this level. Even at the lowest level of induction (0.125% arabinose) the OD of the cells at 20 hours was significantly lower, with around a 90% reduction (Figure 33 and Figure 34). This is due to ACC-overexpression-mediated cellular toxicity [202]. The strain carrying just *rppA* and the *rfp* control strain did not show any detrimental effects, regardless of level of arabinose. This further indicates that the stressor is the overproduction of a non-native ACC and is not due to the presence of the biosensor gene. Overall, the presence of the ACC increased the relative signal of the biosensor, and therefore, presumably, the malonyl-CoA levels. However, the observed detrimental effects of the *acc* expression approach need to be taken into consideration when constructing 3-HP producing strains.

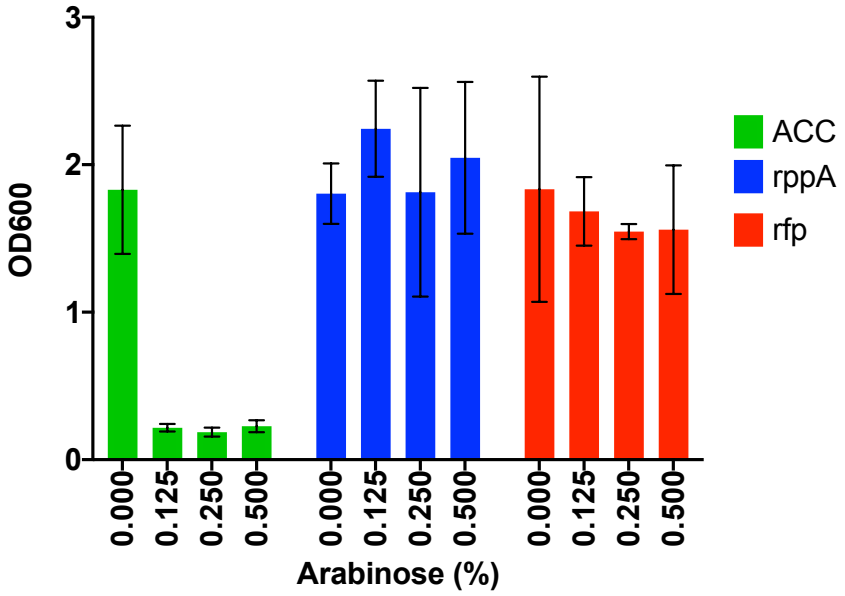

Figure 33 - Optical density of H16 Δ3 *Δmcd* derivative cultures in the presence of arabinose. H16 Δ3 *Δmcd* with reporter derivative pMTL71301_*acc_rppA* (green), pMTL71301_*rppA* (blue) and control pMTL71301_*rfp* (red). Cultures were grown in SG-MM medium at the indicated arabinose concentrations and the final OD600 determined after 20 hours. Error bars mean: ± SD, n = 3.

Lower concentrations of arabinose between 0 and 0.125% (w/v) were investigated to see if a balance could be found between cell growth and expression and therefore, presumably, malonyl-CoA level. Growth data showed that any induction of the ACC leads to a reduction in OD at 20 hours. Even the addition of the lowest concentration (0.016%) caused a dramatic decrease (56%) in OD600.

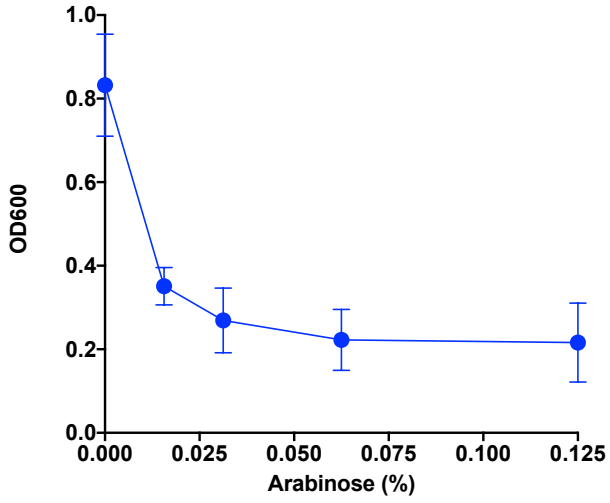

Figure 34 - Optical density of strain H16 Δ3 Δmcd ACC after 20 hours of growth in SG-MM medium at the indicated arabinose concentrations. The starting OD of the cultures was approximately 0.05. Error bars mean: ± SD, n = 3.

A further derivative was constructed, pMTL71301_ACC_*YDFGEC_rppA*, containing the *E. coli ydfG*$_{Ec}$ gene in addition to the *C. glutamicum acc* genes. This was done because the encoded *YdfG*$_{Ec}$ malonate semialdehyde reductase efficiently converts its substrate to 3-HP. It is a vital step in the production of 3-HP (see Chapter 3). As this gene changes the configuration of the plasmid (Figure 9), further experiments were undertaken to confirm that expression of this gene had no effect on malonyl-CoA accumulation. The plasmid pMTL71301_*acc_ydfGEc_rppA* was introduced into strain H16 Δ3 Δ*mcd* and tested with different arabinose levels as before (Figure 35). No significant different difference was found between this strain and the H16 Δ3 Δ*mcd* carrying pMTL71301_*acc_rppA*.

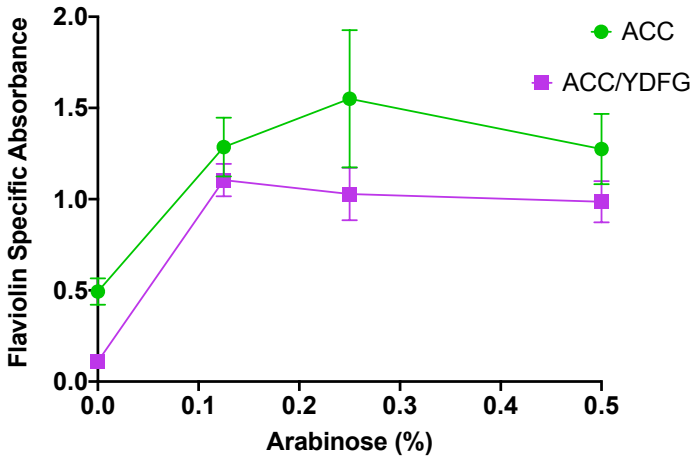

Figure 35 - Flaviolin-specific absorption for H16 Δ3 *Δmcd* carrying reporter derivatives pMTL71301_*acc_rppA* (green) and pMTL71301_*acc_ydfGEc_ rppA* (pink). Cells were grown in SG-MM medium for 20 hours at the indicated arabinose concentrations before absorption of the culture supernatants was analysed at 340 nm. Error bars mean: ± SD, n = 3.

4.4 Discussion

4.4.1 Characterisation of the RppA biosensor in *E. coli*

The wavelength scan of strains DH5α *rppA* reporter and DH5α *rfp* control showed that 340 nm was the most appropriate wavelength at which to relatively quantify the flaviolin level in M9 medium. This was contrary to another study by Tarasava that found 520 nm to be a more suitable wavelength [216]. However, in that study only wavelengths between 400 nm and 600 nm were checked. The results of this thesis agreed with the findings by Yang *et al*., using 340 nm to detect flaviolin in the culture [150].

Interestingly, in this study cerulenin at the used concentrations did not have any significant effect on the final growth of the DH5α cultures. Further work would need to be undertaken to compare growth profiles in *E. coli* strains (however, this work was completed in *C. necator* strains as it was deemed more relevant to the final aims of the project). Although no recent data could be found investigating cerulenin concentration and growth rate in *E. coli*, a concentration of 112 µM has been reported to cause complete and irreversible growth elimination [222]. However, Goldberg *et al.* found that all concentrations of cerulenin had an effect on cell density [223].

The flaviolin specific absorption for DH5α pMTL71301_*rppA* reporter does show a dose-dependent response to increasing levels of cerulenin, presumably as a result of an increasing intracellular malonyl-CoA availability. The flaviolin-producing strain (DH5α pMTL71301_*rppA*) showed a clear increase as cerulenin was titrated, up to approximately 3 µM (Figure 23). Above this concentration, no further statistically significant increase was observed regardless of cerulenin level. This suggests that the cerulenin had a strong effect on the *E. coli* reporter strain, achieving intracellular malonyl-CoA concentrations that were saturating with respect to flaviolin production. In a previous study by Yang *et al.* an *E. coli* strain carrying the *rppA* gene under control of the P_{tac} promoter gave a normalised absorption at 340 nm of ~1 [150], however the signal was lower in the strain created for this study. This could be due to the plasmid backbone used in this study (pMTL71301) not being designed for expression in *E. coli*, but rather contains a *C. necator* optimised replicon.

The background level of absorption at 340 nm was high. The M9 media was checked and did not significantly absorb the light at this wavelength. This suggests that other compounds produced by the growing strain have a similar wavelength to flaviolin and were being detected. It is unknown what these extracellular compounds may be.

In the previous studies, the IPTG inducible *rppA*-dependent flaviolin signal was compared to that of a non-induced *rppA* control [150]. However, the promoter used in this study when constructing the reporter plasmid pMTL71301_*rppA* was a mutated constitutive tac promoter (without *lacI* repressor gene) that no longer requires induction with IPTG. This promoter was chosen because the final host strain (*C. necator*) is unable to take up IPTG from medium, making it unable to activate inducible versions of the tac promoter [35].

4.4.2 Testing the effect of cerulenin on *C. necator* H16 Δ3 Δ*mcd*

The cerulenin had an unanticipated effect on the health of *C. necator* H16 Δ3 *Δmcd*, with strong negative correlation between cerulenin concentration and final optical density (Figure 26C). These results are contrary to those published by Johnson, who tested strain *C. necator* H16 with the same range of cerulenin concentrations and found no inhibition of growth [202]. This suggests that the differences between H16 and H16 Δ3 Δ*mcd* may have an effect of cerulenin resistance. This is most likely to be because the deletion of the malonyl-CoA decarboxylase gene (*mcd*) stops the ability to convert malonyl-CoA back to acetyl-CoA. When cerulenin is added the malonyl-CoA levels are hypothesised to increase and which may result in significant accumulation. This toxicity is also seen when ACC is overexpressed. It has been suggested that this is due to the depletion of free CoAs, resulting in a metabolic imbalance [176]. In H16, *Mcd* could act as a shunt to correct this imbalance, but the removal of it results in decreased growth rate and final OD600.

4.4.3 Characterization of the RppA biosensor in *C. necator*

The RppA biosensor was shown to work well in *C. necator*, producing the heavily coloured flaviolin, that was released into both liquid media and solid agar. There was

a clear dose dependent response, as the cerulenin concentration increased, as did the flaviolin specific absorption. A maximum signal was seen with cerulenin levels between 12.5 µM and 25 µM. Similarly, Johnson found that 20 µM cerulenin was enough to show maximum signal using the FapR/*fapO* biosensor in *C. necator* H16 [202]. This allows the biosensor to be used alongside other genetic engineering techniques (e.g., strain development and overexpression) to evaluate their effect on intracellular malonyl-CoA levels.

The flaviolin concentration appeared to be much higher in *C. necator* H16 Δ3 Δ*mcd* compared to the same reporter plasmid in *E. coli* DH5α. This does not necessarily indicate that there is a higher amount of intracellular malonyl-CoA available in the *C. necator* strain compared to the *E. coli* strain. This is because it cannot be confirmed that the lower signal in DH5α is not due to promoter inactivity, resulting in suboptimum conversion of malonyl-CoA to THN and then to detectable flaviolin. As the origin of replication (pBBR1) is compatible with the strain, this is likely to have arose due to the tac promoter being inducible in *E. coli* due to presence of the native, chromosomal *lacI* gene, whereas it is a strong constitutive promoter in *C. necator*, which lacks this repressor [35]. No IPTG was added when the *E. coli* DH5α was tested, but this could be future work. The background signal produced by H16 Δ3 Δ*mcd* pMTL71301_*rfp* was much lower than that seen in DH5α pMTL71301_*rfp* control. It is uncertain why this is the case but could be due to media or promoter strength.

The RppA biosensor appeared to increase the health of the H16 Δ3 Δ*mcd* in the presence of cerulenin. Previously, as the cerulenin concentration increased, the final optical density of the cells decreased. However, in strain H16 Δ3 Δ*mcd* carrying pMTL71301_*rppA* there was no significant change in final OD600, regardless of cerulenin concentration. This could be due to high malonyl-CoA levels leading to cell toxicity or could relate to the lack of free CoAs. The mechanism for growth inhibition is unknown and cannot be determined in this experiment. However, the addition of a malonyl-CoA shunt, RppA converting 5 malonyl-CoA molecules to 1 THNS molecule alleviated the stress experienced.

4.4.4 Comparison of biosensor signal between genetically engineered strains of *C. necator*

The best strain for 3-HP production would presumably be the strain with the highest available malonyl-CoA level. In order to test this, previously designed strains with genes knocked out were transformed with plasmid pMTL71301_*rppA*. It was previously hypothesised that deleting genes coding for *Mcd*, the *phaCAB* operon and the 3 MmsA ((methyl)malonate semialdehyde dehydrogenases) homologues would increase the malonyl-CoA availability. However, the flaviolin specific absorption in the absence of cerulenin was very similar for all 4 tested strains. This suggests that the pool of malonyl-CoA is unaffected by any of the knockouts necessary to stop 3-HP consumption. This is interesting because it suggests that availability is the same in the absence of inhibitor (cerulenin). However, more malonyl-CoA is available in the strain that is completely blocked for malonyl-CoA degradation (H16 Δ3 *Δmcd*) when fatty acid biosynthesis is inhibited by cerulenin. This could suggest that fatty acid synthesis is the main and most efficient pathway of malonyl-CoA utilisation, as would be expected.

Further work needs to be undertaken to establish whether there is a significant difference between the H16 Δ4 strain when corrected not for OD but cell number. Until the effect of low OD is accounted for, it is not possible to say whether malonyl-CoA levels or availability is higher in H16 Δ4 that cannot produce PHB compared to the other tested strains.

4.4.5 Investigating the effect of ACC on biosensor signal

The effect of overexpression of the *acc* gene from *C. glutamicum* in *C. necator* is hard to predict due to stringent feedback inhibition of the ACC enzyme, although it has worked well in *E. coli* [139]. The gene was designed into a plasmid with the reporter gene to match the plasmid designed for 3-HP production (Chapter 3). The advantage of this plasmid design is only a single plasmid needs to be maintained, with a single antibiotic resistance. However, the disadvantage is that it is unknown how this may affect copy number or expression of the reporter. Ideally, given more time, another plasmid could have been created and tested with *rfp* control instead of

rppA gene. This would allow for testing to see the effect on the strain without the reporter, using *rfp* output as a marker.

The flaviolin specific absorption increased when the *acc* gene was present, controlled by the P_{BAD} promoter, compared to *rppA* gene alone (Figure 32). This implies that the ACC enzyme is converting more acetyl-CoA into malonyl-CoA, that can then be combined to create THNS, leading to flaviolin. This suggests that the addition of the ACC enzyme in the pathway to 3-HP could increase yields. However, the addition of arabinose caused a dramatic decrease in final optical density. This dramatic decrease was apparent even at very low arabinose concentrations (0.016% (w/v)). It is likely that any expression of the enzyme will have an effect on growth, although this will continue to be investigated. Toxicity and the negative impact on cell health due to *acc* overexpression is well documented, but no defined mechanism has been established [181]. It is currently unknown if the final ODs of the strains would eventually be the same if left for a longer incubation time. Further work needs to be done to investigate this, such as measuring the specific activity of the RppA enzyme in extracts.

4.5 Key Outcomes

The work in this chapter aimed to design and implement a malonyl-CoA biosensor in *Cupriavidus necator* strains and to evaluate the previously used methods to increase this. The specific outcomes were –

- A plasmid-based malonyl-CoA biosensor, using a type III polyketide gene (*rppA*) from *S. griseus* was shown to work effectively in *C. necator.*
- Addition of cerulenin, known to inflates malonyl-CoA levels through inhibition of fatty acid biosynthesis, had a detrimental effect on growth in some strains that are lacking the malonyl-CoA decarboxylase (*mcd*) gene.
- The biosensor was used to evaluate the strains designed the increase malonyl-CoA levels/availability, but data suggest that there was no significant difference in malonyl-CoA availability in these strains.
- The biosensor was used to evaluate the use of a heterologous acetyl-CoA carboxylase (ACC) to amplify the amount of intracellular malonyl-CoA available. Increased reporter output was indeed observed when the *acc* gene cluster was expressed. Unfortunately, this overexpression also caused cellular toxicity, even at very low induction levels

Chapter 5 –
Repression of fructose catabolism by 3-HP

Chapter 5 - Repression of fructose catabolism by 3-HP

5.1 Introduction

5.1.1 Metabolic versatility in bacteria

As a potential industrial strain for biosynthesis of commodity chemicals, it is vital to understand the metabolism of *C. necator*. In addition to chemolithotrophic metabolism, using H_2 and CO_2 as energy and carbon sources respectively, this soil dwelling bacteria has the ability to grow on a vast number of heterotrophic carbon sources [7]. Genetic engineering and directed evolution experiments have allowed even more compounds to be utilised [26], [59].

However, many of these investigations and engineering attempts focus on the assimilation of a single carbon source. This means that comparatively little is known about the organism's preferences in the presence of multiple carbon sources and the resulting metabolic consequences and regulatory interactions. In order to design the ideal chassis organism for biotechnological purposes, the intricate regulation of the utilisation of multiple compounds must be understood.

In nature, it is unlikely that bacteria will live in an environment with only a single carbon source available. The ability to adapt to multiple nutrient sources in the most efficient manner can be the vital in a competitive ecosystem. However, most experimental data related to bacterial consumption of carbohydrates is simplistic and mono-source. This does not reflect the natural habitat in which the organisms have evolved [224]. Although a hierarchy of preferred carbon sources can be established, the underlying mechanisms are complex and often unpredictable. For example, if a species has two available, consumable sugars, priority is generally given to the pathway that is less metabolically costly to achieve maximum growth. This behaviour is classified as diauxic growth, with one compound being completely depleted before the second begins to be consumed [225]. The classic example of this hierarchical process is the pattern of assimilation of sugars in *E. coli*, as diauxic growth is seen in a medium containing a mixture of glucose and lactose [226].

5.1.2 Metabolism of 3-HP in *C. necator*

Interest in 3-HP is discussed in previous chapters in detail, as the chemical has been described as an environmentally friendly alternative to fossil fuel derived products. Previous work has shown that *C. necator* can use 3-HP as a sole carbon source, metabolised by the route shown in Figure 36A [63]. It is not known how the compound is transported into the cell, but once internalised 3-HP is converted into malonate semialdehyde by a 3-hydroxypropionate dehydrogenase (*hpdH*, H16_A3663). This toxic intermediate is converted to acetyl-CoA by 3 homologous (methyl)malonate semialdehyde dehydrogenases (*mmsA1*, H16_A0273; *mmsA2*, H16_A3664; *mmsA3*, H16_B1191) which enters central carbon metabolism.

All 3 *mmsA* genes must be deleted in *C. necator* H16 to stop the degradation of 3-HP, whereas deletion of the *hpdH* gene alone only delayed the degradation [63]. In *C. necator*, the 3 *mmsA* homologues are located and regulated separately (Figure 36B). The *mmsA1* operon encodes a β-alanine-pyruvate transaminase, designated *aptA*, and is involved in utilisation of β-alanine [131]. The operon that contains *mmsA2* also encodes the aforementioned *hpdH* and is regulated by a LysR-type transcriptional regulator named HpdR. The corresponding system in *P. putida* was shown to be responsive to 3-HP. In *P. putida* it can confidently be theorised that the *hpdR* is a regulator that binds to the intergenic region under uninduced conditions and is derepressed in the presence of 3-HP [39]. Previous work suggests that the favoured physiological substrate of the *C. necator* MmsA3 is methylmalonate semialdehyde, rather than malonate semialdehyde, but it has flexible specificity. The encoding operon has been shown to play a role in valine and 3-hydroxyisobutyrate degradation and is assumed to be controlled by a AraC transcriptional regulator [63].

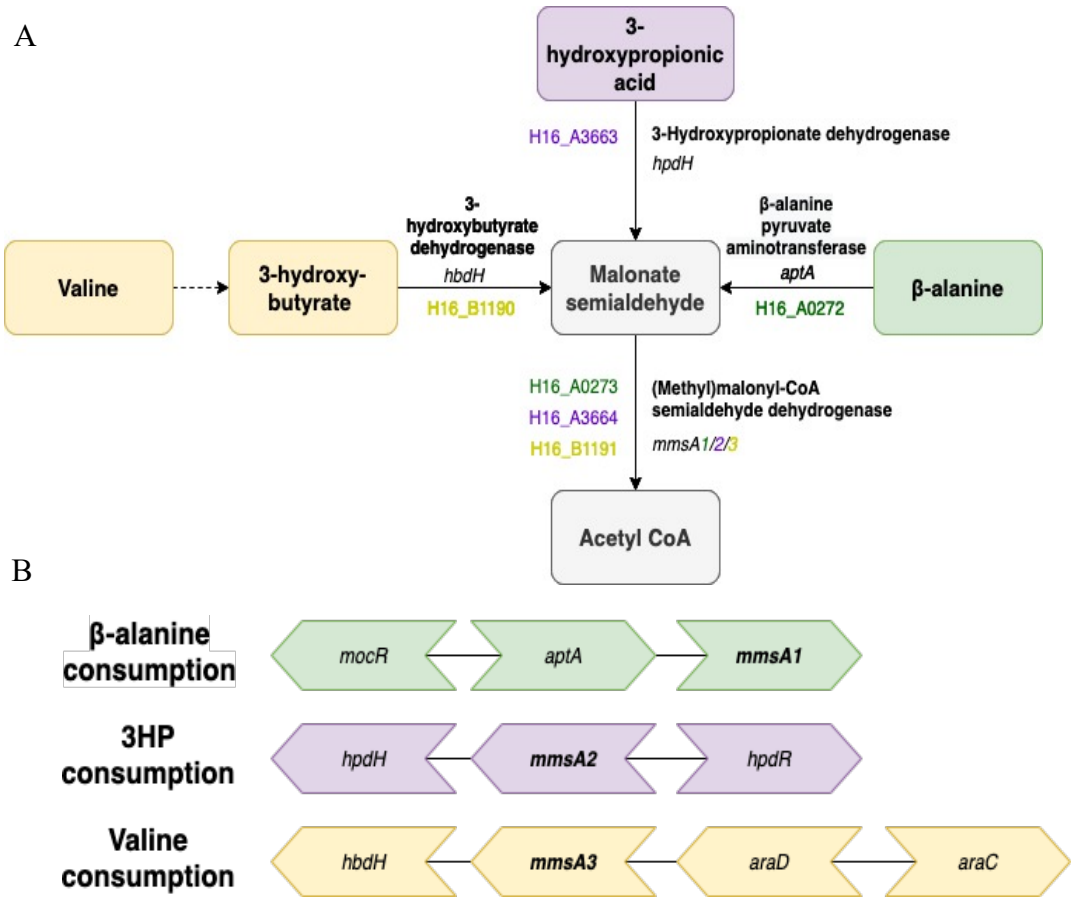

Figure 36 – 3-HP degradation in *C. necator* H16 (A) Schematic of metabolism via malonate semialdehyde to acetyl-CoA. Enzyme names and corresponding gene names shown on arrows. Locus tags shown in corresponding colours to the operons in Figure 37B. (B) The operons involved in 3-HP degradation in *C. necator* H16. Genes shown in green are involved in β-alanine degradation. Genes shown in purple are related to 3-HP degradation. Genes shown in yellow are responsible for valine degradation. Each (methyl)malonate semialdehyde dehydrogenase (mmsA) gene is separately controlled by oppositely transcribed transcriptional regulators (homologs of MocR, LysR and AraC, respectively), and presumably activated by intermediates of the consumption pathways (indicated on the left). *aptA* encodes a β-alanine pyruvate aminotransferase, *acaD* encodes acyl-CoA dehydrogenase. *hpdH* and *hbdH* are genes for 3-hydroxypropionate dehydrogenase and 3-hydroxybutyrate dehydrogenase respectively.

5.1.3 Catabolic repression of fructose by 3-hydroxypropionic acid

In a production scenario it is likely that substrate and product will both be present in a fermentation mixture. For this reason, any strain used for biosynthesis needs to have a high tolerance to the product, without re-consuming it or initiating regulatory systems that may limit productivity.

Previous work by Arenas-Lopez generated *C. necator* H16 Δ3, a strain engineered to not consume 3-HP [24]. This strain grew well when maintained on fructose alone. However, when incubated in a medium containing 25 mM fructose and 50 mM 3-HP,

the strain did not grow for at least 48 hours, in contrast to the wild type. The H16 Δ3 culture remained at the starting OD, and neither fructose nor 3-HP was used. After this prolonged lag phase, the cultures consumed only the fructose. However, when the H16 Δ3 cells were collected from finishing cultures and regrown in the same medium, no lag phase was seen, and fructose was consumed immediately. No 3-HP was consumed [63]. Interestingly, the ability to consume fructose in the presence of 3-HP was maintained when cells from the adapted H16 Δ3 cultures were grown on fructose only, either on agar plates or in liquid, before being transferred back into medium containing both fructose and 3-HP. The presence of 3-HP, even though it could not be metabolised, appeared to prevent the utilisation of fructose.

Using transcriptome analysis of *C. necator* H16 grown 3-HP, Arenas *et al.* showed upregulation of the *mmsA2* operon, with the *hpdH* and *mmsA2* genes being upregulated 154 and 156 fold [63]. This RNA-seq data also showed significant down-regulation of the fructose catabolism genes (H16_B1497- H16_B1501) in the presence of 3-HP. These genes were expressed at levels 70 to 200-fold lower than in cells grown on fructose [63].

No obvious connection between fructose and 3-HP utilisation is apparent. As the repression of fructose breakdown is established, further work needs to look at the utilisation of other compounds that may also be interrupted by 3-HP. Although the asynchronous depletion of compounds in commixture is commonly observed for prokaryotes, more can be gleaned about the regulation through the use of gene knockouts and evolution experiments [227]. This can allow more productive strains to be engineered. If 3-HP is to be synthesised biologically from organic carbon sources in a commercial setting, any undesirable consequences of product accumulation must be understood.

5.1.4 Metabolism of carbon sources *via* ED pathway in *C. necator*

Fructose, *N*-acetylglucosamine and gluconate are the only substrates naturally metabolised by the ED pathway in *C. necator* [228]. The encoding genes for proteins transporting and phosphorylating these compounds are located distally and regulated separately [21], [228].

The two enzymes of the main ED pathway (Figure 37) are phosphogluconate dehydratase and phosphogluconate aldolase (encoded by *edd* and *eda* respectively), which catalyse conversion of 6-phosphogluconate to 2-keto-3-deoxy-6-phosphogluconate (KDGP) and cleavage of the latter to pyruvate and glyceraldehyde-3-phosphate [229]. Deletion of *eda* in *C. necator* was shown to prevent growth on fructose and gluconate [230]. This is the sole glycolytic pathway in *C. necator* H16 as it lacks a phosphofructokinase required to complete glycolysis *via* Embden-Meyerhof-Parnas (EMP). As the three main sugar substrates pass through this pathway, the effect of 3-HP in combination with each of these carbohydrates was investigated.

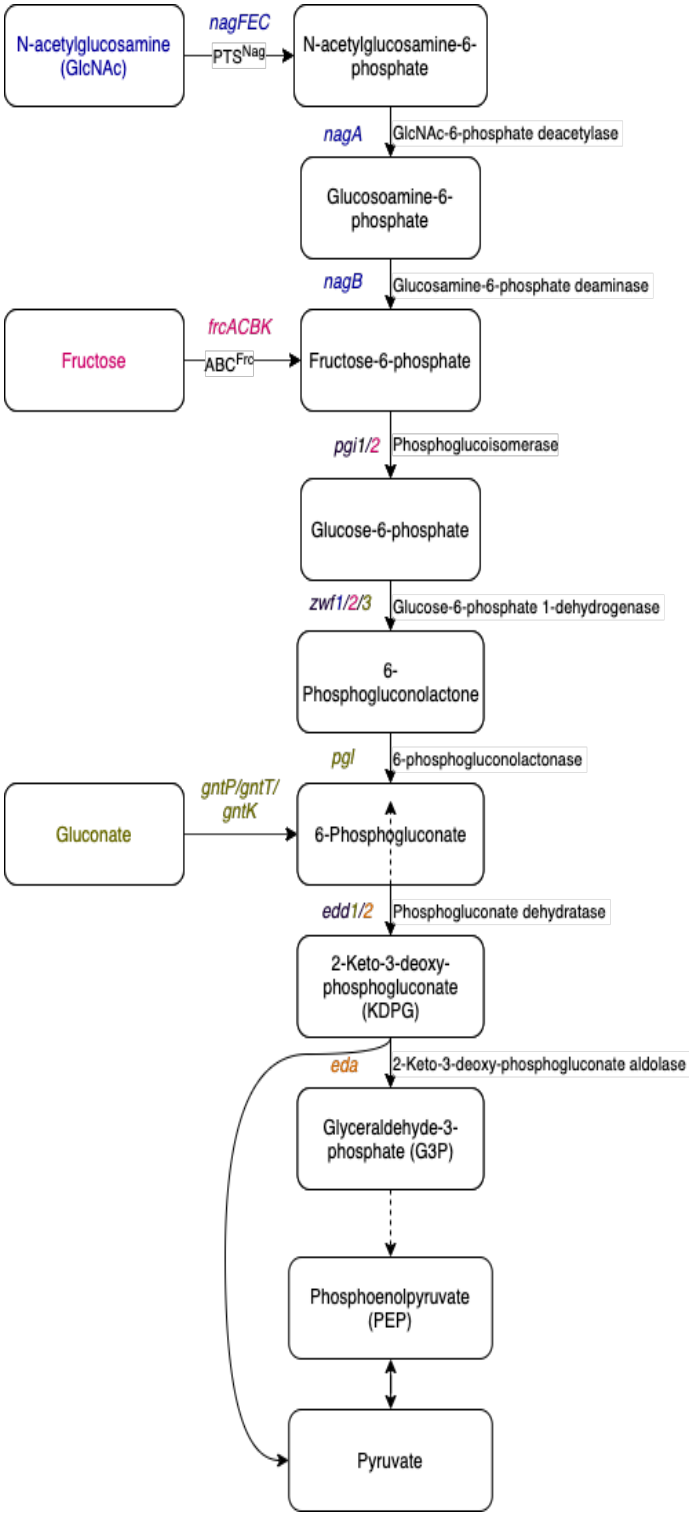

Figure 37 – The pathway for 3 commonly used substrates that are metabolised via the ED pathway to pyruvate in *C. necator* H16. Gene abbreviations are on the left of the arrows. Enzyme names are right of the arrows. Gene names in blue are related to N-acetylglucosamine metabolism. Names in pink indicate genes involved in fructose utilisation. Genes related to gluconate are indicated in green. Genes encoding enzymes of the ED pathway are shown in orange. Figure constructed using information collected from Pohllman *et al*., [7], Raberg *et al*. [21] and González-Villanueva *et al.* [59]

5.2 Aims and objectives of chapter

Using a range of approaches, including growth experiments on different carbon sources, and sequencing of adapted strains, the overall aim of this chapter was to gain further insights into the mechanisms underlying 3-HP mediated catabolite repression. More specifically, the objectives were to

- Further explore the connection between fructose and 3-HP utilisation in a range of engineered *C. necator* strains
- Use genomic sequencing tools to determine the cause(s) of the observed adaptation effects
- Investigate the effect of the presence of 3-HP on the consumption of other carbohydrates
- Explore any emerging hypotheses behind the inhibition of growth on compounds metabolised by the ED pathway

5.3 Results

5.3.1 Effect of 3-HP and fructose on wild type *C. necator* H16 growth

To begin the investigation into 3-HP metabolism and the effect on sugar uptake, wild type *C. necator* H16 cells were grown in F+3HP-MM (Figure 38). The OD, fructose and 3-HP concentrations were quantified at regular intervals. In the wild type, growth started immediately with no lag phase, reaching maximum OD by 48 hours. All fructose and 3-HP were consumed by 72 hours, in the first 24 hours only 3-HP was consumed. The OD reduced somewhat when the carbon sources were depleted.

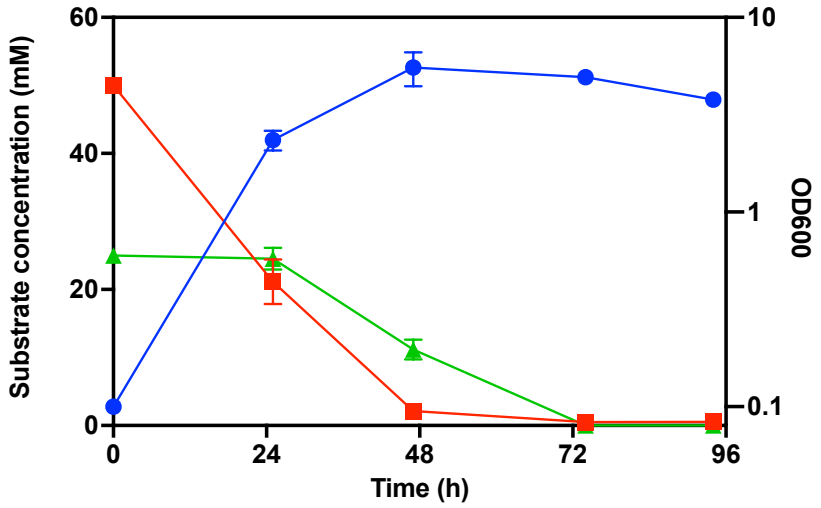

Figure 38 – *C. necator* H16 grown in F+3HP-MM. Blue circles = OD; red squares = 3-HP concentration; and green triangles = fructose concentration. Data points shown are means. Error bars mean ± SD, n = 3. F+3HP-MM contains 25 mM fructose and 50 mM 3-HP.

5.3.2 Effect of 3-HP and fructose on *C. necator* H16 Δ3 growth

Following this, 10 replicates of H16 Δ3 were grown in F+3HP-MM for 192 hours. As seen in Figure 39, there was no consumption of fructose or increase in OD before 48-72 hours, but after that timespan cultures started to grow and reached ODs similar to those seen for the wild type. No 3-HP was consumed throughout the experiment (as expected for H16 Δ3). It was suspected that the strains were adapting to the presence of 3-HP, so the genomic DNA was extracted from the final samples of each of the replicates, alongside the initial inoculum, and all were sent for whole genome sequencing as outlined in Section 2.21.

Upon completion of the growth experiment, the H16 Δ3 cultures were plated on F-MM, then fresh F+3HP-MM was inoculated from these plates. In this experiment, no lag/delay was seen in OD increase or fructose concentration decrease, as seen in Figure 40. All the fructose was consumed by 72 hours, when the bacteria entered stationary phase. Overall, the 3-HP concentration remained static over the course of the experiment.

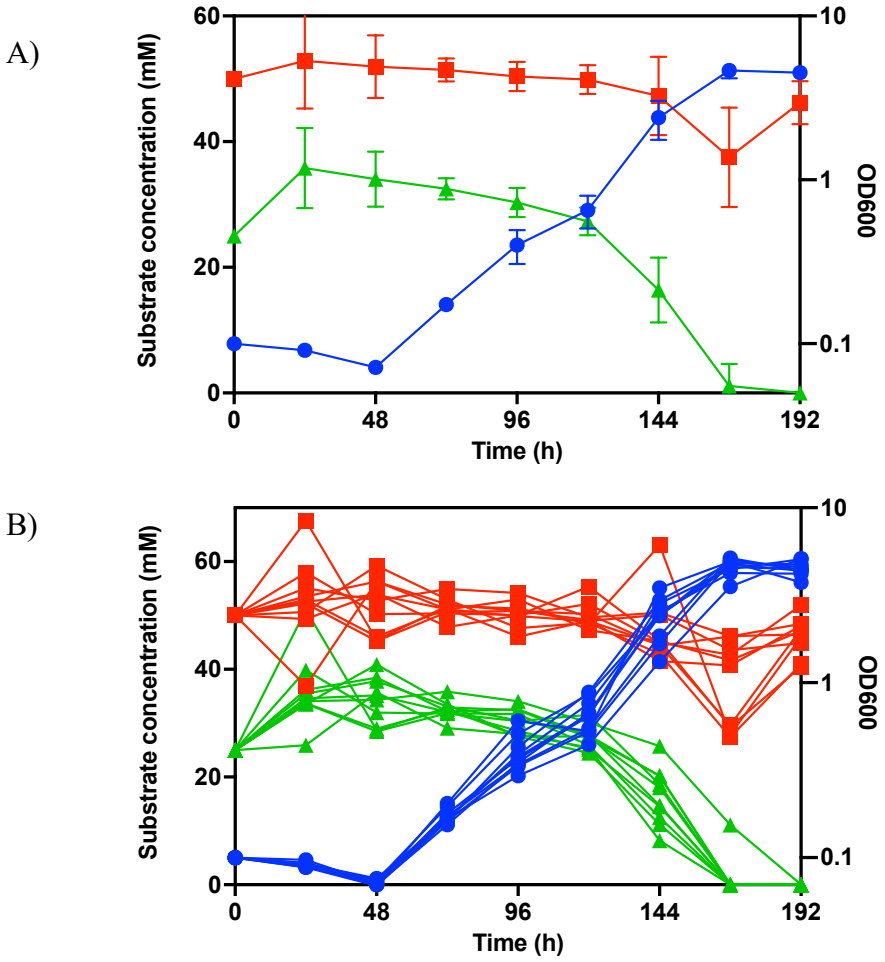

Figure 39 – A) Averaged and B) individual growth curves for 10 replicates of *C. necator* H16 Δ3 grown in F+3HP-MM. Blue circles = OD, red squares = 3-HP concentrations and green triangles = fructose concentration. Data points shown are means. Error bars mean ± SD, n = 10. F+3HP-MM contains 25 mM fructose and 50 mM 3-HP.

Comparison of the obtained genome sequencing data to that of the H16 Δ3 parent strain (see 2.21 for details) showed that many of the strains (70%) had mutations in the *mmsA2* operon region. In the H16 Δ3 strain this region carried a defined *mmsA2* deletion but was otherwise intact, i.e., still contained the intact and convergently transcribed *hpdH* and *hpdR* genes. In most of the isolated mutants, however, mutations were found throughout both *hpdR* and *hpdH* genes, as detailed in Table 15. Their

distribution and relative positions can be seen in Figure 41. This strongly suggested that activity of the encoded proteins was required for the observed 3-HP mediated repression of fructose utilisation to occur. These isolates also contained other SNPs deemed not to play a role, a complete list of all determined changes is given in the appendix 7.2.

It was not possible to identify any relevant SNPs in two of the sequenced strains. It is likely that mutations were missed due to the stringent criteria for identification of variants. Furthermore, in one replicate a mutation was found in *gntP,* and this may be related to the release of repression seen, but no experimental data can currently be found on the gene involved.

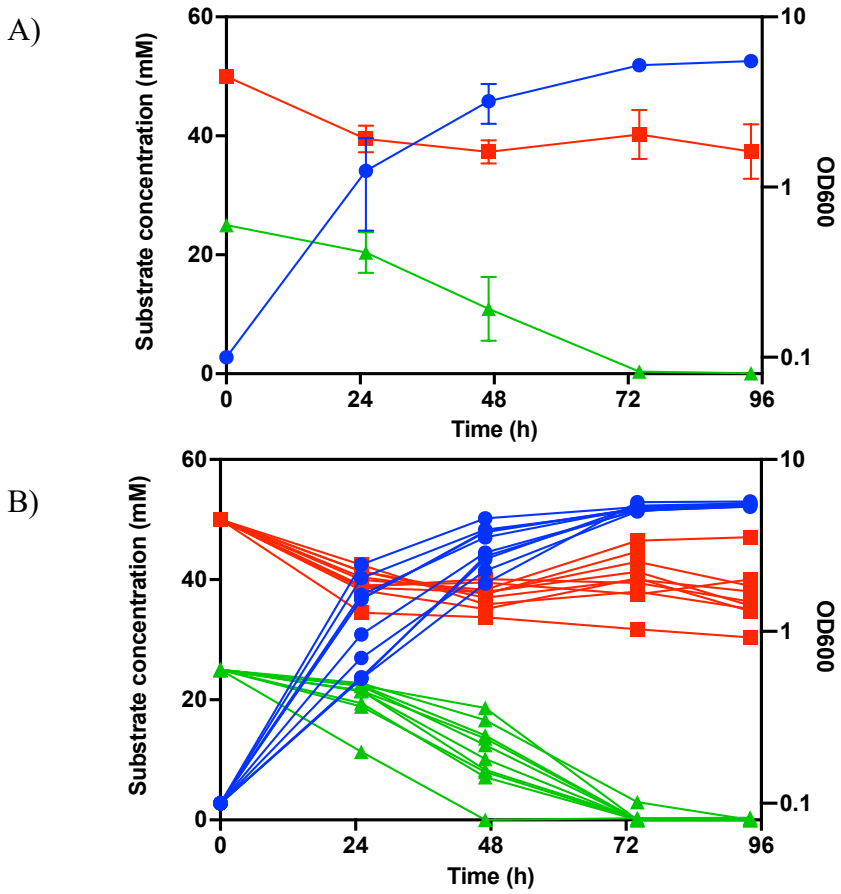

Figure 40 – A) Averaged and B) individual growth curves for 10 adapted replicates of H16 Δ3 grown in F+3HP-MM for a second time. Blue circles = OD; red squares = 3-HP concentrations; and green triangles = fructose concentration. Data points shown are means. Error bars mean ± SD, n = 10. F+3HP-MM contains 25 mM fructose and 50 mM 3-HP.

Table 15 - Mutations in H16 Δ3 after adapting growth in F+3HP-MM over 192 hours. Strain names refer to replicate number

Strain	Locus tag	Gene Name	Functional Description of Encoded Protein	Type	Length	Sequence in Reference	Sequence in strain	Effect of mutation	Frequency (%)
Δ3.1	H16_A3663	***hpdH***	3-hydroxypropionate dehydrogenase	Insertion	5	-	GGCCT	Frameshift	86.76
Δ3.2	H16_A3665	***hpdR***	LysR family transcriptional regulator of *mmsA2-hpdH* operon	Insertion	8	-	CGAACACT	Frameshift	93.75
Δ3.5	H16_A3665	***hpdR***	LysR family transcriptional regulator of *mmsA2-hpdH* operon	SNP	1	C	T	Missense Ala → Val	100
Δ3.6	H16_A3011	***gntP***	Member of the Gnt family of gluconate transporters; unknown function	SNP	1	C	T	Missense Ser → Leu	100
Δ3.7	H16_A3665	***hpdR***	LysR family transcriptional regulator of *mmsA2-hpdH* operon	SNP	1	C	T	Nonsense Trp → Ter*	65.38
	H16_A3663	***hpdH***	3-hydroxypropionate dehydrogenase	SNP	1	C	T	Missense Thr → Ile	38.75
Δ3.8	H16_A3665	***hpdR***	LysR family transcriptional regulator of *mmsA2-hpdH* operon	SNP	1	A	G	Missense Asp → Gly	100
Δ3.9	H16_A3663	***hpdH***	3-hydroxypropionate dehydrogenase	Deletion	1	A	-	Frameshift	100
Δ3.10	H16_A3663	***hpdH***	3-hydroxypropionate dehydrogenase	SNP	1	T	C	Missense Lys → Glu	58.06
				SNP	1	C	G	Silent	58.06
				SNP	1	G	A	Missense Ser → Leu	62.06

Figure 41 – Distribution of mutations throughout *hpdH* and *hpdR*. Mutation sites indicated in green.

5.3.3 Growth of *C. necator* strains in the presence multiple carbon sources

To see if 3-HP mediated repression of growth extended to other sugars, *C. necator* H16 Δ3 was grown on range of minimal medium variants containing 50 mM 3-HP plus either 25 mM gluconate, *N*-acetylglucosamine or succinate. All cultures were also grown on the latter (the non-3-HP substrate) as the sole carbon source and grew well in the absence of 3-HP (data not shown). As previous experiments only observed the wild type and H16 Δ3 during growth on mixed carbon sources, and because of the results shown in Table 15, additional strains were studied. The 5 strains tested were wild type, H16 Δ3, H16 Δ*hpdH*, H16 Δ3Δ*hpdH* and H16 Δ3.1 (a strain adapted to 3HP and fructose in the previous experiment).

5.3.3.1 Fructose

Precultures of different *C. necator* strain were grown on fructose alone. As seen before, when moved to a medium containing fructose and 3-HP, the wild type strain showed no lag phase (Figure 42A). The strain reached peak optical density and depleted the fructose and 3-HP within 48 hours, as previously seen. The only strain to show an increased lag phase was H16 Δ3. The other 3 strains showed immediate growth, but the growth rate was slower than that seen in the wild type. The consumption of fructose supported this. No 3-HP was consumed by any of the gene deletion strains.

A

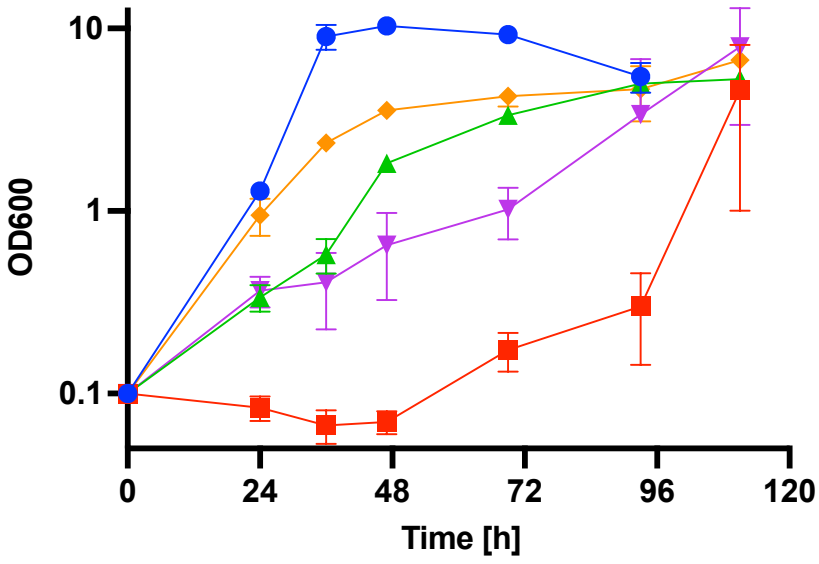

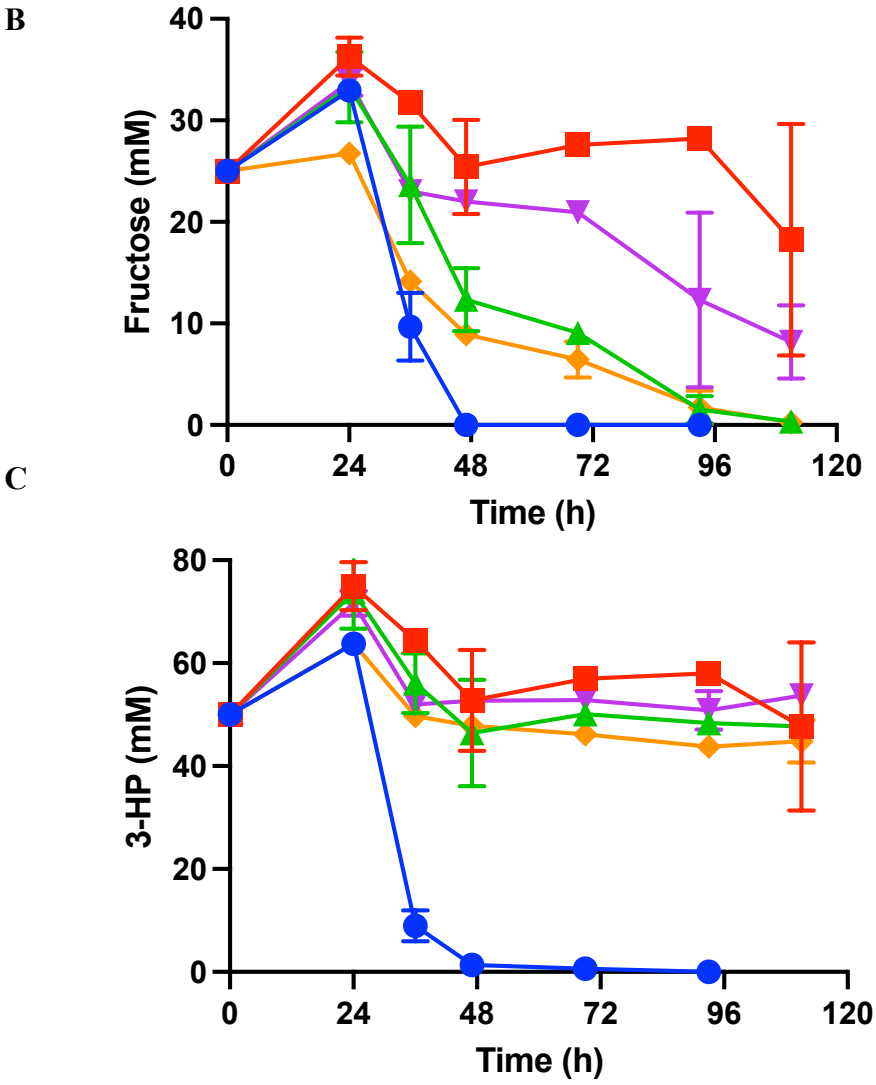

Figure 42 – Growth and substrate consumption of *C. necator* H16 derived strains in minimal medium supplemented with 25 mM fructose and 50 mM 3-HP. Strain were incubated for 120 hours. (A) Optical density measured at 600 nm; (B) Fructose concentration; (C) 3-HP concentration. Blue circles = H16 WT; red squares = H16 Δ3; green upward triangles = H16 Δ*hpdH*; pink downward triangles = H16 Δ3 Δ*hpdH*; and orange rhombus = H16 Δ3.1 (adapted strain from previous experiment). Data points and error bars are the mean ± SD, n = 3.

5.3.3.2 Gluconate

The same strains were grown in gluconate to establish if the repression extended to other ED pathway-metabolised compounds. Precultures were grown on a medium containing gluconate only. These cultures were used to inoculate the dual-source medium. No extended lag phase was seen for any of the strains on gluconate media with 3-HP (Figure 43). However, strain H16 Δ3 had a much slower growth rate. The strain took 72 hours to deplete the gluconate and reach peak OD, as opposed to 24 hours for all other strains.

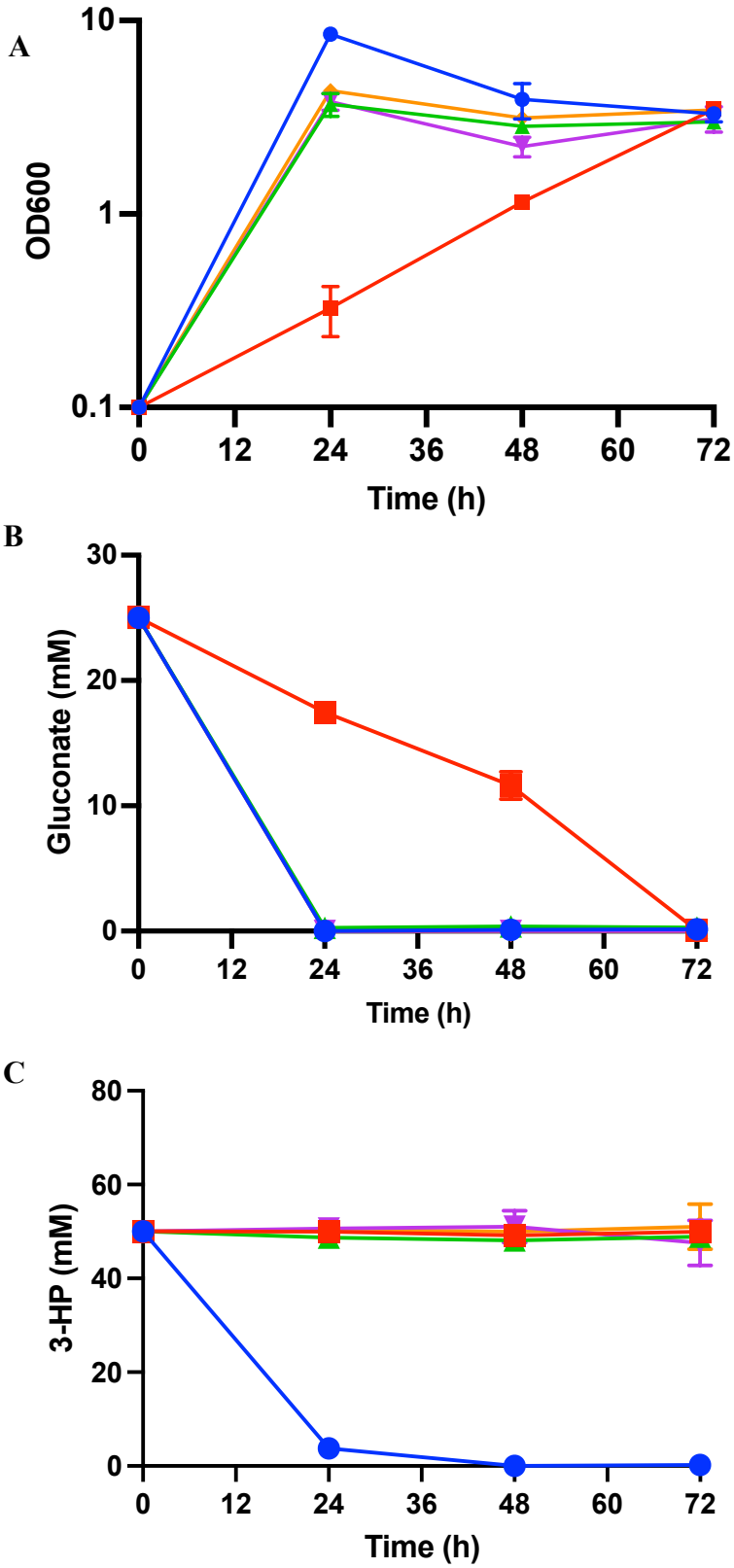

Figure 43 - Growth and substrate consumption of *C. necator* H16 derived strains in minimal medium supplemented with 25 mM gluconate and 50 mM 3-HP. Strains were incubated for 72 hours. (A) Optical density measured at 600 nm; (B) gluconate concentration; (C) 3-HP concentration. Blue circles = H16 WT; red squares = H16 Δ3; green upward triangles = H16 Δ*hpdH*; pink downward triangles = H16 Δ3 Δ*hpdH*; and orange rhombus = H16 Δ3.1 (adapted strain from previous experiment) Data points and error bars are the mean ± SD, n = 3.

5.3.3.3 *N*-acetyl glucosamine

The final sugar to be tested was *N*-acetylglucosamine. Precultures were grown on medium containing only *N*-acetylglucosamine. No growth was seen for the Δ3-derived gene deletion strains on this compound, when 3-HP was present (Figure 44A). All strains grew in media with *N*-acetylglucosamine as a sole carbon source (data not shown). In the presence of 3-HP, growth of H16 Δ3 and H16 Δ3 Δ*hpdH* was completely inhibited on *N*-acetylglucosamine. H16 Δ*hpdH* showed intermediate growth but didn't seem to consume *N*-acetylglucosamine. It is suspected that this strain began to consume 3-HP, however, issues arose with quantification of 3-HP and *N*-acetylglucosamine in the supernatant of later time points (seen in Figure 44B and Figure 44C)

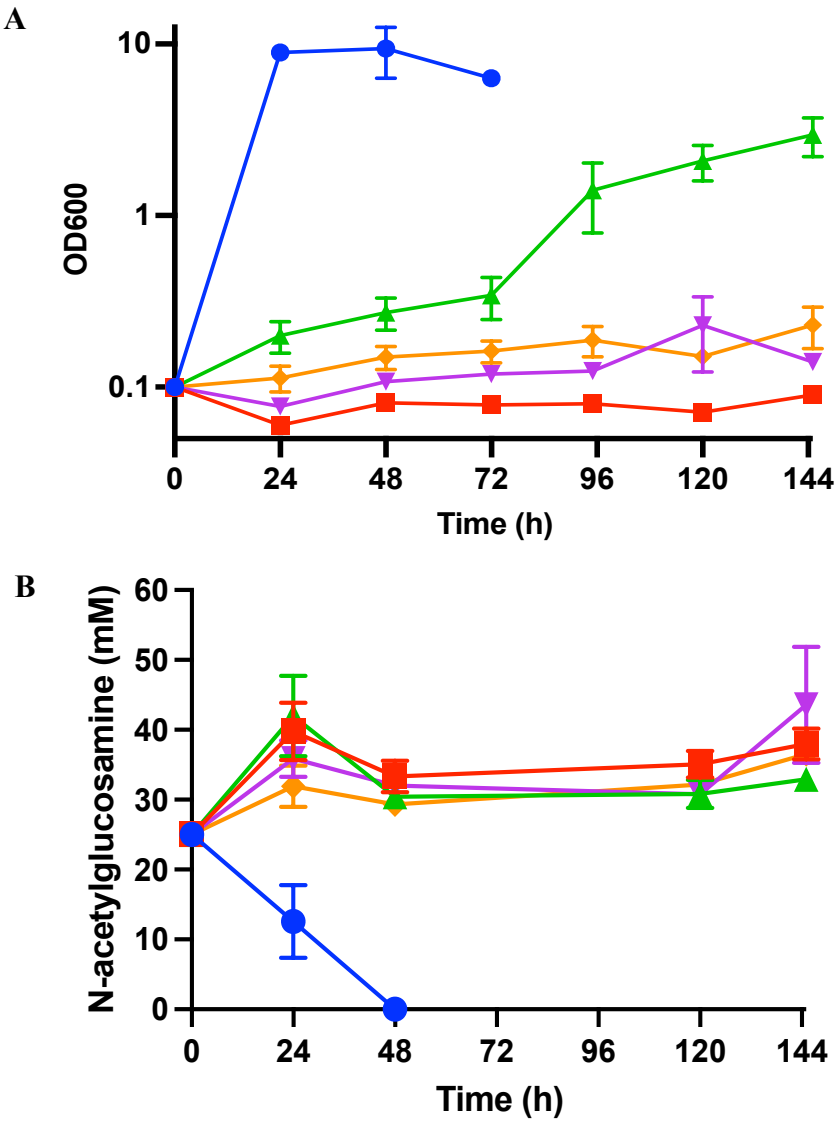

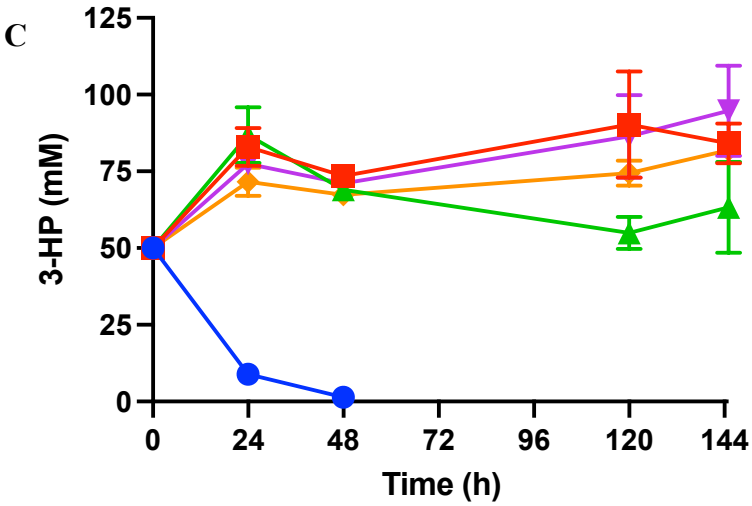

Figure 44 - Growth and substrate consumption of *C. necator* H16 derived strains in minimal medium supplemented with 25 mM N-acetylglucosamine and 50 mM 3-HP. Strains were grown for 144 hours. (A) Optical density measured at 600 nm; (B) N-acetylglucosamine concentration; (C) 3-HP concentration. Blue circles = H16 WT; red squares = H16 Δ3; green upward triangles = H16 Δ*hpdH*; pink downward triangles = H16 Δ3 Δ*hpdH*; and orange rhombus = H16 Δ3.1 (adapted strain from previous experiment) Data points and error bars are the mean ± SD, n = 3.

5.3.3.4 Succinate

The previously tested carbon sources were all metabolised by the ED pathway. For comparison, strains were also tested in succinate plus 3-HP medium. All strains grew in quickly in succinate as sole carbon source. As hypothesised, all the strains grew without any visible signs of repression to the same final OD, with the same growth rate (Figure 45A). No difference in succinate consumption was seen for any strain, apart from slightly lower consumption by H16 Δ3 (Figure 45B). A small amount (~10 mM) of 3-HP was consumed initially by the wild type strain but did not continue after 24 hours (Figure 45C).

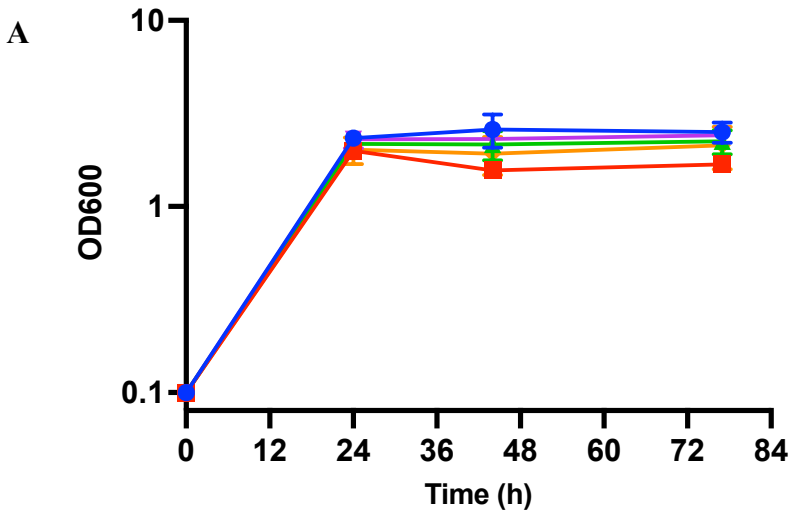

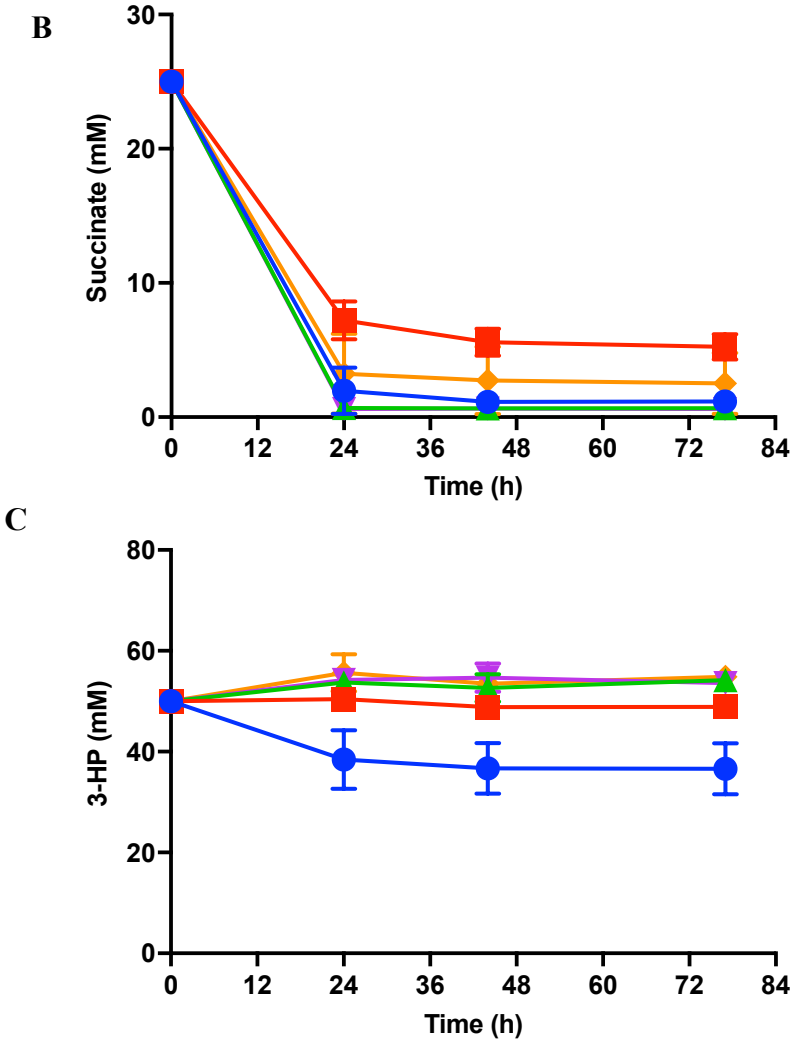

Figure 45 - Growth and substrate consumption of *C. necator* H16 derived strains in minimal medium supplemented with 25 mM succinate and 50 mM 3-HP. Strains were incubated for 144 hours. (A) Optical density measured at 600 nm; (B) succinate concentration; (C) 3-HP concentration. Blue circles = H16 WT; red squares = H16 Δ3; green upward triangles = H16 Δ*hpdH*; pink downward triangles = H16 Δ3 Δ*hpdH* and orange rhombus = H16 Δ3.1 (adapted strain from previous experiment). Data points and error bars are the mean ± SD, n = 3

5.4 Discussion

Due to the variety of reasons discussed throughout this work, *C. necator* H16 has the potential to become an industrially relevant producer of commodity chemicals. The high cell density and the ability to utilise waste products, and the synthetic toolbox available make *C. necator* an ideal organism for commodity chemical production. Many aspects of the organism's metabolism and its regulation remain poorly understood, leading to disappointing results for engineered strains and low yields.

5.4.1 Growth and substrate utilisation of *C. necator* in the presence of 3-HP and fructose

As expected, *C. necator* H16 wild type consumed both fructose and 3-HP when present in the media (Figure 38). Fructose is transported and phosphorylated by an CUT2-type ABC (ATP binding cassette) transporter (encoded by *frcACB*) and a fructokinase (*frcK*). These genes appear in an operon (H16_B1497-1503) with ED pathway genes; *zwf2* (glucose-6-phosphate 1-dehydrogenase, often just referred to as glucose-6-phosphate dehydrogenase) and *pgi2* (glucose-6-phosphate isomerase). Fructose-6-phosphate (derived from *N*-acetylglucosamine or fructose) is first converted to glucose-6-phosphate and then to glucolactone-6-phosphate (also known as 6-phosphogluconolactone). In a study by Arenas-Lopez *et al.* [63], the fructose utilisation operon, was downregulated when *C. necator* wild type cells were grown in the presence of 3-HP [63]. In this experiment, consumption of 3-HP began first, before fructose utilisation started at 24 hours. This delayed carbon utilisation and selective use of preferred sources is likely an example of catabolite repression [231], [232].

This non-classical version of catabolic repression has been documented in the *Pseudomonas* genus [233]. In these bacteria, organic and amino acids are preferred over sugars, with succinate, acetate and other organic acids inhibiting the expression of genes involved in glucose, fructose, gluconate, glycerol and mannitol utilisation [231]. This is an example of reverse carbon catabolism, where an acid is preferred over an available sugar. This form of reverse catabolite repression appears to be seen in *C. necator*, where an organic acid (3-HP) is preferentially consumed over a sugar (fructose).

This could occur *via* a regulatory mechanism known as inducer exclusion, where the nutritionally inferior compound remains in the medium, with transport or phosphorylation blocked. Without the internalisation of the substrate, the degradative enzyme operons are not induced [227]. In this case, 3-HP could be inhibiting fructose transport into the cell, so the operon is not induced. This could explain the RNA-seq data from Arenas-Lopez *et al.* that showed down-regulation of the fructose operon when 3-HP was present, possibly as a method of preventing internalisation of the sugar by the encoded ABC-transporter [63].

The wild type strain was engineered for 3-HP biosynthesis, deleting the genes (*mmsA1*/2/3) required for 3-HP degradation [63]. The production strain, H16 Δ3 was tested, and showed an extended lag phase of 72 hours, where no fructose or 3-HP was consumed (Figure 39B and Figure 39C). Growth of H16 Δ3 is unhindered on fructose as a sole carbon source. This implies that the presence of the 3-HP in the media, or, after uptake, in the cell is the cause of the repression. Despite the lack of a utilisation pathway, the 3-HP-mediated repression remains, halting growth on the available fructose.

A similar situation has been seen in *C. necator* regarding the degradation of benzoate and phenol. A strain with a deletion of the 1,2-dihydro-1,2-dihydroxybenzoate (DHB) dehydrogenase gene was unable to metabolise benzoate and was similarly unable to grow on benzoate-phenol mixtures. The authors concluded that this showed that benzoate was responsible for the repression, but it was not possible to elucidate the mechanism at the time [234].

In this study, after 72 hours, the H16 Δ3 cultures began to grow, using the fructose as a carbon source, but still no 3-HP was consumed. This growth was expected to be as a result of mutations arising in the DNA. This was confirmed by whole genome sequencing of the 10 strains and identification of single nucleotide polymorphisms (SNPs) and other mutations (Table 15). Of the sequenced strains, 70% had mutations within the remaining 3-HP utilisation genes, *hpdR* or *hpdH* (in the operon that previously contained the *mmsA2* gene). This was surprising as the ability to use 3-HP was not restored, but the SNPs released the repression of fructose utilisation. The mutations were distributed throughout the *hpdH* and *hpdR* genes (Figure 41).

Interruption of only *hpdR* was seen in 3 strains, each showing different single nucleotide variations or insertions. The *hpdH* gene only was mutated in a further 3 strains. One strain had variations in both the *hpdH* and *hpdR* regions.

In *C. necator*, 3-HP degradation is predicted to be regulated by HpdR [39], and HpdH catalyses the first step of 3-HP breakdown by converting it to malonate semialdehyde (MSA), a toxic metabolite that might be contributing to fructose inhibition [65], [235]. It can be theorised that the different observed mutations have the same/similar effects, reducing the activity of the encoded 3-hydroxypropionate dehydrogenase by preventing or reducing *hpdH* expression (mutations in *hpdR*) or HpdH catalytic activity (mutations in *hpdH*). Previously, the Δ*hpdH* strain was shown to consume 3-HP in longer cultivations following a longer lag phase, but this was not further explored [63]. As malonate semialdehyde is not commercially available, it was not possible to test this hypothesis in the time available. Future experiments might also be designed to test and compare expression and HpdH activity in the various H16 Δ3 Δ*hpdH* variants.

A further mutation was found in the gene *gntP* (H16_A3011*)*, a gene predicted to encode a component of a putative gluconate transporter. No additional information could be found on this gene, so the link to catabolic repression of fructose was not clear. Of the 10 strains, 2 did not contain any mutations that could be identified by the techniques used.

Given more time, future key experiments could have included introducing intact copies of the mutated genes to restore the repression phenotype. In addition, the selected SNPs in *hpdH* and *hpdR* could be introduced into H16 Δ3, to alleviate the repression of fructose in the presence of 3-HP. These experiments would confirm the hypothesis that 3-HP conversion to MSA is key for the observed repression.

5.4.2 Repression of substrate utilisation by 3-hydroxypropionic acid

In order to elucidate more information on the connection between 3-HP and fructose utilisation, further carbon sources (gluconate and *N*-acetylglucosamine) that enter the ED pathway were evaluated. As it was suspected that the 3-hydroxypropionic

dehydrogenase (or the malonate semialdehyde product) was involved, further strains were also tested. In addition to the wild type and H16 Δ3, 3 more strains were tested, these were: H16 *ΔhpdH*, H16 Δ3 Δ*hpdH* and H16 Δ3.1, and an adapted strain from the previous experiment in this study with a mutation (insertion) in *hpdH*.

5.4.2.1 Fructose

The utilisation of wild type and H16 Δ3 on fructose has already been discussed. All three strains carrying mutations in *hpdH* were able to grow on fructose+3-HP MM, albeit more slowly than the WT. The adapted strain Δ3.1 consumed fructose immediately, as seen previously, and did not consume 3-HP (Figure 42). The peak OD was lower than the wild type, due to less usable carbon in the media. The growth pattern of the adapted strain Δ3.1 was similar to the Δ*hpdH* strain, suggesting that the mutation in this strain caused HpdH to be inactive or reduced its activity greatly.

Surprisingly, no 3-HP appeared to be consumed by H16 Δ*hpdH* over 112 hours. This may occur once the fructose was completely utilised, but this does not match the pattern of reverse catabolic repression seen in the wild type, where 3-HP was utilised first. Nor does it agree with previous data showing eventual 3-HP consumption by H16 Δ*hpdH* [63].

The strain H16 Δ*hpdH* did not utilise measurable amounts of 3-HP, yet growth on fructose was not strongly inhibited in its presence. A possible conclusion from this is that 3-HP alone by itself and unutilised has no strong inhibitory effects. Whilst 3-HP may delay fructose consumption slightly, a stronger effect is seen on all carbon sources tested (in particular on fructose), if the first step of its conversion is fully active (i.e., HpdH present) and MSA breakdown blocked (i.e., MmsAs absent). This suggests that MSA is the key effector. However, further, higher resolution experiments are required.

The growth of H16 Δ3*ΔhpdH* was an intermediate between the delayed growth of H16 Δ3 and the unhindered growth of H16 Δ*hpdH*. These results suggest that deletion of the *hpdH* gene results in a certain alleviation in fructose inhibition. As stated previously, the encoded enzyme converts 3-HP into MSA. The deletion of the *mmsA* genes in H16 Δ3 prevents the conversion of MSA to acetyl-CoA, and hence its entry

into central carbon metabolism. The accumulation of a toxic intermediate could be a possible cause for the counterintuitive inhibition of sugar utilisation, but a role as effector molecule in the repression of alternative carbon sources is also a possibility. The deletion of the *hpdH* gene in a wild type background should result in the 3-HP remaining in the medium, as was observed. It is possible that two or more factors are at play: perhaps both 3-HP and MSA may play roles in repression of fructose utilisation.

Very little information is available on the MSA intermediate and how it may link to carbohydrate utilisation. MSA, also known as 3-oxopropanoic acid, is a compound that has been rarely studied, despite being a metabolite in both prokaryotic and eukaryotic organisms [236] [237]. Previously known as formylacetic acid and malonaldehydic acid, it is a known competitive inhibitor of two enzymes: phosphonoacetaldehyde hydrolase and a succinic semialdehyde dehydrogenase from *Pseudomonas fluorescens* [238] [239]. However, inhibition of these enzymes in *C. necator* would still not explain why fructose is not being consumed when 3-HP/MSA is present.

MSA is an intermediate in a number of reactions, including the degradation of myo-inositol, chloroalkanes and 3-nitropropionic acid (3-NPA) [240]–[242]. In *Pseudomonas aeruginosa*, *nmoA* encodes a nitronate monooxygenase that converts 3-NPA to MSA, then to acetyl CoA (using *ddlA*). These genes are located in an operon with the self-regulating LysR type regulator named NmoR. This protein binds in the intergenic region between *nmoR* and *nmoA* and is derepressed in the presence of an activating molecule. No ligand has been confirmed for NmoR, but Vercammen *et al.* established that it was not 3-NPA (or the conjugate base version, propionate-3-nitronate (P3N). This research group suspected the ligand to be malonate semialdehyde, but it was not possible to test due to lack of stable, commercially available substrate. For a *P. aeruginosa nmoA* deletion strain, a lag phase delay was seen when the culture was supplemented with dual carbon sources, 3-NPA and glucose [242]. This effect is similar to the inhibition seen in this study. However, the *Pseudomonas* strains were not sequenced after any adaptations and no glucose consumption data is available for the experiment.

Deletion of the regulator NmoR in *P. aeruginosa* resulted in a strong decrease in expression of *gloA2* [242]. A homologue of this gene, *gloA* is found in *C. necator*. Kohlmann discovered that the regulator of *gloA*, assigned GloR, controls carbohydrate consumption. Deletion of *gloR* resulted in the inability to utilise fructose or *N*-acetylglucosamine as carbon sources [243]. Literature research has not shown any other regulator that is activated/repressed by malonate semialdehyde.

Evidence against the hypothesis that MSA represses sugar utilisation arises from other work within the research group [131]. 3-HP has been produced from β-alanine *via* MSA in the H16 Δ3 strain and no growth inhibition was observed on that occasion. This biosynthetic pathway was modelled mathematically by Dalwadi *et al.* who acknowledged the need to remove the toxic MSA [197]. However, the co-carbon source used in this experiment was gluconate (alongside the β-alanine), which may have different consequences. When fructose was used as a co-substrate, no growth of the strain was seen, similar to this study (unpublished, Katalin Kovács, University of Nottingham, personal communication).

5.4.2.2 Gluconate

Growth on gluconate was significantly less affected by the presence of 3-HP, for all strains but H16 Δ3 (Figure 43). H16 Δ3 had a slower growth rate than the other strains and consumed the fructose slower. However, the final OD was the same. Only the wild type consumed the 3-HP. This is interesting as it suggests that not all ED pathway metabolised carbon sources are subject to the same degree (or mechanism) of repression. The strongest effects may involve genes earlier in the pathway described in Figure 37**.**

In *C. necator,* gluconate is exclusively metabolised by the ED pathway. It is the final 6 carbon compound that enters the ED pathway. After phosphorylation and dehydration to KDGP and the carbon skeleton is broken down to pyruvate [26], [59], [228]. Gluconate enters the cells by an unstudied transporter and then the substrate is phosphorylated in an ATP-dependent manner by a gluconate permease (GntP). Transport is thought to be mediated by a gluconate-H^+ symporter, predicted to be encoded by *gntT*.

The proposed genes for gluconate utilisation are spread over two regions, suggested to be regulated by HexR type regulators encoded by H16_A1177 and H16_B1210 [244]. The operon on chromosome 1 contains the genes for a glucokinase (*gntK*) that presumably phosphorylates gluconate and the first enzyme of the ED pathway, phosphogluconate dehydratase (*edd1*).

The 6-phosphogluconate dehydratase gene *edd1* was downregulated 38-fold in the presence of 3-HP, although the result was not significant, most likely due to an insufficient number of replicates [63]. The HexR regulator, indicated to be responsible for controlling expression of *edd1* (and *gntK*), showed downregulation as well (25-fold), but again this was not significant either ($p_{adj} = 0.228$).

It is currently not known if the HexR regulator is involved in repression of gluconate, fructose or *N*-acetylglucosamine in the presence 3-HP, but down regulation of *edd* could result in slower production of KDGP, and hence reduced growth rate of H16 Δ3. An interesting working hypothesis to be tested in the future might be that HexR is responsible for modulating the expression of ED pathways genes in *C. necator* [245]. In *C. necator* H16 only the *edd1* gene is suggested to be regulated by HexR, although a patent by Foster and Kennedy suggest that it is part of a regulatory network involving glycerol [244], [246].

In *P. putida* when KDGP binds to HexR, the repression of the target operators is released [247]. The HexR regulator from the γ-proteobacterium *Shewanella oneidensis* has been studied in detail. In the presence of metabolisable sugars, the KDPG concentration increases as they pass through the ED pathway. KDPG binds to HexR, causing dissociation of HexR from the DNA complexes. This leads to derepression of genes of required ED pathway genes (*zwf*, *pgl*, *edd*, *eda* and *pyk*) and genes involved in gluconeogenesis are deactivated. When carbohydrates are limited, but acids such as lactate or pyruvate are provided, the KDPG level is decreased. This leads to HexR binding to its operator sites promoting repression of the glycolytic genes mentioned earlier [245]. If a similar mechanism is seen in *C. necator*, then reduction of the HexR controlled *edd1* could limit growth and cause the lag phase seen on ED-

pathway substrates. However, it does not explain the highly downregulated fructose operon (seen in RNA seq data), which implies a different mechanism.

Less is known about the proposed gluconate utilisation genes in operon on chromosome 2, H16_B2562 - H16_B2567. Genes encoding for a putative glucokinase (*glk*), 6-phosphogluconolactonase (*pgl*), another glucose-6-phosphate 1-dehydrogenase (*zwf3*) and a second phosphogluconate dehydratase (*edd2*), all genes necessary for conversion of glucose to PEP and pyruvate. These genes are found in an operon together with genes encoding a signal transduction histidine kinase and a response regulator of the OmpR family. No studies have looked at these genes. In the presence of 3-HP, the *edd2* homologue present on the second chromosome (H16_B2567) did not show the same downregulation as *edd1* in the presence of 3-HP [63].

5.4.2.3 N-acetylglucosamine

As seen in Figure 37, *N*-acetylglucosamine (GlcNac or NAG) is deacetylated to glucosamine-6-phosphate, which is subsequently deaminated into fructose-6-phosphate. *N*-acetylglucosamine is transported by a PTS transporter, the components encoded by *nagFEC*. NagF is composed of three *N*-acetylglucosamine-specific PEP-PTS domains (EI^{Nag} -HPr^{Nag} -$EIIA^{Nag}$) and delivers phosphoryl groups (donated from PEP) to the final membrane spanning domain, NagE ($EIIC^{Nag}$). After internalisation, the deacetylation and deamination are catalysed by NagA and NagB respectively. The operon is regulated by NagR. Mutational analysis of this regulator showed that inactivation leads to derepression, resulting in constitutive overexpression of the *nag* operon comprised of *nagFECAB-zwf1 (zwf1* encodes a glucose-6-phosphate 1-dehydrogenase). Other mutations in the operon have been shown to change the specificity to glucose [21]

This operon has been reported to have close links to nitrogen regulation in *C. necator* due to the signalling role of the PTS. Other parts of the system, EI^{Ntr} and HPr^{Ntr} are phosphorylated by PEP when *N*-acetylglucosamine is present. This can result in phosphorylation of $EIIA^{Ntr}$. The unphosphorylated $EIIA^{Ntr}$ interacts with an enzyme of the stringent response SpoT1 and is thought to be responsible for global metabolic

changes unrelated to nitrogen, such as PHB formation [13]. However, the underlying mechanisms are yet to be determined [248].

Only the wild type *C. necator* grew immediately in the NAG+3HP-MM, and no growth was seen for H16 Δ3, H16 *ΔhpdH*, H16 Δ3Δ*hpdH* or the adapted strain (Figure 43). These strains did not adapt to consume *N*-acetylglucosamine during the first 144-hours of the experiment (consumption data was not collected after 144 hours). Growth of H16 strains Δ3, H16 *ΔhpdH*, H16 *Δ3ΔhpdH* and H16 Δ3.1 on *N*-acetylglucosamine was completely inhibited as the strains continued to be incubated for 14 days, but no growth was seen within this time frame (data not shown). This inhibitory effect was stronger than that seen for fructose, which is interesting as *N*-acetylglucosamine enters the ED pathway *via* conversion to fructose-6-phosphate. This observation might be explained by very strong inhibition/down-regulation of the first step.

Previously, interruption of the *ptsN* gene has been found to change the growth rate on *N*-acetylglucosamine [228]. This gene is part of a HPr mediated nitrogen regulation system, previously described in *C. necator* H16. Work by Kraußе *et al.* [249] established the activity of a nitrogen PTS system EIIA component, $EIIA^{Ntr}$ denoted as *ptsN*. This gene is found in an operon with essential *hprK*, encoding a HPr kinase/phosphorylase that phosphorylates HPr at Ser-46 in an ATP-dependent manner [249]. It was hypothesised that PEP donates a phosphoryl group to EI and then HPr to phosphorylate $EIIA^{Ntr}$, resulting in downregulation of utilisation genes when the pyruvate levels are high, or nitrogen levels are low. However, as pyruvate levels would be low in the non-consuming cells, this is does not explain the delayed growth of H16 Δ3 on fructose and reduced growth rate on gluconate, only when 3-HP is present.

Curiously, the strain H16 Δ3.1, adapted to growth on fructose and 3-HP, did not grow in this experiment, suggesting that the mutations in *hpdH* were not sufficient to allow growth on this carbon source. It was hypothesised that the growth should have been more similar to H16 Δ*hpdH*, which showed intermediate growth on an undetermined carbon source (as *N*-acetylglucosamine concentrations remained unchanged). Strain H16 Δ*hpdH* is able to utilise 3-HP after a delay [24] but this was not possible to confirm as HPLC quantification of later stage culture supernatants showed increasing levels of both 3-HP and *N*-acetylglucosamine, likely due to interfering metabolites.

5.4.2.4 Succinate

In order to establish a non-sugar comparison, succinate was used as a carbon source. None of the cultures showed any lag phase delay and all consumed the succinate. The growth rate and final OD was consistent for all cultures. During the experiment, only the wild type cultures consumed any 3-HP. The amount was small and only occurred in the first 24 hours. All the succinate was depleted in every culture. However, it is not known if the cultures would have continued to be viable and consume 3-HP at a later time.

Although not reported for *C. necator*, it was expected that this TCA cycle intermediate would be the preferred substrate, similar to what has been observed for some *Pseudomonas* spp. In *C. necator,* succinate inhibits the uptake of phenol [234]. The results also show that the growth of the deletion strains is comparable when using non-EDI substrates. This shows that succinate is clearly the preferred carbon source over 3-HP, expanding the hierarchy of substrates discussed by Ampe *et al.* [234]. It is also interesting to note that no repression of growth was seen when *C. necator* H16 Δ3 was grown on a gas mixture of $CO_2/H_2/O_2$, in the presence of 3-HP [63].

5.5 Key Outcomes

Results in this chapter suggest that presence of 3-HP represses the utilisation of fructose. This repression was strengthened when the organism's ability to degrade the pathway intermediate MSA was abolished. Interestingly though, in this background, mutation of genes required for full activity of the preceding step, the generation of MSA, alleviated the observed repression to varying degrees. The underlying mechanisms remain unclear, however.

More work is needed, but the 3-HP-mediated catabolic repression seen in H16 Δ3 is likely to be specific to carbohydrates metabolised by the ED pathway, as no inhibition of succinate or CO_2/H_2/O_2 was seen in presence of 3-HP.

In previous chapters in this work, it has not proved possible to produce 3-HP in *C. necator*, despite strain engineering and efforts to balance enzyme expression. More work is required but the unknown effects of 3-HP, and its degradation products, on the central carbon metabolism of *C. necator* could be the reason behind the failed biosynthesis efforts.

Future work could include additional RNA-seq studies, which would allow for a more global picture of which genes are repressed for the various substrate combinations. This would allow identification of the precise target genes and may facilitate the identification of the regulatory factors involved.

Chapter 6 – General Discussion

Chapter 6 - General Discussion

6.1 Outcomes of PhD project

The starting aim of this project was to produce 3-HP in *C. necator*, via malonyl-CoA. Literature indicated that overexpression of the ACC from *C. glutamicum* increased the conversion of acetyl-CoA to malonyl-CoA in some species [137], [139], [250]. Coupled with the *C. aurantiacus* derived MCR enzyme, the malonyl-CoA is converted into 3-HP *via* malonate semialdehyde, as has been observed in *E. coli*, *S. cerevisiae* and *K. pneumoniae* [109], [113], [137], [193]. However, plasmid-based expression of the pathway genes in *C. necator* was not successful. The large size of the genes involved suggested that their expression from two compatible vectors would facilitate 3-HP biosynthesis in this species. However, issues with consistent plasmid maintenance necessitated the construction of large, complex plasmids. Whilst the generation of these plasmids was carried out in *E. coli* without observing any negative effects on viability in the absence of gene induction, their transfer into *C. necator* strongly affected growth in minimal medium.

To understand the reasons behind the lack of 3-HP production in strains carrying the dual plasmid system, each stage of the pathway was assessed. The activities of multiple thermophilic MCR enzymes were tested. Both *N. maritimus and C. aurantiacus* were shown to be active at 30ºC, but *C. aurantiacus* (encoded by mcr_{635}) had the highest activity. The measured specific activity (0.025 µmol min^{-1} mg^{-1}) of the *C. aurantiacus* enzyme in *C. necator* crude extracts at 30°C were similar to those reported for cell extracts of the native organism at 55°C [133], indicating that conversion of malonyl-CoA to 3-HP was a viable option in *C. necator*. Further work created plasmids with modifications to the mcr_{635} gene that have been demonstrated to improve activity of the resulting enzyme, but it was not possible to test these plasmids due to time constraints and the emergence of an unforeseen pandemic.

Literature suggests that low intracellular malonyl-CoA levels are one of the factors limiting 3-HP production [144]. It was hypothesised that this may also be the case for the engineered *C. necator* strains and hence work focused on the expression of the *acc* genes from *C. glutamicum* (acc_{Cg}), or an alternative MMC enzyme from *P.*

freudenreichii. Regulation of the ACC is known to be strict. Although no mechanism has been described for the native *C. necator* enzyme, it has been shown that transcriptional and translational regulation, and allosteric inhibition, contribute to regulating malonyl-CoA levels within other bacteria [170], [172], [174]. Initially, a spectrophotometric coupled enzyme assay was used to evaluate the effect of expression the acc_{Cg} in *C. necator*, but this was unsuccessful.

An alternative, biosensor-based method was employed to measure malonyl-CoA levels, by converting the compound into flaviolin, a red coloured polyketide whose production results in a measurable absorbance change. Production of flaviolin from malonyl-CoA is reliant on the polyketide synthase RppA from *S .griseus* This biosensor was also utilised to measure the malonyl-CoA levels in strains of *C. necator* with gene deletions (*mcd* and *phaCAB*) theorised to improve malonyl-CoA accumulation. The outcomes showed that neither of these deletions had any significant effect of flaviolin production, indicating that available malonyl-CoA levels were unperturbed, and likely tightly regulated.

The reporter was first used to monitor the response to cerulenin, which is an inhibitor of beta-ketoacyl-ACP synthases, vital in the fatty acid biosynthesis pathway and known to increase malonyl-CoA levels *in E. coli* [164]. In *E. coli*, this resulted in increased output without affecting growth. However, in *C. necator* strains (wild type, H16 Δ3, H16 Δ3Δ*mcd* and H16 Δ*mcd*) the addition of cerulenin reduced growth.

Implementation of this *rppA* biosensor in *E. coli* and *C. necator* H16 Δ3 successfully showed that induction of acc_{Cg} resulted in increased malonyl-CoA availability. However, *acc* overexpression also had a drastic effect on growth, with even the lowest amount of arabinose inducer (0.016%) reducing the OD at 20 hours to 56% of the uninduced culture. Hence that from these data it seems that within the tested strains malonyl-CoA overproduction was detrimental.

Further work with the *rppA*-based biosensor demonstrated that plasmid pMTL71301_*acc_rppA* worked as expected. Arabinose induction of *acc* expression increased specific (OD-corrected) reporter output, indicative of an increased malonyl-CoA availability, but induction also dramatically decreased growth. However, it was

not possible to grow *C. necator* carrying pMTL71301_*acc_mcr*, a plasmid only differing in one gene. This suggested that the mcr_{635} was responsible for lack of growth. As activity of the MCR_{635} enzyme had already been demonstrated in *C. necator*, accumulation of the toxic pathway intermediate MSA was suggested to be the source. Other hypotheses include the large plasmid size adding a burden to the cells, and the previously established detrimental effect of overexpressing heterologous ACC_{Cg}.

Related work investigated the repression of sugar utilisation and growth when 3-HP is present in the medium. For the *C. necator* strain H16 Δ3, which lacks the MmsA enzymes required to convert MSA to acetyl-CoA, growth on 3-HP plus another carbon source was shown to be inhibited to varying degrees. For fructose and *N*-acetylglucosamine, complete repression was seen. For gluconate, growth was slowed. Growth on succinate inhibited the use of 3-HP as a carbon source in all of the *C. necator* strains, including the wild type.

Despite complete inhibition of growth of *C. necator* H16 Δ3 in fructose and 3HP medium for the first 48 hours, mutations occurred in the H16 Δ3 strains that allowed for subsequent consumption of fructose. Interestingly, genomic analyses revealed that SNPs and insertion/deletion events had materialised in *hpdR* and *hpdH* in 70% of the strains sequenced. These genes are part of a cluster responsible for 3-HP degradation [63]. The likely outcome of the mutations is inactivation (or reduction of activity) of HpdH that converts 3-HP to MSA, either directly or by inactivating HpdR that regulates expression of the operon. In the hindered strain H16 Δ3, the enzymes responsible for the degradation of MSA to acetyl-CoA have been eliminated. This suggests that accumulation of MSA may result, either directly or indirectly, in the repression of fructose (and other ED pathway) utilisation genes.

Growth and consumption profiles of gene deletion strains of *C. necator* on fructose and 3-HP further supported this hypothesis. Bacteria with the *hpdH* deletion only did not show the pattern of complete repression of fructose consumption and growth, nor did H16 Δ3 Δ*hpdH*. In these strains, 3-HP cannot be converted to MSA. The results of this work imply 3-HP weakly inhibits fructose consumption, but MSA is largely responsible for the full repression seen.

This work highlighted that in the presence of common growth substrates, native gene regulatory systems may interfere with the implementation of heterologous metabolic pathways: implementation of a functional pathway may lead to 3-HP production, but this may in turn prevent growth of the generated strain. Hence, when isolating candidate clones during the process of pathway engineering, those emerging first or growing fastest may represent disabled mutant strains.

Previous literature had hinted that efficient conversion of MSA to 3-HP was required to prevent a bottleneck and toxicity issues [144], [188], [236]. Plasmids were created including *ydfG*$_{Ec}$ whose protein product (3-hydroxypropionic acid dehydrogenase) has been reported to reduce MSA. Furthermore, plasmids bearing a dissected *mcr*$_{635}$ were also generated, as separation into the alcohol dehydrogenase and aldehyde dehydrogenase domains have been shown improve the overall activity and prevent MSA accumulation and resulting growth repression. Nonetheless, since both 3-HP and MSA appear to have an inhibitory effect on sugar consumption (although the strength of repression differs) ED pathway carbohydrates are unsuitable carbon sources when engineering *C. necator* for 3-HP production.

In summary, despite promising properties of the malonyl-CoA pathway to 3-HP, it appears multiple mechanisms may be at play, preventing biosynthesis of this commodity chemical. It is likely that malonyl-CoA levels are strictly controlled, and conversion of this compound to 3-HP must be appropriately balanced to prevent accumulation of toxic intermediates.

6.2 Future work

Unfortunately, it was not possible to test the final, 4th generation 3-HP pathway plasmids in *C. necator*. These plasmids were the proposed solution to the identified issues with MSA, and stability of the 2nd generation "two plasmid system", but time restraints emerged due to COVID-19 related restriction of laboratory access. As little is known about the regulation of the native ACC in *C. necator*, it is unlikely that the issues with the expression of the heterologous *acc*$_{Cg}$ can easily be remedied. Nevertheless, the demonstrated RppA-based biosensor was constructed as part of a

modular plasmid, hence allowing for other ACC candidates from different organisms to easily be cloned and tested.

The repression of carbohydrates metabolised by the ED pathway must be investigated further if *C. necator* is to be established as a chassis for biosynthesis of industrial compounds such as 3-HP. Whilst the ultimate aim is to achieve 3-HP production from CO_2/H_2, or other economically viable and environmentally sustainable carbon and energy sources, at least the initial pathway assembly and testing will continue to rely on the use of conventional organic substrates. In this study, no definite mechanism was established for the reported repression of the fructose utilisation operon, or those of the other tested ED substrates, but is likely due to MSA. Reporter systems (or larger scale approaches such as RNA-seq) monitoring transcription of the ED pathway and 3-HP consumption operons, will allow for a more detailed demonstration of the affected genes. Larger scale analysis of spontaneous mutant strains, that are able to grow (or grow more quickly) on ED substrates in the presence of 3-HP may reveal other genes involved.

Catabolic repression has been previously been reported in *C. necator*, where phenol catabolism is inhibited by the presence of acetate. It is apparent that multiple systems control substrate utilisation in *C. necator*. Investigating and expanding this hierarchy of compounds is indispensable for understanding the complex metabolism of this industrial strain. Based on this study, future strain engineering aiming to establishing 3-HP production should be undertaken for cells growing on succinate. This compound was found to support growth in the presence of high 3-HP concentrations, and this is unlikely to change in the presence of 3-HP production.

6.3 Conclusions

Although it is not possible to make 3-HP by the methods developed during this study, knowledge was gained into the mechanisms obstructing the biosynthesis of this compound. Despite the pathway comprising of a small number of genes and linking directly to central metabolism, this work demonstrates how complex interactions occurring inside the cell can prevent introduction and use of heterologous metabolic routes to new products.

References

[1] W. J. Ripple *et al.*, "World scientists' warning to humanity: A second notice," *Bioscience*, vol. 67, no. 12, pp. 1026–1028, Dec. 2017.

[2] A. Kätelhön, R. Meys, S. Deutz, S. Suh, and A. Bardow, "Climate change mitigation potential of carbon capture and utilization in the chemical industry," *Proc. Natl. Acad. Sci. U. S. A.*, vol. 166, no. 23, pp. 11187–11194, Jun. 2019.

[3] Procter and Gamble, "Method of making acrylic acid from hydroxypropionic acid," US20180126187A1, 04-Jan-2018.

[4] S. Phillips, B. Flach, S. Lieberz, and S. Bolla, "EU-28 Biofuels Annual 2019," 2019.

[5] F. Bauer and C. Hulteberg, "Is there a future in glycerol as a feedstock in the production of biofuels and biochemicals?," *Biofuels, Bioprod. Biorefining*, vol. 7, no. 1, pp. 43–51, Jan. 2013.

[6] F. M. Liew, M. E. Martin, R. C. Tappel, B. D. Heijstra, C. Mihalcea, and M. Köpke, "Gas fermentation - A flexible platform for commercial scale production of low-carbon-fuels and chemicals from waste and renewable feedstocks," *Front. Microbiol.*, vol. 7, p. 694, May 2016.

[7] A. Pohlmann *et al.*, "Genome sequence of the bioplastic-producing 'Knallgas' bacterium *Ralstonia eutropha* H16.," *Nat. Biotechnol.*, vol. 24, no. 10, pp. 1257–62, 2006.

[8] R. Repaske, "Characteristics of hydrogen bacteria," *Biotechnol. Bioeng.*, vol. 8, no. 2, pp. 217–235, 1966.

[9] D. H. Davis, M. Doudoroff, R. Y. Stanier, and M. Mandel, "Proposal to reject the genus *Hydrogenomonas*: Taxonomic implications," *Int. J. Syst. Bacteriol.*, vol. 19, no. 4, pp. 375–390, Oct. 1969.

[10] E. Yabuuchi, I. Yano, H. Hotta, Y. Nishiuchi, and Y. Kosako, "Transfer of two *Burkholderia* and an *Alcaligenes* species to *Ralstonia* gen. Nov.: proposal of *Ralstonia pickettii* (Ralston, Palleroni and Doudoroff 1973) Comb. Nov., *Ralstonia solanacearum* (Smith 1896) Comb. Nov.," *Microbiol. Immunol.*, vol. 39, no. 11, pp. 897–904, Nov. 1995.

[11] M. Vaneechoutte, P. Kämpfer, T. De Baere, E. Falsen, and G. Verschraegen, "*Wautersia* gen. nov., a novel genus accomodating the phylogenetic lineage including *Ralstonia eutropha* and related species, and proposal of *Ralstonia* [*Pseudomonas*] *syzygii* (Roberts et al. 1990) comb. nov," *Int. J. Syst. Evol. Microbiol.*, vol. 54, no. 2, pp. 317–327, Mar. 2004.

[12] P. Vandamme and T. Coenye, "Taxonomy of the genus *Cupriavidus*: A tale of lost and found," *Int. J. Syst. Evol. Microbiol.*, vol. 54, no. 6, pp. 2285–2289, Nov. 2004.

[13] N. S. Makkar and L. E. Casida, "*Cupriavidus necator* gen. nov., sp. nov.; a nonobligate bacterial predator of bacteria in soil," *Int. J. Syst. Bacteriol.*, vol. 37, no. 4, pp. 323–326, 1987.

[14] R. Moriuchi, H. Dohra, Y. Kanesaki, and N. Ogawa, "Complete genome sequence of 3-chlorobenzoate-degrading bacterium *Cupriavidus necator* NH9 and reclassification of the strains of the genera *Cupriavidus* and *Ralstonia* based on phylogenetic and whole-genome

sequence analyses," *Front. Microbiol.*, vol. 10, no. FEB, p. 133, Feb. 2019.

[15] D. Pérez-Pantoja, R. De La Iglesia, D. H. Pieper, and B. González, "Metabolic reconstruction of aromatic compounds degradation from the genome of the amazing pollutant-degrading bacterium *Cupriavidus necator* JMP134," *FEMS Microbiol. Rev.*, vol. 32, no. 5, pp. 736–794, Aug. 2008.

[16] A. Poehlein, B. Kusian, B. Friedrich, R. Daniel, and B. Bowien, "Complete genome sequence of the type strain *Cupriavidus necator* N-1," *J. Bacteriol.*, vol. 193, no. 18, p. 5017, Sep. 2011.

[17] E. Schwartz, A. Henne, R. Cramm, T. Eitinger, B. Friedrich, and G. Gottschalk, "Complete nucleotide sequence of pHG1: A *Ralstonia eutropha* H16 megaplasmid encoding key enzymes of H_2-based lithoautotrophy and anaerobiosis," *J. Mol. Biol.*, vol. 332, no. 2, pp. 369–383, Sep. 2003.

[18] J. Yu and P. Munasinghe, "Gas fermentation enhancement for chemolithotrophic growth of *Cupriavidus necator* on carbon dioxide," *Fermentation*, vol. 4, no. 3, p. 63, Aug. 2018.

[19] G. T. Little *et al.*, "Complete Genome Sequence of *Cupriavidus necator* H16 (DSM 428)," *Microbiol. Resour. Announc.*, vol. 8, no. 37, Sep. 2019.

[20] C. Bi *et al.*, "Development of a broad-host synthetic biology toolbox for *Ralstonia eutropha* and its application to engineering hydrocarbon biofuel production," *Microb. Cell Fact.*, vol. 12, no. 1, p. 107, 2013.

[21] M. Raberg *et al.*, "Proteomic and transcriptomic elucidation of the mutant *Ralstonia eutropha* G+1 with regard to glucose utilization," *Appl. Environ. Microbiol.*, vol. 77, no. 6, pp. 2058–2070, Mar. 2011.

[22] J. Lu, C. J. Brigham, C. S. Gai, and A. J. Sinskey, "Studies on the production of branched-chain alcohols in engineered *Ralstonia eutropha*," *Appl. Microbiol. Biotechnol.*, vol. 96, no. 1, pp. 283–297, Oct. 2012.

[23] S. Sato, T. Fujiki, and K. Matsumoto, "Construction of a stable plasmid vector for industrial production of poly(3-hydroxybutyrate-co-3-hydroxyhexanoate) by a recombinant *Cupriavidus necator* H16 strain," *J. Biosci. Bioeng.*, vol. 116, no. 6, pp. 677–681, Dec. 2013.

[24] C. A. Lopez, "The genetic basis of 3-hydroxypropanoate metabolism in *Cupriavidus necator* H16," 2017.

[25] J. Mifune, S. Nakamura, and T. Fukui, "Engineering of *pha* operon on *Cupriavidus necator* chromosome for efficient biosynthesis of poly(3-hydroxybutyrate-co-3-hydroxyhexanoate) from vegetable oil," in *Polymer Degradation and Stability*, 2010, vol. 95, no. 8, pp. 1305–1312.

[26] E. Volodina, M. Raberg, and A. Steinbüchel, "Engineering the heterotrophic carbon sources utilization range of *Ralstonia eutropha* H16 for applications in biotechnology," *Crit Rev Biotechnol*, vol. 36, no. 6, pp. 1549–7801, 2016.

[27] C. Fleige, J. Kroll, and A. Steinbüchel, "Establishment of an alternative phosphoketolase-dependent pathway for fructose catabolism in *Ralstonia eutropha* H16," *Appl. Microbiol. Biotechnol.*, vol. 91, no. 3, pp. 769–776, 2011.

[28] J. S. Chen, B. Colón, B. Dusel, M. Ziesack, J. C. Way, and J. P. Torella, “Production of fatty acids in *Ralstonia eutropha* H16 by engineering β -oxidation and carbon storage,” *PeerJ*, vol. 3, p. e1468, 2015.

[29] J. Lu, C. J. Brigham, S. Li, and A. J. Sinskey, *Ralstonia eutropha H16 as a platform for the production of biofuels, biodegradable plastics, and fine chemicals from diverse carbon resources*. Elsevier B.V., 2016.

[30] S. E. Nybo, N. E. Khan, B. M. Woolston, and W. R. Curtis, “Metabolic engineering in chemolithoautotrophic hosts for the production of fuels and chemicals,” *Metab. Eng.*, vol. 30, pp. 105–120, 2015.

[31] S. Gruber *et al.*, “Design of inducible expression vectors for improved protein production in *Ralstonia eutropha* H16 derived host strains,” *J. Biotechnol.*, vol. 235, pp. 92–99, 2016.

[32] I. Voss and A. Steinbüchel, “Application of a KDPG-aldolase gene-dependent addiction system for enhanced production of cyanophycin in *Ralstonia eutropha* strain H16,” *Metab. Eng.*, vol. 8, no. 1, pp. 66–78, Jan. 2006.

[33] S. Lütte *et al.*, “Autotrophic production of stable-isotope-labeled arginine in *Ralstonia eutropha* strain H16,” *Appl. Environ. Microbiol.*, vol. 78, no. 22, pp. 7884–7890, 2012.

[34] J. Kroll, S. Klinter, C. Schneider, I. Voss, and A. Steinbüchel, “Plasmid addiction systems: perspectives and applications in biotechnology.,” *Microb. Biotechnol.*, vol. 3, no. 6, pp. 634–57, Nov. 2010.

[35] T. Fukui, K. Ohsawa, J. Mifune, I. Orita, and S. Nakamura, “Evaluation of promoters for gene expression in polyhydroxyalkanoate-producing *Cupriavidus necator* H16,” *Appl. Microbiol. Biotechnol.*, vol. 89, no. 5, pp. 1527–1536, Mar. 2011.

[36] L. Crépin, E. Lombard, and S. E. Guillouet, “Metabolic engineering of *Cupriavidus necator* for heterotrophic and autotrophic alka(e)ne production,” *Metab. Eng.*, vol. 37, pp. 92–101, Sep. 2016.

[37] A. O. Johnson, M. Gonzalez-Villanueva, K. L. Tee, and T. S. Wong, “An engineered constitutive promoter set with broad activity range for *Cupriavidus necator* H16,” *ACS Synth. Biol.*, vol. 7, no. 8, pp. 1918–1928, Aug. 2018.

[38] S. Alagesan, E. K. R. Hanko, N. Malys, M. Ehsaan, K. Winzer, and N. P. Minton, “Functional genetic elements for controlling gene expression in *Cupriavidus necator* H16,” *Appl. Environ. Microbiol.*, vol. 84, no. 19, Oct. 2018.

[39] E. K. R. Hanko, N. P. Minton, and N. Malys, “Characterisation of a 3-hydroxypropionic acid-inducible system from *Pseudomonas putida* for orthogonal gene expression control in *Escherichia coli* and *Cupriavidus necator*,” *Sci. Rep.*, vol. 7, no. 1, p. 1724, 2017.

[40] E. K. R. Hanko, A. C. Paiva, M. Jonczyk, M. Abbott, N. P. Minton, and N. Malys, “A genome-wide approach for identification and characterisation of metabolite-inducible systems,” *Nat. Commun.*, vol. 11, no. 1, pp. 1–14, Dec. 2020.

[41] J. M. Reyrat, V. Pelicic, B. Gicquel, and R. Rappuoli, “Counterselectable markers: Untapped tools for bacterial genetics and pathogenesis,” *Infect. Immun.*, vol. 66, no. 9, pp. 4011–4017, 1998.

[42] B. Xiong, Z. Li, L. Liu, D. Zhao, X. Zhang, and C. Bi, “Genome editing of *Ralstonia eutropha* using an electroporation-based CRISPR-Cas9 technique,” *Biotechnol. Biofuels*, vol. 11, no. 1, p. 172, Dec. 2018.

[43] J. A. Englaender, J. A. Jones, B. F. Cress, T. E. Kuhlman, R. J. Linhardt, and M. A. G. G. Koffas, “Effect of genomic integration location on heterologous protein expression and metabolic engineering in *E. coli*,” *ACS Synth. Biol.*, vol. 6, no. 4, pp. 710–720, Apr. 2017.

[44] J. Müller *et al.*, “Engineering of *Ralstonia eutropha* H16 for autotrophic and heterotrophic production of methyl ketones,” *Appl. Environ. Microbiol.*, vol. 79, no. 14, pp. 4433–4439, Jul. 2013.

[45] E. Grousseau, J. Lu, N. Gorret, S. E. Guillouet, and A. J. Sinskey, “Isopropanol production with engineered *Cupriavidus necator* as bioproduction platform,” *Appl. Microbiol. Biotechnol.*, vol. 98, no. 9, pp. 4277–4290, 2014.

[46] R. R. Bommareddy *et al.*, “A sustainable chemicals manufacturing paradigm using CO_2 and renewable H_2,” *iScience*, vol. 23, no. 6, 2020.

[47] S. Srinivasan, G. C. Barnard, and T. U. Gerngross, “Production of recombinant proteins using multiple-copy gene integration in high-cell-density fermentations of *Ralstonia eutropha*,” *Biotechnol. Bioeng.*, vol. 84, no. 1, pp. 114–120, Oct. 2003.

[48] L. Qin, X. Jiang, Z. Dong, J. Huang, and X. Chen, “Identification of two integration sites in favor of transgene expression in *Trichoderma reesei*,” *Biotechnol. Biofuels*, vol. 11, no. 1, p. 142, Dec. 2018.

[49] S. Sichwart, S. Hetzler, D. Bröker, and A. Steinbüchel, “Extension of the substrate utilization range of *Ralstonia eutropha* strain H16 by metabolic engineering to include mannose and glucose,” *Appl. Environ. Microbiol.*, vol. 77, no. 4, pp. 1325–1334, Feb. 2011.

[50] B. Bowien and B. Kusian, “Genetics and control of CO_2 assimilation in the chemoautotroph *Ralstonia eutropha*,” *Arch. Microbiol.*, vol. 178, no. 2, pp. 85–93, 2002.

[51] T. Buhrke, O. Lenz, N. Krauss, and B. Friedrich, “Oxygen tolerance of the H_2-sensing [NiFe] hydrogenase from *Ralstonia eutropha* H16 is based on limited access of oxygen to the active site,” *J. Biol. Chem.*, vol. 280, no. 25, pp. 23791–23796, Jun. 2005.

[52] S. Gruber, H. Schwab, and P. Heidinger, “CbbR and RegA regulate *cbb* operon transcription in *Ralstonia eutropha* H16,” *J. Biotechnol.*, vol. 257, pp. 78–86, Sep. 2017.

[53] M. S. Islam Mozumder, L. Garcia-Gonzalez, H. De Wever, and E. I. P. Volcke, “Poly(3-hydroxybutyrate) (PHB) production from CO_2: Model development and process optimization,” *Biochem. Eng. J.*, vol. 98, pp. 107–116, Jun. 2015.

[54] D. Heinrich, M. Raberg, and A. Steinbüchel, “Studies on the aerobic utilization of synthesis gas (syngas) by wild type and recombinant strains of *Ralstonia eutropha* H16,” *Microb. Biotechnol.*, vol. 11, no. 4, pp. 647–656, Jul. 2018.

[55] P. Dürre, B. J. Eikmanns, P. Durre, and B. J. Eikmanns, “C1-carbon sources for chemical and fuel production by microbial gas fermentation,” *Curr. Opin. Biotechnol.*, vol. 35, pp. 63–72, Dec. 2015.

[56] B. F. Johnson and R. Y. Stanier, “Dissimilation of aromatic compounds by *Alcaligenes*

eutrophus.," *J. Bacteriol.*, vol. 107, no. 2, pp. 468–475, 1971.

[57] C. J. Brigham *et al.*, "Elucidation of β-oxidation pathways in Ralstonia eutropha H16 by examination of global gene expression," *J. Bacteriol.*, vol. 192, no. 20, pp. 5454–5464, Oct. 2010.

[58] P. K. Sharma *et al.*, "Global changes in the proteome of *Cupriavidus necator* H16 during poly-(3-hydroxybutyrate) synthesis from various biodiesel by-product substrates," *AMB Express*, vol. 6, no. 1, p. 36, Dec. 2016.

[59] M. González-Villanueva *et al.*, "Adaptive laboratory evolution of *Cupriavidus necator* H16 for carbon co-utilization with glycerol," *Int. J. Mol. Sci.*, vol. 20, no. 22, Nov. 2019.

[60] T. Fukui, M. Mukoyama, I. Orita, and S. Nakamura, "Enhancement of glycerol utilization ability of *Ralstonia eutropha* H16 for production of polyhydroxyalkanoates," *Appl. Microbiol. Biotechnol.*, vol. 98, no. 17, pp. 7559–7568, Sep. 2014.

[61] S. Y. Ong, J. Y. Chee, and K. Sudesh, "Degradation of polyhydroxyalkanoate (PHA): a review," *J. Sib. Fed. Univ. Biol.*, vol. 10, no. 2, pp. 21–225, 2017.

[62] S. Povolo, P. Toffano, M. Basaglia, and S. Casella, "Polyhydroxyalkanoates production by engineered *Cupriavidus necator* from waste material containing lactose," *Bioresour. Technol.*, vol. 101, no. 20, pp. 7902–7907, Oct. 2010.

[63] C. Arenas-López *et al.*, "The genetic basis of 3-hydroxypropanoate metabolism in *Cupriavidus necator* H16," *Biotechnol. Biofuels*, vol. 12, no. 1, p. 150, Dec. 2019.

[64] P. Lee, S. M. Raj, S. Zhou, S. Ashok, S. Edwardraja, and S. Park, "3-Hydroxyisobutyrate dehydrogenase-I from *Pseudomonas denitrificans* ATCC 13867 degrades 3-hydroxypropionic acid," *Biotechnol. Bioprocess Eng.*, vol. 19, no. 1, pp. 1–7, 2014.

[65] S. Zhou, S. K. Ainala, E. Seol, T. T. Nguyen, and S. Park, "Inducible gene expression system by 3-hydroxypropionic acid," *Biotechnol. Biofuels*, vol. 8, no. 1, p. 169, 2015.

[66] S. Zhou, S. Ashok, Y. Ko, D.-M. M. Kim, and S. Park, "Development of a deletion mutant of *Pseudomonas denitrificans* that does not degrade 3-hydroxypropionic acid," *Appl. Microbiol. Biotechnol.*, vol. 98, no. 10, pp. 4389–4398, May 2014.

[67] F. H. Isikgor and C. R. Becer, "Lignocellulosic biomass: a sustainable platform for the production of bio-based chemicals and polymers," *Polym. Chem.*, vol. 6, no. 25, pp. 4497–4559, Jun. 2015.

[68] S. J. Park, T. W. Kim, M. K. Kim, S. Y. Lee, and S. C. Lim, "Advanced bacterial polyhydroxyalkanoates: Towards a versatile and sustainable platform for unnatural tailor-made polyesters," *Biotechnol. Adv.*, vol. 30, no. 6, pp. 1196–1206, Nov. 2012.

[69] F. Mravec *et al.*, "Accumulation of PHA granules in *Cupriavidus necator* as seen by confocal fluorescence microscopy," *FEMS Microbiol. Lett.*, vol. 363, no. 10, p. 94, May 2016.

[70] F. Muneer, I. Rasul, F. Azeem, M. H. Siddique, M. Zubair, and H. Nadeem, "Microbial polyhydroxyalkanoates (PHAs): efficient replacement of synthetic polymers," *J. Polym. Environ.*, vol. 28, no. 9, pp. 2301–2323, Sep. 2020.

[71] F. Masood, "Polyhydroxyalkanoates in the food packaging industry," in *Nanotechnology Applications in Food: Flavor, Stability, Nutrition and Safety*, Elsevier Inc., 2017, pp. 153–

177.

[72] E. Bugnicourt, P. Cinelli, A. Lazzeri, and V. Alvarez, “Polyhydroxyalkanoate (PHA): Review of synthesis, characteristics, processing and potential applications in packaging,” *Express Polym. Lett.*, vol. 8, no. 11, pp. 791–808, 2014.

[73] I. Isak *et al.*, “Quantification of polyhydroxyalkanoates in mixed and pure cultures biomass by Fourier transform infrared spectroscopy: comparison of different approaches,” *Lett. Appl. Microbiol.*, vol. 63, no. 2, pp. 139–146, Aug. 2016.

[74] M. Koller, “Biodegradable and biocompatible polyhydroxy-alkanoates (PHA): Auspicious microbial macromolecules for pharmaceutical and therapeutic applications,” *Molecules*, vol. 23, no. 2. MDPI AG, 2018.

[75] “Polyhydroxyalkanoate (PHA) Market Analysis | Recent Market Developments | Industry Forecast to 2019-2024 | MarketsandMarkets™,” *Markets and Markets*, 2019. [Online]. Available: https://www.marketsandmarkets.com/Market-Reports/pha-market-395.html. [Accessed: 30-Nov-2020].

[76] K. W. Meereboer, M. Misra, and A. K. Mohanty, “Review of recent advances in the biodegradability of polyhydroxyalkanoate (PHA) bioplastics and their composites,” *Green Chem.*, vol. 22, no. 17, pp. 5519–5558, Aug. 2020.

[77] P. R. Rodrigues, J. M. N. Nunes, L. N. Lordelo, and J. I. Druzian, “Assessment of polyhydroxyalkanoate synthesis in submerged cultivation of *Cupriavidus necator* and *Burkholderia cepacia* strains using soybean as substrate,” *Brazilian J. Chem. Eng.*, vol. 36, no. 1, pp. 73–83, 2019.

[78] “VIMSS2037523: H16_A1178 edd1 phosphogluconate dehydratase (NCBI), 631 a.a. [Ralstonia eutropha H16].” [Online]. Available: http://www.microbesonline.org/cgi-bin/fetchLocus.cgi?locus=2037523&disp=0. [Accessed: 12-Feb-2021].

[79] R. A. Verlinden, D. J. Hill, M. A. Kenward, C. D. Williams, Z. Piotrowska-Seget, and I. K. Radecka, “Production of polyhydroxyalkanoates from waste frying oil by Cupriavidus necator,” *AMB Express 2011 11*, vol. 1, no. 1, pp. 1–8, Jun. 2011.

[80] Y. Jung Sohn *et al.*, “Chemoautotroph Cupriavidus necator as a potential game-changer for global warming and plastic waste problem: A review,” *Bioresour. Technol.*, p. 125693, Jul. 2021.

[81] B. S. Kim, S. C. S. Y. Lee, H. N. Chang, Y. K. Chang, and S. I. Woo, “Production of poly(3-hydroxybutyric acid) by fed-batch culture of *Alcaligenes eutrophus* with glucose concentration control,” *Biotechnol. Bioeng.*, vol. 43, no. 9, pp. 892–898, Apr. 1994.

[82] T. Fukui, M. Suzuki, T. Tsuge, and S. Nakamura, “Microbial synthesis of poly((R)-3-hydroxybutyrate-co-3-hydroxypropionate) from unrelated carbon sources by engineered Cupriavidus necator,” *Biomacromolecules*, vol. 10, no. 4, pp. 700–706, Apr. 2009.

[83] C. S. McGregor, “Production of 3-hydroxypropionate- containing polymers by engineered Cupriavidus necator H16,” University of Nottingham, 2020.

[84] A. Aramvash, Z. Akbari Shahabi, S. Dashti Aghjeh, and M. D. Ghafari, “Statistical physical and nutrient optimization of bioplastic polyhydroxybutyrate production by Cupriavidus

necator," *Int. J. Environ. Sci. Technol. 2015 127*, vol. 12, no. 7, pp. 2307–2316, Feb. 2015.

[85] T. G. Volova and N. A. Voinov, "Kinetic parameters of a culture of the hydrogen-oxidizing bacterium *Ralstonia eutropha* grown under conditions favoring polyhydroxybutyrate biosynthesis," *Appl. Biochem. Microbiol. 2003 392*, vol. 39, no. 2, pp. 166–170, Mar. 2003.

[86] K. Y. Sen, M. H. Hussin, and S. Baidurah, "Biosynthesis of poly(3-hydroxybutyrate) (PHB) by Cupriavidus necator from various pretreated molasses as carbon source," *Biocatal. Agric. Biotechnol.*, vol. 17, pp. 51–59, Jan. 2019.

[87] A. F. Mohidin Batcha, D. M. R. Prasad, M. R. Khan, and H. Abdullah, "Biosynthesis of poly(3-hydroxybutyrate) (PHB) by Cupriavidus necator H16 from jatropha oil as carbon source," *Bioprocess Biosyst. Eng. 2013 375*, vol. 37, no. 5, pp. 943–951, Sep. 2013.

[88] C. Windhorst and J. Gescher, "Efficient biochemical production of acetoin from carbon dioxide using *Cupriavidus necator* H16," *Biotechnol. Biofuels*, vol. 12, no. 1, p. 163, 2019.

[89] J. Marc, E. Grousseau, E. Lombard, A. J. Sinskey, N. Gorret, and S. E. Guillouet, "Over expression of GroESL in *Cupriavidus necator* for heterotrophic and autotrophic isopropanol production," *Metab. Eng.*, vol. 42, pp. 74–84, Jul. 2017.

[90] H. Li *et al.*, "Integrated electromicrobial conversion of CO_2 to higher alcohols," *Science (80-.).*, vol. 335, no. 6076, p. 1596, Mar. 2012.

[91] S. N. Nangle *et al.*, "Valorization of CO_2 through lithoautotrophic production of sustainable chemicals in *Cupriavidus necator*," *bioRxiv*, p. 2020.02.08.940007, Feb. 2020.

[92] C. Jers, A. Kalantari, A. Garg, and I. Mijakovic, "Production of 3-hydroxypropanoic acid from glycerol by metabolically engineered bacteria," *Front. Bioeng. Biotechnol.*, vol. 7, p. 124, May 2019.

[93] C. Della Pina, E. Falletta, and M. Rossi, "A green approach to chemical building blocks. The case of 3-hydroxypropanoic acid," *Green Chem.*, vol. 13, no. 7, p. 1624, 2011.

[94] A. Corma Canos, S. Iborra, and A. Velty, "Chemical routes for the transformation of biomass into chemicals," *Chem. Rev.*, vol. 107, no. 6, pp. 2411–2502, Jun. 2007.

[95] B. Andreeßen, N. Taylor, and A. Steinbüchel, "Poly(3-hydroxypropionate): A promising alternative to fossil fuel-based materials," *Appl. Environ. Microbiol.*, vol. 80, no. 21, pp. 6574–6582, 2014.

[96] P. Bonnafous *et al.*, "Treatment of influenza virus with beta-propiolactone alters viral membrane fusion," *Biochim. Biophys. Acta - Biomembr.*, vol. 1838, no. 1 PARTB, pp. 355–363, Jan. 2014.

[97] PubChem, "beta-Propiolactone | C3H4O2 - PubChem," 2020. [Online]. Available: https://pubchem.ncbi.nlm.nih.gov/compound/beta-Propiolactone#section=GHS-Classification. [Accessed: 02-Feb-2021].

[98] National Toxicology Program, "βPropiolactone.," *Rep. Carcinog.*, vol. 12, pp. 366–367, 2011.

[99] ICIS Chemical Business, "Chemical profile: US acrylic acid," 2013. [Online]. Available: https://www.icis.com/explore/resources/news/2016/12/01/10059851/chemical-profile-us-acrylic-acid/. [Accessed: 14-May-2020].

[100] M. Bihani, T. N. Ansari, J. D. Smith, and S. Handa, “The magical but endangered metal: searching for sustainable palladium catalysis,” *Curr. Opin. Green Sustain. Chem.*, vol. 11, pp. 45–53, Jun. 2018.

[101] C. Della Pina, E. Falletta, and M. Rossi, “Oxidation of allyl alcohol in the presence of a gold catalyst: A route to 3-Hydroxypropionic acid,” *ChemSusChem*, vol. 2, no. 1, pp. 57–58, Jan. 2009.

[102] J. A. Moma, T. A. Ntho, and M. Scurrell, “Gold-catalysed reactions,” in *Catalytic Application of Nano-Gold Catalysts*, InTech, 2016.

[103] Research Dive Analysis, “3-hydroxypropionic acid market report,” 2020. .

[104] L. Wu, S. Dutta, and M. Mascal, “Efficient, chemical-catalytic approach to the production of 3-hydroxypropanoic acid by oxidation of biomass-derived levulinic acid with hydrogen peroxide,” *ChemSusChem*, vol. 8, no. 7, pp. 1167–1169, Apr. 2015.

[105] L. Matsakas, K. Hrůzová, U. Rova, and P. Christakopoulos, “Biological production of 3-hydroxypropionic acid: an update on the current status,” *Fermentation*, vol. 4, no. 1, p. 13, Feb. 2018.

[106] T. Werpy and G. P. Petersen, “Top value added chemicals from biomass,” p. 66, 2004.

[107] T. Warnecke and R. T. Gill, “Organic acid toxicity, tolerance, and production in *Escherichia coli* biorefining applications.,” *Microb. Cell Fact.*, vol. 4, no. September 2005, p. 25, Aug. 2005.

[108] H. S. Chu *et al.*, “Metabolic engineering of 3-hydroxypropionic acid biosynthesis in *Escherichia coli*,” *Biotechnol. Bioeng.*, vol. 112, no. 2, pp. 356–364, Feb. 2015.

[109] Y. Li, X. Wang, X. Ge, and P. Tian, “High production of 3-hydroxypropionic acid in *Klebsiella pneumoniae* by systematic optimization of glycerol metabolism,” *Sci. Rep.*, vol. 6, p. 26932, May 2016.

[110] Z. Chen, J. Huang, Y. Wu, W. Wu, Y. Zhang, and D. Liu, “Metabolic engineering of *Corynebacterium glutamicum* for the production of 3-hydroxypropionic acid from glucose and xylose,” *Metab. Eng.*, vol. 39, pp. 151–158, Jan. 2017.

[111] Y. S. Jang *et al.*, “Bio-based production of C2-C6 platform chemicals,” *Biotechnol. Bioeng.*, vol. 109, no. 10, pp. 2437–2459, 2012.

[112] E. I. Lan, D. S. Chuang, C. R. Shen, A. M. Lee, S. Y. Ro, and J. C. Liao, “Metabolic engineering of cyanobacteria for photosynthetic 3-hydroxypropionic acid production from CO_2 using *Synechococcus elongatus* PCC 7942,” *Metab. Eng.*, vol. 31, pp. 163–170, Sep. 2015.

[113] C. Liu, Y. Ding, R. Zhang, H. Liu, M. Xian, and G. Zhao, “Functional balance between enzymes in malonyl-CoA pathway for 3-hydroxypropionate biosynthesis,” *Metab. Eng.*, vol. 34, pp. 104–111, Mar. 2016.

[114] S. Takayama *et al.*, “Enhancing 3-hydroxypropionic acid production in combination with sugar supply engineering by cell surface-display and metabolic engineering of *Schizosaccharomyces pombe*,” *Microb. Cell Fact.*, vol. 17, no. 1, pp. 1–11, Nov. 2018.

[115] C. W. Song, J. W. Kim, I. J. Cho, and S. Y. Lee, “Metabolic engineering of *Escherichia coli*

for the production of 3-hydroxypropionic acid and malonic acid through β-alanine route," *ACS Synth. Biol.*, vol. 5, no. 11, pp. 1256–1263, Nov. 2016.

[116] I. Borodina *et al.*, "Establishing a synthetic pathway for high-level production of 3-hydroxypropionic acid in *Saccharomyces cerevisiae* via β-alanine," *Metab. Eng.*, vol. 27, pp. 57–64, Jan. 2015.

[117] A. Kalantari *et al.*, "Conversion of glycerol to 3-hydroxypropanoic acid by genetically engineered *Bacillus subtilis*," *Front. Microbiol.*, vol. 8, no. APR, Apr. 2017.

[118] M. Delample *et al.*, "Glycerol as a cheap, safe and sustainable solvent for the catalytic and regioselective β,β-diarylation of acrylates over palladium nanoparticles," *Green Chem.*, vol. 12, no. 5, pp. 804–80, May 2010.

[119] Y. S. Park *et al.*, "Engineering an aldehyde dehydrogenase toward its substrates, 3-hydroxypropanal and NAD+, for enhancing the production of 3-hydroxypropionic acid," *Sci. Rep.*, vol. 7, no. 1, Dec. 2017.

[120] S. K. Brar, S. J. Sarma, K. Pakshirajan, S. Kaur Brar, S. Jyoti Sarma, and K. Pakshirajan, *Platform Chemical Biorefinery: Future Green Chemistry*. Elsevier Science, 2016.

[121] Y. Ko *et al.*, "Coenzyme B_{12} can be produced by engineered *Escherichia coli* under both anaerobic and aerobic conditions," *Biotechnol. J.*, vol. 9, no. 12, pp. 1526–1535, Dec. 2014.

[122] Cargill Incorporated, "3-hydroxypropionic acid and other organic compounds," WO2002042418 A2, 2002.

[123] V. Kumar, S. Ashok, and S. Park, "Recent advances in biological production of 3-hydroxypropionic acid," *Biotechnol. Adv.*, vol. 31, no. 6, pp. 945–961, 2013.

[124] H. Liao, R. Gokarn, S. J. Gort, H. J. Jessen, and O. Selifonova, "US8124388B2 - Production of 3-hydroxypropionic acid using beta-alanine/pyruvate aminotransferase."

[125] C. S. Henry, L. J. Broadbelt, and V. Hatzimanikatis, "Discovery and analysis of novel metabolic pathways for the biosynthesis of industrial chemicals: 3-hydroxypropanoate," *Biotechnol. Bioeng.*, vol. 106, no. 3, pp. 462–473, Jun. 2010.

[126] M. López-Sámano *et al.*, "De novo β-alanine synthesis in α-proteobacteria involves a β-alanine synthase from the uracil degradation pathway," *bioRxiv*, p. 663849, Jun. 2019.

[127] C. Kennes, *Bioconversion Processes*. MDPI AG, 2018.

[128] K. R. Kildegaard, Z. Wang, Y. Chen, J. Nielsen, and I. Borodina, "Production of 3-hydroxypropionic acid from glucose and xylose by metabolically engineered *Saccharomyces cerevisiae*," *Metab. Eng. Commun.*, vol. 2, pp. 132–136, Dec. 2015.

[129] M. Zampieri, M. Hörl, F. Hotz, N. F. Müller, and U. Sauer, "Regulatory mechanisms underlying coordination of amino acid and glucose catabolism in *Escherichia coli*," *Nat. Commun.*, vol. 10, no. 1, pp. 1–13, Dec. 2019.

[130] B. Wu, W. Szymański, M. M. Heberling, B. L. Feringa, and D. B. Janssen, "Aminomutases: Mechanistic diversity, biotechnological applications and future perspectives," *Trends Biotechnol.*, vol. 29, no. 7, pp. 352–362, Jul. 2011.

[131] D. Orol Gómez, "Characterisation of the native β-alanine pathway in *Cupriavidus necator* H16: an attractive route towards 3-hydroxypropionic acid production.," 2020.

[132] I. A. Berg, D. Kockelkorn, W. Buckel, and G. Fuchs, “A 3-hydroxypropionate/4-hydroxybutyrate autotrophic carbon dioxide assimilation pathway in archaea,” *Science (80-.).*, vol. 318, no. 5857, pp. 1782–1786, Dec. 2007.

[133] M. Hügler, C. Menendez, H. Schägger, and G. Fuchs, “Malonyl-coenzyme a reductase from *Chloroflexus aurantiacus*, a key enzyme of the 3-hydroxypropionate cycle for autotrophic CO_2 fixation,” *J. Bacteriol.*, vol. 184, no. 9, pp. 2404–10, May 2002.

[134] T. J. Erb, “Carboxylases in natural and synthetic microbial pathways.,” *Appl. Environ. Microbiol.*, vol. 77, no. 24, pp. 8466–77, Dec. 2011.

[135] C. Liu *et al.*, “Malonyl-CoA pathway: a promising route for 3-hydroxypropionate biosynthesis,” *Crit. Rev. Biotechnol.*, vol. 0, no. 0, pp. 1–9, Oct. 2017.

[136] Y. Sasaki and Y. Nagano, “Plant acetyl-CoA carboxylase: structure, biosynthesis, regulation, and gene manipulation for plant breeding,” *Biosci. Biotechnol. Biochem.*, vol. 68, no. 6, pp. 1175–1184, Jan. 2004.

[137] C. Rathnasingh, S. M. Raj, Y. Lee, C. Catherine, S. Ashok, and S. Park, “Production of 3-hydroxypropionic acid via malonyl-CoA pathway using recombinant *Escherichia coli* strains,” *J. Biotechnol.*, vol. 157, no. 4, pp. 633–640, 2012.

[138] Q. Wang, C. Liu, M. Xian, Y. Zhang, and G. Zhao, “Biosynthetic pathway for poly(3-Hydroxypropionate) in recombinant *Escherichia coli*,” *J. Microbiol.*, vol. 50, no. 4, pp. 693–697, 2012.

[139] Z. Cheng, J. Jiang, H. Wu, Z. Li, and Q. Ye, “Enhanced production of 3-hydroxypropionic acid from glucose via malonyl-CoA pathway by engineered *Escherichia coli*,” *Bioresour. Technol.*, vol. 200, no. March 2016, pp. 897–904, 2016.

[140] M. S. Davis, J. Solbiati, and J. E. Cronan, “Overproduction of acetyl-CoA carboxylase activity increases the rate of fatty acid biosynthesis in *Escherichia coli*,” *J. Biol. Chem.*, vol. 275, no. 37, pp. 28593–28598, Sep. 2000.

[141] W. Cao *et al.*, “Enhanced pinocembrin production in *Escherichia coli* by regulating cinnamic acid metabolism,” *Sci. Rep.*, vol. 6, no. 1, pp. 1–9, 2016.

[142] W. Zha, S. B. Rubin-Pitel, Z. Shao, and H. Zhao, “Improving cellular malonyl-CoA level in *Escherichia coli* via metabolic engineering,” *Metab. Eng.*, vol. 11, no. 3, pp. 192–198, May 2009.

[143] S. W. Polyak, A. D. Abell, M. C. J. Wilce, L. Zhang, and G. W. Booker, “Structure, function and selective inhibition of bacterial acetyl-coA carboxylase,” *Appl. Microbiol. Biotechnol.*, vol. 93, no. 3, pp. 983–992, Feb. 2012.

[144] C. Liu, Q. Wang, M. Xian, Y. Ding, and G. Zhao, “Dissection of malonyl-Coenzyme A reductase of *Chloroflexus aurantiacus* results in enzyme activity improvement,” *PLoS One*, vol. 8, no. 9, Sep. 2013.

[145] Y. Wang *et al.*, “Biosynthesis of platform chemical 3-hydroxypropionic acid (3-HP) directly from CO_2 in cyanobacterium *Synechocystis sp.* PCC 6803,” *Metab. Eng.*, vol. 34, pp. 60–70, Mar. 2016.

[146] R. E. Davis, “Microbial community dynamics and carbon fixation in dark oligotrophic

volcanic ecosystems," Oregon Health & Science University, 2014.

[147] K. Umenhoffer *et al.*, "Reduced evolvability of *Escherichia coli* MDS42, an IS-less cellular chassis for molecular and synthetic biology applications," *Microb. Cell Fact.*, vol. 9, no. 1, p. 38, May 2010.

[148] R. Simon, U. Priefer, and A. Pühler, "A broad host range mobilization system for *in vivo* genetic engineering: transposon mutagenesis in Gram negative bacteria," *Bio/Technology*, vol. 1, no. 9, pp. 784–791, Nov. 1983.

[149] C. Harwood and S. Cutting, *Molecular Biological Methods for Bacillus*, Illustrate., vol. 3. Wiley, 1991.

[150] D. Yang *et al.*, "Repurposing type III polyketide synthase a malonyl-CoA biosensor for metabolic engineering in bacteria," *PNAS*, vol. 115, no. 40, pp. 9835–9844, Oct. 2018.

[151] J. M. Park, Y.-S. Jang, T. Y. Kim, and S. Y. Lee, "Development of a gene knockout system for *Ralstonia eutropha* H16 based on the broad-host-range vector expressing a mobile group II intron," *FEMS Microbiol. Lett.*, vol. 309, no. 2, p. no-no, Jul. 2010.

[152] J. K. Kroeger, J. Zarzycki, and G. Fuchs, "A spectrophotometric assay for measuring acetyl–coenzyme A carboxylase," *Anal. Biochem.*, vol. 411, no. 1, pp. 100–105, 2011.

[153] D. Yang *et al.*, "Repurposing type III polyketide synthase as a malonyl- CoA biosensor for metabolic engineering in bacteria," *Proc. Natl. Acad. Sci. U. S. A.*, vol. 115, no. 40, pp. 9835–9844, Oct. 2018.

[154] CLC Genomics, "CLC Genomics Workbench User Manual," 2021. [Online]. Available: http://resources.qiagenbioinformatics.com/manuals/clcgenomicsworkbench/current/User_Manual.pdf.

[155] M. Hachisu, K. Mori, K. Hyodo, S. Morimoto, T. Yamazaki, and Y. Ichiyanagi, "Selective aerobic oxidation of 1,3-propanediol to 3-hydroxypropanoic acid using hydrotalcite supported bimetallic gold nanoparticle catalyst in water," in *AIP Conference Proceedings*, 2015, vol. 1649, no. 20, pp. 20–26.

[156] L. Mika, E. Csealvay, and R. Neeth, "Catalytic conversion of carbohydrates to initial platform chemicals: chemistry and sustainability," *Chem. Rev.*, vol. 118, pp. 505–613, 2018.

[157] L. Tong, "Acetyl-coenzyme A carboxylase: Crucial metabolic enzyme and attractive target for drug discovery," *Cell. Mol. Life Sci.*, vol. 62, no. 16, pp. 1784–1803, Aug. 2005.

[158] C. O. Rock, "Fatty acid and phospholipid metabolism in prokaryotes," in *Biochemistry of Lipids, Lipoproteins and Membranes*, Elsevier, 2008, pp. 59–96.

[159] Y. Kimura, R. Miyake, Y. Tokumasu, and M. Sato, "Molecular cloning and characterization of two genes for the biotin carboxylase and carboxyltransferase subunits of acetyl coenzyme a carboxylase in *Myxococcus xanthus*," *J. Bacteriol.*, vol. 182, no. 19, pp. 5462–5469, 2000.

[160] A. C. Smith and J. E. Cronan, "Dimerization of the bacterial biotin carboxylase subunit is required for acetyl coenzyme A carboxylase activity *in vivo*," *J. Bacteriol.*, vol. 194, no. 1, pp. 72–78, Jan. 2012.

[161] A. L. Livieri, L. Navone, E. Marcellin, H. Gramajo, and E. Rodriguez, "A novel multidomain acyl-CoA carboxylase in *Saccharopolyspora erythraea* provides malonyl-CoA for *de novo*

fatty acid biosynthesis," *Sci. Rep.*, vol. 9, no. 1, pp. 1–10, Dec. 2019.

[162] R. W. Brownsey, A. N. Boone, J. E. Elliott, J. E. Kulpa, and W. M. Lee, "Regulation of acetyl-CoA carboxylase," *Biochem. Soc. Trans.*, vol. 34, no. 2, pp. 223–227, Apr. 2006.

[163] T. Konishi, K. Shinohara, K. Yamada, and Y. Sasaki, "Acetyl-CoA carboxylase in higher plants: Most plants other than Gramineae have both the prokaryotic and the eukaryotic forms of this enzyme," *Plant Cell Physiol.*, vol. 37, no. 2, pp. 117–122, 1996.

[164] R. J. Heath and C. O. Rock, "Regulation of malonyl-CoA metabolism by acyl-acyl carrier protein and β- ketoacyl-acyl carrier protein synthases in *Escherichia coli*," *J. Biol. Chem.*, vol. 270, no. 26, pp. 15531–15538, Jun. 1995.

[165] M. A. Silvers, G. T. Robertson, C. M. Taylor, and G. L. Waldrop, "Design, synthesis, and antibacterial properties of dual-ligand inhibitors of acetyl-CoA carboxylase," *J. Med. Chem.*, vol. 57, no. 21, pp. 8947–8959, Nov. 2014.

[166] R. Gande *et al.*, "The two carboxylases of *Corynebacterium glutamicum* essential for fatty acid and mycolic acid synthesis," *J. Bacteriol.*, vol. 189, no. 14, pp. 5257–5264, Jul. 2007.

[167] L. Milke, N. Kallscheuer, J. Kappelmann, and J. Marienhagen, "Tailoring *Corynebacterium glutamicum* towards increased malonyl-CoA availability for efficient synthesis of the plant pentaketide noreugenin," *Microb. Cell Fact.*, vol. 18, no. 1, p. 71, Apr. 2019.

[168] A. L. Evans, "The distinctive regulatory mechanisms of bacterial acetyl-CoA carboxylase," Louisiana State University, 2018.

[169] G. Meades, B. K. Benson, A. Grove, and G. L. Waldrop, "A tale of two functions: Enzymatic activity and translational repression by carboxyltransferase," *Nucleic Acids Res.*, vol. 38, no. 4, pp. 1217–1227, Dec. 2009.

[170] E. S. James and J. E. Cronan, "Expression of two *Escherichia coli* acetyl-CoA carboxylase subunits is autoregulated," *J. Biol. Chem.*, vol. 279, no. 4, pp. 2520–2527, 2004.

[171] "Regulon of FasR in *Corynebacterium glutamicum* ATCC 13032." [Online]. Available: http://regprecise.sbpdiscovery.org:8080/WebRegPrecise/regulon.jsp?regulon_id=36238. [Accessed: 13-Mar-2021].

[172] J. Nickel, K. Irzik, J. Van Ooyen, and L. Eggeling, "The TetR-type transcriptional regulator FasR of *Corynebacterium glutamicum* controls genes of lipid synthesis during growth on acetate," *Mol. Microbiol.*, vol. 78, no. 1, pp. 253–265, Aug. 2010.

[173] M. S. Davis and J. Cronan, "Inhibition of *Escherichia coli* acetyl coenzyme A carboxylase by acyl-acyl carrier protein," *J. Bacteriol.*, vol. 183, no. 4, pp. 1499–1503, Feb. 2001.

[174] A. Evans, W. Ribble, E. Schexnaydre, and G. L. Waldrop, "Acetyl-CoA carboxylase from *Escherichia coli* exhibits a pronounced hysteresis when inhibited by palmitoyl-acyl carrier protein," *Arch. Biochem. Biophys.*, vol. 636, pp. 100–109, Dec. 2017.

[175] L. M. Salati and A. G. Goodridge, "Fatty acid synthesis in eukaryotes," in *New Comprehensive Biochemistry*, vol. 31, no. C, 1996, pp. 101–127.

[176] D. Liu, Y. Xiao, B. S. Evans, and F. Zhang, "Negative feedback regulation of fatty acid production based on a malonyl-CoA sensor-actuator," *ACS Synth. Biol.*, vol. 4, no. 2, pp. 132–140, Feb. 2015.

[177] E. Leonard, K. H. Lim, P. N. Saw, and M. A. G. Koffas, "Engineering central metabolic pathways for high-level flavonoid production in *Escherichia coli*," *Appl. Environ. Microbiol.*, vol. 73, no. 12, pp. 3877–3886, Jun. 2007.

[178] M. Hügler, R. S. Krieger, M. Jahn, and G. Fuchs, "Characterization of acetyl-CoA/propionyl-CoA carboxylase in *Metallosphaera sedula*: Carboxylating enzyme in the 3-hydroxypropionate cycle for autotrophic carbon fixation," *Eur. J. Biochem.*, vol. 270, no. 4, pp. 736–744, Feb. 2003.

[179] R. Gande *et al.*, "Acyl-CoA carboxylases (*accD2* and *accD3*), together with a unique polyketide synthase (Cg-pks), are key to mycolic acid biosynthesis in *Corynebacterianeae* such as *Corynebacterium glutamicum* and *Mycobacterium tuberculosis*," *J. Biol. Chem.*, vol. 279, no. 43, pp. 44847–44857, Oct. 2004.

[180] W. Jäger, P. G. Peters-Wendisch, J. Kalinowski, and A. Pühler, "A *Corynebacterium glutamicum* gene encoding a two-domain protein similar to biotin carboxylases and biotin-carboxyl-carrier proteins," *Arch. Microbiol.*, vol. 166, no. 2, pp. 76–82, 1996.

[181] K. S. Shin and S. K. Lee, "Introduction of an acetyl-CoA carboxylation bypass into *Escherichia coli* for enhanced free fatty acid production," *Bioresour. Technol.*, vol. 245, pp. 1627–1633, Dec. 2017.

[182] L. A. Stirling, P. M. Ahmad, and F. Ahmad, "Acyl coenzyme A carboxylase of *Propionibacterium shermanii*: Detection and properties," *J. Bacteriol.*, vol. 148, no. 3, pp. 933–940, 1981.

[183] H. Holo, "*Chloroflexus aurantiacus* secretes 3-hydroxypropionate, a possible intermediate in the assimilation of CO_2 and acetate," *Arch. Microbiol.*, vol. 151, no. 3, pp. 252–256, Feb. 1989.

[184] J. Zarzycki, V. Brecht, M. Müller, and G. Fuchs, "Identifying the missing steps of the autotrophic 3-hydroxypropionate CO_2 fixation cycle in *Chloroflexus aurantiacus*," *Proc. Natl. Acad. Sci. U. S. A.*, vol. 106, no. 50, pp. 21317–21322, 2009.

[185] P. M. Shih, L. M. Ward, and W. W. Fischer, "Evolution of the 3-hydroxypropionate bicycle and recent transfer of anoxygenic photosynthesis into the *Chloroflexi*," *Proc. Natl. Acad. Sci. U. S. A.*, vol. 114, no. 40, pp. 10749–10754, Oct. 2017.

[186] C. G. Klatt *et al.*, "Temporal metatranscriptomic patterning in phototrophic *Chloroflexi* inhabiting a microbial mat in a geothermal spring," *ISME J.*, vol. 7, no. 9, pp. 1775–1789, Sep. 2013.

[187] A. B. Hawkins, M. W. W. Adams, and R. M. Kelly, "Conversion of 4-hydroxybutyrate to acetyl coenzyme A and its anapleurosis in the *Metallosphaera sedula* 3-hydroxypropionate/4-hydroxybutyrate carbon fixation pathway," *Appl. Environ. Microbiol.*, vol. 80, no. 8, pp. 2536–2545, 2014.

[188] M. P. Dalwadi and J. R. King, "An asymptotic analysis of the malonyl-CoA route to 3-hydroxypropionic acid in genetically engineered microbes," *Bull. Math. Biol.*, vol. 82, no. 3, pp. 1–31, Mar. 2020.

[189] B. B. Kuznetsov *et al.*, "Draft genome sequence of the anoxygenic filamentous phototrophic

bacterium *Oscillochloris trichoides* subsp. DG-6," *J. Bacteriol.*, vol. 193, no. 1, pp. 321–322, Jan. 2011.

[190] J. Otte, A. Mall, D. M. Schubert, M. Könneke, and I. A. Berg, "Malonic semialdehyde reductase from the archaeon *Nitrosopumilus maritimus* is involved in the autotrophic 3-hydroxypropionate/4-hydroxybutyrate cycle.," *Appl. Environ. Microbiol.*, vol. 81, no. 5, pp. 1700–7, Mar. 2015.

[191] H. Liao *et al.*, "Monofunctional *mcr* + 3-HP dehydrogenase," US2015O119601A1, 30-Apr-2015.

[192] R. N. Ivanovsky *et al.*, "Evidence for the presence of the reductive pentose phosphate cycle in a filamentous anoxygenic photosynthetic bacterium, *Oscillochloris trichoides* strain DG-6," *Microbiology*, vol. 145, no. 7, pp. 1743–1748, 1999.

[193] K. R. Kildegaard *et al.*, "Engineering and systems-level analysis of *Saccharomyces cerevisiae* for production of 3-hydroxypropionic acid via malonyl-CoA reductase-dependent pathway," *Microb. Cell Fact.*, vol. 15, no. 1, p. 53, Mar. 2016.

[194] J. M. Ellis and M. J. Wolfgang, "A genetically encoded metabolite sensor for malonyl-CoA," *Chem. Biol.*, vol. 19, no. 10, pp. 1333–1339, Oct. 2012.

[195] M. Szostková and D. Horáková, "The effect of plasmid DNA sizes and other factors on electrotransformation of *Escherichia coli* JM109," *Bioelectrochemistry Bioenerg.*, vol. 47, no. 2, pp. 319–323, Dec. 1998.

[196] U. E. Cheah, W. A. Weigand, and B. C. Stark, "Effects of recombinant plasmid size on cellular processes in *Escherichia coli*," *Plasmid*, vol. 18, no. 2, pp. 127–134, Sep. 1987.

[197] M. P. Dalwadi, J. R. King, and N. P. Minton, "Multi-timescale analysis of a metabolic network in synthetic biology: a kinetic model for 3-hydroxypropionic acid production via beta-alanine," *J. Math. Biol.*, vol. 77, no. 1, pp. 165–199, Jul. 2018.

[198] A. P. Golovanov, G. M. Hautbergue, S. A. Wilson, and L. Y. Lian, "A simple method for improving protein solubility and long-term stability," *J. Am. Chem. Soc.*, vol. 126, no. 29, pp. 8933–8939, Jul. 2004.

[199] S. Shi, Y. Chen, V. Siewers, and J. Nielsen, "Improving production of malonyl coenzyme A-derived metabolites by abolishing Snf1-dependent regulation of Acc1," *MBio*, vol. 5, no. 3, Jul. 2014.

[200] J. D. McGarry, M. J. Stark, and D. W. Foster, "Hepatic malonyl-CoA levels of fed, fasted and diabetic rats as measured using a simple radioisotopic assay," *J. Biol. Chem.*, vol. 253, no. 22, pp. 8291–8293, 1978.

[201] L. Gao, W. Chiou, H. Tang, X. Cheng, H. S. Camp, and D. J. Burns, "Simultaneous quantification of malonyl-CoA and several other short-chain acyl-CoAs in animal tissues by ion-pairing reversed-phase HPLC/MS," *J. Chromatogr. B Anal. Technol. Biomed. Life Sci.*, vol. 853, no. 1–2, pp. 303–313, Jun. 2007.

[202] A. O. Johnson *et al.*, "Design and application of genetically-encoded malonyl-CoA biosensors for metabolic engineering of microbial cell factories," *Metabolic Engineering*, vol. 44. Academic Press Inc., pp. 253–264, 01-Nov-2017.

[203] T. Fehér *et al.*, “A sense of balance: experimental investigation and modeling of a malonyl-CoA sensor in *Escherichia coli*,” *Front. Bioeng. Biotechnol.*, vol. 3, no. APR, p. 46, Apr. 2015.

[204] Y. Takamura, Y. Kitayama, A. Arakawa, S. Yamanaka, M. Tosaki, and Y. Ogawa, “Malonyl-CoA: acetyl-CoA cycling. A new micromethod for determination of acyl-CoAs with malonate decarboxylase,” *Biochim. Biophys. Acta (BBA)/Lipids Lipid Metab.*, vol. 834, no. 1, pp. 1–7, Mar. 1985.

[205] Y. Tsuchiya, U. Pham, and I. Gout, “Methods for measuring CoA and CoA derivatives in biological samples,” *Biochem. Soc. Trans.*, vol. 42, no. 4, pp. 1107–1111, Aug. 2014.

[206] O. Hayashi and K. Satoh, “Determination of acetyl-CoA and malonyl-CoA in germinating rice seeds using the LC-MS/MS technique,” *Biosci. Biotechnol. Biochem.*, vol. 70, no. 11, pp. 2676–2681, 2006.

[207] MyBioSource, “Human Malonyl Coenzyme A ELISA Kit Catalog Number. MBS705079 48T,” 2019. .

[208] I. M. Vincent, D. E. Ehmann, S. D. Mills, M. Perros, and M. P. Barrett, “Untargeted metabolomics to ascertain antibiotic modes of action,” *Antimicrob. Agents Chemother.*, vol. 60, no. 4, pp. 2281–2291, Apr. 2016.

[209] J. B. Parsons, M. W. Frank, C. Subramanian, P. Saenkham, and C. O. Rock, “Metabolic basis for the differential susceptibility of gram-positive pathogens to fatty acid synthesis inhibitors,” *Proc. Natl. Acad. Sci. U. S. A.*, vol. 108, no. 37, pp. 15378–15383, Sep. 2011.

[210] K. Kawahara, K. Uchida, and K. A. Aida, “Isolation and partial characterization of a cerulenin-sensitive mutant of *Pseudomonas aeruginosa*,” *J. Antibiot. (Tokyo).*, vol. 36, no. 10, pp. 1329–1335, 1983.

[211] P. Xu, W. Wang, L. Li, N. Bhan, F. Zhang, and M. A. G. G. Koffas, “Design and kinetic analysis of a hybrid promoter−regulator system for malonyl-CoA sensing in *Escherichia coli*,” *ACS Chem. Biol.*, vol. 9, no. 2, pp. 451–458, Feb. 2014.

[212] F. David, J. Nielsen, and V. Siewers, “Flux control at the malonyl-CoA node through hierarchical dynamic pathway regulation in *Saccharomyces cerevisiae*,” *ACS Synth. Biol.*, vol. 5, no. 3, pp. 224–233, Mar. 2016.

[213] Y. Du, H. Hu, X. Pei, K. Du, and T. Wei, “Genetically encoded FapR-NLuc as a biosensor to determine malonyl-CoA *in situ* at subcellular scales,” *Bioconjug. Chem.*, vol. 30, no. 3, pp. 826–832, Mar. 2019.

[214] G. E. Schujman, L. Paoletti, A. D. Grossman, and D. de Mendoza, “FapR, a bacterial transcription factor involved in global regulation of membrane lipid biosynthesis,” *Dev. Cell*, vol. 4, no. 5, pp. 663–672, May 2003.

[215] H. G. Garcia, H. J. Lee, J. Q. Boedicker, and R. Phillips, “Comparison and calibration of different reporters for quantitative analysis of gene expression,” *Biophys. J.*, vol. 101, no. 3, pp. 535–544, Aug. 2011.

[216] K. Tarasava, “Development of novel Crispr-based methods for transcriptional control over bacterial gene expression,” University of Colorado at Boulder, 2019.

[217] E. S. Gomes, V. Schuch, and E. G. de M. Lemos, “Biotechnology of polyketides: New breath of life for the novel antibiotic genetic pathways discovery through metagenomics,” *Brazilian Journal of Microbiology*, vol. 44, no. 4. Sociedade Brasileira de Microbiologia, pp. 1007–1034, 2013.

[218] C. P. Ridley, Y. L. Ho, and C. Khosla, “Evolution of polyketide synthases in bacteria,” *Proc. Natl. Acad. Sci. U. S. A.*, vol. 105, no. 12, pp. 4595–4600, Mar. 2008.

[219] N. Funa, Y. Ohnishi, Y. Ebizuka, and S. Horinouchi, “Properties and substrate specificity of RppA, a chalcone synthase-related polyketide synthase in *Streptomyces griseus*,” *J. Biol. Chem.*, vol. 277, no. 7, pp. 4628–4635, Feb. 2002.

[220] J. Cheng, J. Ma, J. Lin, Z. C. Fan, J. E. Cronan, and H. Wang, “Only one of the five *Ralstonia solanacearum* long-chain 3-ketoacyl-acyl carrier protein synthase homologues functions in fatty acid synthesis,” *Appl. Environ. Microbiol.*, vol. 78, no. 5, pp. 1563–1573, Mar. 2012.

[221] K. H. Kim, “Regulation of acetyl-CoA carboxylase,” in *Current Topics in Cellular Regulation*, vol. 22, no. C, 1983, pp. 143–176.

[222] T. M. Buttke, L. O’, and N. Ingram, “Inhibition of unsaturated fatty acid synthesis in *Escherichia coli* by the antibiotic cerulenin,” *Biochemistry*, vol. 17, no. 24, pp. 5282–5286, 1978.

[223] I. Goldberg, J. R. Walker,’ And, and K. Bloch, “Inhibition of lipid synthesis in *Escherichia coli* cells by the antibiotic cerulenin,” *Antimicrob. Agents Chemother.*, vol. 3, no. 5, pp. 549–554, 1973.

[224] E. Perrin *et al.*, “Diauxie and co-utilization of carbon sources can coexist during bacterial growth in nutritionally complex environments,” *Nat. Commun.*, vol. 11, no. 1, p. 3135, Dec. 2020.

[225] X. Wang, K. Xia, X. Yang, and C. Tang, “Growth strategy of microbes on mixed carbon sources,” *Nat. Commun.*, vol. 10, no. 1, pp. 1–7, Dec. 2019.

[226] B. Magasanik, “Glucose effects: inducer exclusion and repression.,” in *The Lactose Operon*, vol. 1, no. 0, 1970, pp. 189–219.

[227] R. Brückner, F. Titgemeyer, R. Brackner, and F. Titgemeyer, “Carbon catabolite repression in bacteria: choice of the carbon source and autoregulatory limitation of sugar utilization,” *FEMS Microbiol. Lett.*, vol. 209, no. 2, pp. 141–148, Apr. 2002.

[228] C. Kaddor and A. Steinbüchel, “Effects of homologous phosphoenolpyruvate-carbohydrate phosphotransferase system proteins on carbohydrate uptake and poly(3-Hydroxybutyrate) accumulation in *Ralstonia eutropha* H16,” *Appl. Environ. Microbiol.*, vol. 77, no. 11, pp. 3582–3590, Jun. 2011.

[229] T. Conway, “The Entner-Doudoroff pathway: history, physiology and molecular biology,” *FEMS Microbiol. Lett.*, vol. 103, no. 1, pp. 1–28, Sep. 1992.

[230] K. Lin, Y. Elbahloul, and A. Steinbüchel, “Physiological conditions conducive to high cell density and high cyanophycin content in *Ralstonia eutropha* strain H16 possessing a KDPG aldolase gene-dependent addiction system,” *Appl. Microbiol. Biotechnol.*, vol. 93, no. 5, pp. 1885–1894, 2012.

[231] D. N. Collier, P. W. Hager, and P. V. Phibbs, “Catabolite repression control in the Pseudomonads,” in *Research in Microbiology*, 1996, vol. 147, no. 6–7, pp. 551–561.

[232] H. Park, S. L. McGill, A. D. Arnold, and R. P. Carlson, “Pseudomonad reverse carbon catabolite repression, interspecies metabolite exchange, and consortial division of labor,” *Cell. Mol. Life Sci.*, vol. 77, no. 3, pp. 395–413, Feb. 2020.

[233] F. Rojo, “Carbon catabolite repression in *Pseudomonas*: Optimizing metabolic versatility and interactions with the environment,” *FEMS Microbiol. Rev.*, vol. 34, no. 5, pp. 658–684, Sep. 2010.

[234] F. Ampe, D. Léonard, and N. D. Lindley, “Repression of phenol catabolism by organic acids in *Ralstonia eutropha*,” *Appl. Environ. Microbiol.*, vol. 64, no. 1, pp. 1–6, Jan. 1998.

[235] H. Den, W. H. Robinson, and M. J. Coon, “Enzymatic conversion of beta-hydroxypropionate to malonic semialdehyde,” *J. Biol. Chem.*, vol. 234, no. 7, pp. 1666–1671, 1959.

[236] R. D. Scholem and G. K. Brown, “Metabolism of malonic semialdehyde in man,” *Biochem. J.*, vol. 216, no. 1, pp. 81–85, 1983.

[237] J. D. Todd *et al.*, “Molecular dissection of bacterial acrylate catabolism - unexpected links with dimethylsulfoniopropionate catabolism and dimethyl sulfide production,” *Environ. Microbiol.*, vol. 12, no. 2, pp. 327–343, Feb. 2010.

[238] D. B. Olsen, T. W. Hepburn, S. lian Lee, B. M. Martin, P. S. Mariano, and D. Dunaway-Mariano, “Investigation of the substrate binding and catalytic groups of the PC bond cleaving enzyme, phosphonoacetaldehyde hydrolase,” *Arch. Biochem. Biophys.*, vol. 296, no. 1, pp. 144–151, Jul. 1992.

[239] W. B. Jackoby and E. M. Scott, “Aldehyde oxidation. III. Succinic semialdehyde dehydrogenase,” *J. Biol. Chem.*, vol. 234, no. 4, pp. 937–940, 1959.

[240] L. Yu, S. Li, W. Gao, Y. Pan, H. Tan, and G. Liu, “Regulation of myo-inositol catabolism by a GntR-type repressor SCO6974 in *Streptomyces coelicolor*,” *Appl. Microbiol. Biotechnol.*, vol. 99, no. 7, pp. 3141–3153, Apr. 2015.

[241] R. Satpathy, V. B. Konkimalla, and J. Ratha, “Microbial dehalogenation: 3-chloropropanoic acid (3-CPA) degradation as a case study,” *Microbiology*, vol. 86, no. 1, pp. 32–41, 2017.

[242] K. Vercammen *et al.*, “*Pseudomonas aeruginosa* LysR PA4203 regulator *nmoR* acts as a repressor of the PA4202 *nmoA* gene, encoding a nitronate monooxygenase,” *J. Bacteriol.*, vol. 197, no. 6, pp. 1026–1039, Mar. 2015.

[243] Y. Kohlmann, “Charakterisierung des Proteoms von *Ralstonia eutropha* H16 unter lithoautotrophen und anaeroben Bedingungen,” 2015.

[244] “HexR: Ralstonia.” [Online]. Available: http://regprecise.sbpdiscovery.org:8080/WebRegPrecise/ort_operons.jsp?project_id=1082&ort_id=19839. [Accessed: 12-Feb-2021].

[245] S. A. Leyn *et al.*, “Control of proteobacterial central carbon metabolism by the HexR transcriptional regulator: A case study in *Shewanella oneidensis*,” *J. Biol. Chem.*, vol. 286, no. 41, pp. 35782–35794, Oct. 2011.

[246] A. B. Foster and J. Kennedy, “Materials and methods for controlling regulation in

biosynthesis in species of the genera *Ralstonia* or *Cupriavidus* and organisms related thereto," 07-Nov-2019.

[247] A. Daddaoua, T. Krell, and J. L. Ramos, "Regulation of glucose metabolism in *Pseudomonas*. The phosphorylative branch and Entner-Doudoroff enzymes are regulated by a repressor containing a sugar isomerase domain," *J. Biol. Chem.*, vol. 284, no. 32, pp. 21360–21368, Aug. 2009.

[248] C. J. Brigham, D. R. Speth, C. K. Rha, and A. J. Sinskey, "Whole-genome microarray and gene deletion studies reveal regulation of the polyhydroxyalkanoate production cycle by the stringent response in *Ralstonia eutropha* H16," *Appl. Environ. Microbiol.*, vol. 78, no. 22, pp. 8033–8044, Nov. 2012.

[249] D. Kraußе *et al.*, "Essential role of the *hprK* gene in *Ralstonia eutropha* H16," *J. Mol. Microbiol. Biotechnol.*, vol. 17, no. 3, pp. 146–152, 2009.

[250] A. B. Hawkins *et al.*, "Bioprocessing analysis of *Pyrococcus furiosus* strains engineered for CO_2-based 3-hydroxypropionate production.," *Biotechnol. Bioeng.*, vol. 112, no. 8, pp. 1533–43, Aug. 2015.

Appendix

7.1 Codon optimised gene strings ordered to construct pMTL71301_*mmc*

Polynucleotides ordered from ThermoFisher in the form of Gene strings. Three sequences were ordered to cover the 4 coding regions of the MMC operon. Each gene of the operon is indicated in a different colour (RM25_1795/*M18870* in orange, RM25_1794/*mmdA* in blue, RM25_1793/*HY* in purple and RM25_1792/*bccP* in green). RBS and spacers (native to *P. freudenreichii*) in grey. Codon optimisation resulted in the alteration of bases, indicated in genes strings 1 and 3, by capitalisation. Overlap sequences allowed for construction of plasmid vectors by HiFi assembly. The restriction digestion cut sites for NdeI and HindIII were restored (indicated in bold).

Gene string 1 – 1587 bp

aatagtgacggcagagagacaatcaa**cat**atgagtccgcgagaaattgaggtttccgagccgcgcgaggttggtatca
ccgagctcgtgctgcgcgatgcccatcagagcctgatggccacacgaatggcaatggaagacatggtcggcgcctgtg
cagacattgatgctgccgggtactggtcagtggagtgttggggtggtgccacgtatgactcgtgtatccgcttcctcaacg
aggatccttgggagcgtctgcgcacgttccgcaagctgatgcccaacagccgtctccagatgctgctgcgtggccagaa
cctgctgggttaccgccactacaacgacgaggtcgtcgatcgcttcgtcgacaagtccgctgagaacggcatggacgtg
ttccgtgtcttcgacgccatgaatgatccccgcaacatggcgcacgccatggctgccgtcaagaaggccggcaagcac
gcgcagggcaccatttgctacacgatcagcccggtccacaccgttgagggctatgtcaagcttgctggtcagctgcttga
catgggtgctgattccatcgccctgaaggacatggccgccctgctcaagccgcagccggcctacgacatcatcaaggcc
atcaaggacacctacggccagaagacgcagatcaacctgcactgccactccaccacgggtgtcaccgaggtctccctc
atgaaggccatcgaggccggcgtcgacgtcgtcgacaccgccatctcgtccatgtcgctcggcccgggccacaacccc
accgagtcggtcgccgagatgctcgagggcaccgggtacaccaccaaccttgactacgatcgcctgcacaagatccgc
gatcacttcaaggccatccgcccgaagtacaagaagttcgagtcgaagacgcttgtcgacacctcgatcttcaagtcgca
gatccccggcggcatgctctccaacatggagtcgcagctgcgcgcccagggcgccgaggacaagatggacgaggtc
atggccgaggttccgcgcgtccgcaaggccgccggTttcccgcccctggtcaccccgtccagccagatcgtcggcac
gcaggccgtgttcaacgtgatgatgggcgagtacaagaggatgaccggcgagttcgccgacatcatgctcggctactac
ggcgccagcccggccgatcgcgatccgaaggtggtcaagttggccgaggagcagtccggcaagaagccgatcaccc
agcgcccggccgatctgctgccccccgagtgggagaagcagtccaaggaggccgcgacgctcaagggcttcaacgg
caccgacgaggacgtgctcacctatgcactgttcccgcaggtcgctccggtcttcttcgagcatcgcgccgagggcccg
cacagcgtggctctcaccgatgcccagctgaaggccgaggccgagggcgacgagaagtcgctcgccgtggccggtc
ccgtcacctacaacgtgaacgtgggcggaaccgtccgcgaagtcaccgttcagcaggcgtgaggatgattgccaatcat
ggctgaaaacaacaatttgaagc

Gene string 2 – 1656 bp

cgaagtcaccgttcagcaggcgtgaggatgattgccaatcatggctgaaaacaacaatttgaagctcgccagcaccatg
gaaggtcgcgtggagcagctcgcagagcagcgccaggtgatcgaagccggtggcggcgaacgtcgcgtcgagaag
caacattcccagggtaagcagaccgctcgtgagcgcctgaacaacctgctcgatccccattcgttcgacgaggtcggcg
ctttccgcaagcaccgcaccacgttgttcggcatggacaaggccgtcgtcccggcagatggcgtggtcaccggccgtg
gcaccatccttggtcgtcccgtgcacgccgcgtcccaggacttcacggtcatgggtggttcggctggcgagacgcagtc
cacgaaggtcgtcgagacgatggaacaggcgctgctcaccggcacgcccttcctgttcttctacgattcgggcggcgcc

cggatccaggagggcatcgactcgctgagcggttacggcaagatgttcttcgccaacgtgaagctgtcgggcgtcgtgc
cgcagatcgccatcattgccggcccctgtgccggtggcgcctcgtattcgccggcactgactgacttcatcatcatgacca
agaaggcccatatgttcatcacgggcccccaggtcatcaagtcggtcaccggcgaggatgtcaccgctgacgaactcg
gtggcgctgaggcccatatggccatctcgggcaatatccacttcgtggccgaggacgacgacgccgcggagctcattg
ccaagaagctgctgagcttccttccgcagaacaacactgaggaagcctccttcgtcaacccgaacaatgacgtcagccc
caataccgagctgcgcgacatcgttccgattgacggcaagaagggctatgacgtgcgcgatgtcattgccaagatcgtc
gactggggtgactacctcgaggtcaaggccggctatgccaccaacctcgtgaccgccttcgcccgggtcaatggtcgtt
cggtgggcatcgtggccaatcagccgtcggtgatgtcgggttgcctcgacatcaacgcctctgacaaggccgccgaatt
cgtgaatttctgcgattcgttcaacatcccgctggtgcagctggtcgacgtgccgggcttcctgcccggcgtgcagcagg
agtacggcggcatcattcgccatggcgcgaagatgctgtacgcctattccgaggccaccgtgccgaagatcaccgtggt
gctccgcaaggcctacggcggctcctacctggccatgtgcaaccgtgaccttggtgccgacgccgtgtacgcctggccc
agcgccgagattgcggtgatgggcgccgagggtgcggcaaatgtgatcttccgcaaggagatcaaggctgccgacga
tcccgacgccatgcgcgccgagaagatcgaggagtaccagaacgcgttcaacacgccgtacgtggccgccgcccgc
ggtcaggtcgacgacgtgattgacccggctgataccgtcgaaagattgcttccgccctggagatctacgccaccaagc
gtcagacccgcccggcgaagaagcatggaaacttcccctgctgagcgaggagagaaattatggctgatgaggaagag
aaggacct

Gene String 3 – 712 bp

gaagcatggaaacttcccctgctgagcgaggagagaaattatggctgatgaggaagagaaggacctgatgatcgccac
gctcaacaagcgcgtcgcgtcattggagtctgagttgggttcactccagagcgatacccagggtgtcaccgaggacgta
ctgacggccatttcggccgccgttgcggcctatctcggcaacgatggatcggctgaggtcgtccatttcgccccgagccc
gaactgggtccgcgagggtcgtcgggctctgcagaaccattccattcgttgatccgggagtaactcacatgaaactgaag
gtaacagtcaacggcactgcgtatgacgttgacgttgacgtcgacaagtcacacgaaaacccgatgggcaccatcctgtt
cggAggcggcacAggcggcgcgccAgcaccgAgAgcagcaggtggAgcaggAgccggtaaggccggaga
gggcgagattcccgctccgctggccggcaccgtctccaagatcctcgtgaaggagggtgacacggtcaaggctggtca
gaccgtgctcgttctcgaggccatgaagatggagaccgagatcaacgctcccaccgacggcaaggtcgagaaggtcct
tgtcaaggagcgtgacgccgtgcagggcggtcagggtctcatcaagatcggctga**agctt**ggcactggccgtcgtttta
caacgtcgtga

Table 16 - Mutations identified in the 10 strains of C. necator Δ3 cultured in F+3-HP MM for 192 hours.

Strain	Mapping	Reference Position	Type	Length	Ref.	Allele	Frequency	New locus tag	Old locus tag	Gene Name	Protein Accession	Functional Description
Δ3.1	Chromosome 1	3945014	Insertion	5	-	GGCCT	86.8	H16_RS18290	H16_A3663	*hpdH*	WP_010811289.1	3-hydroxypropionate dehydrogenase
Δ3.2	Chromosome 1	3948467	Insertion	8	-	CGAACACT	93.8	H16_RS18300	H16_A3665	*hpdR*	WP_041687575.1	LysR family transcriptional regulator
Δ3.5	Chromosome 1	3947702	SNV	1	C	T	100.0	H16_RS18300	H16_A3665	*hpdR*	WP_041687575.1	LysR family transcriptional regulator
Δ3.5	Chromosome 1	159883	Deletion	1	G	-	75.0	H16_RS33595	H16_A0146	Hypothetical protein	Unknown	Unknown
Δ3.6	Chromosome 2	2379715	Insertion	12	-	CGGCCT TGCCAG	61.8	H16_RS29225	H16_B2107	-	WP_011617648.1	Type IV secretion protein Rhs
Δ3.6	Chromosome 1	3259616	SNV	1	C	T	100.0	H16_RS15010	H16_A3011	*GntP*	WP_011615955.1	Member of the Gnt family of gluconate transporters; unknown function
Δ3.7	Chromosome 1	3945474	SNV	1	C	T	38.8	H16_RS18290	H16_A3663	*hpdH*	WP_010811289.1	3-hydroxypropionate dehydrogenase
Δ3.7	Chromosome 1	3947723	SNV	1	C	T	65.4	H16_RS18300	H16_A3665	*hpdR*	WP_041687575.1	LysR family transcriptional regulator
Δ3.8	Chromosome 1	3948311	SNV	1	A	G	100.0	H16_RS18300	H16_A3665	*hpdR*	WP_041687575.1	LysR family transcriptional regulator
Δ3.8	Chromosome 2	1056872	SNV	1	C	T	100.0	H16_RS23920	H16_B1032	-	WP_011616965.1	DUF2188 domain-containing protein
Δ3.9	Chromosome 1	3944734	Deletion	1	A	-	100.0	H16_RS18290	H16_A3663	*hpdH*	WP_010811289.1	3-hydroxypropionate dehydrogenase
Δ3.9	Chromosome 1	3174086	SNV	1	C	T	100.0	H16_RS14640	H16_A2937	*fdhA1*		Formate dehydrogenase
Δ3.10	Chromosome 1	159883	Deletion	1	G	-	75.0	H16_RS33595	H16_A0146	Hypothetical protein	Unknown	Unknown
Δ3.10	Chromosome 1	3944725	SNV	1	T	C	58.1	H16_RS18290	H16_A3663	*hpdH*	WP_010811289.1	3-hydroxypropionate dehydrogenase
Δ3.10	Chromosome 1	3944729	SNV	1	C	G	58.1	H16_RS18290	H16_A3663	*hpdH*	WP_010811289.1	3-hydroxypropionate dehydrogenase
Δ3.10	Chromosome 1	3944733	SNV	1	G	A	62.1	H16_RS18290	H16_A3663	*hpdH*	WP_010811289.1	3-hydroxypropionate dehydrogenase